SYNTHESIS, CHARACTERIZATION AND APPLICATIONS OF MORPHOLOGICALLY VARYING ORGANIC-INORGANIC DIELECTRICS AND AMINO ACID BASED BIOCOMPATIBLE COPOLYMERIC NANOMATERIALS

Dissertation submitted in partial fulfillment of the requirements for the degree of

Doctor of Philosophy (Ph.D.)

in

MATERIALS ENGINEERING

By

Debasrita Bharatiya

(Registration No: 15ETPM02)

Under the guidance of

Dr. PRADIP PAIK and Prof. M. GHANASHYAM KRISHNA



SCHOOL OF ENGINEERING SCIENCES AND TECHNOLOGY

UNIVERSITY OF HYDERABAD

HYDERABAD-500046

India

February 2020

DECLARATION

I hereby declare that the work embodied in this dissertation entitled,

"Synthesis, Characterization and Applications of Morphologically Varying Organic-

inorganic **Dielectrics** and Amino acid Based **Biocompatible** Copolymeric

Nanomaterials" submitted to University of Hyderabad for the award of Doctor of

Philosophy in **Materials Engineering**, is a record of original research work carried out by

me under the supervision of Dr. Pradip Paik, Associate Professor, School of Engineering

Sciences and Technology, University of Hyderabad (Presently at IIT BHU) and Prof. M.

Ghanashaym Krishna, Professor & Dean, School of Engineering Sciences and Technology.

The plagiarism of this dissertation has been checked and satisfied the requirement. None of

part of this work has been submitted for any degree in any University or Institute.

DEBASRITA BHARATIYA

Reg No: 15ETPM02

Ph.D. Materials Engineering

School of Engineering Sciences and Technology

University of Hyderabad

Hyderabad, 500046, India

Place:

Date:

ii

OF HIS AND ADDRESS OF THE PARTY OF THE PARTY

CERTIFICATE

This is to certify that the work contained in this dissertation entitled, "Synthesis, Characterization and Applications of Morphologically Varying Organic-inorganic Dielectrics and Amino acid Based Biocompatible Copolymeric Nanomaterials", has been carried out by Ms. Debasrita Bharatiya under my supervision and the same has not been submitted for the award of research degree to any university or Institute.

This dissertation is free from plagiarism and has not been submitted previously in part or full to any other University or Institutions for the award of any degree or diploma.

Parts of this thesis have outcomes

A. List of publications from this dissertation

- 1. <u>Bharatiya</u>, <u>Debasrita</u> & Kumar, K Santhosh & Raghunandan, S & Paik, Pradip. (2019). Dielectrics of graphene oxide decorated with nanocomposite silica-coated calcium copper titanate (CCTO) nanoparticles. **Journal of Materials Science**. 54. 10.1007/s10853-019-03336-8.
- **2.**Bharatiya Debasrita, Kumar K Santhosh, S Raghunandan& Paik Pradip. (2019). A detailed study on the dielectric properties of CCTO@SiO2 core-shell nanoparticles: Role of SiO2-NH2 shell over CCTO core surface. **Journal of Solid State Chemistry**. 10.1016/j.jssc.2019.06.023

B. List of conference presentations based on dissertation work

- 1. **Debasrita Bharatiya** (Poster Presentation, International Conference Nano Sci Tech 2017)
- 2. **Debasrita Bharatiya** (Poster Presentation, 2nd International Conference on Nano & Science and Engineering Applications-2018), (ISBN:978-81-924726-4-5)
- **3. Debasrita Bharatiya** (Short invited talk/ Oral Presentation, 4th International Conference on Nanomaterials-2019)
- **4. Debasrita Bharatiya** (Poster, International Conference on Functional Materials-2020)

Further, the student has passed the following courses towards the fulfilment of coursework requirement for Ph.D.

Course Code	Name	Credits	Pass/Fail
MT402	Characterization of Materials -Microscopy	4	Pass
MT403	Introduction to Nano Science and Engineering	4	Pass
MT404	Composites	4	Pass
MT406	Concepts in Materials Science and Engineering	4	Pass
MT407	Materials Processing and Characterization	4	Pass
	Laboratory		
MT408	Seminar	2	Pass
MT460	Nano Biotechnology	4	Pass
MT601	Research Methodology	4	Pass

	(Dr. PRADIP PAIK)
Date:	
Place:	

Supervisor

(Prof. M. GHANASHYAM KRISHNA)

Supervisor

DEAN

School of Engineering Sciences and Technology

University of Hyderabad

ACKNOWLEDGEMENTS

This Ph.D. tenure is a wonderful journey in my life with a lot of hard work, knowledge, struggle and patience. I got an opportunity to learn a lot not only from science but also from different people, place and mentality. In this period, I have observed myself with a better human being, as each passing day hurdles made me realize the strongest inner part of mine. So here I would like to thank each and everyone, who has supported in this vital period of my life.

First and foremost I wish to offer my sincerest gratitude and respect to my Ph.D. supervisor **Dr. Pradip Paik**, for introducing the current interdisciplinary topic of nanomaterials and for his inspiring guidance, patience and valuable suggestions throughout my research work. I consider myself to be fortunate to work under him as he is a very supportive, understanding and eminent scientist in the field of nano-biotechnology. His guidance, teaching classes, and lessons to live life healthy with peace made our team more strong day by day. The most important factor about my supervisor is to follow the foreign research culture in the lab, which helps me to learn the research working skill. Beyond professionalism, I would also like to thank him personally for the valuable statement which makes my life better at my difficult times.

I am also very thankful to my supervisor **Prof. M. Ghanashyam Krishna**, for his support, suggestions and guidance during my Ph.D. tenure and DRC meetings. He is a person who showed me the right pathway to overcoming the academic and research-related issues with his most valuable suggestions. I admired his way of scientific thinking, possessed of many innovative ideas and a great personality. I am fortunate to have a great supervisor in this tenure.

I would like to thank Prof. R. Singh and Prof. M. Sundararaman former deans and all other faculties in the department for providing me with the facilities and the guidance to carry out my research work. In particular, I would like to give my sincere gratitude to **Dr. Raghunandan Seelaboiyna** (BHEL, Hyderabad, R&D) for the research related help.

I am very much thankful to **Dr. Swati Ghoshachharrya** (Asst. Prof., SEST, UoH) and **Dr. Santhosh Padhi** (Asst. Prof., School of Life Sciences, UoH) for their constant

encouragement and support during the doctoral committee meetings with the most helpful research suggestions which helped me to develop my research work.

I would also especially like to thank Dr. Biswajit Parhi (IISER Bhopal), Dr. Rajendra Kumar Mallick (UoH), Ms. Rutuparna Jena (UoH), Dr. Anupama Swain (UoH), Ms. M Supriya (IIT Bombay), Dr. Binoy (UoH), Dr. Siba Soren (Ravenshaw University), Mr. Sarat (UoH) for their assistance in Physical, Chemical and Biological characterizations.

I would sincerely like to thank all my lab mates Dr. Koushi Kumar, Dr. Santhosh Kumar, Dr. Chander A, Dr. Himadri Medhi, Ms. Monica Pandey, Mr. Anil Kumar, Ms. Somedutta Maity and Ms. Monami Das and other research scholars in SEST for providing a joyful environment in the lab and helping me in all ways. I am sincerely thankful to Ms. S Saritha for the accommodation help at UoH.

I would also like to thank the technicians and non-teaching staff of SEST Mr. Mallesh, Mr. Dinakar, Mr. Pankaj, Mr. Venu, Ms. Malathy, Mr. Bala Kishan and TEM technician Mr. Durga Prasad Sir, CD technician Mr. Prasad, TGA operator Mr. Rajesh for their help in helping to do research related experiments at UoH.

I would like to thank all my batch mates especially Ms. J Sravani and batch cum lab mate Ms. Monica Pandey for their supports during my course work and in my research work.

I would like to acknowledge the (funding bodies) BHEL (sanction number BHEL/10/1001/2013/00724) for providing the facilities for the project, UGC-NFO for providing me with the fellowship, University of Hyderabad for providing me with fellowship

Finally, I would like to thank my parents, husband and brother for their constant support and encouragement.

CONTENTS

SL No	Title	Page No
I	Title Page	i
п	Declaration	ii
Ш	Certificate	iii
IV	Acknowledgements	v
Ш	Contents	vii
IV	List of Figures	xvii
V	List of Tables	xxvi
VI	Abbreviations	xxvii
VII	Abstract	xxix

CHAPTER-1

Introduction and Literature Review

Introduction

- 1. Natural Science, Material Chemistry and Nanotechnology
- 1.1. Natural Science
- 1.2. Material Chemistry
- 1.3. Nanotechnology
- 1.4. Nanomaterials

1.4.1. Classification of Nanomaterials

1.5. Part I - Dielectric Nanocomposites

- 1.5.1. Inorganic-inorganic nanocomposites
- 1.5.2. Organic-Inorganic dielectric Solids
- 1.5.3. Organic-organic hybrid nanocomposites Dielectrics
- 1.5.4. History of Dielectric materials
- 1.5.5. Effect of Dielectric materials
- 1.5.5.1. Insulator
- 1.5.5.2. Dielectric materials
- 1.5.5.3. Types of Dielectric materials
- 1.5.5.3.1. Dielectric materials have been classified based on dielectric constant strength
- 1.5.5.3.2. Dielectric materials have been classified based on Polarity
- 1.5.5.4. Terms Associated with Dielectric Study
- 1.5.5.4.1. Dielectric Constant
- 1.5.5.4.2. Dielectric Loss
- 1.5.5.4.3. Breakdown voltage
- 1.5.5.5. Polarizations involved in Dielectric medium
- 1.5.5.6. Major challenges of Dielectric Organic-Inorganic hybrid materials
- 1.5.6. Calcium copper titanate
- 1.5.7. Silica (SiO₂ NPs)
- 1.5.8. Amine functionalized SiO₂ NPs
- 1.5.9. Core-Shell Inorganic NPs
- 1.5.10. Graphene Oxide (GO)

- 1.5.11. GO NPs Synthesis Method
- 1.5.12. GO NPs Functionalization
- 1.5.13. GO NPs Conjugation functionalization

1.6. Part II - Polymeric Nanomaterials

- 1.6.1. History of Polymeric materials
- 1.6.2. Effect of Polymeric materials
- 1.6.3. Classification of Polymeric nanomaterials
- 1.6.3.1. Classification by Monomer and building blocks
- 1.6.3.2. Classification by Origin
- 1.6.3.3. Classification by Structure
- 1.6.3.4. Classification by Polymerization method
- 1.6.3.5. Classification on Tacticity
- 1.6.3.6. Classification based on Self-assembly
- 1.6.4. Important Chemical and Physical properties of triblock copolymers
- 1.6.5. Challenges of Block Copolymer
- 1.6.6. Importance of Block copolymer
- 1.6.7. Monomer Blocks
- 1.6.7.1. [α-Methoxy-ω-Amino-Polyethylene Glycol] / [α-OMe-ω-NH-PEG]
- 1.6.7.2. L-Glutamic Acid-β-Benzyl Ester
- 1.6.7.3. L-Aspartic Acid-δ-Benzyl Ester
- 1.6.8. MTT/ Biocompatibility Assay Test
- 1.6.9. Antibacterial Study

Literature Review

1.7. Part I-Dielectric Nanocomposites

- 1.7.1. Inorganic Dielectric Material
- 1.7.1.1. Calcium Copper Titanate
- 1.7.1.2. Synthesis of CCTO materials
- 1.7.1.3. CCTO based Composites
- 1.7.1.4. Barium Titanate, Lead Titanate and PZT
- 1.7.1.5. Silicon Oxide Nanoparticles (SiO₂ NPs)
- 1.7.2. Organic Dielectric Material
- 1.7.2.1. Graphene Oxide (GO)
- 1.7.2.2. Synthesis of GO NPs
- 1.7.2.3. GO based nanocomposites and its dielectric behaviour
- 1.7.3. Composite Dielectric Material

1.8. Part II - Amino acid based Block Copolymer

- 1.8.1. Synthesis and Development of Amino acid based Block Copolymer
- 1.8.2. Development of Amino acid based Block Copolymer for anticancer activity
- 1.8.3. Protein Folding Study of Block copolymers
- 1.8.4. Antimicrobial activity of Block copolymer
- 1.8.5. PEG and Amino acid based Di and Triblock Copolymer activity towards drug delivery
- 1.8.6. [PEG-b-L-GluA] Di- Block Copolymer for therapeutic application
- 1.8.7. [α -MeO- ω -NH-PEG]-b-(L-AspA)] for cancer and bacterial treatment

1.9. Motivations

1.10. Objectives

CHAPTER-2

Materials, Experimental Procedures and Characterization Techniques

Materials

- 2.1. Introduction
- 2.2. Chemicals, Solvent and materials used for applicative purpose
- 2.3. Synthesis of core-shell like amine functionalized SiO₂ NPs on CCTO NPs
- 2.3.1. Synthesis of CCTO NPs
- 2.3.2. Synthesis of CCTO@SiO₂-NH₂ NPs
- 2.3.3. Preparation of Pellet for Dielectric analysis
- 2.4. Synthesis of CCTO@SiO₂ core-shell NPs decorated on sheet like Graphene oxide (GO) nanocomposites
- 2.4.1. Synthesis of GO
- 2.4.2. Synthesis of CCTO@SiO₂ NPs:
- 2.4.3. Synthesis of CCTO@SiO₂-GO
- 2.5. Amino-acid based stimuli responsive biocompatible [PEG-b-PBLG-b-PBLA] nano micelles synthesis
- 2.5.1. Synthesis of NCA BLG and NCA BLA
- 2.5.2. Synthesis of Diblock copolymer [PEG-b-PBLG]
- 2.5.3. Synthesis of a triblock copolymer of [PEG-b-PBLG-b-PBLA]
- 2.6. Synthesis of polypepto vesicle sized [[(α -OCH₃- ω -NH-PEG)-b-(PBLA)₇-b-(PBLG)₁₇]
- 2.6.1 Synthesis of NCA BLA and NCA BLG
- 2.6.2. Development of triblock copolymer of $[(\alpha \text{-OCH}_3 \omega \text{-NH-PEG}) b (\text{PBLA})_7 b (\text{PBLG})_{17}]$

- 2.7. In Vitro Studies
- 2.7.1. In Vitro Antibacterial activities with different stains
- 2.7.2. In Vitro Cell maintenance for Cytotoxicity assay test

Characterization Techniques/Instrumentation

2.8. Instrumentation

2.8.1. Physical Study Characterizations

- 2.8.1.1. TEM (Morphology Analysis)
- 2.8.1.2. FESEM (Morphology)
- 2.8.1.3. EDX (Elemental Analysis)
- 2.8.1.4. XRD (Crystalline nature)
- 2.8.1.5. TGA (Thermal Stability)
- 2.8.1.6. Raman Spectra (Atomic order)

2.8.2. Structural Characterization

- 2.8.2.1. FTIR (Identification of Chemical Functionality)
- 2.8.2.2. H¹ NMR (positioning of hydrogen)
- 2.8.2.3. MALDI TOF (exact molecular weight)
- 2.8.2.4. DLS size of macromolecules)

2.8.3. Biological and Physical Applicative Characterization

- 2.8.3.1. Dielectric Study (Dielectric constant and loss)
- 2.8.3.2. Zeta (Electro-kinetic potential)
- 2.8.3.3. CD (Secondary structure of proteins)
- 2.8.3.4. UV (Absorbance band)
- 2.8.3.5. LCSM (Morphology)

- 2.8.3.6. MTT Assay (Biocompatibility against human carcinoma cell)
- 2.8.3.7. Antibacterial Susceptibility test (Killing Efficiency Bacteria)

CHAPTER-3

Results and Discussion

- 3.1 Results and Discussion: Part IA
- 3.3.1. Abstract
- 3.1.2. Synthesis Procedures
- 3.1.3. Introduction and Motivation
- 3.1.4. Reaction Pathway
- 3.1.5. Morphological Characterization
- 3.1.6. XRD and Thermal analysis
- 3.1.7. FTIR Spectra
- 3.1.8. Comparative Raman Study
- 3.1.9. Ultraviolet Measurement
- 3.1.10. Frequency dependence dielectric study of nonsintered samples
- 3.1.11. Frequency dependence dielectric study of sintered samples
- 3.1.12. Temperature dependence dielectric bahaviour of CCTO@SiO₂ NPs
- 3.1.13. Analysis of Cole-Cole plots
- 3.1.14. Conclusions for Part IA
- 3.2 Results and Discussion: Part IB
- 3.2.1. Abstract
- 3.2.2. Synthesis of CCTO@SiO₂-GO nanocomposites
- 3.2.3. Introduction and Motivation

- 3.2.4. Reaction Mechanism for CCTO@SiO₂-GO nanocomposites
- 3.2.5. Shape and Morphology Study via HRTEM
- 3.2.6. Crystalline nature and Thermal Stability Study
- 3.2.7. Chemical Functionality through FTIR Spectra
- 3.2.8. Raman Spectra for CCTO@SiO₂-GO nanocomposites
- 3.2.9. UV analysis for CCTO@SiO2-GO nanocomposites
- 3.2.10. Dielectrics behaviour with respect to change in frequency
- 3.2.11. The temperature dependence of the dielectric study of silica coated CCTO-GO nanocomposite
- 3.2.12. Cole-Cole plot for nanocomposites
- 3.2.13. Part IB-Conclusion of CCTO@SiO₂-GO nanocomposites
- 3.3 Results and Discussion: Part IIA
- 3.3.1. Abstract
- 3.3.2. Synthesis of a triblock copolymer of [PEG-b-PBLG-b-PBLA]
- 3.3.2.1. Cell Viability Study and MTT assay
- 3.3.2.2. Antibacterial activities Studies against different bacterial models
- 3.3.3. Introduction and Motivations
- 3.3.4. Reaction Pathway
- 3.3.5. ¹H NMR Analysis
- 3.3.6. FTIR and MALDI-TOF Analysis
- 3.3.7. Morphology and Size Analysis
- 3.3.8. XRD and TGA Analysis
- 3.3.9. Ultraviolet-Visible Spectra

- 3.3.10. Laser Confocal Scanning Microscopy
- 3.3.11. Zeta Potential Measurements
- 3.3.12. CD analysis for amino-acid based polymeric proteins with varying pH and temperature
- 3.3.13. *In vitro cytotoxicity assay*
- 3.3.14. In vitro antibacterial activity
- 3.3.15. Conclusion for Part IIA
- 3.4 Results and Discussion: Part IIB
- 3.4.1. Abstract
- 3.4.2. Introduction and Motivations
- 3.4.3. Synthesis of a triblock copolymer of [PEG-*b*-(PBLA)₇-*b*-(PBLG)₁₇]
- 3.4.4. Reaction Mechanism
- 3.4.5. Morphological Study of Polymer via HRTEM
- 3.4.6. LCSM analysis of copolymer [PEG-*b*-(PBLA)₇-*b*-(PBLG)₁₇]
- 3.4.7. Position of Hydrogen by ¹HNMR
- 3.4.8. FTIR and MALDI-TOF
- 3.4.9. XRD and TGA analysis for polymers
- 3.4.10. Zeta Potential measurement at different pH medium
- 3.4.11. UV-Vis Measurements at different pH medium
- 3.4.12. CD Spectra at different pH medium and temperature range
- 3.4.13. Antimicrobial Resistance
- 3.4.14. *In vitro* MTT assay test
- 3.4.15. Conclusion for Part IIB

CHAPTER 4

Summary and conclusions

- 4.1. Summary
- 4.2. Conclusions

CHAPTER 5

Future scopes from this dissertation

REFRENCES

LIST OF FIGURES

Chapter 1-Introduction and Literature Review

- Figure 1.1. Schematic Classification of areas associated with the development of nanomaterials
- Figure 1.2. Showing the different sized nanomaterials
- Figure 1.3. Types of classification of polymer based nanomaterials
- Figure 1.4. Represent the different Polarization Mechanisms (i) Electronic polarization (ii) ionic polarization (iii) orientation/dipolar polarization and (iv) space charge polarization respectively.
- Figure 1.5. CaCu₃Ti₄O₁₂, shown as TiO₆ octahedra, Cu atoms (blue) bonded to four oxygen atoms (red), and large Ca atoms (yellow) without bonds.
- Figure 1.6. SiO₂ (silica), shown as, Si atoms (blue) bonded to two oxygen atoms (red).
- Figure 1.7. Shows the functionalization of -NH₂ with SiO₂ (silica), shown as, Si atoms (blue) bonded to two oxygen atoms (red) and one organic amine (-NH₂) group (yellow).
- Figure 1.8. Chemical Structure of Graphene Oxide.
- Figure 1.9. Polymer-based materials and its wide ranges of usage.
- Figure 1.10. Polymeric nanostructures: (a) Dendrimers, (b) Liposomes and (c) Micelles.
- Figure 1.11. Schematic illustration for recent used polymeric materials, its side effects and armour to save the globe.
- Figure 1.12. 2D Ball and stick model of PEG polymeric materials, its side effects and armour to save the globe.
- Figure 1.13. 2D Ball and stick model of L-Glutamic Acid-β-Benzyl Ester polymeric materials as an amino acid based precursor
- Figure 1.14. 2D Ball and stick model of L-Aspartic Acid-δ-Benzyl Ester polymeric materials as an amino acid precursor

Chapter 3-Results and Discussion Part IA

Figure 3.1.A. Objective diagram of CCTO@SiO₂core-shell nanoparticles synthesis.

Schematic 3.1.1: Schematic illustration of the formation of core-shell CCTO@SiO₂-NH₂ NPs with a stepwise mechanism via sol-gel method.

Figure 3.1.1. High resolution TEM images with varying shell thickness of aminated SiO₂ on CCTO core (a) PCNS (uncoated CCTO) (b) CS1NS NPs, 3-4 nm (c) CS2NS NPs, 7-10 nm (d) CS3NS NPs 15-20nm (e) IFTT image of PCNS and (f) IFTT image of coated CCTO@SiO₂-NH₂ NPs, (g) and (h) illustrate the length and diameter of uncoated PCNS NPs of 500 nm-700 nm and (h) 100 nm-200 nm, respectively.

Figure 3.1.2. (a) X-Ray Diffractrogram pattern for nonsintered uncoated PCNS and coated CCTO@SiO₂-NH₂ NPs and Fig 3.1.2 (b) represents JCPDS file for CS3NS NPs.

Figure 3.1.2(c), 3.1.2(d) and 3.1.2(e) EDX graph and table obtained from FESEM of CS1NS, CS2NS and CS3NS NPs respectively.

Figure 3.1.2(f) and 3.1.2(g) represents TGA and DTA thermogram for nonsintered uncoated PCNS and coated CCTO@SiO₂-NH₂ NPs with a heating rate of 10° C per minute in N₂ atmosphere respectively.

Figure 3.1.3. Comparison between FTIR spectrums for (a) non-sintered PCNS, CS1NS, CS2NS and CS3NS NPs (b) sintered PCS, CS1S, CS2S and CS3S NPs respectively.

Figure 3.1.4. Comparative study of RAMAN spectrums for (a) non-sintered PCNS, CS1NS, CS2NS and CS3NS NPs (b) sintered PCS, CS1S, CS2S and CSNS) NPs respectively

Figure 3.1.5. Ultra-Violet measurement of non-sintered PCNS, CS1NS, CS2NS and CS3NS NPs from 180 nm-700 nm respectively

Figure 3.1.6. (a), (b), (c) and (d) represent the variation of the real part of dielectric constant (ε') and imaginary part of dielectric constant (ε'') with respect to frequency (20 Hz to 2 MHz) for PCNS NPs.

Figure 3.1.6. (e), (f), (g) and (h) represent the variation of impedance constant (Z') and impedance loss (Z") loss with respect to frequency (20Hz to 2MHz) for nonsintered PCNS NPs.

- Figure 3.1.6. (i) ϵ' as a function of the frequency of PCNS NPs at different temperature range between RT to 200 °C.
- Figure 3.1.7. represent (a), (b), (c) and (d) represents the variation of real part of dielectric constant (ϵ') and imaginary part of dielectric constant (ϵ'') with respect to frequency (20Hz to 2MHz) for CS1NS NPs.
- Figure 3.1.7. (e), (f), (g) and (h) represent the variation of impedance constant (Z') and impedance loss (Z") loss with respect to frequency (20Hz to 2MHz) for nonsintered CS1NS NPs.
- Figure 3.1.7. (i) ε' as a function of the frequency of CS1NS NPs at different temperature range between RT to 400°C.
- Figure 3.1.8. represent (a), (b), (c) and (d) represents the variation of the real part of dielectric constant (ϵ') and imaginary part of dielectric constant (ϵ'') with respect to frequency (20Hz to 2MHz) for CS2NS NPs.
- Figure 3.1.8. (e), (f), (g) and (h) represent the variation of impedance constant (Z') and impedance loss (Z") loss with respect to frequency (20 Hz to 2 MHz) for nonsintered CS2NS NPs.
- Figure 3.1.8. (i) ϵ' as a function of the frequency of CS2NS NPs at different temperature range between RT to 400 °C.
- Figure 3.1.9. represent (a), (b), (c) and (d) represents the variation of the real part of dielectric constant (ϵ') and imaginary part of dielectric constant (ϵ'') with respect to frequency (20Hz to 2MHz) for CS3NS NPs.
- Figure 3.1.9. (e), (f), (g) and (h) represent the variation of impedance constant (Z') and impedance loss (Z") loss with respect to frequency (20 Hz to 2 MHz) for nonsintered CS3NS NPs.
- Figure 3.1.9. (i) ε' as a function of the frequency of CS3NS NPs at different temperature range between RT to 400 °C.
- Fig 3.1.10 represents the frequency dependence ϵ' for PCS NPs from 20Hz to 1×10^4 Hz.

Figure 3.1.11. (a), (b), (c) and (d) represents the variation of dielectric constant (ϵ '), dielectric loss (ϵ "), impedance constant and impedance loss with respect to frequency (20Hz to 2MHz) for sintered uncoated (PCS) and coated CCTO@SiO₂ (CS1S, CS2S and CS3S) NPs, respectively at 25°C.

Fig: 3.1.12 (a), (b), (c) and (d) ε'as a function of the frequency of sintered uncoated CCTO, coated CS1S, coated CS2S and coated CS3S NPs at different temperature range between RT to 250°C.

Figure 3.1.13 (a), (b), (c) and (d) shows the Cole-Cole plot of sintered uncoated PCSNPs, coated CS1S, coated CS2S and coated CS3S NPs, respectively.

Figure 3.1.14 represents the Cole-Cole plot for PCS NPs.

Chapter 3-Results and Discussion Part IB

Figure 3.2.A. Objective Diagram for Dielectrics of the noble synthesized nanocomposite silica coated CCTO over Graphene oxide with the efficacy of CCTO@SiO₂ NPs decoration.

Scheme 3.2.1. Schematic steps of the sol-gel synthesis method of CCTO@SiO₂ NPs

Figures 3.2.1. (a), (b) and (c) are the HRTEM images of pure CCTO NPs, coated CCTO@SiO₂NPs and GO, respectively. Figs. 3.2.1. (d), (f) and (h) illustrate the coating CCTO@SiO₂ NPs GO named as CSG1, CSG2 and CSG3, respectively. Figs. 3.2.1. (e), (g) and (i) show the shell thickness of silica coated on CCTO NPs which are attached on the surface of GO layers of thickness 2-4 nm, 5-7 nm and 15-17 nm respectively. Figs. 3.2.1. (j), (k) and (l) illustrates IFTT images with d-spacing values of pure CCTO NPs, CCTO@SiO₂ core-shell NPs and CCTO@SiO₂ NPs over GO, respectively.

Figure 3.2.2. (a), (b), (c) and (d) illustrates FESEM images of CSG1, CSG2 and CSG3 derived nanocomposites synthesized from 2-4 nm, 5-7 nm and 15 nm CCTO@SiO₂ core-shell NPs. Fig. 3.2.2 (e) and Table 3.2.2 represents EDX data for CSG 2 nanocomposite.

Figure 3.2.3. (a) and (b) represents well spread silica-CCTO over GO for CSG2 and CSG3 nanocomposites respectively.

Figure 3.2.4. (a) and (b) illustrates XRD Pattern and TGA Thermogram of CSG1, CSG2 and CSG3 nanocomposites synthesized from 2-4 nm, 5-7 nm and 15-17 nm Si coated CCTO NPs, respectively.

Figure 3.2.5. (a) illustrates the FTIR Spectra of CSG1, CSG2 and CSG3 nanocomposites synthesized from 2-4nm, 5-7 nm and 15-17 nm Si coated CCTO NPs, respectively. Fig. 3.2.5. (b) represents the FTIR Spectra for precursor materials.

Figure 3.2.6. (a) illustrates the Raman Spectra of CSG1, CSG2 and CSG3 nanocomposites synthesized from 2-4nm, 5-7 nm and 15-17 nm Si coated CCTO NPs, respectively. Fig 3.2.6. (b) represents FTIR Spectra for precursor materials.

Figure 3.2.7.(a) and (b) illustrate UV-Vis NIR Spectrums of pure CCTO NPs, GO NPS, CSG1, CSG2 and CSG3 nanocomposites synthesized from 2-4 nm, 5-7 nm and 15-17 nm Si coated CCTO NPs, respectively.

Figures 3.2.8. (a), (b), (c) and (d) Illustrate the Variation of dielectric constant (ϵ'), dielectric loss (ϵ''), impedance constant (Z') and impedance loss (Z'') with respect to frequency of CSG1, CSG2 and CSG3 nanocomposites synthesized from 2-4 nm, 5-7 nm and 15-17 nm Si coated CCTO NPs, respectively.

Figure 3.2.9. (a), (b) and (c) Illustrate the Variation of dielectric constant with different temperature from RT to 400°C at variable frequency region for of CSG1, CSG2 and CSG3 nanocomposites synthesized from 2-4 nm, 5-7 nm and 15-17 nm Si coated CCTO respectively.

Figure 3.2.10. represents temperature-dependent plot with a variable frequency of highest thickness coated silica-CCTO over GO for CSG3 nanocomposite.

Figure 3.2.11. (a), (b) and (c) represent the Cole-Cole plot in the low and high-frequency region for of CSG1, CSG2 and CSG3, nanocomposites respectively.

Chapter 3-Results and Discussion Part IIA

Figure 3.3.A. Objective diagram for stimuli responsive biocompatible synthetic polypetidic nano micelles [α -OMe- ω -NH-PEG-b-(PBLG)₅-b-PBLA)₁₈]

Schematic 3.3.1: The mechanistic pathway involved in the synthesis approach of polymers through ring-opening polymerization of [PEG-*b*-PBLG-*b*-PBLA].

Figure 3.3.1. (a), (b), (c) and (d) represent the ¹HNMR results of diblock copolymer [PEG-*b*-BLG] and triblock copolymer of [PEG-*b*-BLG₅-*b*-BLA₁₈] before catalytic hydrogenation, respectively. Where p= no. of CH₂ units of PEG, n= no. of CH₂ units of glutamate and m= no. of CH₂ units of aspartate, (See Scheme 3.3.1). Figs. 3.3.1. (c) and (d) represent the cross-sectional H¹NMR data of diblock copolymer of [PEG-*b*-PBLG] and triblock copolymer of [PEG-*b*-PBLG-*b*-PBLA] after catalytic hydrogenation respectively. Where n= no. of CH₂ units of glutamate and m= no. of CH₂ units of aspartate

Figure 3.3.2. (a) represents the FTIR spectra of type triblock copolymer of [PEG-*b*-PBLG-*b*-PBLA], before [PEG-*b*-BLG-*b*-BLA] and after catalytic hydrogenation [PEG-*b*-PBLG-*b*-PBLA], respectively and (b) MALDI-TOF of triblock copolymer of [PEG-*b*-BLG₅-*b*-BLA₁₈] before catalytic hydrogenation.

Figure 3.3.2. (a) and (b) represent the MALDI data of NCA BLG which is a precursor for the synthesis of diblock copolymer [[PEG-b-PBLG-b-PBLA] before catalytic hydrogenation respectively.

Figures 3.3.3. (a), (b) and (c) are the HRTEM micrographs of diblock copolymer micelles of [PEG-b-PBLG] from lower to higher resolution. Fig 3.3.3 (d), (e) and (f) illustrate the distorted shape of the triblock copolymer micelles of [PEG-b-PBLG-b-PBLA]. Figs. 3.3.3. (g), (h) and (i) show the ribbon type triblock copolymer of [PEG-b-PBLG-b-PBLA] at various ranges of 100 nm-200 nm. Figs. 3.3.3. (j) and (k) are the particle size distribution of [PEG-b-PBLG-b-PBLA] triblock copolymer and [PEG-b-PBLG] diblock copolymer, respectively.

Figures 3.3.4. (a) and (b) represent XRD plots and TGA thermogram of [PEG-b-PBLG-b-PBLA] triblock copolymer and an a-AB diblock copolymer of [PEG-b-PBLG], respectively.

Figures 3.3.5. (a) and (b) represent the UV-Vis spectra for triblock copolymer of [PEG-*b*-PBLG-*b*-PBLA] at the range 190-300 nm and 450-550 nm, respectively.

Figure 3.3.5. (c) illustrates the UV graph of an a-AB diblock copolymer of [PEG-b-PBLG]

Figures 3.3.6. (a) and (b) illustrate Laser Confocal images of diblock [PEG-b-PBLG], and Fig. 3.3.6(c) and (d) represent triblock copolymer [PEG-b-PBLG-b-PBLA] for laser and bright-field images, respectively.

Figures 3.3.7. (a) and (b) show the profile for Zeta potential for triblock copolymer [PEG-b-PBLG-b-PBLA] and di-block copolymer [PEG-b-PBLG], respectively at different pH (pH 4 to10) and 25°C.

Figure 3.3.8. illustrates CD results for triblock copolymer of [PEG-*b*-PBLG-*b*-PBLA] at 20 to 50 °C with different pH (a) pH 4, (b) pH 5, (c) pH 6, (d) pH 7, (e) pH 8, (f) pH 9 and (g) pH 10, respectively.

Figure 3.3.9. illustrates Circular Dichroism analysis for a-AB diblock copolymer of [PEG-*b*-PBLG] over a change of temperature range 20°C to 50°C with respect to different pH conditions (a) pH 4, (b) pH 5, (c) pH 6, (d) pH 7, (e) pH 8, (f) pH 9 and (g) pH 10 respectively.

Figure 3.3.10. Cell viability results for diblock copolymer of [PEG-b-PBLG] and triblock copolymer [PEG-b-PBLG-b-PBLA], respectively.

Schematic 3.3.2. Probable schematic representation of *Reactive Oxygen Species Pathway* (*ROS*) mechanism to kill the bacteria by tri-block-copolymer.

Figures 3.3.11. (a) and (b) show the *in vitro* antimicrobial activity results for diblock copolymer of [PEG-b-PBLG] and triblock copolymer of [PEG-b-PBLG-b-PBLA] for *Gram* (+) *Staphylococcus aureus* and Gram (-) *E.Coli, respectively*.

Chapter 3-Results and Discussion Part IIB

Figure 3.4.A. Objective diagram for Designing of a new polypepto based nanovesicles sized macromolecular triblock biomaterials for [PEG-*b*-(PBLA)₇-*b*-(PBLG)₁₇].

Scheme 3.4.1. Mechanistic pathway for [PEG-b-(PBLA)₇-b-(PBLG)₁₇] via modified ring-opening polymerization where p= no of –CH₂ units for α -CH₃- ω -NH₂-PEG, n= no of –CH₂ units for NCA-BLA and m= no of –CH₂ units for NCA-BLG respectively

Figures 3.4.1. (a) and (b) represent the HRTEM micrograph of [PEG-b-(PBLA)₇] and Fig 3.4.1(c) and (d) show for [PEG-b-(PBLA)₇-b-(PBLG)₁₇] respectively. Fig 3.4.1. (e) and (f) illustrate the average size for [PEG-b-(PBLA)₇] nano micelles of average size 8 nm and [PEG-b-(PBLA)₇-b-(PBLG)₁₇] nanovesicles.

Figure 3.4.1. (g) EDAX analysis for [PEG-b-(PBLA)₇-b-(PBLG)₁₇] block copolymer

Figures 3.4.3. (a) and (b) represent the H^1NMR spectra for diblock[PEG-b-(PBLA)₇], triblock [PEG-b-(PBLA)₇-b-(PBLG)₁₇] and precursor [α -OCH₃- ω -NH-PEG] respectively with CDCl₃ as solvent and tetramethylsilane (TMS) as an internal reference. Where p=no. of CH₂ units in a-MeO-PEG-NH₂ n= no. of CH₂ units in b-(NCA-BLA)₇ and m= no. of CH₂ units in b-(NCA-BLG)₁₇.

Figures 3.4.2. (a) and (b) represented LCSM images for of [PEG-b-(PBLA)₇] whereas Fig. 3.4.2.(c) and (d) indicated the LCSM images for [PEG-b-(PBLA)₇-b-(PBLG)₁₇] respectively. Fig 3.4.2. (e) represents the axial view of [PEG-b-(PBLA)₇-b-(PBLG)₁₇] at a magnification of 50 μ m.

Figure 3.4.3. (a) and (b) represent the H¹NMR spectra for diblock [PEG-b-(PBLA)₇], triblock [PEG-b-(PBLA)₇-b-(PBLG)₁₇] and precursor [α -OCH₃- ω -NH-PEG] respectively with CDCl₃ as solvent and tetramethylsilane (TMS) as an internal reference. Where p=no. of CH₂ units in a-MeO-PEG-NH₂, n= no. of CH₂ units in b-(BLA)₇ and m= no. of CH₂ units in b-(NCA-BLG)₁₇.

Figures 3.4.4. (a) and (b) illustrates the FT-IR spectra and MALDI-TOF data for [PEG-b-(PBLA)₇] and [PEG-b-(PBLA)₇-b-(PBLG)₁₇] respectively with DCM and CHCl₃ as a standard soluble solvent.

Figures 3.4.5. (a) and (b) illustrates the XRD and TGA data for [PEG-b-(PBLA)₇] and [PEG-b-(PBLA)₇-b-(PBLG)₁₇] respectively.

Figures 3.4.6. (a) and (b) show the ζ potential value for [PEG-b-(PBLA)₇] and [PEG-b-(PBLA)₇-b-(PBLG)₁₇] respectively with DDI H₂O as a standard soluble solvent.

Scheme 3.4.2. Plausible acid-base interaction in the colloidal solution in of nanovesicular [PEG-*b*-(PBLA)₇-*b*-(PBLG)₁₇].

Figures 3.4.7. (a) and (b) represent the UV spectra for [PEG-b-(PBLA)₇] and [PEG-b-(PBLA)₇-b-(PBLG)₁₇] respectively at room temperature with a variation of pH from 4 to 10.

Figure 3.4.8. illustrates the CD component spectra showing deconvoluted protein folding behaviour of [PEG-*b*-(PBLA)₇-*b*-(PBLG)₁₇], the concentration of solution 0.5mg/ml with the variation of pH 4 to 10 and temperature from 20°C to 50°C with 23 reference proteins.

Figure 3.4.9. illustrates the CD spectra showing protein folding behaviour of [PEG-*b*-(PBLA)₇] at acidic pH 4, neutral pH 7 and basic pH 8 with the temperature ranged from 20°C to 45°C.

Figures 3.4.10. (a) and (b) represents the antibacterial susceptibility test showing the inhibition of growth for [PEG-b-(PBLA)₇] and [PEG-b-(PBLA)₇-b-(PBLG)₁₇] at room temperature with two different bacterial strains of *gram* (-) *E.coli and gram* (+) *Staphylococcus aureus* respectively. Fig 3.4.10 (c): Probable Reductive Oxygen-Free radical mechanism against antibacterial infection.

Figure 3.4.11. Cytotoxicity MTT assay test of [PEG-b-(PBLA)₇] and [PEG-b-(PBLA)₇-b-(PBLG)₁₇] solution in solvent medium towards MDA-MB231after 24 h incubation.

LIST OF TABLES

- Table 1.1: Reported research work for CCTO, Silica and GO nanomaterials dielectric study
- Table 1.2: Reported research work for amino acid based polymers and its application
- Table 2.2.1: List of precursor materials used
- Table 2.2.2: List of solvents used
- Table 2.2.3: List of materials used for application purpose
- Table 2.3.1: Show the details of the sintered CCTO@SiO₂-NH₂ NPs sample properties
- Table 2.4.1: Synthesis of CCTO@SiO₂-GO nanocomposites at different condition
- Table 3.1.1: The dielectric constant ε' values for nonsintered and sintered samples core-shell NPs with varying frequency have been elucidated
- Table 3.1.2: The dielectric loss ε'' values for nonsintered and sintered samples attached
- Table 3.1.3: Frequency with respect Z' for nonsintered and sintered samples attached
- Table 3.1.4: Frequency-dependent impedance loss for nonsintered samples (PCNS, CS1NS, CS2NS and CS3NS) core-shell NPs along with sintered samples (PCS, CS1S, CS2S and CS3S) core-shell NPs have been elucidated
- Table 3.2.1: Synthesis of CCTO@SiO₂-GO nanocomposites at different condition
- Table 3.2.3: Raman modes of vibration of newly synthesized nanocomposites of CCTO@SiO₂-GO
- Table 3.2.4: Frequency with respect to ε' and ε'' of GO based nanocomposites
- Table 3.2.5: Frequency with respect to Z' and Z" of GO based nanocomposites
- Table 3.3.1: Data Obtained from Zeta experiment for nano micelles
- Table 3.4.1: EDAX Data of nanosized Vesicles
- Table 4.2.1: List of properties and the details have been attached below in the table for designed materials of this dissertation

ABBREVIATIONS

ССТО	$CaCu_3Ti_4O_{12}$
GO	Graphene Oxide
RT	Room Temperature
NPs	Nanoparticles
XRD	X-Ray Diffraction
SEM	Scanning Electron Microscopy
FESEM	Field Emission Scanning Electron Microscopy
TEM	Transmission Electron Microscopy
CD	Circular Dichroism
DSC	Differential Scanning Calorimetry
PEG	Polyethylene Glycol
EDX	Energy Dispersive X-Ray Spectroscopy
MBA-MD231	M D anderson Metastasis Breast Human Carcinoma cell
Rh6G	Rhodamine 6G
nm	nanometer
μm	micrometer
TGA	Thermo-Gravimetric Analysis
FTIR	Fourier Transform Infrared
UV-Vis	Ultraviolet-Visible Spectroscopy
SiO ₂	Silica
MTT	Dimethythiazol-diphenyl tetrazolium bromide
E.coli	Escherichia Coli
S.aureus	Staphylococcus aureus
вто	BaTiO ₃
ТВР	Trriblock copolymer
рН	Concentration of Hydrogen ions

PAA	Poly Aspartic Acid
PGA	Poly Glutamic Acid
ROP	Ring-opening polymerization
RAFT	Reversible addition-fragmentation radical transfer
BCC	Body centred Cubic

ABSTRACT

Being small and compact structures, nanomaterials are regarded as smart materials. Since the creation of this earth until now, the existence of nanomaterials has been proved by many pioneer researchers with interesting phenomena at several stages. There are wide varieties of designing procedures for different morphological nanomaterials to be used for numerous purposes. Looking towards the development of interesting behaviour and application of nanomaterials, this dissertation is mainly focusing on the synthesis and study of morphologically varying organic-inorganic dielectrics and amino acid based biocompatible copolymeric nanomaterials for electrical and biomedical applications. Morphologically varying polymeric self-assembled nanomaterials have been synthesized by ring-opening polymerization techniques with other chemical purification methods like condensation, crystallization, separation and recrystallization methods whereas organic-inorganic nanocomposites followed the modified sol-gel method, nano chemical processes like ultrasonication, ultracentrifugation, hydrolysis, dehydrolysis and drying. The organicinorganic dielectric nanocomposites have developed by solid-state route and mainly focused towards the development of charge storage devices, sensors and electronic application purpose. The synthesis of very small sized morphologically changed amino acid based polymeric nanomaterials have attracted many researchers to focus on their application towards anticancer therapy, antibacterial treatment and as drug carriers into the human cell line due to its small size ranges from 10^1 - 10^2 nm, biochemical properties and surface functionalities. To overcome few hurdles in the field of electrical and biological applications, self-assembled organic-inorganic nanocomposites along with block copolymeric nanostructures are designed for human need.

The first chapter of this dissertation is about the introduction and literature review of organic-inorganic dielectrics and amino acid based block copolymer nanoparticles respectively. This chapter includes various topics i.e. Natural science, nanomaterials, nanocomposites, organic-inorganic dielectrics, calcium copper titanate, silica, grapheme oxide, dielectric study for electrical and storage application, amino acid based peptides, polyethylene glycol, block copolymer, challenges, biocompatibility test/MTT assay, antibacterial treatment and therapeutic applications. The last section of this chapter summarizes with motivation and objectives towards the development of morphologically biased nanomaterials.

The second chapter includes the chemicals required, experimental procedures and characterization techniques performed for the synthesis and the purpose of investigation on physical, structural, biophysical, chemical and biological behaviours.

The third chapter is the results and discussion part & has been classified into four different parts with the detailed application of nanomaterials. The synthesis and applications of core-shell CCTO@SiO₂ NPs and sheet like CCTO@SiO₂-GO nanocomposites in nanodevice applications with a high dielectric constant is the main aim to develop the different morphological appearance of organic-inorganic dielectrics. The synthesis of amino acid based organic block copolymer and its biological applications is another aim of this dissertation. The dissertation is targeted to use different morphological based nanomaterials for different applications including nanodevices and nanomedicines.

The fourth chapter of this dissertation summarizes with the significant conclusion and future scopes in the field of electrical and biological applications. This chapter of this dissertation concludes with the summary of different nanosized designed nanomaterials and their exceptional application features in electrical nanodevices and biotechnology area. The benefits and use of morphologically varied synthesized nanomaterial with concrete proofs for our future development is also depicted and discussed.

The fifth chapter concisely discussed the future scope of the dissertation including the development of different dielectrics and the amino acid based block copolymers towards various usage.

CHAPTER-1

INTRODUCTION AND LITERATURE REVIEW

INTRODUCTION

- 1. Natural Science, Material Chemistry and Nanotechnology
- 1.1. Natural science
- 1.2. Material chemistry
- 1.3. Nanotechnology
- 1.4. Nanomaterials
- 1.4.1. Classification of nanomaterials
- 1.5. Section I Dielectric nanocomposites
- 1.5.1. Inorganic-inorganic nanocomposites
- 1.5.2. Organic-Inorganic dielectric solids
- 1.5.3. Organic-organic hybrid nanocomposites dielectrics
- 1.5.4. History of dielectric materials
- 1.5.5. Details of dielectric materials
- 1.5.6. Calcium copper titanate
- 1.5.7. Silica (SiO₂ NPs)
- 1.5.8. Amine functionalized SiO₂ NPs
- 1.5.9. Core-Shell Inorganic NPs
- 1.5.10. Graphene Oxide (GO)
- 1.5.11. GO Synthesis method
- 1.5.12. GO Functionalization

- 1.5.13. GO NPs Conjugation functionalization
- 1.6. Section II- Polymeric nanomaterials
- 1.6.1. History of polymeric materials
- 1.6.2. Effect of polymeric materials
- 1.6.3. Classification of polymeric Nanomaterials
- 1.6.4. Important chemical and physical properties of triblock copolymers
- 1.6.5. Challenges of block copolymer
- 1.6.6. Importance of block copolymer
- 1.6.7. Monomer blocks
- 1.6.8. MTT/ Biocompatibility Assay Test
- 1.6.9. Antibacterial Study

LITERATURE REVIEW

- 1.7. Literature Review for Organic-inorganic dielectrics
- 1.8. Literature Review for amino acid based polymeric nanomaterials
- 1.9. MOTIVATIONS
- 1.10. OBJECTIVES

CHAPTER-1

INTRODUCTION AND LITERATURE REVIEW

INTRODUCTION

The life has first started emerging on this earth from water, carbon with the energy from the Sun. Much more life formed starting from simple unicellular to complex multicellular organisms. The outcome of modernization is possible because of accurate development in the field of materials research available on this earth. The effective growth in science and technology comforts human need and become more effective with sustainable and green research with many applications.

1. Natural Science, Material Chemistry and Nanotechnology

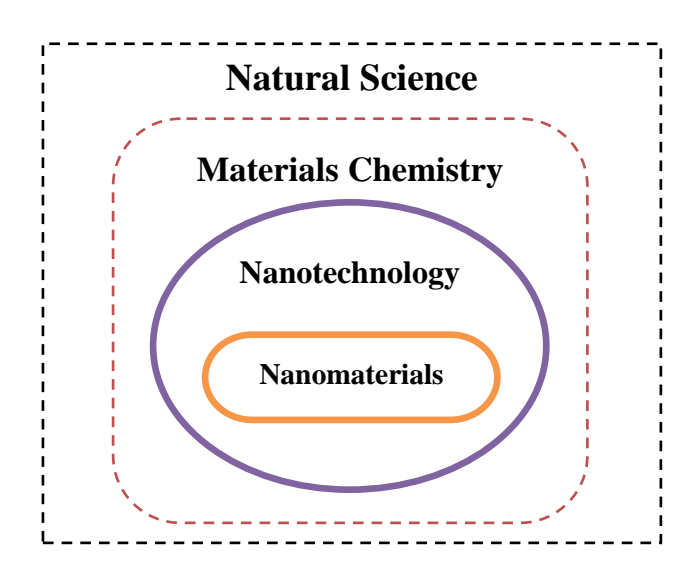


Figure 1.1. Schematic Classification of areas associated with the development of nanomaterials.

1.1. Natural Science

Natural science is associated with the understanding of natural phenomenon with the help of experiments and scientific proofs. The branches like Chemistry, Physics and Biology are very influential for the study of natural science leading to understanding. The journey from the ancient time to the modern world, Chemistry became a salient area of research which provides suitable solutions for mankind as well as flora and fauna. The study of chemical science is divided mainly into three categories i.e. physical, inorganic and organic

chemistry, respectively. History of chemistry was mainly focused on the study of chemical physics, inorganic and organic chemistry and prominent examples are common salt, Ayurvedic medicines consist of metallic components, organic polymers and natural steroids [1]. But contemporary physical chemistry research leads to various interdisciplinary research topics like green chemistry, environmental chemistry, materials science and nanotechnology. This dissertation is mainly focused on Nanotechnology and Nanomaterials. A schematic is depicted as **Fig 1.1.**

1.2. Material Chemistry

Among the above-mentioned topics, materials science and nanotechnology have impacted several aspects in the human development process with the elements of Physics, Chemistry, Biology and Mathematics. Ages like Bronze, Stone and Iron were excellent examples of metal ages which were prominently used by our ancestors in the very early stages of civilization process. But later to the end of the nineteenth century, the interdisciplinary materials science has developed significant roles among the researchers and attracted many pioneer scientists towards itself. This field includes an area of research like biomaterials [2], nanomaterials [3], polymers, magnetic materials, ceramics, metals and alloys [4-5]. With these very broad research fields, scientists from all over the world have made this field of research very effective and useful for the human being.

1.3. Nanotechnology

The existence of nanotechnology started from the date of the evolution of this earth, which later was discovered by scientists in the form of DNAs, RNAs, size of microorganism, metals and alloys and many more. Nanotechnology is an applied science which studies materials at the nanoscale. The word **nano** is used to define objects that are 10^{-9} m in size and materials belong to nanoscience and technology range from 1 to 100 nm in size. The American Physicist Richard Feynman is known to have predicted the various possibilities of nanoscience and technology in his famous lecture "**There's Plenty of Room at the Bottom**" at American Physical Society, Caltech on 29 Dec 1959 [6]. He even has suggested another term "**on the head of a pin**" which also opened a pathway for contemporary scientists to the world of interesting, obscure and unknown nanomaterials search at a very small level. The usage of nanotechnology and nanomaterials reached 1.6 trillion Dollar value as shown by a survey on the importance of the current technology [3].

1.4. Nanomaterials

Nanomaterials are the materials at its molecular level size in nanometer with unique behaviour which enable significant applications. These are categorised various manners according to their structures, size, morphology, physical and chemical properties, synthesis methods, dimensions etc. Structures like 0D, 1D, 2D and 3D nanomaterials are available in the literature, however, 3D nanomaterials are much optimized and useful than the other dimensions due to their extraordinary properties [7]. Nanomaterials possess all the dimensions such as micelles [8], metal nanoparticles [9], biomaterials [10], polymer-metallic vesicles [11, 12], and nanocomposites [13-15] are very popular. They can be synthesized by direct or modified top-down, bottom-up, sol-gel, hydrolysis, polymerization methods [16-19] and other nano chemical processes keeping other environmental parameters as a change [20]. The positive impacts of nanomaterials are like high stability, high carrier capacity, easy synthesis, good storage capacity, compatibility with animal cell lines. Nature has included the best examples of varying size of nanomaterials from decimal to hundredth value, as shown in

Fig 1.2.

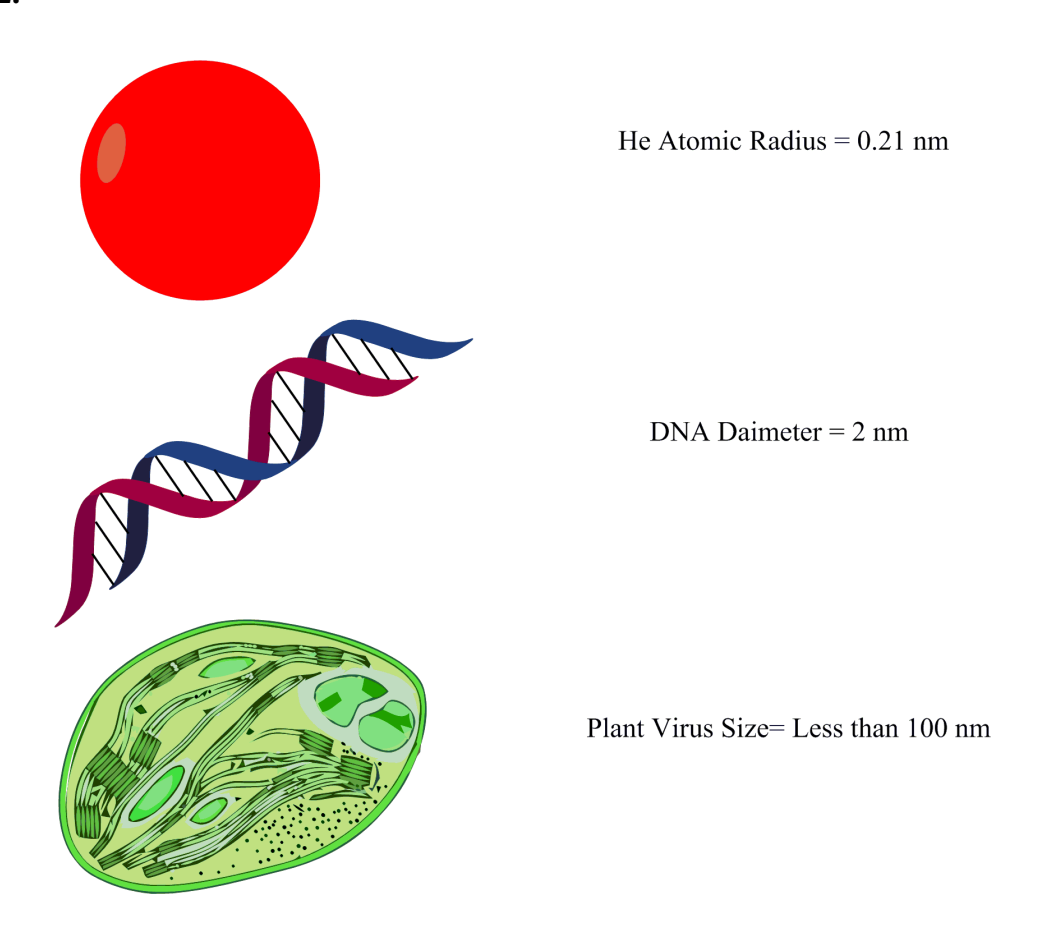


Figure 1.2. Showing the different sized nanomaterials [21].

1.4.1. Classification of Nanomaterials

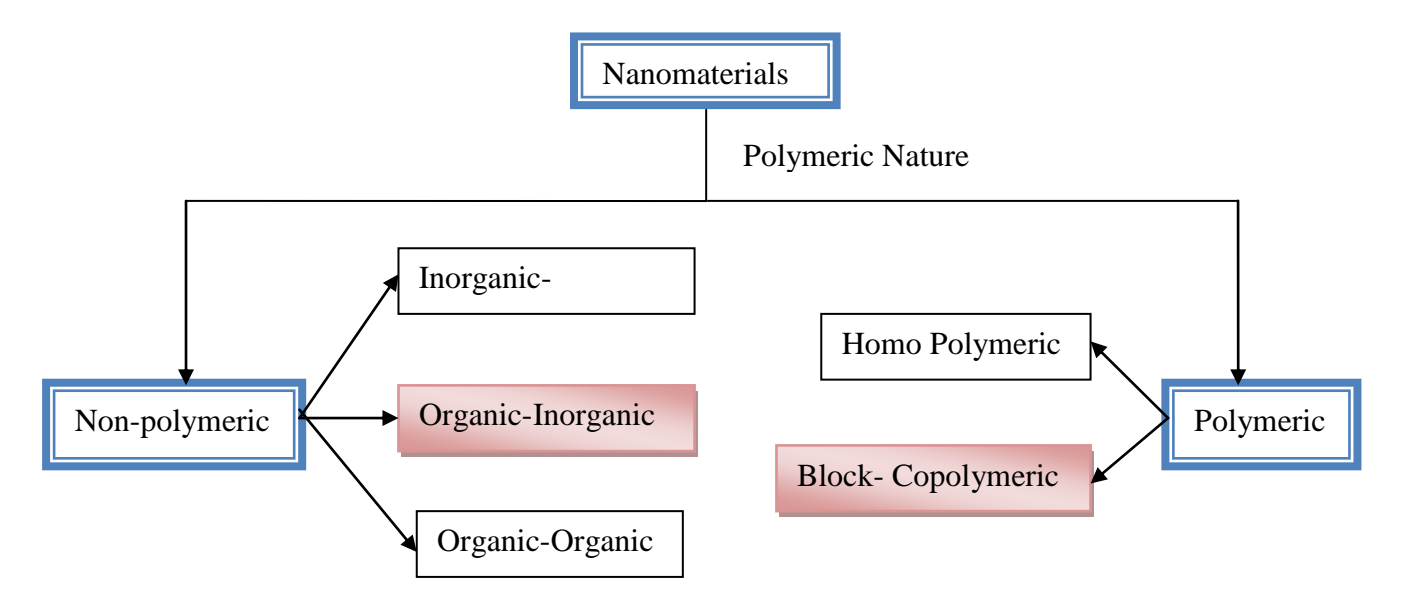


Figure 1.3. Types of classification of polymer based nanomaterials [22].

There are many factors available in literature based on which nanomaterials classification established [22]. This dissertation is mainly focused on the classification of viapolymeric nature. Based on the polymeric nature, the nanomaterials have been categorised into non-polymeric and polymeric nanomaterials, as shown in **Fig. 1.3**.

Non-polymeric nanomaterials are associated with the materials composed of organic and inorganic groups from the periodic table. Focusing on the chemical composition of the nanomaterials, it has been categorised into inorganic-inorganic, organic-inorganic and organic-organic non-polymeric nanomaterials. Many theories are available in the literature to classify the non-polymeric nanomaterials concentrating on their composition, structure, and nature. But in this dissertation, we will be mainly focusing on the development of organic-inorganic nanomaterials. The discussion is associated with the dielectric and impedance study, its scientific behaviour via-numerous characterization techniques along with elaborate applications. Such type of non-polymeric nanomaterials mostly come under ceramics or metal nanocomposites category. The presence of more than one solid phase with at least one phase dimension in the nanoscale range (50-100) nm is the basic synthetic principle of such nanocomposites. Physical methods like spray pyrolysis, vapour deposition methods and chemical methods like sol-gel, precipitations and reverse micro-emulsions are mostly used for preparations of such composites [23].

1.5. Section I - Dielectric Nanocomposites

Nanocomposites consist of more than one phase with the size in nanometer range of each phase. These are broadly classified into metal [24, 25], polymer matrix [26], ceramics [27], and magnetic matrix composites [28]. Recent research is mainly focused on their novel application in numerous areas of human civilization including health, medicine, medical apparatus, electronics and daily uses. To realize these requirements with less cost, time and effective results the study of nanocomposites came into play. The structural and compositional differences of composites have led their uses in different areas according to their behaviour. Ceramics matrix composites are used in the electronic device uses. Metal matrix composites based on single metal oxide, double metal oxides mostly used for drug delivery carrier. Polymer matrix composites are also very prominent in drug delivery study [29].

The best dielectric nanocomposites are made up of inorganic metal based materials like CCTO, BaTiO₃, PbTiO₃, PZT etc. due to their perovskite lattice positions and structures [30, 31]. Reports are available for such nanocomposites with a very wide direction of applications including insulator, filler, integral/thin-film capacitors and charge storage device. Important properties of such nanocomposites are good transparency due to nanosize, improved mechanical performance, large surface area, good adhesive nature and high aspect ratio [31].

1.5.1. Inorganic-inorganic nanocomposites

Elements other than C, H, N, O, S and P consist of inorganic materials which mostly include metals, non-metals, and metalloids in these classifications. The modified inorganic material at the nanoscale is otherwise called as inorganic hybrid nanomaterial with numerous physical and chemical properties for wide practical applications. The very suitable examples of these composites are based on BaTiO₃, CaTiO₃ and other perovskites like structure and mainly used for electrical and insulation purpose [32].

Historically, there are many man-made inorganic hybrid materials like bronze, brass while other alloys like silica-aluminium, silica- magnesium present in the earth's crust. The classification based on chemical composition, the nanomaterials are divided into inorganic-inorganic, organic-inorganic and organic-organic nonpolymeric nanomaterials [33, 34]. This dissertation is based on organic-inorganic nanomaterials, composed of organic and inorganic

groups brought together via electrostatic interaction along with other chemical bonding mechanisms. The dielectric constant possessed by such type of materials is very high in nature of the order of 10^5 - 10^6 . These composites possess very good optical, electronic, catalytic, magnetic properties compared to bulk inorganic composites.

1.5.2. Organic-Inorganic Dielectric Solids

The literature has revealed the study of metallo-organic nanocomposites e.g. Al-Propylene [35], Pt-NPG leaves [36-38], Au-PS [39], GO-MO [40], PolyVinylSulfonate-Co [41], PolyMethaMAcrylate-MnO₂-AgO [42, 43] for electro-catalysis, optical phenomenon, energy harvester, inverter, transistor, biosensing, dielectric and supercapacitor purposes. Organic compounds based metal oxide nanocomposite/nanomaterials have shown highest dielectric constant from 10¹-10² for pendant-type poly-(acetoxystyrene-co-isobutylstyrylpolyhedral oligomeric [44], poly(vinylidene fluoride)-barium titanate (PVDF-BaTiO₃) [45], Mixed-Metal Phenylphosphonates, ATi(C₆H₅PO₃)₃, A= Ca, Mg, Ba, Sr and Pb [46], PVDF- $BaTiO_3[47,$ 48], Silicotungstic Acid-H₃PO₄-Poly(vinyl alcohol) [49] dielectric nanocomposites. The contemporary material science research is growing with the development of this category of nanomaterials which show a moderate range of dielectric constant with low loss. The materials designed under this category are cost-effective, easy to synthesize and handle for better electrical application compared to the pure organic based dielectric materials.

1.5.3. Organic-organic hybrid nanocomposites Dielectrics

Nanomaterials associated with polymer-polymer or polymer-organic nanocomposites fall in this category with very low dielectric constant (ϵ ') and loss (ϵ ") less than 10^{-2} . Organic based material with different organic concentrations and polymer-modified layers used as a dielectric material is mostly used for the development of transparent and environmentally safe gate dielectric materials [50]. These are not effectively used for the electrical insulation properties due to the availability of more number of free conducting electrons in the polymeric structure influencing the current flow. Generally, such dielectric materials are used for electrical application purpose like coating on the surface of electrical wires.

1.5.4. History of Dielectric Materials

Since 1945, after the discovery of capacitors by Cunaeus and Mussachenbroek, the study of inorganic dielectrics has gained interest and become useful. Thereafter, dielectric research has been shown its significance and importance by many pioneer scientists. William Whewell first coined the term "**Dielectric**" (**Dia+Electric**) along with Michael Faraday (1836) [51]. The influence of an external electrical field on dielectrics materials is to causes the shifting of atomic nuclei towards the negative side and electrons towards the positive side resulting in several types of polarization [52].

1.5.4. Details of Dielectric Materials

1.5.4.1. Insulators

The material which does not allow the free flow of current through itself acts as an insulator upon application of the externally applied field. There is no perfect insulator except few materials like wood, paper, glass etc. [53], which duplicate its behaviour. The excitation of electrons from the valence band to the conduction band requires applied parameters like temperature and electric field due to the giant magnitude of the energy gap. The high energy gap is the main reason behind the insulators to act as a barrier to the current flow [54].

1.5.4.2. Dielectric Materials

A dielectric material is a type of electrical insulator e.g. silica having very low ε' , which stores electrical energy with the externally applied field [55]. The presence of dielectrics causes no flow of electric charges through the material, but only a little change in dipole position resulting in dipolar polarization [56, 57]. Piezoelectric ceramics, ferroelectric relaxor materials, magnetic polymer and perovskite like materials are mostly associated with a high value of dielectric constant [58]. On the application of a field, positive charges move toward the field and negative charges shift away from the field. Creation of another field inside dielectric material opposing the flowing external electric field is the main reason for observed dielectric behaviour [59-62].

1.5.4.3. Types of Dielectric Materials

1.5.4.3.1. Dielectric materials have been classified based on dielectric constant strength

- (i) Electrical dependence properties like dielectric constant, refractive index, tensile strength, electrical conductivity, low dissipation, low leakage current, low charge trapping property due to presence of an insulator, high electric-field strength, high reliability and chemical properties like chemical resistance, microfabrication of chemicals, low moisture uptake, low solubility in H_2O , low gas permeability, high purity, anticorrosion towards metals, long storage life and environmentally safe are required to be a very good low dielectric material. Including few other mechanical and thermal parameters like thickness uniformity, good adhesion, low stress, high hardness, crack resistance, high tensile modulus and high thermal stability with low coefficient of thermal expansion is also required to act very good low dielectrics [63]. Low dielectric constant materials which are composed of polymer and organic framework, possess $\varepsilon' < 4$ (SiO₂ = 3.9) and have less ability to polarize. Due to the less polarization caused by the material, they have less tendency to hold the charges. Being low dielectric constant materials like SiO₂, Air, Polyethylene, Polypropylene, Polystyrene and Perylene, they are mostly used for the insulating purpose at higher frequencies [64].
- (ii) High dielectric constant materials have high ϵ' with numerous applications discussed in the later section of the dissertation. Si₃N₄ is a primary high dielectric strength material and the materials possessing $\epsilon' > 7$ are generally considered as good dielectric strength materials [64]. Alumina possesses high surface area, highly porous material with a dielectric constant >10⁸ and it is evident that this class of material with dielectric constants greater than 10⁵ at low frequency also. Applications like storage devices, adhesion layers, coatings of nanoporous materials, photoelectron chemical cells, protective coatings, electroluminescence and microwave electronics are associated with high dielectric strength materials [65].

1.5.4.3.2. Dielectric Materials have been classified based on Polarity

- (i) Polar dielectrics are mainly possessed of permanent dipole moment due to the dipolar molecules associated with the material. The asymmetrically shaped molecules like HCl, NH₃ and H₂O mostly fall in this category with intrinsic permanent dipole moment [66].
- (ii) Nonpolar dielectrics are of symmetrical shape with no dipole moment. Here the charges cancel each other resulting, μ =0. The best examples of nonpolar dielectrics are C_6H_6 , CH_4 etc. [67].

1.5.4.4. Terms Associated with Dielectric Study

1.5.4.4.1. Dielectric Constant

It is a parameter to calculate the electrical energy storage in a material [68]. Mathematically, it can be defined as the ratio between the permittivity of medium and free space.

$$k = \frac{\varepsilon'}{\varepsilon_{\circ}} \tag{1}$$

Where,

k = Dielectric Constant

 $\varepsilon'_{=}$ real permittivity of the material

 ε_{o} = permittivity of free space

If the dielectric constant value is high then there will be more chances of charge storage in the material.

The relation between capacitance and dielectric permittivity is

$$C = \frac{\varepsilon'\varepsilon_{\circ}A}{d}$$
 (2)

Where,

C= Capacitance of dielectric material

A = Area of the electrodes

d = Thickness of material

1.5.4.4.2. Dielectric Loss

The dissipated energy produced due to the charge motion in an alternating filed medium is a dielectric loss. The phenomenon mainly occurs due to the polarization mechanism involved in the material depending on the force applied on the system and the resonance associated with the various transitions like electronic, rotational and vibrational transitions [69]. It is measured as Loss tangent ($\tan \delta$).

Mathematically,

$$Tan \delta = \frac{\varepsilon''}{\varepsilon'}$$
(3)

Where,

 ε' = real permittivity of material

 ε'' = permittivity of free space

 δ = Tangent

1.5.4.4.3. Breakdown Voltage

Dielectric strength, which is also known as breakdown voltage is a very important property of a dielectric material. The mechanism behind the breakdown associated with the dielectric material is due to the sudden excitation of more number of electrons from the valence band to the conduction band with the effect of the external electric field. The sudden change in current flow causes few phenomena like melting, burning and vaporizations which led to degradation and failure of the material. The magnitude of the electric field required for the breakdown of dielectric material is known as dielectric strength. Generally, it is hypothesized that the strength is related to the dielectric constant of a material.

1.5.4.5 Polarizations involved in Dielectric medium

Dielectric materials possess various polarizations caused dielectrics with respect to frequency and temperature dependence.

The relation between flux density and dielectric gradients can be represented,

$$D = \mathcal{E}_r \, \mathcal{E}_i \, E$$
(4)

Where, D= Electric Flux density

 $\mathcal{E}_r / \mathcal{E}'_=$ real part of dielectrics/ permittivity of free space

 $\mathcal{E}_{i}/\mathcal{E}''=$ imaginary part of dielectrics/ relative permittivity of material

E=applied electric field

There are four types of polarization processes involved including electronic polarization (P_e), ionic polarization (P_i), orientation/dipolar polarization (P_d) and space charge polarization (P_s) [70]. These four polarizations are the important backbone of dielectrics behaviour (**Fig. 1.4.**) [71].

$$P(t) = P\left[1 - exp(-\frac{t}{t_r})\right]$$
(5)

Where,

P(t) = Polarization as a function of time

P = Maximum Polarization

 $t_r = Relaxation time$

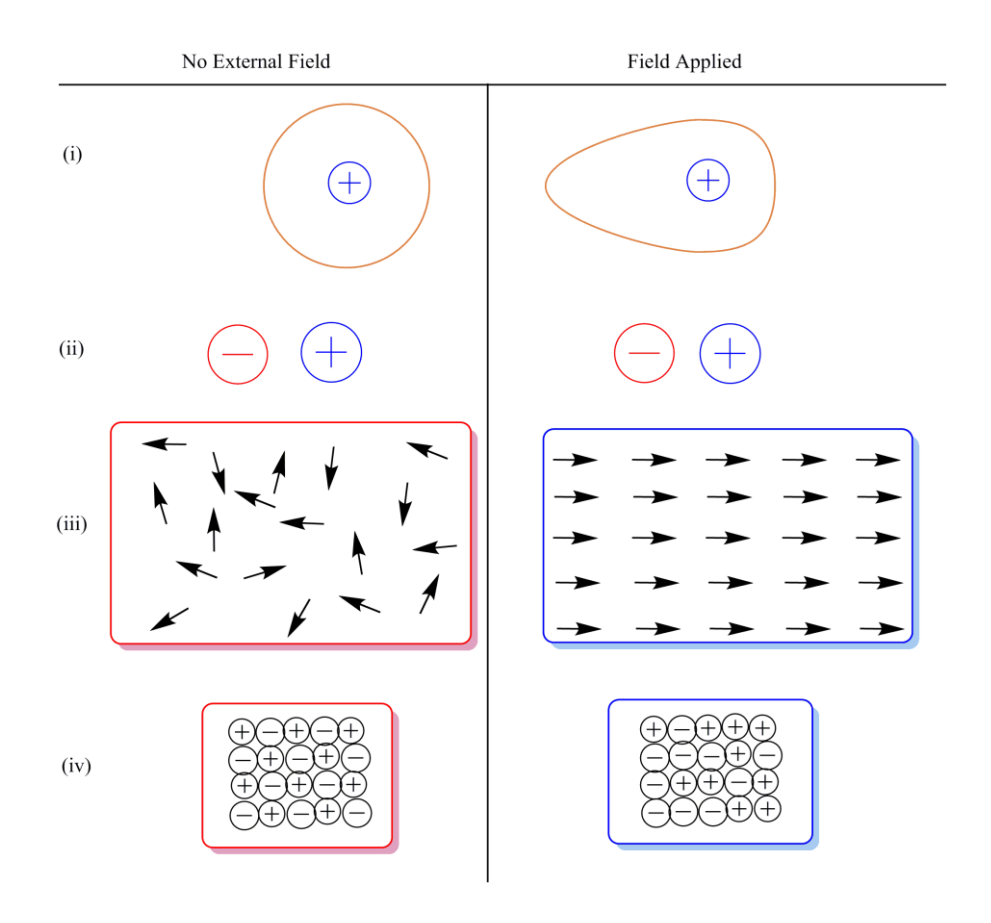


Figure 1.4. Represent the different Polarization Mechanisms (i) Electronic polarization (Pe) (ii) Ionic polarization (Pi) (iii) Orientation/dipolar polarization (Pd) and (iv) Space charge polarization (Ps), respectively [70].

The prime factor for the generation of polarization is the structural and atomic rearrangement inside the material and solution during the synthesis parameters [72, 73]. The

temperature and frequency parameters are associated with polarization processes. Under an applied field, the relation between the function of time and polarization is depicted as in **Fig. 1.4.**

The shifting of the positive nucleus and negative electrons in opposite directions to each other under application of an external electric flow is the reason for electronic polarization. This polarization helps in the displacement of the electron cloud to the positive end of the applied field. The formation of ionic bonds by acquiring the excess of ions under the application of electric field cause a shift of ions relative to the oppositely charged neighbours and is the main cause of ionic polarization in dielectrics. Both the electronic and ionic polarizations are independent of temperature. The dipolar polarizations are mainly caused by the presence of permanent dipoles which tend to flow in the direction of the applied field and dependent on temperature. Mostly this type of polarization occurs in the low frequency region due to the relaxation processes. Lastly, the space charge polarization occurs due to the gathering of charges or ions at the interfaces in phases of dielectric materials [74, 751.

Electronic polarization occurs very fast in the optical range of frequency 10^{15} Hz, whereas ionic, dipolar and space charge polarization found to be placed in the infrared range $(10^{13}$ Hz), audio range and 10^2 Hz respectively. Frequency increment has a direct impact on polarization with an increase in frequency, space, orientation and ionic polarization become ineffective in order [64].

Mathematically it is represented as,

$$P_{total} = P_e + P_i + P_d + P_s$$
(6)

1.5.4.6. Major challenges of Dielectric Organic-Inorganic Hybrid Materials

Dielectric breakdowns are the most disadvantage features for dielectric material. Since 1745, scientists are trying to develop the best dielectric material as a charge storage device along with high capacitance property [76]. The breakdowns like electric, intrinsic, thermal and defective breakdowns are caused by excessive charge displacement by increased field strength, excitation of electrons by excess voltage, over dissipated heat and presence of pores and cracks on the dielectric material surface respectively [77, 78]. Current research is mainly focused on to avoid such type of irregular breakdown using high dielectric constant and low loss dielectric materials. This dissertation has also led to the synthesis of two

different types of dielectrics with high dielectric constant and low loss compared to previously reported work.

The challenges of organic-inorganic dielectrics are breakdowns caused due to different environmental factors, high loss, hard synthesis procedure at high temperature >1000°C, high sintering temperature, the formation of cracks and pores due to thermal, electrical breakdowns in the interface and not suitable for biomedical application. But the extensive and significant reasons of such dielectrics like possibility of high real part dielectrics [35], easy attachment of inorganic and organic groups [42, 48], minimum toxicity [79] with the presence of essential metal groups [80], probability of high energy storage density of CCTO [25, 81-82], low loss, good thermal stability at 1000°C, can be used in capacitors, microelectronic devices [57, 60] made our motivations to work on it.

1.5.5. Calcium copper titanate

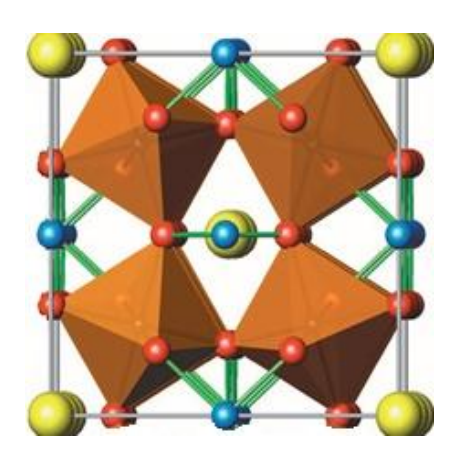


Figure 1.5. CaCu₃Ti₄O₁₂, shown as TiO₆ octahedral, Cu atoms (blue) bonded to four oxygen atoms (red), and large Ca atoms (yellow) without bonds [75].

Till date, Calcium copper titanate (CaCu₃Ti₄O₁₂) has been reported one of the most eligible and best dielectrics for applications required high dielectric constant and low loss. Being a perovskite and body centred cubic (BCC) type structured material (**Fig. 1.5.**) it possessed dielectric constant up to 10⁶ and 10⁴ in crystal and bulk medium respectively with a very low loss [78-81]. The elemental composition of Ca, Cu, Ti and O make the composite toxic-free and stable at room temperature (RT). Hence for this dissertation work, we have targeted the development of new dielectric material with CCTO NPs as a base material. The important factors like chemical functionalization on the surface, the microstructure of composite and nano or microparticles of CCTO strongly control the dielectric property as

well as impedance properties of the nanocomposites. This study has targeted for the development of this core-shell material as a better dielectric than few other lanthanide series perovskite materials such as ACu₃M₄O₁₂ (where, A= Ca, M=La, Nd, Sm, Gd and Y) at 100K Hz [82]. Previously it is elucidated about perovskite oxides as excellent dielectrics material. This reason attracted us to focus CCTO as a base material for the development of this dielectric material [83].

1.5.6. Silica (SiO₂) NPs

The previous study has proved silica as a smart material and is one of the best inorganic filler with less dielectric behaviour. SiO_2 has $\epsilon'<10$ and very useful for insulating application [84]. SiO_2 is considered as a shell material due to factors like eligibility of forming uniform shell thickness, amorphous nature, absence of organic functional group, less chance of groups lost after sintering at high temperature, high optical transparency, low toxicity, inert to all pH medium, easy functionalization [85] with organic life making groups, broad range of accessible sizes form 5 nm-2000 nm, low dielectric loss due to change of charge polarization and dipole moment due to presence of various polar groups, we consider SiO_2 as a shell material [86-88]. It is also proved that silica can entrap fluorescent dyes for applicative purpose easily without any structural changes (**Fig. 1.6.**). Its excellent morphology, inorganic filler property and enhanced chemical functional group incorporations influenced its positive action for the dielectric study.

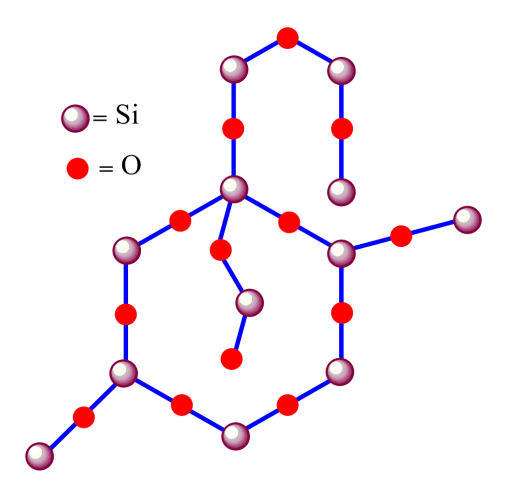


Figure 1.6. Shows the structure of SiO_2 (silica), shown as, Si atoms (blue) bonded to two oxygen atoms (red) [85].

1.5.7. Amine functionalized SiO₂ NPs

Few functionalizations of organic/inorganic groups on CCTO have been reported previously [89], but no research has been done with amine functionalization of silica on CCTO yet. We aimed for a unique modification of amine coated silica on CCTO NPs (shown in Fig.1.7.) and found to be effective for dielectric study. Herein, we have functionalized silica with an amine by using (3-Aminopropyl) triethoxysilane (ATPS) with tetraethyl orthosilicate (TEOS) for the better core-shell interaction to generate the required shell thickness along with covalent [90, 91] interaction and synthesized by the modified Stober method. There is no literature available with amine functionalized metal or non-metal embedded on organic or inorganic base precursors. This dissertation will have a detail explanation and analysis for such materials in the **chapter-3** sections. Typical functionalization of silica with organic amine is shown in schematically in **Fig. 1.7**.

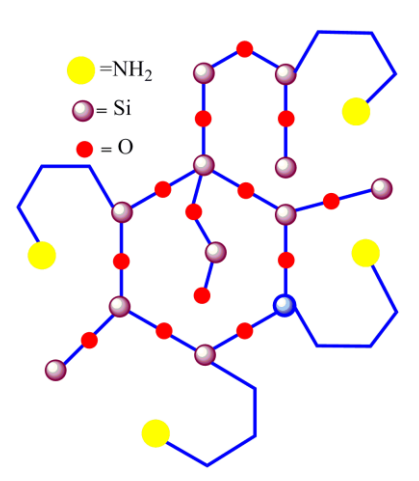


Figure 1.7. Shows the functionalization of –NH₂ with SiO₂ (silica), shown as, Si atoms (blue) bonded to two oxygen atoms (red) and one organic amine (NH₂) group (yellow) [87].

1.5.8. Core-Shell Inorganic Nanoparticles

The nanoparticles prepared with an inorganic core and one or more inorganic shell layer is defined as core-shell based inorganic nanomaterials. The applications of inorganic core-shell NPs are found to be very useful in many fields including Biology, Chemistry, Physics and Engineering in the recent development of science age [92-94]. The surface functionalization chemistry of shell on the surface of core remained a great hope for many suitable applications in the field of current technology.

1.5.9. Graphene Oxide (GO)

Ali *et al.* [98] and Cheon *et al.* [99] have mentioned about the multiple emulsion templating route and chemo-photothermal therapy of GO. The chemical functionality of GO made our target to a new pathway for the development of noble dielectric material. In addition to other applications, GO plays an important role in making optoelectronic device, fuel cells, supercapacitors, lithium ion batteries and biocomposites to various applications such as drug delivery, tissue engineering purposes.

In this study, GO (Fig.1.8.) is chosen instead of graphene due to the availability of less number of electrons (presence of lesser double bonds) which is also a suitable non-/semi-conducting material and is useful as good storage material. These are the factors for which, we have focused on GO as substitute dielectric component which is further synthesized viamodified sol-gel method leading to the development of nanocomposites. The functionalization of GO is shown in **Fig. 1.8.**

Figure 1.8. Chemical Structure and arrangement of functional groups in Graphene Oxide sheet [93].

1.5.10. GO NPs Synthesis Methods

The Graphene oxide based materials seemed to have many advantages which we have discussed in the previous paragraph. The most used Hummers method has been used for the development of GO NPs from Graphite flakes being reduced in acidic medium. There are also many reports are associated with the development of GO NPs. Daniela *et al.* [100] in the year 2010, have developed GO excluding the NaNO₃. The higher amount of hydrophilic oxidized graphene material has been obtained compared to Hummers method with the increased concentration of KMnO₄ [100]. In a few other reports, graphene sheets have shown

its outstanding thermal, mechanical, and electrical properties, incorporating its one property material with its structural property enhancements. Such sheets are being used as electrically conducting polymers and inks and ultracapacitors [101, 102].

1.5.11. GO Functionalization

The functional approach of organic and inorganic based groups on any type of matrix has shown its excellent significance towards many directions of scientific applications. The oxidized GO shows significant properties including high mechanical strength, adsorbent nature, optical transparency, easy surface functionalization of organic groups present on the surface of GO and association of both nucleophilic and nucleophobic functional groups which make itself much useful in the fields ranging from medicine to solar cells [103]. To solve the insoluble property, functionalization methods were followed. The chemically modified GO functionalizations also have shown its great efficiency in its mechanical, chemical thermal behaviour.

The GO modification with tris-hydroxymethyl)aminomethane (TRIS) and PVA matrix has shown a very strong interaction of covalent amine and amide bond with epoxy and carboxylic acid groups on the basal plane and edge of GO nanosheets [104]. Even GO has been functionalized with hexamethylene diisocyanate (HDI) with a lot of optimizations. The hydrophobic behaviour of HDI-GO sheets seemed to have higher tin nature than unspoilt GO. To check the suspension property, HDI-GO were allowed to disperse in few polar aprotic solvents like N,N-dimethylformamide (DMF), N-methylpyrrolidone (NMP) and dimethyl sulfoxide (DMSO) along with non-polar solvents such as tetrahydrofuran (THF), chloroform (CHCl₃) and toluene (C₆H₅CH₃). The modified GO sheets left an impression of being a suitable candidate as nanofillers for high-performance GO-based polymer nanocomposites [105].

1.5.12. GO NPs Conjugation Functionalization

The tuning of GO NPs and its conjugation effect with polymers or other inorganic particles have been reported [106]. The strategy of fabrication of functional 3D nitrogen-doped graphene aerogel and spinel oxides composite materials acts as a very good as electrocatalysts for the application in batteries [107]. The in-situ reprecipitation poly(3-hexylthiophene) (P₃HT) NPs with GO exhibited exciton coupling constants and indicated favourable charge separation due to π - π interface interactions between the P₃HT NPs and GO

sheets.GO open new pathways for the fabrication of improved optoelectronic thin-film devices [108, 109]

1.6. Section II-Block copolymeric Nanomaterials

After metal ages from ancient time, contemporary society is known as polymer age. The urbanization is solely dependent on smart materials like polymers. The molecular approaches and maximum performance phenomenon of organic polymers are quite interesting for which they are otherwise known as smart and intelligent materials [110, 111]. The identification and use of amino acid based polymeric nanomaterials have gained popularity due to the longevity, biocompatibility and cost-effective nature [112, 113]. The polymeric nanomaterials seem to be useful as drug conjugates, nanocarriers, biomedical equipment and anti-disease ailments, as shown in **Fig. 1.9.**

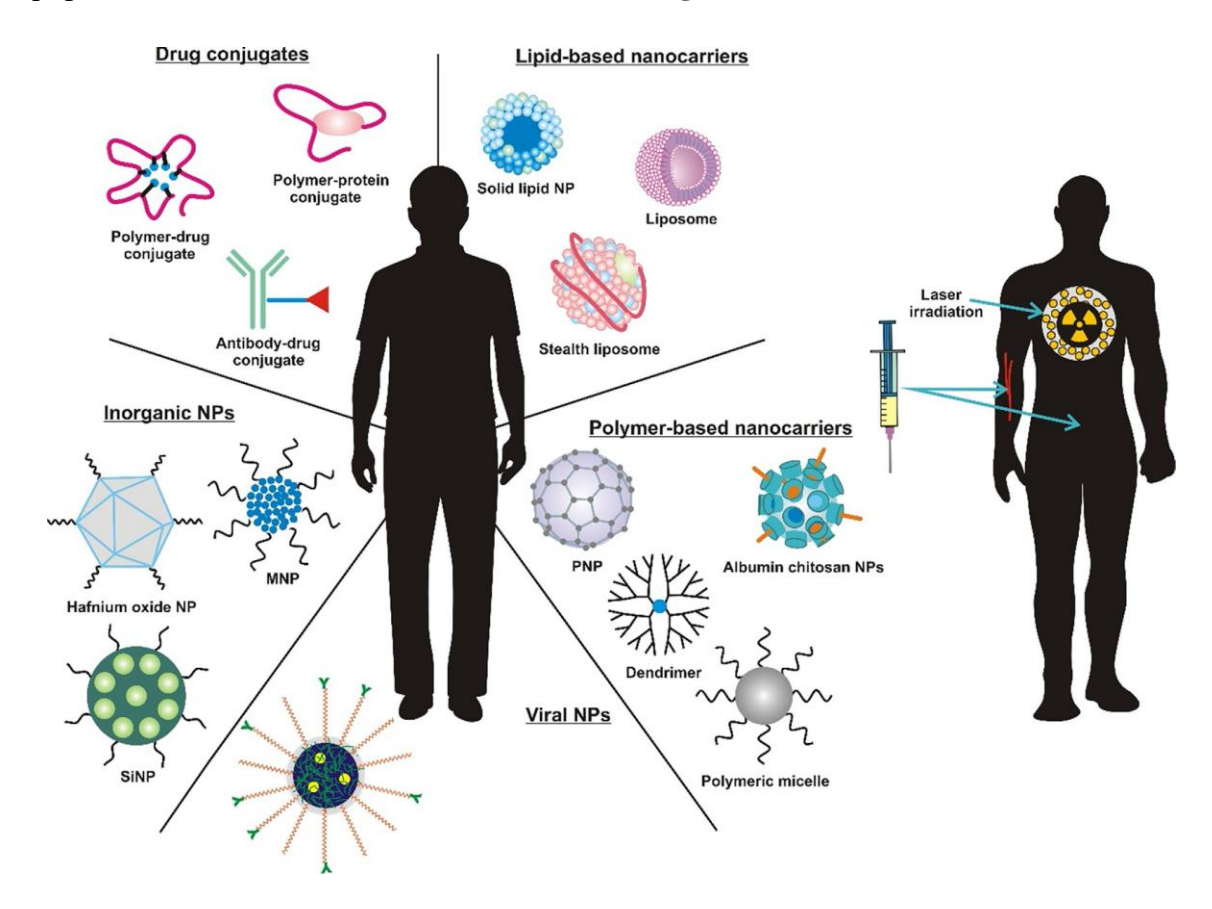


Figure 1.9. Schematic shows the different polymer-based materials and a wide range of usage [17]

1.6.1. History of Polymeric Materials

In this modern time, humans require polymeric materials for their essential need everywhere to their presence naturally. Natural polymers like proteins, carbohydrates, lipids, and nucleic acids are mainly found in all living things. Further, the scientists modified them and used enormously. Herman Francis Mark, Austrian American (1895-1992) chemist is known as the father of polymer science [114], even though he is not the first person associated with the polymer. Before his research, many pioneer scientists like Henri Braconnot (1777), Christian Schonbein (1846) have opened a pathway for polymer science in the use of human need [115]. Polymer word was given by a Swedish chemist, Jons Jakob Berzelius in 1833 [116]. The journey of the synthetic polymer was started nearly around 250 years ago. But after 176 years of polymer research by prominent scientists, in the year 1953, Hermann Staudinger [117] who is also known as the father of polymer chemistry was awarded the Nobel Prize for the first time in the polymer research area for the explanation of bonding association in the polymer [118]. Starting from 1777 to 2019 the research and development of polymer are still going on and progressing rapidly [119-121].

1.6.2. Effect of Polymeric Materials in the current situation

We can not live our life without using a polymer. From cell phone to aircraft, plastic bags to the home decorator, everywhere you look around where you are now, any corner in the World you can see the use of polymer. We can't think of a better and easy World. Synthetic polymers like nylon, polyethylene, polyester, Teflon etc. have become a human necessity. Nowadays the use of polymeric nanomaterials have been increasing more due to cost-effective nature, self-assembled nature, temperature and pH responsive behaviour, nano sized drug carrier, biocompatible, sustainable synthesis procedure, pure form of samples and for other biomedical applications including antibacterial susceptibility. Polymeric nanomaterials are very easy to clean and sterilize for which the medical persons prefer to use to reduce infections in the hospital as well as outside premises. It has increased hopes for a better and healthy World.

1.6.3. Classification of Polymeric Nanomaterials

1.6.3.1. Classification by Monomer and Building blocks

Polymeric nanomaterials are the nanosized materials whose building block is a **mer**. Based on structure, polymeric particles are classified into homopolymer and copolymer [117,

122]. Homopolymers consist of similar block throughout the long chain whereas copolymer may consist of two or more than that in the polymeric chain. Recent research has targeted the drug delivery application via polymeric nanomaterials to the animal cell line based on their chemical and physical properties. These polymers are classified into diblock, triblock, tetrablock, pentablock copolymer and so on based on block attachment of different monomers. But current research is mainly focused on the synthesis of tri and tetrablock copolymers.

This dissertation is partially based on triblock copolymers. The polymer which consists of two or three different monomers via covalent linkage in a block like strategy is called tri-block copolymer. They are mostly amphiphilic. The arrangement of blocks is found in ABC, ABA, BAB and ACB types [115].

1.6.3.2. Classification by Origin

Polymeric particles are divided into synthetic organic, semi synthetic, inorganic and natural bio polymers. Modern polymer technology is mainly dependent on semi synthetic and synthetic polymers [123]. Synthetic organic polymers are polymers which consist of essential elements like C, H, N, O, S and P where Carbon acts as long chain backbone of the polymer. They include fibres, paints, plastics etc. and mostly derived from flora, fauna and microorganisms. Synthetic Inorganic polymers are polymers which consist of chains of elements belong to the group 13, 14, 15 and 16 elements along with few transition metals. Natural silicates, polymeric chain of Si, P, Ge, Sn and S come under this type of polymers. Natural polymers are the most vital part of polymer science which consists of DNAs, RNAs, Proteins, Carbohydrates, Peptides, Amino Acids, natural rubbers etc. Semi synthetic polymers are the modified form of natural polymers which includes cellulose nitrates and acetates.

There are twenty essential amino acids which are biocompatible with nature. Choosing the effective and useful amino acids is a not a very tough job but the attachment of these amino acids with various types of metal, organic and inorganic network, block copolymers and even with other amino acid is a tricky job. The presence of chemical groups in amino acid has helped us for the synthesis of artificial peptide bond which is otherwise called as proteins.

1.6.3.3. Classification by Structure

Polymers are again classified based on their structure to linear, branched and cross-linked polymers [124]. Linear polymers possess a high degree of unsymmetry and density which includes polymers like polyethylene, PVC, Polyesters, Nylons etc. Branched chain polymers are low dense polymers including-glycogen, starch. Cross-linked polymers are 3D network type polymer formed from linear polymers. Bakelite is an example of cross-linked polymers.

1.6.3.4. Classification by Polymerization Method

Polymerization is divided into additional and condensational polymers based on synthesis [115, 125]. Additional polymers do not produce any byproducts whereas condensational polymer mainly produces byproducts like CO₂, H₂O etc. Common examples of additional polymers are polystyrenes, polyacrylates, BuNa-S, Teflon etc. whereas condensation polymers are cellulose, polypeptide chains etc. [117].

1.6.3.5. Classification by Tacticity

Tacticity refers to the arrangement of atoms or molecule in a long chain format. According to tacticity, polymers are classified as isotactic, synditactic and atactic polymers. Isotactic polymers are defined as polymers which have similar d-, l- arrangement of atoms, whereas synditactic polymers have alternate d-, l- arrangement but atactic polymer is having random d-, l- arrangements [126].

1.6.3.6. Classification based on Self-assembly Structure

Self-assembly is the rapid and reversible organization of molecules via noncovalent bonding. There are three distinct features help in self-assembly process order, interactions and building blocks [7, 117]. Polymers mostly follow the building block path as these are made up from monomer blocks. This property looks important for phenomenons like synthesis, functional properties and biomedical applications. The polymer structures are classified into dendrimers, liposomes and micelles as shown schematically in **Fig. 1.10**. Dendritic polymers are tree like in structure and growth. They are three dimensional and regular branches in nature. Liposomes are normally bigger compared to micelles. Liposomes are synthesized by bi-layer lipids with hydrophobic chains where micelles are monolayer which consists of hydrophobic cores.

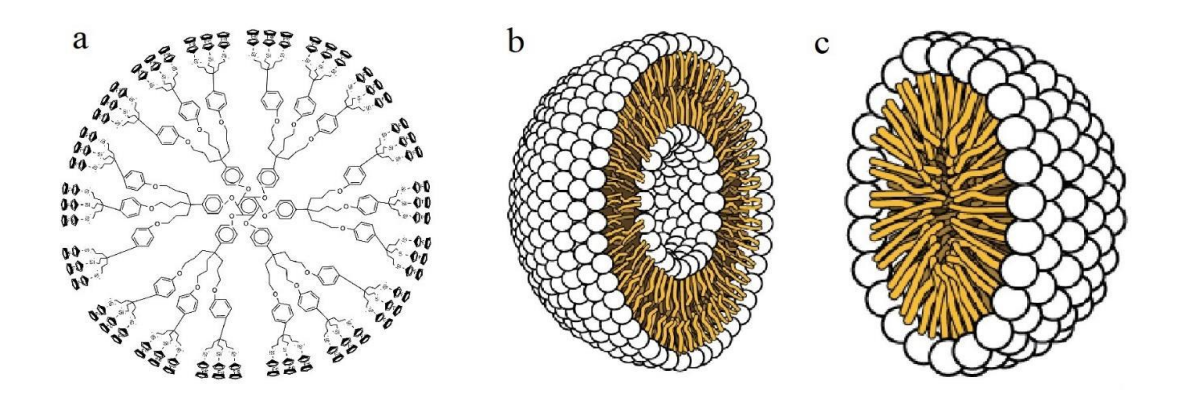


Figure 1.10. Polymeric nanostructures: (a) Dendrimers, (b) Liposomes and (c) micelles [7].

1.6.4. Important Physical and Chemical Properties of Triblock Copolymers

Two or three different types of blocks attached via covalent bonding are known to form as triblock copolymers. There may be a repetition of block copolymers (BCPs) occurred during the formation of a large segment of a block copolymer. Generally, these polymers are formed with the attachment of the type head to tail, whereas other variations like head-head and tail-tail are also possible.

Physical Properties of Triblock Copolymer

The properties of polymer which can be determined without changing the skeletal backbone or composition are known as physical properties. Solubility, viscosity, density, crystallinity are the main properties studied under the physical category. The complete physical properties study of the triblock copolymer has not been established for a general trend due to the variety of structures [127]. Due to heavy mass with a large segment of monomer, the triblock copolymers are not completely soluble in water irrespective of the presence of the hydrophilic group. Triblock copolymers are highly tensile, which support the mechanical strength for many applications. The melting point of these block copolymers normally falls under high range revealed from the TGA data. Usually, the monomeric unit of block copolymers for bioapplications is amino acids. The acidity (pKa) of block copolymer depends upon the amino-acids structure. If the amino acid contains more acidic (carboxylic acid) group then the corresponding block copolymer will be acidic and if the amino acid is basic then the corresponding block copolymer will be basic. For amphiphilic amino acids, the block copolymer is neutral with regards to acidity.

(i) The solubility of Triblock Copolymer

Most of the polymers are less soluble in a particular solvent due to the coiled and entangled structure along with the high molecular weight. Those polymers which dissolve in a solvent have greater solvent-solute interaction over solute-solute and solvent-solvent. The polymers are generally solubilised through the process of swelling in which solvent molecule penetrate the space between the polymer chain [127]. Polar polymers are usually soluble in polar solvents and non-polar polymers are solubilised in a nonpolar solvent. The polymers having linear sigma polar linkage like -O-, -S- are more soluble than the polymers having rigid pi linkage like -C=C-, -N=N- due to the flexible nature of polymer [128]. The low solubility of polymers is mainly due to the high secondary interactions present between polymers.

(ii) The viscosity of Triblock Copolymer

The resistance to flow under external conditions like temperature, force, the pressure is known as viscosity. The polymers with the flexible structure are less viscous than the polymer having rigid structures. As most of the polymers have coiled or entangled structure, so the viscosity increases with the increase in molecular weight. Also more cross-linked or branched polymers show high viscosity [128].

(iii) The density of Triblock Copolymer

The polymers normally have low density than other material for which these are widely used for various applications. Polymers having heavy elements like heavy metals, bromine or metalloids show high density [128].

(iv) The crystallinity of Triblock Copolymer

Most of the polymers are amorphous due to long chain length, coiled and entangled structure. Only those polymers show crystallinity for which the molecular arrangement is long range order in nature. Those polymers tend to crystalize which have simple and highly regular structural units [125]. This property of polymers is known as crystallizability. The rate of crystallization is very slow in case of polymers due to its coiled structure with high molecular weight. The study of polymers based on its physical properties is very useful for the application with the toughness, stiff behaviour, elasticity and viscous properties in many areas of polymer science.

Chemical Properties of Triblock Copolymer

The tendency of a material to react chemically with another material through chemical bonding is named as chemical properties and the process is called chemical process. In this process the composition of material changes from one form to another. This tendency arises due to the reactive functionality like -NH₂, -OH, -COOH, -CHO, -CONH₂, -X (Halogen or any good leaving group), -COX (X= electronegative element or group) etc. present in the polymer [128, 129]. In solid-state or concentration solution at ambient temperature, the linear polymers react slowly due to the availability of less number of functional groups for reaction whereas branched polymers react faster due to availability of more reactive centre. With an increase in temperature, the rate of reactivity increases for most of the polymers.

The number of monomer units present in a polymer is called as **degree of polymerization** and mathematically it is expressed as,

Degree of Polymerization (p) =
$$\frac{\{\text{Molar Mass of Polymer (M)}\}}{\{\text{Molar mass of Monomer (m)}\}}$$
 (7)

Calculation of Molecular weight of Polymers

There are different methods available in the literature by which the molecular weights of polymers can be determined. The most used equations are based on the molar mass of polymers as seen from equation (8)-(11) including number average, mass average, Z-average and V-average molar masses, respectively.

1.6.5. Challenges associated with Block Copolymer

There is a saying "every coin has two sides". The same principle rules to the application and use of synthetic polymers. If we-see the disadvantaged part it has many like improper degradation, increased risk of global warming, emission of toxic fumes, people do not prefer to stay nearby polymer industry for increased risk of diseases. According to a Slate article 2007, scientists estimated that a single plastic bag could take as much as 500 years to break down. Forty-four percentages of seabird species are known to have ingested synthetic polymers that have been mistaken for food, with millions dying from this indigestion every year reported in a survey of U.S. National Institutes of Health. If we do not control the pollution caused by the toxic chemicals then, maybe the term "a rapidly increasing, long-term threat." given by NIH, US, will be seen true and will not able to wipe the tear of this globe (see Fig. 1.11.).



Figure 1.11. Schematic representation of recently used polymers, its side effects and armour to save the globe.

The Challenges of this dissertation was to overcome the non degradation, cytotoxicity [2, 4-8], side effects, less drug loading efficiency [10, 11] and biocompatible [118-120] issue of block copolymer which can lower environmental pollution risk and can be used in various domains of chemistry and biology. The factors like the availability of naturally occurring polymeric proteins sufficiency, possibility of biocompatible nature, biodegradation in animal cell line, smart material, less side effects with essential amino acid, highly stable colloid, self-assembled in nature, temperature and pH responsive, antibacterial resistive [118] in nature have made us to focus to develop artificial proteins along with various amino acids. There are

twenty essential amino acids which are biocompatible with nature. The presence of chemical groups in amino acid helps us for the synthesis of the peptide bond and produces long-chain proteins. Many studies have fulfilled the target of biodegradability of few block copolymers and proved a lot of application in the biomedical domain. In this dissertation, we have shown the cost-effective and smart polymer, which is affordable and available for everyone's use.

1.6.6. Importance of Block Copolymer in wide areas

(i) Thermoplastic Elastomers as Primary Block Polymer

The current world needs advance technology with low cost, durability and low MW. The first thermoplastic polymer was synthesized by Menon *et al.* [8] from urathanes via two step condensation polymerization. Following at his work, Legge *et al.* have developed a noble TPE, commercially called Kraton in 1965. Later to these TPEs, polyester and polyamides were synthesized for better access to society [8, 11, 42].

(ii) Self-assembly behaviour of the Copolymer in selective Solvents

The self-assembly property of block copolymers can be determined by using a solvent. The soluble organic groups become soluble whereas the insoluble part remained separated in the solvent [111]. Based on the micellar theory, the insoluble part forms core while the soluble part acts as a shell in the solution. This property is very suitable for encapsulation and drug delivery applications [112, 113].

(iii) Block Polymer usage in Biomedical Applications

The self-assembly nature, biocompatibility, numerous functional groups attached to the backbone, economical, low density, easy chemical interactions, interesting morphology in a medium and easy degradation theory help block copolymer to be effectively used for biomedical applications [26].

(iv) Drug delivery and DNA effect of Block Copolymer

The importance of functional groups helps the polymer to change its morphology in the medium. Due to different morphological features like micelles, vesicles, dendrimers, nanogels and liposomes [8], these are quite easy to implicate as good drug carrier [29, 113]. In spite of a large number of chemotherapeutics and powerful drugs, the current research is focusing on the smart material of amino acid based block copolymers.

(v) Block Polymer as Anticancer and Antibacterial agent

The variant functional properties of amino acid based block copolymers help the inhibition of cancer and bacterial growth. Even the presence of a very low concentration of polymeric samples, the probability of inhibition of infected cells is more due to the dissociation of COO and NH₄⁺ ions and formation of ammonium salt in the medium at different stimuli condition [126]. The stimulus responsive segments have notable factors of smart functional groups, self-assembly nature, stimuli active property caused the resistance of cancer and other microbes. In spite of more antibiotics and therapeutic medicines due to the high possibility of side effects in the later stage of human life, the amino acid based polymers seem to be very effective and multi resistant microbe material with minimal side effects.

1.6.7. Monomer Blocks associated with the development of amino acid based Polymers

1.6.7.1. [α-Methoxy-ω-Amino-Polyethylene Glycol] or [α-OMe-ω-NH-PEG]

Organic polymeric materials have a significant outcome in comparison to the inorganic and other metal based NPs. Organic framework consisting of polymers will have a very unique effective result for numerous biological applications due to the presence of life making elements like C, H, N, O, S and P. Due to the amphiphilic nature of di- and tri-block co-polymers in many solvents, it provides a broad space for parameters responsive research. There are many reports available for the synthesis of self-assembled di-block/tri-block-copolymers having pH and temperature-responsive nature using two to three identical or non-identical monomers. There are also few reports available with the application in the effective antibacterial study of di and tri-block polymers.

However, very few reports are available with three or more than three distinct monomer units to form synthetic block-copolymers with a wide range of biological applications. Clinically, PEG has proven to be very good for constipation in children with long term safety depending on their alkyl chains associated with the polymer [130, 131]. Nalam *et al.* [132] have discussed the surface association mechanism that arose from the PEG polymeric chains and its suitable interaction with other biological polymeric materials. The reduced entropy caused by such force also acts as a partition between the polymeric solution and allowed PEG based material for biological applications [132, 133]. The helical conformation confirmed that the PEG based chain has an easy interaction with cationic polymers due to the oxygen in PEG and with the ammonium ions in polymers via hydrogen bonding and electrostatic interactions [134]. The hydrophobic PEG conjugated polymers

have shown their advantages in chemotherapy, artificial protein chain, helical structures [135-138].

The precursors of the above triblock polymers are consist of PEG (**Fig. 1.11.**), [NCA glutamate (NCA-BLG)] derivative (**Fig. 1.12.**) and [NCA aspartate (NCA-BLA)] derivative (**Fig. 1.13.**), respectively shown below. Among these three monomers, the later two monomers come under essential amino acids whereas the former one is completely biocompatible. PEG acts as a very biocompatible backbone of any macromolecule due to its amphiphilicity which attracted our team to work on it with other essential amino acids.

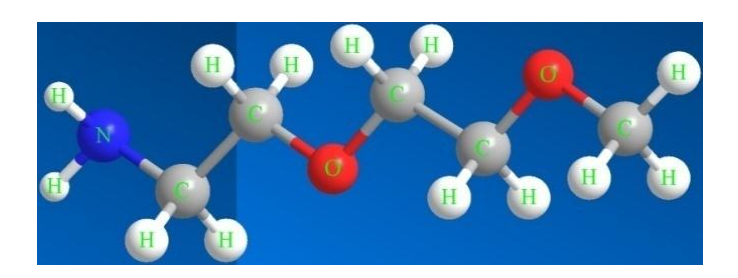


Figure 1.11. 2D Ball and stick model of PEG polymeric materials [131]

1.6.7.2. L-Glutamic Acid-β-Benzyl Ester

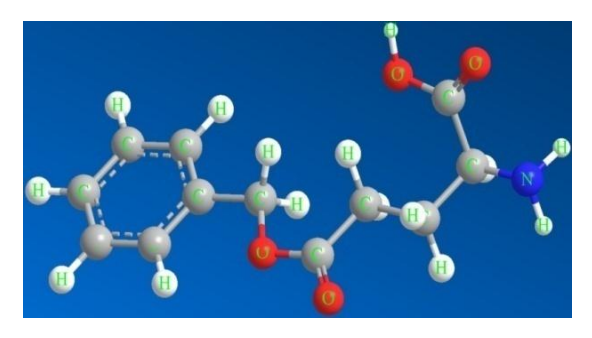


Figure 1.12. 2D Ball and stick model of L-Glutamic Acid-β-Benzyl Ester polymeric materials as an amino acid based precursor [131].

We have considered amino acid chain as our primary backbone of the polymer due to its associative nature, unique colloidal properties, numerous functional groups present in them, and high lifetime, more durability and biocompatible nature which further can be used for various pharmaceutical and medical applications. Morphology of numerous shapes of these type polymers can also exhibit significant results in physio-chemical behaviour.

1.6.7.3. L-Aspartic Acid-δ-Benzyl Ester

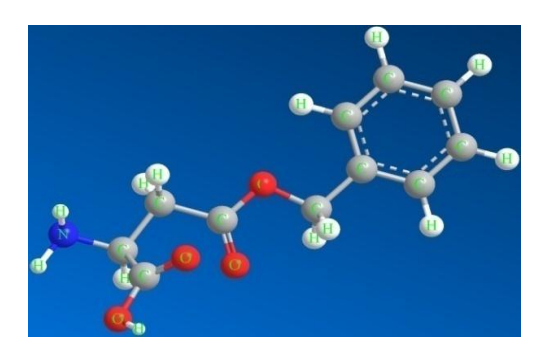


Figure 1.13. 2D Ball and stick model of L-Aspartic Acid-δ-Benzyl Ester polymeric materials as an amino acid precursor [131].

Noble vesicle sized macromolecular polymeric nano-bio compounds for the biomedical applications have been designed considering (α-CH₃-ω-NH-PEG), (L-AspA-4-BE) and (L-GluA-5-BE) as starting materials. The bio-chemical behaviour of polypepto vesicles includes self assembly nature [131-144] in presence of the solvent medium, biocompatibility with human carcinoma cells [145, 146], antibacterial active agent [147, 148], possessed of helical proteins [149], responsive experimental parameter and possessed of chirality. Due to the multipurpose behaviour of the macromolecule, it can be defined as a smart material. We have focused on the modified synthesis of newly designed macromolecule through ring-opening polymerization and succeded with the application *in vitro* biotechnology process. Due to the spherical vesicular property, it can be used for the drug delivery process and tissue engineering application [150, 151].

1.6.8. MTT/ Biocompatibility Assay Test

The primary technique to know the biological behaviour of the newly designed materials is an assay test. Among many assay tests, the MTT assay test is known to be very easy, accurate and time saving procedure. The chemical MTT is used as a dye to know the survival percentage of carcinogenic or non-carcinogenic cells in the human. This experiment is most favoured to perform in the human cell lines [152-154]. In brief, the MTT assay experiment performed in 96 well plates using several cell lines. The required medium contained 5000 cells in each block and allowed for incubation. After an estimated time interval, the targeted material is allowed to pass through the assay tray. The biocompatibility otherwise known as cell viability is represented mathematically by using below equation,

Cell Viability (%) =
$$\frac{ABST}{ABSC} * 100$$
(12)

Where,

ABST= Absorbance of treated culture

ABSC= Absorbance of controlled culture at a given wavelength (say 570nm)

1.6.9. Antibacterial Study

Across the globe, diseases are spreading epidemically be it cancer, dengue, malaria, diabetes, skin problem or bacterial growth. Bacterial growth may occur in both plants and animals. It seems to be very minute micro-organisms but their negative effect can cause severe damage to the living world. To avoid the bacterial infection many researchers have made easy way outs, but still, the research to inhibit the growth of bacterial infection is going on. If we look at previous literature, nanomaterials like metal oxide, polymer composite, bio drugs are available to kill the bacteria in the environment. This dissertation also includes bacterial study with biocompatible triblock copolymers with interesting morphology at nanolevel [155-157]. The methods like micro broth dilution method, agar disc diffusion methods are quite easy and cost-effective experiments against pathogenic and non-pathogenic bacteria cell line [140, 141]. Previously, the literature also suggested techniques like the Stokes method, Kirby Bauer method for the estimation of bacterial growth in the medium [142].

This dissertation will be mainly focusing on the bacterial susceptibility test through a broth dilution method. The optical density calculation for broth dilution method with positive inhibition represented mathematically,

Inhibition Percentage =
$$1 - \frac{OD \ Test}{OD \ Control} * 100$$
 (13)

Mathematically,

Inhibition Percentage =
$$\frac{OD\ Test}{OD\ Control} * 100$$
 (14)

There are many mechanisms are associated with the antibacterial behaviour towards both the pathogenic and nonpathogenic bacterial world [158]. The mechanisms are described shortly in this section. The very common mechanism is alterations in the cell membrane and its lipid profile and mostly useful for *Grampositive* bacteria due to its simple wall which allows the penetration of antibiotics [159]. The mechanism is difficult to apply in *gramnegative* bacteria due to the complex cell wall. The other mechanisms are inhibition of ATPase, cell division, motility and biofilm formation and membrane porins, anti quorum sensing effects [160]. The inhibition of ATP phase is related to the performance of many enzymes with ATP phase activity inhibits the growth of bacteria. The bacterial cell division is another mechanism of antibacterial action by a prokaryotic element [155]. The hydrophobicity of materials also led to a better antibacterial therapy following to porin membrane inhibition. An intracellular sensing effect, as well as biofilm formation, develops the proliferation and adhesion to develop the growth of useful bacteria [160].

LITERATURE REVIEW

1.7. Section I Dielectric Nanocomposite

1.7.1. Inorganic Dielectric Material

Prolonged research based on inorganic dielectric composite received a lot of attention towards the end of the twentieth century due to its functional and variable properties [30, 31]. Mainly the dielectric behaviour of materials has been carried out concerning frequency and temperature as the structural and atomic arrangement can be affected by these two parameters.

1.7.1.1. Calcium Copper Titanate

Dielectric materials have huge applications in the fabrication of microelectronic and energy storage devices. Homes *et al.* discovered $TiO_2@Co$ material, which has shown an extremely high dielectric constant and negligible dielectric losses [161]. In 2013, Hao *et al.* mentioned a review of dielectric materials with high permittivity and low losses being used in making the capacitors [162]. His team even suggested about four kinds of materials of antiferroelectrics, dielectric glass-ceramics, relaxor ferroelectric and polymer-based ferroelectrics with high energy-storage density, low loss, and good temperature stability. For metals, relative permittivity is negative and the surface charge dissipates at a faster rate. On the other hand, the surface charge dissipates very slowly for dielectrics. Materials with colossal permittivity used in capacitor design meet the limited success. However, because of the evolution of the materials with high dielectric constant, like $ATiO_3$ -type perovskite titanates (where, A = Ca, Sr, Ba, Pb or their solid solution), the making of a large number of electronic devices with variable capacitance can be possible.

The perovskite, calcium copper titanium oxide (CCTO, $CaCu_3Ti_4O_{12}$) is an excellent dielectric material, having a very high dielectric constant ($\varepsilon' \sim 10^4 - 10^5$) with a low dielectric loss. Fundamental dielectric study has established calcium copper titanate (CCTO, $CaCu_3Ti_4O_{12}$) as the best dielectric material, which possesses a high dielectric constant of $\sim 10^5$ and a low loss due to its perovskite nature having a wide area of applications in charge storage devices, sensors, etc. as compared to other ferroelectric materials (ε' , $1\times 10^3 - 5\times 10^4$).

1.7.1.2. Synthesis of CCTO Materials

In 1967, the synthesis of the highest possessing dielectric constant material with low loss calcium copper titanate / (CaCu₃Ti₄O₁₂) / CCTO was discovered by Deschenes *et al.* [163]. In the year 2000, Subramanian *et al.* became the first team to introduce the high dielectric value for CCTO more than 10⁴, at 1 kHz and 300°C along with its cubic centred structural determination [164]. ACu₃Ti₄O₁₂ based CaCu₃Ti₄O₁₂ showed a dielectric constant of 1.2×10⁵ at 1 kHz and nearly constant from room temperature 573K. Even his team mentioned that due to the perovskite nature of CCTO, TiO₆ can produce a square planar environment that leads to higher dielectric values. There is a very low dissipation of heat released from the surface of perovskite like structure.

Following Subramanian *et al.* work, Homes *et al.* studied the optical conductivity associated with the physics of CCTO. This team was able to find *e'* of 80 at RT due to the presence of dipolar relaxation at very low frequencies [165]. Optical conductivity measurement on CCTO was observed with a giant dielectric effect at low frequency range of ≤ 1 kHz. Later in 2000, many researchers like Lunkenheimer *et al.* [166], Thomas *et al.* [167] and Si *et al.* [168] have established CCTO and studied the dielectrics with different temperature and frequency. Lunkenheimer *et al.* have mentioned about the large magnitude of a colossal constant of transition metal oxide NPs and their application in capacitance based storage devices. The generation of interfacial effects from external and internal boundaries and electronic phase separation led La₂−xSrxNiO₄ NPs to generate high dielectric constant. Tang *et al.* [59] extended the CCTO synthesis method with the attachment of polymers on the surface of CCTO to increase the dielectric value of both CCTO and polymer matrix. The aspect ratio phenomenon of dispersed filler CCTO NPs increased the aspect ratio of polymer based nanowires with a higher yield of the nanomaterials.

Turky *et al.* [78] in 2015 developed CCTO NPs by using the organic acid precursors and allowed for annealing at 1000°C for 2hrs. CCTO NPs have shown its size from 40-60nm and effective porous nature with suppression of loss value to a very minimal extent [80]. The promising synthesis method for the development of $CaCu_3Ti_4O_{12}$ NPs was developed by Chen *et al.* by using a stoichiometric amount of $CaCO_3$, CuO and TiO_2 in molten NaCl-KCl and Na_2SO_4 - K_2SO_4 medium. A giant dielectric constant of up to 10^4 was observed for corresponding CCTO NPs with a very low loss tangent ≤ 0.2 at RT in the frequency range from 100 Hz to 100 kHz and used suitably for technological applications. In the previous year in 2019, Tripathy *et al.* [81] synthesized CCTO ceramic pellets of 10 mm dia. by solid state

route. The sample has shown a dielectric constant of around 5×10^3 at 1 kHz frequency due to capacitance of the grain boundaries associated with the IBLC model with a loss of 0.14.

1.7.1.3. CCTO based Composites

In 2009, Thomas *et al.* [167] observed a complex oxalate precursor containing CCTO, CaCu₃ (TiO)₄ (C₂O₄)₈·9H₂O, (CCT-OX) which exhibited giant dielectric constants up to 4×10⁵ (1 kHz) at 25°C with dielectric losses, <0.07. Even the dielectric material has shown very good sintering capacity at high temperature, the particle size of 30 nm-80 nm. Pulsed-laser deposition CaCu₃Ti₄O₁₂ on LaAlO₃ and SrTiO₃ substrates was performed by Si et al. in 2000. His team was able to develop the epitaxial thin films of CCTO composites with or without various conducting buffer layers. Earlier researchers performed against the frequency dependence study of CCTO based composite but in this year they observed the temperature-dependent dielectric study of nanocomposites and also the frequency dependence of its dielectric properties below 150 K indicated an activated relaxation process.

Pandirengan *et al.* [75] in 2017 modified CCTO NPs with $(Bi_4Ti_3O_{12})$ X as thin films and allowed to grow on a platinized silicon substrate using the spin-coating technique. He observed two different crystal phases of orthorhombic BTO and cubic CCTO exist together in the film matrices. The percolation theory also proved the better dielectric constant of $(Bi_4Ti_3O_{12})$ and used as a suitable candidate for the modern microelectronic devices.

The dielectric behaviour of CCTO-Fe₃O₄/polyimide (PI) hybrid films was studied by Chi *et al.* [79] in 2016 with the application of an external magnetic field. His team observed that Fe₃O₄ NPs were deposited on the surface of CCTO with a substantial increase in dielectric permittivity (10²-10³), a slight increase in dielectric loss, and a decrease in the percolation threshold for the hybrid composites subjected to a magnetic field treatment.

Following the interesting dielectric study of CCTO NPs, Krohns and Lunkenheimer developed lanthanide titanate based dielectric which has shown the value of the dielectric from 10⁴-10⁵at 300C, 10 kHz [166]. In 2009 Wang *et al.* [172] reported an exceptional work on organic polymer based nanocomposite which showed its dielectric constant less than 10² due to the unavailability of polarization like electronic, atomic, etc. Dielectric material including CCTO has invaded the area of capacitors, as they do not allow conductivity of electricity and used as charge storage devices with high dielectric property [169]. Substantial lattice vibrations (phonons) results in the intrinsic dipole moment and yield giant dielectric permittivity of CCTO which could be explained by the Lyddane-Sachs-Teller model [170,

171]. CCTO can be synthesized by a solid-state reaction using the stoichiometric amount of CaCO₃, TiO₂, and CuO as precursor materials [172].

Many theories [173-177] have been reported to explain the origin of the giant dielectric permittivity. It has been observed that several factors like shape, sizes, surface morphology; grain boundary contributions, internal material layers, and distribution of ions of doping, etc. are the possible contributors for the giant high dielectric properties. Apart from these, the high dielectric phenomenon is appeared due to the extrinsic properties such as the interfacial polarization of highly delocalized electrons at the interface of the grain boundaries [161]. A report by Hu and co-workers have found out that doping of In³⁺ (electron acceptors) with Nb⁵⁺ (co-dopant) into rutile, lower the dielectric losses. This is happened due to the stoichiometric local lattice defects (defect clusters due to the conversion of Ti⁺⁴ to Ti⁺³) and is responsible for the extraordinarily high value of intrinsic permittivity in the radio frequency range [178]. Recently, it is observed that core-shell nanomaterials have a great impact on fabricating charge storage devices, microelectronic devices etc. [179].

1.7.1.4. Barium Titanate, Lead Titanates and PZT

BaTiO₃ is the first ferroelectric perovskite ceramics and used for different electrical applicative purposes. Since 1940, BaTiO₃ has been used as a mica substitute in the capacitors. Chen *et al.* [180] in 2003 has synthesized BaTiO₃ by hydrothermal method at a temperature between 75°C and 180°C and for 10 min to 96 hr in an alkaline medium. Physical characterization has proven the influence of Ti NPs on the size and morphology of barium titanate of 0.1 μm size. More *et al.* [181] discussed the dopants and their role in the development of the dielectric behaviour of BaTiO₃ at A and B site cations. Solid-state reaction method for the synthesis of barium titanate was established by Andreda *et al.* in 2014 [182] with significant dielectric behaviour. The doping process made the of BaTiO₃ nanocomposites very effective at different temperatures.

BaTiO₃ based composites have shown a greater effect in the development of better dielectric behaviour with respect to frequency and temperature. Jiang *et al.* in 2018 [183] have developed numerous types of nanoparticles, nanorods, nanotubes and nanowires and controlled crystal phases like cubic, tetragonal and multi-phase of BaTiO₃/polymer nanocomposites. Even his team mentioned the advantages of simple solution processibility, high breakdown strength, lightweight device scalability and high dielectric constant.

After a few decades later, Lead Titanate (PbTiO₃), Lead Zirconate Titanate (PZT) and Lead Lanthanum Zirconate Titanate (PLZT) came in to picture with moderate dielectric properties [23-24]. Being a ferroelectric ceramics, PbTiO₃, possessed of high capacitance value. Nurbaya *et al.* [184] have discussed the synthesis and dielectric properties at low temperatures. They have explained the process involved for the uniform grain size possessing stable dipole moment leading to better dielectric values at different temperature ranges.

Mridula *et al.* [185] designed via solid-state reaction technique. The dielectric constant was found to be 515.50 at 1 K Hz with the loss tangent is 0.005 due to the migration of oxygen ions towards the electrodes. But among all the materials, BaTiO₃ seems to have a better dielectric property with more constant and strength than other inorganic based nanocomposites reviewed by Chaudhuri *et al.* [186]. Being economical, easily synthesized, environmentally friendly and unique crystalline solid, it is possessed of fascinating ferroelectric, piezoelectric and dielectric properties.

1.7.1.5. Silicon Oxide Nanoparticles (SiO₂ NPs)

In late 1960, Stober *et al.* [187] were taken the initiative to synthesize uniform spherical shaped particles. Till today, this synthesis method is used extensively in all the fields of applied sciences. The interesting uniform size and morphology were controlled via the addition of surfactants by this team. Later to this research, SiO₂ NPs acts as a best known inorganic insulator possessing a very low dielectric constant (~50-100) and have a good impact on environmental compatibility [133, 135]. Due to its surface functionality and presence of a lone pair of oxygen associated with the main non-metal silica, the pathway of chemical functionality became very easy. Volksen *et al.* [188] have mentioned many significant effects of low dielectric constant materials and their effect against porosity. The thermal stability of a porous thin film of silica seemed to show any appreciable loss of samples up to 600°C. Esposito *et al.* [189] mentioned the loss of weight % of silica sample at 700°C due to less polarizable bonds.

Tang *et al.* [82] have developed CCTO based polymer film@ SiO₂ nanocomposites with the effect of an aspect ratio of filler CCTO NPs on SiO₂ and polymer matrix viahydrothermal process. This effect led to lower dielectric loss value 0.081 and constant up to 68 of this composite is due to the core-shell structure of the composite.

1.7.2. Organic Dielectric Materials

The organic polymer based nanocomposite is otherwise known as organic dielectric material. These dielectrics mostly possessed of very low ε' [29] and ε'' due to unavailability of conducting electrons [32].

1.7.2.1. Graphene Oxide (GO Sheets)

In the year 2007, Geim *et al.* [190] have mentioned the history and rise of graphene oxide very briefly. GO is a two-dimensional (2D) material, a flat monolayer of sp² hybridized carbon atoms, tightly packed into a honeycomb lattice and basic synthetic frame for all graphene materials have been reported a few decades ago [191].

Following this work, others such as Bonaccorso *et al.* [192]. Stankovich *et al.* [193] and Lee *et al.* [194] have studied the photonics-optoelectronics, elastic properties and intrinsic strength of monolayer graphene. Bonaccorso *et al.* described the high mobility and optical transparency, flexibility and environmental stability. They also mentioned about the benefits of the presence of exfoliation present in GO due to which tuning occurred even with the absence of band gap leading to the linear dispersion responsible for the optoelectronic activity. The elastic properties and intrinsic breaking strength of GO were first studied by Lee *et al.* via nanoindentation process. The nonlinear elastic stress-strain response was observed to be 340 Newtons per meter (N m⁻¹) for GO NPs and found to be the strongest material till that year. Their research on of GO also suggested many significant advantages of electrical stability, highly stable thermal and mechanical properties along with biocompatible nature.

Contemporary researchers, Cai *et al.* and Zeng *et al.* discussed the applications of GO for the development of 3D smart material, biosensors and nanohybrid materials due to variant groups association[195-197]. The association of GO with impermeable membranes leads to the creation of pressure differences between itself and atmosphere became an advantage for the microfabrication of devices by calculating its mass and elastic constants [198]. GO has shown its significant roles towards the application in biology, chemistry and engineering field due to the structural distortion phenomena with the presence of various oxygen moiety on its surface [199-201]. Gupta *et al.* have reported that GO-MnO₂ nanosheets possessed of 10³ with low loss, became useful for electronic applications, optical devices, thin films and sensors [202]. In detail, GO@MnO₂ nanocomposites have been synthesized by a chemical

route. The existence of MnO₂ in GO@MnO₂ nanocomposites led to the effective enhancement of the electronic polarization, interfacial polarization and anisotropy energy in the presence of microwaves and used suitably in microwave applicative purpose.

1.7.2.2. Synthesis of GO NPs

Singh *et al.* [203] synthesized GO by modified Hummer's method with the exfoliation of graphene sheets. These GO composites act as a suitable material for solar cell, water purification, supercapacitors, and an antibacterial agent. Paulchamy *et al.* also developed GO in a very simple approach. This team confirmed the existence of oxygen, C-O, and C=C by physical characterization techniques [204]. Yu *et al.* in 2016 [205] reported an economical and efficient by removing NaNO₃ from established Hummers method and replacing KMnO₄ with K₂FeO₄. He also performed such type of GO to the super electrode application purpose.

In 2017, Sharma *et al.* [206] reported a simple and convenient method for synthesis of GO by using a reducing agent hydrazine hydrate to yield reduced graphene oxide with the elimination of oxygen containing functional groups and acts as a very potential material for the purpose. Ranjan *et al.* [207] have synthesized GO via improved Hummers' approach by not using hydrogen peroxide in the reaction medium. This procedure led to a higher yield of GO NPs with the release of excess toxic gas to the environment.

Following the previous work, Santhosh *et al.* introduced very few-layered GO synthesis with the ultrasonication method. His team has also suggested a very high dielectric constant of 10⁶ and a very low loss at 1 kHz, 30°C due to the mechanistic approach and the role of functional groups, defects [208].

1.7.2.3. GO NPs based Nanocomposites and its Dielectric behaviour

Zhang *et al.* [209] developed silica-graphene oxide GO@SiO by the hydrolysis of tetraethylorthosilicate (TEOS) in the presence of hydrophilic GO NPs via modified Hummers method. The dielectric constant of GO@SiO₂ was found to be less than 10 from a frequency range of 20-10⁶ Hz. Sang *et al.* [210] also designed GO@SiO₂ nanocomposites to enhance the electrorheological activity and suitable for the use in smart suspensions with high ER responses.

Song *et al.* [211] have synthesized GO/-PDMS-PGMA by the molecular design process. The composites had shown a high dielectric constant of 40 at 1 kHz frequency at RT and used in the electronics and engineering fields.

1.7.2.4. Composite Dielectric Material

The literature review on CCTO, other perovskites like BaTiO₃, PZT, PbTiO₃, SiO₂, GO and GO based nanocomposites discussed in detail above. The significant change of dielectric behaviour from low to high constant with very minimal loss tangent at different temperature and frequency has been a great interest for the development of dielectric materials based on their chemical composition and its suitable use in electronics and storage applications. However, an exception to the ferroelectric material, temperature-dependent behaviour of CCTO from RT to 500K, with a giant dielectric constant and a very low loss showed an exceptional result to the dielectrics study which encourages us to go for further development of new nanocomposites including CCTO nanoparticles (NPs) and GO Sheets. GO and silica coated calcium copper titanate (CCTO@SiO₂) NPs were synthesized from the established Hummer's method and sol-gel process, respectively [212-220]. **Table 1.1** with reported research work for CCTO, Silica, GO and composite based dielectric nanomaterials, composition, real part permittivity values and dielectric study has been attached below for a better understanding of the background of such materials.

Table 1.1: Reported Research work for CCTO, Silica and GO nanomaterials dielectric study

Dielectric	Journal	Composition	Real part	Temperature	Reference
Type			(ε')		
Onconio	Nancanana	CoCo Ti O	70	101-11-	Tono et al [50]
Organic-	Nanoenergy,	CaCu ₃ Ti ₄ O ₁₂	70	10 kHz	Tang <i>et al</i> . [59]
inorganic	(2015), 17,	Nanowires			
	302-207				
Inorganic	Thin Solid	(Bi ₄ Ti ₃ O ₁₂)X-	9×10^{3}	100 Hz	Pandirengan et
	Films 628	$(CaCu_3Ti_4O_{12})$			al. [75]
	(2017) 117–126	1-X,			
		[(BTO)X-			
		(CCTO)1 – X]			
Organic-	RSC Adv.,	CaxCu ₃ _xTi ₄ O	0.05×10^3	1.75 Hz	Turkey et al.
inorganic	2015, 5, 18767	12 synthesized			[78]
		by organic acid			
Organic-	J. Mater. Chem.	ССТО-	308	100 Hz, 363K	Chi <i>et al</i> . [79]
inorganic	C, 2016,	Fe ₃ O ₄ /PI			
	4, 8179				
Inorganic	Materials	CaCu ₃ Ti ₄ O ₁₂	5×10 ³	1 kHz	Tripathy et al.
Pellet	Science and				[81]
	Engineering				
	115,(2016),				
	012022				
Inorganic	Journal of Solid	CaCu ₃ Ti ₄ O ₁₂	12,000	573 K, 1kHz	Subramanian <i>et</i>
	State Chemistry				al. [164]
	151, 323-325				
	(2000)				
	, ,				
Inorganic	Science	CaCu ₃ Ti ₄ O ₁₂	80	RT	Homes et al.
	(80) 293,				[165]
	673–676				
	(2001)				
<u> </u>	l .	I	<u> </u>	L	

Inorganic	Eur. Phys. J.	CaCu ₃ Ti ₄ O ₁₂	10^{4}	473 K, 28 Hz	Lunkenheimer
	Spec. Top. 180				et al. [166]
	(2009) 61–89				
Organic	Journal of	CaCu ₃ Ti ₄ O ₁₂	4×10 ⁴	278K, 1kHz	Thomas et al.
Organic	Thermal	CaCu3114O12	4/10	270K, 1KHZ	[167]
	Analysis and	$(C_2O_4)_8 \cdot 9H_2O$			[107]
	Calorimetry,				
	Vol. 95 (2009)				
	1, 267–272				
Inorganic	Appl Phys Lett	CaCu ₃ Ti ₄ O ₁₂	1.5×10^3	300 K, 100	Si et al.
morganic	81:11	on LaAlO $_3$ and	1.5×10	kHz	[168]
	01.11	SrTiO ₃		KIIZ	[100]
Dolyman	Progress in	CCTO	1.5×10 ⁵	1 kHz	Single at al
Polymer		CCIO	1.5×10	1 КПХ	Singh et al.
	growth and characterization				[169]
	,				
	60, 2014 (15-				
Inonconio	62)	CCTO@S:O	12.78×10 ⁴	100 Hz 202	Wong at al
Inorganic	Electron.	CCTO@SiO ₂	12.78×10	100 Hz, 293	Wang et al.
	Mater. 43,2607-			K	[172]
	2613,2014	G0	5000	100 5111	
Organic	RSC Adv	GO	5000	180, 5 kHz	Santhosh et al.
	5:14768-				[208]
	14779, 2015	0000:0	4.5	10-111	
Inorganic-	Langmuir 2012,	GO@SiO ₂	4.5	10 ⁻¹ Hz	Zhang et al.
organic	28, 7055–7062				[209]
Polymer	ACS Appl	GO/PDMS-P	25	10^4Hz	Song S et al.
	Mater	GMA			[211]
	Interfaces				
	8:31264–				
	31272,2016				

LITERATURE REVIEW

1.8. Section II Block Copolymer

Many polymer reports are available with polyethylene glycol which is low toxic, high biocompatibility [8], amphiphilic [9], higher thermal stability up to 400°C, higher presence of methylene groups in longer chains [12].

1.8.1. Synthesis and Development of Amino acid based Block Copolymer

There are numerous amino acids available in nature, but among them, twenty amino acids play a vital role in the survival of human being. These amino acids constitute of -NH₂, -COOH-, -CONH₂, -CH₃, -CH₂- and few cases N, S related functional groups. The properties like hydrophobic, hydrophilic character, charge density, chirality, reversible cross-linking, numerous chances of various bond formation etc. are the important factors why scientists focusing these bio-based amino acids for nanomedicine, drug delivery, anticancer and bacterial agent.

A very simple amino-acid block copolymer [poly(ethylene glycol) (PEG)-poly(amino acids) (PAA)] has developed by Miyazaki *et al.* [214] via ring-opening polymerization (ROP) method with biocompatible nanostructures. The polymeric micellar solution showed a significant blood circulation and biodistribution in the solvent medium.

Ladmiral *et al.* [215] have synthesized amino acid based poly (amino acid methacrylate) via reversible addition-fragmentation chain reaction (RAFT) polymerization with the effective biomedical application. Their electrophoresis solution study has also proved that the polymer possessed of the cationic character below pH 3.5 and anionic character above pH 3.5.

1.8.2. Study of Amino acid based Block Copolymer for Anticancer activity

Kumar *et al.* [216] tried to develop safe and effective nanocarriers for multi type of delivery system, gene engineering and succeeded at their aim. They have designed the amino acid based polymer of monomethoxy poly(ethylene glycol)-b-poly(Boc-amino acid methacryloyloxyethyl ester) (mPEGn-b-P(Boc-AA-EMA)) via RAFT polymerization, *In vitro* experiments by encapsulation of nile red dye, doxorubicin drug into the core of the micellar nanoaggregates has performed along with high cytotoxicity performance

Levit *et al.* [217] have synthesized amphiphilic block copolymers PMAG-*b*-PAA RAFT polymerization. The encapsulation of paclitaxel drug into the desired polymer and its cytotoxicity effect on human lung carcinoma cells (A549) and human breast adenocarcinoma cells (MCF-7) were observed to be more significant. In Situ, polymerization method was followed by Liang *et al.* [218] strategy to develop PS-*b*-P₄VP with a higher degree of freedom for tailoring the surface functionality in the pores. Osada *et al.* [219] have discussed DDS based on polymeric micelles for anti-cancer drug and gene delivery.

Ponta *et al.* [220] have developed and collected six block copolymers possessed of drug-binding linkers. They performed the conjugation of anticancer drugs to these polymers which resulted in nano micelles of size <50 nm. These PEG-poly(amino acid) block copolymer has shown a promising effect for chemotherapeutic treatment due to its self-assembly nature and pH-responsive behaviour.

1.8.3. Protein Folding Study of Block copolymers

The chirality properties are mostly associated with organic based compounds. The circular dichroism (CD) study helps the chirality behaviour of organic based materials very easily. Hawkins *et al.* [221] have measured the CD spectra for optically active (a-aminocarboxylate) pentaamminecobalt (111) complexes under different pH conditions with the presence of salts of polarizable anions. The observed spectra associated with significant chiral properties with the Cotton effects.

The hydrophobic P(Boc-L-Ile-HEMA)-b-PMMA and P(Boc-L-Leu-HEMA)-b-PMMA was reported by Bauri *et al.* [222] with the formation of optical activity and α-helical structures. The study was performed by RAFT polymerization in N, N-dimethylformamide (DMF) medium. The side chain amine functionality initiates the pH-responsive behaviour of such cationic polymers due to -NH₃ became a suitable candidate for drug delivery applications and conjugation of biomolecules.

1.8.4. Antimicrobial activity of Block copolymer

Reports proved that synthetic polymer-based antimicrobial materials destroy the conventional antibiotic-resistant microorganisms. The block copolymer of (poly(l-lysine·hydrochloride)₁₀₀-b-poly(l-leucine)₄₀) was synthesized by Bevilacqua *et al.* [223] and performed against few *Gram-positive* and *Gram-negative* bacteria and yeast with different multidrug-resistant strains. The long-chain, cationic and hydrophobic properties enhance the polymer to acts as a very good antimicrobial agent and to prevent wound infections.

In 2017, Szczeblinska *et al.* [224] have synthesized poly(ester-amide)-PEG block copolymers and discussed the preparation and antibiotic loading of polymeric microspheres, composed of copolymers. The streptomycin, chloramphenicol and amphotericin B antibiotics were used against bacteria like *E. coli* bacteria, and *C. albicans* and exhibited a strong antibacterial activity.

The morphological change of a bacterial cell from rod to spherical shape in the presence of antimicrobial polymers [P(Boc-Ala-HEMA)₁₄-b-PPEGMA₆₀] and [P(Boc-Ala-HEMA)₁₄-b-PMMA₃₇], were designed by Mukherjee *et al.* [225] in 2017. The desired polymer showed a great efficiency towards antibacterial activity against *E. coli* and *Bacillus subtilis* bacteria.

1.8.5. PEG and Amino acid based Di and Triblock Copolymer activity towards drug delivery

Previous polymer study has proven that polyolefins are mostly nondegradable. But in 2010, Gandhiraman *et al.* have studied the organic amine group functionalization of cycloolefin polymer for bio diagnostics purpose [226]. His team created amino functional coatings on COP substrates by PECVD and the use of mixtures of APTES and EDA has been mainly emphasized in this case. The chemical composition, homogeneity, stability, reactivity and morphological properties were developed through chemical and physical characterizations. They published the siloxane functionality as essential to creating a stable, adherent amine reactive network on COP substrates along with the application of siloxane surfaces to biomolecule binding.

Nano and micro sized polymeric materials have been receiving recognition due to several uses in chemistry, medical technology, therapeutics, biosensors (diagnostics), etc. in recent times. Shixian*et et al.* have studied PEG-*b*-P(Glu-co-Phe) amphiphilic triblock copolymer synthesis and its use as doxorubicin-loaded drug delivery for cancer treatment [227, 228]. The current authors developed an anionic mPEG-*b*-P(Glu-co-Phe) block copolymer and a model cationic anticancer drug, DOX. The excellent biocompatibility, easy fabrication, strong self-assembling structure under the physiological conditions, a high drug-loading capability and an intracellular pH-triggered drug release capability revealed its great potential for delivering anticancer drugs have been discussed by his team. Polymerized DOX-NP has shown a high level of tumour cell uptake along with high inhibition of cancer cell growth compared to virgin DOX was confirmed by biological imaging assays like CLSM and

flow cytometry and *in vitro* cytotoxicity and the cell apoptosis studies, respectively. Hence, the self-assembled polymer/drug complexes driving power of electrostatic interactions of self-assembled polymerized drugs remained a suitable platform for cancer therapy.

The self-assembled smart polymeric materials with different morphological features along with their nanostructures are used as potential drug carriers, site-specific drug vehicles, scaffolds, stents, catheters, plastics, things for conventional uses. These smart polymers exhibit more advantages over low molecular weight polymers. Reynhout et al. have reported the self-assembled nature of biohybrid triblock copolymers [229]. His team mentioned the advantages of block copolymer use by varying the length and composition of the monomers provided. In 2013, Kang et al. have developed PEG-b-PCL-grafted poly(β-amino ester) diblock copolymer which originally was a pH-triggered and biodegradable. The former polymer has shown a very effective anti-cancer drug delivery [230]. Further in 2015, Shao et al. have reported the cytotoxicity study of polymeric NPS for zeta potential gradient [231]. Interestingly, the responsive behaviour of polymeric macromolecules towards pH, temperature, solvent system and reaction time advances its use in biomedical sciences and technology [232, 233]. However, polymeric vesicles and micelles with different morphologies are trending nowadays in all the areas of bioscience and technology due to their biocompatible nature, cost-effectiveness, easy synthesis, stable nature at body temperature (37°C) and therapeutic importance such as for targeted drug delivery [233].

Currently, in 2017, Galiano *et al.* [234] have reported the polymeric organic acryloyloxyalkyltriethyl ammonium salts responsible for an effective antibacterial result against several bacteria cell line concerning variant parameters [234]. Wang *et al.* have developed a novel temperature-responsive PNIPAM polymer based hierarchical surface. In this work, they performed bactericidal experiments through a temperature-triggered hydration. They mentioned that the release of dead bacterial cells by the inhibition of bacterial cells at a certain temperature, RT was due to the formation of a hierarchical surface by switching to a zwitterionic ions mechanism [235]. Many polymeric-inorganic and organic-inorganic nanocomposites also have shown its significant effect from device applications to biological applications including its effective result towards antibacterial susceptibility.

1.8.6. [PEG-b-L-GluA] Di- Block Copolymer for Therapeutic application

In 2010, Yang *et al.* have developed an amino acid based diblock copolymer [poly(l-glutamic acid)-*b*-poly(lactic-co-glycolic acid)] with self assembly and pH dependent property

[236]. Here in this work, his team suggested the polymer behaviour towards high pH response and distinct self-assembly property. The shape and size variation of the polymer was caused by carboxylic ions on PGA block of the copolymer, the in the diffusion of alkaline water into the core and by the solvation of the inner carboxylic ions in the medium, which have shown its efficacy for drug control release and bio applications. Further in 2016, Xu et al. have developed a similar type of morphological dependent polymer for drug delivery applications. The chemical functionality of hydrophobic and hydrophilic groups have enhanced the biofeasible application of copolymers [237]. In the same year, Amgoth et al. [238] have developed the [PEGlyted-b-(L-GluA)]-PCL block copolymer for therapeutic applications [167]. Priftis et al. have reported a very interesting study of block copolymer related to the protein folding nature. Here they have discussed the self assembly nature and helical properties of block copolymer [239]. However, organic polymeric materials have a significant outcome in comparison to the former. Organic framework consisting of polymers will have a very unique effective result to numerous biological applications due to the presence of life making elements like C, H, N, O, S and P. Due to the amphiphilic nature of di- and tri-block-co-polymers in many solvents; it provides a broad space for parameters responsive research. There are many reports available for the synthesis of self-assembled diblock/tri-block-copolymers having pH and temperature-responsive nature using two to three identical or non-identical monomers [240].

In 2009, Paik *et al.* [241] have reported the enantioselective separation process of block copolymers. They have separated mesoporous spherical silica enantioselectivity by using chiral block copolymers of [PEG-b-L GluA]. His team has clearly described the impact of chirality on almost any chemical and biological process. They have shown that CBCs based on a PEO block and an amino acid block is good surfactant templates for the fabrication of CMPPy. The CMPPy has shown high enantioselectivity after the extraction of the CBCs.

Only very few reports are available with three or more than three distinct monomer units to form synthetic block-copolymers with a wide range of biological applications. Therefore, in this work, we have focused on the synthesis of a triblock copolymer [MeO-PEG-NH]-*b*-(L-GluA)₅-*b*-(L-AspA)₁₈ and its numerous applications in the various fields of medical biotechnology.

Herein, we have synthesized ABC type triblock copolymer of α-methoxy-ω-amino-(poly ethylene glycol)–L-glutamic acid-L-aspartic acid, i.e., [MeO-PEG-NH]-b-(PBLG)₅-b-(PBLA)₁₈] by ring-opening polymerization method of NCAs and studied various biomedical applications including antibacterial activity due to its colloidal properties like self-assembled nature with temperature and pH responsive behaviour for biological activities inside the body, very minute sized micelle morphology and thermal stability. We have earlier reports on diblock copolymer [PEG-b-PBLG] with its characteristic properties, however, the detailed study on folding, morphology, versatile biological application scope and size variation with the adverse effects such as pH and temperature have never been reported yet. We have considered amino acid chain as our primary backbone of the polymer due to its associative nature, unique colloidal properties, and biocompatible nature which further can be used for various pharmaceutical and medical applications [242-245]. Morphology of numerous shapes of these type polymers can also exhibit significant results in physio-chemical behaviour [246-248]. Very few reports are available with the application in the effective antibacterial study of di and tri-block polymers [231, 233].

1.8.7. [MeO-ω-NH-PEG]-b-(L-AspA)] for Cancer and Bacterial Treatment

The era of nanoparticles is the platinum age of the world as it troubleshot many of the problems which are generated due to micro- or nano-devils like bacteria, virus, fungi, etc. [249-250]. Nanoparticles perfectly counter-attack these microorganisms for their growth which keeps the human habitat healthy. Various forms of nanoparticles have been reported with their broad applications in the research of chemistry, physics, material science with the major contribution in the biological field [226, 231, 240 251]. The major challenge remains with nanoparticles in the field of biology with the pathway of carriers to the affected site for the counter attack. Block co-polymers play a vital role in the transfer of nanoparticles to the desired site by forming non-covalent interactions with nanoparticles. Protein based copolymer is amazing copolymer for the carrier of nanoparticles as they possess many polarized functional group which involved in non-covalent interaction [236, 246, 252]. Research has been done for different micelles and vesicle sized self-assembled polymeric nanoparticles but our study based on a very small size is very exception result which attracted our target towards biological application [229, 230, 253]. Many of the anti-microorganisms possess chirality for the complete protection of the antimicrobial effect [254, 255]. Recently few groups have focused their attention on designing a new class of chiral amino acid based copolymer for its application in bio-field [256, 257].

In general, self-assembled nanosized amphiphilic polymeric materials are playing a vital role in biology as well as in chemistry for biocompatible nature, antimicrobial activity, as site specific drug vehicles, material synthesis and many more. In 2015, Li *et al.* have reported about the reversibly cross-linked PEG-poly(amino acid)s copolymeric micelles and its drug release study at different cell lines [245, 258]. The previous study regarding the zwitterionic colloidal solution of the polymer has gained attention from scientists for its variable property in different solutions of solvents [259,260]. Table 2 with reported research work for PEG and essential amino acid based polymers has been attached below with a better understanding of the background of such materials with its numerous applications and morphology.

Table 2: Reported Research work for amino acid based polymers and its application

	Composition				
	Composition		rial	Survival	ence
			stability		
ACS biomaterials	PEG-PLL	Micelles like	-	-	[214]
Science and		Sphere			
Engineering					
Polymer	GSHMA	Worm like	-	-	[215]
Chemistry, 2015,					
805					
Lamgmuir, 2013,	PEGn-CTA		-	Gene and	[216]
29, 15375–15385				Drug	
				delivery	
Polymers, 2020,	PMAG-b-	-	-	Drug	[217]
2,183;					r ,
loi:10.3390/poly					
m12010183					
Chinese chemical	PS-b-	Spherical with			[218]
Letter, 2019	P4VP(Py-	good mechanical			
	Phe)1	property			
Pharm Res (2010)	PEG				[220]
27:2330–2342					
ActaBiomater.,	mPEG-b-	Micelles 140nm	-	5 mg/l	[227]
2013, 9, 9330–	P(Glu-co-			DOX	
9342	Phe)				
. Am. Chem.	PS _m -b-	micelle rods,	-	-	[229]
Soc., 2007, 129,	PEG ₁₁₃	vesicles, toroids,			
2327–2332		Figure eight ,			
	cience and ngineering olymer themistry, 2015, 805 amgmuir, 2013, 9, 15375–15385 olymers, 2020, 2,183; oi:10.3390/poly 12010183 thinese chemical etter, 2019 harm Res (2010) 7:2330–2342 actaBiomater., 013, 9, 9330–342 Am. Chem. oc., 2007, 129,	cience and ngineering olymer Chemistry, 2015, 805 amgmuir, 2013, PEGn-CTA 9, 15375–15385 olymers, 2020, PMAG-b- 2,183; PAA oli:10.3390/poly 12010183 Chinese chemical PS-b- etter, 2019 P4VP(Py- Phe)1 ctaBiomater., mPEG-b- 013, 9, 9330– 342 mPEG-b- 1342 Phe) Am. Chem. PS _m -b- peG ₁₁₃	cience and ngineering olymer Olymer Chemistry, 2015, 805 amgmuir, 2013, PEGn-CTA 9, 15375–15385 olymers, 2020, PMAG-b- 2,183; oi:10.3390/poly 112010183 Chinese chemical etter, 2019 P4VP(Py- Phe)1 property harm Res (2010) PEG 7:2330–2342 ctaBiomater., 013, 9, 9330– 342 Am. Chem. PS _m -b- peG ₁₁₃ worm like Worm like Worm like Morm like Morm like Morm like Spherical with good mechanical property Micelles 140nm Micelles 140nm micelle rods, vesicles, toroids,	Sphere Spherical Sphere Spherical Sphere Spherical Spherical	Sphere S

			structures,spheres			
S. W. Kang <i>et</i> al.	Polymer (Guildf)., 2013, 54, 102–110	PAE-b-PCL- PEG	Spherical 100nm	-	Anticancer less than 70%	[230]
X.R. Shao et al.	Cell Prolif., 2015, 48, 465–474	poly-3- hydroxybutyr ateco-3- hydroxyhexa noate (PHBHHx)	-30 mV		50%	[231]
Galiano et al.	Chempluschem, 2017, 82, 1235– 1244	Acryloxyalky ltriethylamm oni bromides (AATEABs)	-	MIC value of 64 mg/mL	-	[234]
Yanan Yang et al.	Polymer (Guildf)., 2010, 51, 2676– 2682	PLGA-b- PGA)	Distorted vesicles 2um	-	-	[236]
Amgoth et al.	Nanotechnology, 2016, 27, 0	MeO-PEG- NH-(L- GluA)10- PCL	Porous capsules 200nm	-	~279 and ~480 ng/µg	[238]
Dimitrio s et al.	Angew. Chemie - Int. Ed., 2015, 54, 11128–11132	$\begin{array}{cc} PPLGPG_{50}/P \\ Glu_{50} & and \\ PLys_{50}/PGlu_{5} \\ 0 \end{array}$	Micelles, 36 nm			[251]
Yuling Li <i>et al</i> .	RSC Adv., 2015, 5, 20025–20034	PEG– PGlu(EDA– LA)–PPhe	Micelles 19 nm19 mV	-	1.0 mg/mL	[258]

1.9. MOTIVATIONS, RESEARCH GAPS AND PROBLEM DEFINITION

This thesis confined to the development of four different types of nanomaterials which are morphologically distinguished. Basically, in this dissertation, the synthesis of organic-inorganic dielectrics and amino-acid based polymeric materials will be discussed. These designed nanomaterials are applied according to their primary composition.

Electronic applications

Organic-inorganic based nanomaterials including CCTO, SiO₂ and GO as precursors were mainly implicated for the electrical insulation. There are many reports available with polymer based CCTO and GO dielectric materials with very low constant and loss [172]. Even possessing very low ε' , polymer-inorganic nanomaterials also have been used in sensor and electric storage applications. This thesis has an elaborate discussion about the amine organic group attachment on the surface of inorganic filler and CCTO. The study suggested that the dielectric behaviour of SiO₂ NPs mostly used for insulating applications whereas the organic groups mostly possessed with very low ε' [261]. Possessing low ε' and ε'' for both the former case, it was quite difficult to develop high ε' for charge storage device applications [156]. But, the precursors like CCTO and GO possessed ϵ' up to 10^5 - 10^6 at higher frequency regions. Even reports are available that the Polymer, organic or silica based CCTO and GO nanocomposites seems to have very low dielectric strength materials due to the disappearance of polarization at the different frequency at external magnetic field [262]. Providing such types of challenges and disadvantages, our team decided to develop an organic-based inorganic dielectric and proved to have better dielectric constant and low loss and can be used for various applications. Extensively we have studied the newly designed organic-inorganic dielectric material for dielectric and impedance study to use these materials or various applications.

Therapeutic applications

Amino acid based polymeric nanomaterials were mainly used for antibacterial applications. The development of biocompatible polymeric micelles and vesicles have done by using organic including α -Methoxy- ω -Amino-Polyethylene Glycol, L-Glutamic Acid- β -Benzyl Ester, L-Aspartic Acid- δ -Benzyl Ester as precursors. The development has been based on modified ring opening polymerization following a few other chemical processes for further purification of material. Previously, the amino acid based diblock polymers has shown

the morphology and few biological applications with some challenges [226]. The diblock polymer was unable to act as a smart material, possessing high protein folding behaviour, effective therapeutic applications and high ζ value remained a challenging situation for current researchers [263]. The attachment of a new block to the diblock polymer and its purification procedure also seemed to be challenged but finally resolved with high yield [264. Even, the disadvantages of [PEG-b-PBLG₅-b-PBLA₁₈] and [PEG-b-(PBLA)₇-b-(PBLG)₁₇] polymers were very unstable at different pH and temperature due to their stimuli and selfassembly behaviour. The instability leads to aggregation of particles and was unable to load at different stimuli conditions [230]. Hence to avoid such situations, we have optimized suitable conditions and parameters after repeated experiments several times and reach a conclusion of the polymers with effective application pH 6-8 and temperature of 25°C to 35°C. However, the synthesized polymers have shown effective in vitro antibacterial and anticancer applications. Further, the polymeric nanomaterials showed high protein folding behaviour and ζ value at different stimuli conditions. To reduce the epidemic diseases in the human world and to overcome non-biodegradable processes, the polymer can be a very good option.

1.10. OBJECTIVES OF THIS DISSERTATION

The objectives of this dissertation are as follows.

- 1. Designing of CCTO@SiO₂core-shell nanoparticles via Sol-gel method following other nano chemical processes like hydrolysis, evaporation, purification, centrifugation, and drying of solvent
- 2. Determination of the physical, structural and chemical characterizations of CCTO@SiO₂ NPs via XRD, EDAX TGA, FTIR, Raman and UV-Vis measurements and to target the design of a different range of the shell thickness
- 3. To study the role of SiO₂ shell over CCTO core surface and CCTO@SiO₂ NPs during dielectric and impedance measurements.
- 4. Developing graphene oxide decorated with nanocomposite silica-coated calcium copper titanate (CCTO) nanoparticles via modified Sol-gel technique and design different sheet type decorated GO-CCTO@SiO₂nanocmposites.

- 5. To investigate the morphology, crystallinity, functionality and vibrational mode arrangement, thermal stability, and electronic excitation phenomenon.
- 6. Dielectric and Impedance study performance on GO-CCTO@SiO₂nanocomposite at different frequency and temperature ranges.
- 7. To prepare polypetidic nano micelles of $[\alpha\text{-OMe-}\omega\text{-NH-PEG-}b\text{-}(PBLG)_5\text{-}b\text{-PBLA})_{18}]$ via ring opening polymerization method at an inert environment and control the morphology over parameters.
- 8. Designing of new triblock polypepto vesicle sized [α -OMe- ω -NH-PEG-b-(PBLA)₇-b-PBLG)₁₇] nanobio materials and its action upon antibacterial activity.
- 9. To study the biological, chemical, structural and physical characterization of artificial peptides via essential techniques of Circular Dichroism, DLS, ZETA, and UV at different temp range 20°C-50°C and pH 4-10.
- 9. The biological study of the amino acid based block copolymeric nanoparticles against several bacteria and cancer cell lines. To investigate the block copolymers through LCSM techniques, MTT assay and broth dilution method
- 10. An extensive study of protein block copolymers via circular dichroism and DLS-Zeta experiment at different environmental conditions including pH and temperature as parameters.
- 10. Structural confirmation analysis of [PEG-*b*-(PBLG)₅-*b*-PBLA)₁₈] and [PEG-*b*-(PBLA)₇-*b*-PBLG)₁₇] will be performed by ¹HNMR, chemical functionality via FTIR spectra and the molecular weight determination via MALDI-TOF analysis.
- 11. Performance of other physical and chemical characterization including XRD, TGA, and other techniques.

CHAPTER-2

MATERIALS, METHODS, EXPERIMENTAL PROCEDURES AND CHARACTERIZATION TECHNIQUES



- 2.1. Introduction
- 2.2. Chemicals, solvent and materials used for the applicative purpose
- 2.3. Synthesis of core-shell like amine functionalized SiO₂ NPs on CCTO NPs
- 2.4. Synthesis of CCTO@SiO₂ core-shell NPs decorated on the sheet like Graphene oxide (GO) nanocomposites
- 2.5. Amino-acid based stimuli responsive biocompatible [PEG-*b*-PBLG-*b*-PBLA] nano micelles synthesis
- 2.6. Synthesis of polypepto vesicle sized [[(α -OCH₃- ω -NH-PEG)-b-(PBLA)₇-b-(PBLG)₁₇]
- 2.7. In vitro studies
- 2.7.1. Antibacterial susceptibility test
- 2.7.2. In Vitro Cell maintenance for cytotoxicity assay test
- 2.8. Characterization Techniques/ Instrumentation

MATERIALS AND METHODS

2.1. Introduction

This chapter includes required chemicals and materials, synthesis methods, experimental procedures and characterization techniques in detail for the study of morphologically varying of organic-inorganic solids and amino acid based triblock copolymeric nanomaterials. Nanomaterials in this dissertation are of two different types (a) organic-inorganic solids (b) amino-acid based triblock copolymeric nanomaterials. Morphologically varying organic-inorganic solids and amino acid based triblock copolymeric nanomaterials were designed by modified sol-gel techniques, various nano chemical processes and modified ring opening polymerization along with catalytic debenzylation, crystallization, recrystallization and purification methods

2.2. Chemicals, Solvent and materials used for the applicative purpose

Table 2.2.1: List of Solvents Used for This Work

Sl No	Solvent name	Make
1	Cyclohexane (C ₆ H ₁₂ , 99.5%)	FINAR
2	Tetrahydro Furan (THF)	FINAR
3	Dimethyl Sulphoxide (DMSO)	Sigma Aldrich
4	Methanol (CH ₃ OH, <99.9% pure)	FINAR
5	Ethanol (C ₂ H ₅ OH, <97.9% pure)	MERCK
6	Acetone (CH ₃ COCH ₃ , <99.9% pure)	SDFCL
7	Iso-Propanol(C ₂ H ₅ OH, <99.9% pure)	FINAR
8	Ethyl Acetate	FINAR
9	Petroleum Ether (n-Hexane)	FINAR
10	Deionized Water (DDI H ₂ O)	UOH
11	Chloroform (CHCl ₃)	Sigma Aldrich
12	Duterated chloroform (CDCl ₃)	FINAR

Table 2.2.2: List of Precursor Materials Used for This Work

S1 N0	Chemicals name	Make
1	Calcium Carbonate (CaCO ₃ , 99%)	Sigma Aldrich
2	Titanium Dioxide (TiO ₂ , 99%)	Sigma Aldrich
3	Cupric Oxide (CuO, 99%)	Sigma Aldrich
4	Tetraethylorthosilicate (TEOS, 98%)	Sigma Aldrich
5	(3-Aminopropyl) triethoxysilane (APTES, 98%)	Sigma Aldrich
6	Ammonium Hydroxide (NH ₄ OH, 95%)	Sigma Aldrich
7	Igepal (99%)	Sigma Aldrich
8	Triphosgene (>99.9%)	Sigma Aldrich
9	L-Glutamic acid-γ- benzyl ester (>98%, Sigma-Aldrich)	Sigma Aldrich
10	L-Aspartic acid-β- benzyl ester (>98%, Sigma-Aldrich)	Sigma Aldrich
1.1	α-Methoxy-ω-amino PEG [MeO-PEG-NH ₂ (>98.5%, 5000	Iris Biotech GMBH,
11	Dalton),	Germany
12	α-Methoxy-ω-amino PEG [MeO-PEG-NH ₂ (>98.5%, 2000	Iris Biotech GMBH,
12	Dalton),	Germany
13	Sodium Bicarbonate (NaHCO ₃) (>98.5%)	SRL
14	Palladium activated carbon charcoal (10%) (>99.9%, sigma- aldrich)	Sigma Aldrich
15	Benzophenone (>99.9%)	Sigma Aldrich
16	Phosphotungstic acid (PTA, >93.8%)	Sigma Aldrich
17	Na metal(>99.9%, dipped in mineral oil),	Sigma Aldrich
18	Potassium Bromide (KBr, >99.9%)	Sigma Aldrich
19	Graphite powder (synthetic powder)	Sigma Aldrich
20	Sulphuric Acid (conc. H ₂ SO ₄ , 95-98%, ACS reagent)	Sigma Aldrich

21	Potassium Persulphate (K ₂ S ₂ O ₈), (99%, ACS reagent)	Sigma Aldrich
22	Phosphorous Pentoxide (P ₂ O ₅ , 99.9%)	Sigma Aldrich
23	Potassium Permanganate (KMnO ₄ , 99.9%)	Sigma Aldrich
24	Hydrogen Peroxide (H ₂ O ₂)	Sigma Aldrich
25	Hydrochloric Acid (dil. HCl solution, 37%, ACS reagent)	Sigma Aldrich

Table 2.2.3: List of Materials Used for Application Purpose of This Work

Sl No	Materials Name	Make
1	Silver Paste cat. no. 735825	Sigma Aldrich
2	Polyvinyl Alcohol (PVA)	Sigma Aldrich
3	MTT (Methyl Thiazolyltetrazolium)	SRL
4	DMEM Medium (Dulbecco's modified eagle medium)	GIBCO
5	MDA-MB231 (Human breast carcinoma cells)	NCCS PUNE, INDIA
6	gram negative Escherichia coli (ATCC-25922)	Supplier Hyderabad
7	gram positiveStaphylococcus aureus (ATCC-25923)	Supplier Hyderabad
8	Medium	Supplier Hyderabad

In detailed, the list of chemicals has been provided for the synthesis of organic-inorganic solids and amino acid based triblock copolymeric nanomaterials from different makers and suppliers. The chemicals with high purity have been used without further purification and modification.

2.3. Synthesis of core-shell like amine functionalized SiO₂ NPs on CCTO NPs

2.3.1. Synthesis of CCTO NPs

CCTO has been synthesized by solid-state reaction method using the stoichiometric amount of CaCO₃, TiO₂ and CuO as a precursor. The precursors were mixed with acetone for 24 hr with the help of an agate mortar followed by drying. Then the mixture was allowed under calcination for 8 hr at 800°C with the atmospheric condition. The CCTO NPs were collected and used for the further synthesis of core/shell materials.

2.3.2. Synthesis of CCTO@SiO₂-NH₂ NPs

CCTO@SiO₂-NH₂NPs have been successfully synthesized by an improved sol-gel method. Pure CCTO NPs (500 mg) were taken with 50 ml of cyclohexane and ultrasonication was performed for 10 minutes. Igepal 50 (2 ml) was added dropwise to the given solution as a surfactant and allowed under ultrasonication for 20 minutes. The same ratio of Igepal 50 and conc.NH₄OH was added to the above solution dropwise and sonicated for 30 minutes. The reaction mixtures were separated into a few sets of the reaction medium with different concentrations of TEOS and APTES (1:2:3) and added to each solution of mixture set. The solution sets were allowed on an orbital shaker (48 hrs, 600 rpm, 25°C). The solid particles were collected by repeated centrifugation (30 mints, 10000 rpm) and washing processes with distilled water followed by ethanol. The purified materials were collected and dried at 100°C. All the samples were characterized by standard methods. Before sintering the synthesized aminated CCTO@SiO2 core-shell NPs, we named the samples as pure CCTO (PCNS), CCTO@SiO₂-NH₂-5 nm (CS1NS), CCTO@SiO₂-NH₂-10 nm (CS2NS), and CCTO@SiO₂-NH₂-20 nm (CS3NS) respectively and after sintering the samples at 1000°C for 6 hrs, the samples are designated as pure CCTO (PCS), CCTO@SiO₂-5 nm (CS1S), CCTO@SiO₂-10 nm (CS2S) and CCTO@SiO₂-20 nm (CS3S) respectively. Samples are prepared as pellets for the dielectric study as listed in **Table** 2.2.3.

2.3.3. Preparation of Pellet for Dielectric analysis

The impedance experiments have been performed by the pellets which were made up of 150 mg of CCTO@SiO₂-NH₂ NPs and 1 mg of PVA. The diameters of the prepared pellets were around 8 mm and thickness around was 1.5 mm. The powder was compressed with 2 tonnes of pressure load for 1 minute. The pellets were allowed to keep in a hot oven at 120°C for the removal of moisture and other impurities in it. To observe the

dielectric behaviour of the material at high temperature, e.g. 1000°C, the proper electroding was done by using silver paste (Cat. No. 735825, Sigma-Aldrich) on both sides of the pellet and allowed for drying further at 50°C for 2 hrs. The final dimensions of the pellets were found to be approximately 8.0 mm in diameter and 1.5 mm in thickness (Shown in **Table** 2.3.1).

Table 2.3.1: Show the details of the sintered CCTO@SiO₂-NH₂ NPs sample properties

Commla	Silica ratio	Thickness of the silica	the diameter of the	The thickness of the
Sample	TEOS: APTS (shell (nm) (measures	sinter palette (mm)	palette (mm), (after
Name	μl)	through TEM)	(after sintering)	sintering)
PCS	0:0	No silica	7.85±0.120	1.25±0.10
CS1S	150:50	(3-5)	7.87±0.11	1.25±0.12
CS2S	300:100	(7-10)	7.86±0.12	1.25±0.11
CS3S	450:150	(15-17)	7.85±0.14	1.25±0.13

2.4. Synthesis of CCTO@SiO₂ core-shell NPs decorated on sheet like Graphene oxide nanocomposites

2.4.1. Synthesis of GO:

Graphene oxide (GO) was synthesized from an established Hummer's method. We have reported the synthetic procedure for GO in our previous work [203].

2.4.2. Synthesis of CCTO@SiO₂ NPs

CCTO@SiO₂ NPs were synthesized by the general sol-gel method and cyclohexane as an appropriate solvent. CCTO@SiO₂NPs have been successfully synthesized by following the sol-gel synthetic method. 1gm of CCTO NPs were taken with 130 ml of cyclohexane and allowed under for few minutes. 5 ml of Igepal-50 was added dropwise to the given solution and allowed under ultrasonication for 30 minutes. The ratio of Igepal-50 and conc.NH₄OH was maintained with the previously used condition and added to the above solution dropwise. The solution mixture was allowed under sonication for 30 minutes. Numerous ratios of silica

(APTS: TEOS) have been used for the synthesis of CCTO@SiO₂ NPs through sonication and centrifugation process maintaining other environmental parameters too. After 48 hrs of reaction on a shaker at 600 rpm, the products were collected by centrifugation and washing processes with distilled water followed by ethanol.

2.4.3. Synthesis of CCTO@SiO₂-GO

CCTO@SiO2-GO nanocomposites were synthesized using the modified sol-gel method in which, CCTO@SiO₂ NPs and GO act as precursor materials which are previously synthesized by hammer's method and sol-gel process respectively. The mixture is allowed under hydrolysis process and sonication for few minutes in different ratios. These solutions are poured into a reagent bottle and allowed for sonication for 4 hours by consistently maintaining room temperature (RT). Several decoration types of CCTO@SiO₂-GO nanocomposites are mainly depended on few environmental parameters given in the belowattached **Table** 2.4.1. The concept of covalent bonding of silica and GO or amide bonds may play the role for the synthesis of CCTO@SiO₂ NPs on the surface GO sheet. The reasons of choosing water as the suitable solvent as FTIR study has shown a clear image of C-N bond present in the composites which may arise due to the interaction between carboxylic -COOH, hydroxyl (-OH) or ether (-O-) of GO and -NH₂ or SiO₂ groups of CCTO@SiO₂ NPs. C-N bond is strongly polarized towards N due to the presence of lone pair in N so why the dipole moment arises making C-N bond soluble in water [208]. After the process of sonication completes the solution bottle is kept in a shaker for 72 hrs at 600 rpm. With the completion of 3days, the composite material was continuously centrifuged with distilled water at high rpm 14000, 30 minutes and very low temperature. Once the centrifugation is over, the material was allowed for drying at 100°C and the grey colour material was collected. Various steps of the sol-gel synthesis method of CCTO@SiO₂ NPs are shown in **Schematic** 3.1.1.

Table 2.4.1: Synthesis of CCTO@SiO₂-GO nanocomposites at different condition

Sample Name	CCTO@ SiO ₂ NPs	Amount of CCTO@SiO ₂ N Ps	Amount of GO NPs	Shell thickness	Sonication Time	rpm
CSG1	CS 3	50	50	3 nm	45 mints	14000
CSG2	CS 7	50	50	5-7 nm	3 hrs	14000
CSG3	CS16	100	25	15-20 nm	3 hrs	12000

Several experiments were performed but among all the synthesis procedure it is confirmed that at higher rpm of the centrifugation process helps in better extraction of water like solvent along with unnecessary surfactant from the final product of the composite material. This method also signifies that more time of shaking also enhances the spreading/decorating capability of silica coated CCTO on the surface of GO.

2.5. Amino-acid based stimuli responsive biocompatible [PEG-b-PBLG-b-PBLA] nano micelles synthesis

2.5.1. Synthesis of NCA BLG and NCA BLA

In brief, a solution of triphosgene (2.5 g, 0.0043 mol) each in 50 mL dry THF was added to a milky white solution of L-glutamic acid γ -benzyl ester (4 g, 0.0085 mol) in 50 mL of THF in round bottom 1 (RB1) and L-aspartic acid- β -benzyl ester (4.2gm) in 50 ml of THF in RB2. The reactions were carried out in an inert atmosphere, as the reducing agent and solvent medium are very sensitive to the moisture. The mixtures were stirred for around 4h at 50 °C and after the initial step completed, the product formation was observed as a clear solution. Purification of NCAs was done by evaporation followed by crystallization and recrystallization methods (Hexane: THF, 1:1). The yield of NCA BLG is 3g (75%) and for NCA BLA 3.2gm (80%).

2.5.2. Synthesis of Diblock copolymer [PEG-b-PBLG]

The synthesis method for AB type [PEG-*b*-PBLG] diblock polymer has been followed in detail as reported in our earlier work.

2.5.3. Synthesis of a triblock copolymer of [PEG-b-PBLG-b-PBLA]

This method involves the conversion of acid to anhydride with the help of a reducing agent triphosgene which is highly hygroscopic. 4 gm PEG was added to a solution of 1.6 gm of NCA BLG and allowed for 72 hrs of reaction till it produced a shiny pale yellow solid. After 72 hrs of reaction, the dissolved solution of NCA BLA with dry THF was added to the [PEG-b-BLG] solution. The reaction mixture turned into a transparent solution after the addition of NCA BLA. The reaction mixture was again allowed to stir for 72 hrs at 600 RPM and 40°C with an inert atmosphere till the completion of the reaction. After the completion of the reaction, the mixture was evaporated and purified through recrystallization method (hexane and THF). Then hydrogenation was performed using Pd-C, H₂/THF to obtain the final block copolymer. The synthesized product was collected and allowed for freeze-drying.

In short, the AB diblock copolymer of PEG-*b*-BLG has been synthesized first then the new block of NCA BLA has been attached to the electron-rich N-terminal of glutamate forming an amide -(C=O)-NH₂ bond. For better understanding, the prepared samples are designated as diblock [PEG-*b*-BLG] polymeric micelles and triblock [PEG-*b*-BLG-*b*-BLA] polymeric micelles before catalytic hydrogenation method.

2.6. Synthesis of polypepto vesicle sized $[(\alpha - OCH_3 - \omega - NH - PEG) - b - (PBLA)_7 - b - (PBLG)_{17}]$

2.6.1 Synthesis of NCA BLA and NCA BLG

NCA-BLA and NCA-BLG were synthesized under an inert atmosphere with dry solvent THF from L-aspartic acid-4-BE and L-glutamic acid-5-BE respectively. Revised ring polymerization of both the NCAs with the precursor (α-OCH₃-ω-NH-PEG) has resulted in nanovesicle sized ABC type triblock copolymer of [PEG-b-(PBLA)₇-b-(PBLG)₁₇]. A solution of triphosgene (5g, 0.0086 mol) in 50 ml dry THF was added to a powdered white solution of L-aspartic acid-4-benzyl ester (8 g, 0.0085mol) in 50 ml of THF in experiment system 1 and milky white solution of L-glutamic acid-5-benzyl ester (8 g, 0.017 mol) in 50 ml of THF in system 2 respectively under an inert atmosphere due to hygroscopic nature of reagent and solvent medium. Purification of NCAs was done when the reactions end after 4 hrs following evaporation and crystallization method (Hexane:THF). The yield of NCA BLA and NCA BLG were found to be 85% and 80% respectively.

2.6.2. Development of triblock copolymer of $[(\alpha\text{-}OCH_3\text{-}\omega\text{-}NH\text{-}PEG)\text{-}b\text{-}(PBLA)_7\text{-}b\text{-}(PBLG)_{17}]$

The previously reported method for the synthesis of AB type [PEG-*b*-(PBLA)₇] was followed [29]. After the synthesis of [PEG-*b*-(BLA)], following the same method we have added NCA GluA to the solution mixture of [PEG-*b*-(BLA)] and allowed for 72 hrs at 600 rpm and 45°C with an inert atmosphere condition so that the polymerization would take place completely. The Di-PA block copolymer of [PEG-*b*-(BLA)] has been synthesized first then the new block of NCA-BLG has been attached to the N-atom of aspartate forming an amide - (C=O)-NH₂ bond. The functional groups like carboxy (-COOH) and amine (-NH₂) helps for further condensation polymerization. The benzylic deprotection method of block copolymer with the help of Pd/C catalyst has led to the formation of benzene free block copolymer of [PEG-*b*-(PBLA)₇-*b*-(PBLG)₁₇]. The purified polymeric particles were collected and allowed for freeze-drying at a low temperature of -20°C.

2.7. In Vitro Studies

2.7.1. In Vitro Antibacterial activities with different stains

In vitro antibacterial susceptibilities of polymeric nanomaterials were investigated by prominent broth micro-dilution method using two microorganism *gram negative ATCC bacterial strains of Escherichia coli* (ATCC-25922) as well as with *gram positive Staphylococcus aureus* (ATCC-25923). The bacterial strains were taken and maintained at 4°C. Briefly, 5μl of the bacterial culture in each segment of 96-well plate followed by 150μl of broth containing 50μl different concentrations (1.25mg/ml with serial dilution up to 0.0048 mg/ml) of samples [PEG-*b*-PBLG-*b*-PBLA], [PEG-*b*-PBLG₅-*b*-PBLA₁₈], [PEG-*b*-(PBLA)₇-*b*-(PBLG)₁₇] and [PEG-*b*-(PBLA)₇] incubated for 24hr at a physiological temperature 37°C for both the bacterial strains. The last segment was the tenth segment consisting of bacterial strains but without any sample medium. We have studied the antibacterial activities of polymeric materials with different types of bacteria and have found the effectiveness of our materials for further biomedical applications. All the polymeric samples were characterized by suitable methods [265-266].

2.7.2. In Vitro Cell maintenance for Cytotoxicity assay test

The standard methyl thiazolyltetrazolium (MTT) assay was used for the biocompatibility test of the above polymeric samples using the human breast carcinoma cell of MDA-MB231 cells (obtained from National Centre for Cell Science (NCCS), Pune, India). Cells were cultured in Dulbecco's Modified Eagle medium (DMEM) supplemented with 10% heat-inactivated fetal bovine serum (FBS), 100 units/ml penicillin, 100µg/ml streptomycin and cultured at 37°C, 5% CO₂ humidified incubator. Details of the methods have been discussed in our previous reports [195,199].

2.8. INSTRUMENTATION

2.8.1. Physical Study Characterizations

- 2.8.1.1. Transmission Electron Microscopy (Morphology Analysis)
- 2.8.1.2. Field Emission Scanning Electron Microscopy (Morphology)
- 2.8.1.3. Energy Dispersive X-Ray Analysis Spectrometer (Elemental Analysis)
- 2.8.1.4. X-ray Diffraction (Crystalline nature)
- 2.8.1.5. Thermo-Gravimetric Analysis (Thermal Stability)
- 2.8.1.6. Raman Spectra (Atomic order)

2.8.2. Structural Characterization

- 2.8.2.1. Fourier Transform Infrared Spectroscopy (Identification of Chemical Functionality)
- 2.8.2.2. Proton Nuclear Magnetic Resonance Spectroscopy (positioning of hydrogens)
- 2.8.2.3. Matrix-assisted Laser Desorption/Ionization Mass Spectrometer (Exact molecular weight)
- 2.8.2.4. Dynamic Light Scattering Method (Size of macromolecules)

2.8.3. Biological and Physical Applicative Characterization

- 2.8.3.1. Dielectric Study (Dielectric constant and loss)
- 2.8.3.2 . Zeta potential measurement (Electro-kinetic potential)
- 2.8.3.3. Circular Dichroism (Secondary structure of proteins)
- 2.8.3.4 . Ultra-violet Spectroscopy (Absorbance band)
- 2.8.3.5. Laser Confocal Scanning Microscopy
- 2.8.3.6 . MTT Assay (Biocompatibility against human carcinoma cell)
- 2.8.3.7 . Antibacterial Susceptibility test (Killing Efficiency Bacteria)

Different Characterization Methods

2.8.1. Physical Study of the nanomaterials

2.8.1.1. Transmission Electron Microscopy (TEM)

Morphology and Elemental detection of four different types of dielectric solids and polymeric based nanomaterials i.e. core-shell like amine functionalized SiO₂ NPs on CCTO NPs, CCTO@SiO₂ core-shell NPs decorated on sheet like Graphene oxide nanocomposites, biocompatible [PEG-b-PBLG-b-PBLA] nano micelles and vesicle sized [[(α-OCH₃-ω-NH-PEG)-b-(PBLA)₇-b-(PBLG)₁₇]were analysed in a Transmission Electron Microscope TEM (Model FEI Technai G2 200 S -Twin).

The transmission electron microscope was used to obtain the size, shape, morphology and structure of the synthesized materials [265].

Sample preparation of organic-inorganic of dielectric solids

Organic-inorganic of dielectric solids were dispersed in ethanol and allowed under ultra sonication to avoid the agglomeration of CCTO NPs for 5 minutes. One drop of the dispersed solution was put on a carbon coated Cu grid followed by proper drying for 12 hrs. The sample containing Cu grid was allowed under accelerating voltage of 200kV and morphology of nanomaterials obtained.

Polymeric Samples preparation for TEM

The amino acid based polymeric samples were dissolved in mili-Q water by using vortex for 30 sec. Following drop casting method, one drop of polymer sample was placed on the Cu grid. The solvent was allowed to evaporate for 10 minutes. As the polymeric samples are very sensitive to voltage and to avoid the damage of samples, the coating of phospho tungstic acid (PTA) was preferred as a stain. PTA also helped to change the contrast of the samples at high voltage. Once the PTA solution dried for some time, the sample based grid was cleaned by casting off 1 drop of water to avoid an excess amount of PTA from the sample surface.

2.8.1.2. Field Emission Scanning Electron Microscopy (FESEM)

The field emission scanning electron microscope model Zeiss UltraTM was used to obtain the images of its surface morphology, patterned nanostructures, shapes and sizes the synthesized materials [265].

Preparation of Samples

The prepared samples were taken and a very small amount of it directly placed on the carbon tape and attached to the stub provided by instrument accessories. The gold coating was preferred to be done for around 50-60 second for the conductivity issue.

2.8.1.3. Energy Dispersive X-Ray Spectroscopy (EDAS)

This is a nondestructive energy dispersive tool to know the elements present in the new and unknown synthesized material. When a sample is allowed under a high energy electron beam, the excitation of electrons from the sample with numerous signals occurs. Among these exciting signals, X-rays happened to interact with the EDXS detector providing the peaks of present atoms in the material [265].

2.8.1.4. X-Ray Diffraction (XRD)

Structural characterization was carried out in a Bruker Powder AXS Model D8 Advanced X-Ray Diffractometer. The X-rays used is Cu K α of wavelength = 1.5408 °A. To investigate the crystalline, amorphous nature of the material, crystalline phase, crystallite size and distance of planes associated in the material, XRD used to be done as a primary assessment. The principle of powder based XRD instrument is that when a monochromatic X-ray beam falls on the synthesized nanomaterial, there are chances of excitation of various signals [265]. The Bragg's Law is the most important formula which satisfies the relation between the crystalline phase, bond angle, planes, diffraction properties and kinetics order of the material by,

$$n\lambda = 2d\sin\theta \qquad \qquad (15)$$

Where, n = integer

 $\lambda =$ Wavelength

d =atomic distance

 θ = Bond angle

Solid state crystal structure of synthesized material was studied through XRD in the range of 2θ value = 10° - 90° and time of 30 minutes.

2.8.1.5. Thermo Gravimetric Analysis (TGA)

TGA technique provides the information of variation of weight loss of synthesized material corresponding to change of temperature. Processes like dehydration after 100C, evaporation of the solvent and volatile materials, phase change at higher temperature and decomposition are the optimum functions [265]. Thermal stability of the materials was studied through TG/DTA (Thermo ONIXS Gas lab 300). The TG/DTA study was done in N₂atmoshpere from 30°C to 1000°C with a heating rate of 10°C/min. The thermal study including the weight loss percentage, amount of heat flow and phase transition was done by TG/DTA experiment. TGA gives the information of precise endothermic, exothermic behaviour along with the phase change study.

2.8.1.6. Raman Spectra (Atomic order)

To investigate the atomic order or disorder movement, Raman scattering study was carried out using Witech alpha 300 Raman Spectrometer. This is also associated with the study of vibrational as well as rotational motions of atoms and molecules present in the bulk and nano material. When the monochromatic light falls on the liquid or gas medium scatterer, a small fraction of beam tends to radiate scattered due to the collision phenomenon between molecules of sample and photons of light [265]. There are possibilities of stokes and antistokes lines mostly caused by lower and higher Raman frequencies respectively. In the Raman spectra, there are also possibilities of elastic and inelastic collisions formation which leads to modification of Raman lines causing various modes in the molecules. The Raman shift is also an important equation which defined as the difference between Rayleigh's line and Raman line;

$$\Delta V = V_R - V_0$$
(16)

Where. $\Delta v = Raman Shift$

 v_R = Rayleigh's line

 $\nu_0 = Raman \ line$

Structural Characterization

2.8.2.1. FTIR (Identification of Chemical Functionality)

Surface chemical structure of the nanomaterials, functional groups were investigated with FT-IR(Nicolet model impact -410) by making KBr by grinding in an agate mortar followed by making pellets. FTIR spectrum was collected after removing unnecessary background format.

This spectroscopy is mostly observed in between visible and microwave region (4000cm⁻¹ to 400cm⁻¹) of the electromagnetic spectrum. Following to Beer Lambert's law and Hooke's law, the principle and mechanism of FTIR are based on [266]. The equation for Hooke's stretching frequency is represented as,

$$\bar{v} = \frac{1}{2\pi\epsilon} \sqrt[2]{k/\mu}$$
(17)

Where, $\bar{\upsilon} =$ Stretching Frequency c = Velocity of light

k= Hooke's Constant

μ=Reduced mass

2.8.2.2. Proton (¹H) Nuclear Magnetic Resonance Spectroscopy

To know the positioning of the Hydrogen at respective functional groups and chemical structures, 1HNMR model no Bruker DPX ¹HNMR (400 MHz) (Ultra ShieldTM) has been used in this dissertation.

The principle and reason of NMR are associated with the presence of positive nuclei which create a magnetic field on their spin rotation with the application of an external magnetic field. In short, this spectroscopy reveals the relationship between the applied magnetic field and magnetic field of H atom. When the sample is placed in a magnetic field region, there is a probability of formation of two types of orientation by H atom i.e. alignment with and against the field. The proton aligned in the direction of the magnetic field generally absorbs energy whereas against the field led to the loss of energy [266]. Hence NMR term is satisfied with the resonance between nucleus and radio frequency together.

2.8.2.3. Matrix-assisted Laser Desorption/Ionization Mass Spectrometer (MALDI-TOF)

The exact molecular weight of the synthesized polymers was confirmed through a MALDI-TOF instrument model MALDI TOF/TOF-Autoflex III smart beam, Bruker Daltonics. In the year 1988, eminent scientist Hillenkemp and Karas have developed the MALDI TOF instrument for the purpose to estimate the molecular weight of protein, peptides, amino acids and other long range biomolecules. This is a quite extensive, non-destructive vaporization technique which provides the accurate weight of the material at a short period time. Here the sample is dissolved in the soluble medium (UV absorbing) forming matrix-matrix mixture and allowed to pass through the laser light. The matrix is the prominent factor due to the absorption phenomenon by laser light energy which found to be the main reason for vaporization and ionisation of the system [266]. During the experiment procedure, the velocity of ions derived from the matrix depends on its mass, energy and time.

Biological and Physical Applicative Characterization

2.8.3.1. Dielectric Study (Dielectric constant and loss)

Dielectric Study (Dielectric constant and loss) The dielectric studies of CCTO and CCTO@SiO₂ NPs/composites were performed after making of pellets within the electromagnetic frequency range of 20 Hz to 2 MHz using an Impedance spectrometer (AGILENT LCR Meter, Model E4980A Precession Impedance Analyzer). The dielectric study of material CCTO@SiO₂-GO nanocomposite was done by Impedance spectrometer after making of pellets. The pellets were prepared by the general method i.e. adding PVA as binder and water to help the powder mixed properly to give a better result.

2.8.3.2 . Zeta Potentia (Electro-kinetic potential)

ZETA analysis was performed through DLS instrument with model no Malvern 92 2008 instrument to give size distribution intensity along with potential raised on the interface of the particles. The principle lies with the illumination of the sample by a laser beam. The scattered light from the beam is detected at a known scattering angle θ by a fast photon detector [266].

2.8.3.3. Circular Dichroism (CD)

The secondary structure, physical properties and folding of proteins, peptides were studied through a Circular Dichroism instrument with model no JASCO Corp., J-810. The

principle deals with the differences between the absorption of left and right circularly polarized lights of molecules containing chiral chromophores [266].

Sample Preparation

The concentration of 0.5mg/1ml followed for each sample with the respective pH. For acidic pH, we have used electrolytes of 1M glacial acetic acid and 1M ammonium hydroxide solution. The UV wavelength recorded between 300-180 nm with the cell path length of 1mm.

2.8.3.4. Ultra-Violet Spectroscopy (UV-Vis)

This is spectroscopy where we can calculate the percentage of transmittance with the passing of a particular range of wavelength and frequency of light through the sample medium. UV-Vis absorption of the samples was studied through a UV-Vis-NIR spectrometer (LAMDA 750 spectrometer, PerkinElmer). The important components of UV instruments are Tungsten filament as light source, a discharge lamp, monochromator, detector, amplifier and recorder. The principle is when the monochromatic beam is allowed to pass through the sample medium and the other beam is passed through the reference sample, at that time the intensities of transmitted beams are compared over the decided instrumental wavelength range [266].

UV spectroscopy analysis based on Beer Lambert's law which stated as,

$$-\frac{dI}{dx} = \varepsilon' \, l \, c \qquad \qquad (18)$$

Where,

c = concentration of solution (mol.dm⁻³)

1 = length of the solution of light passes through (cm)

The structural elucidation of UV spectroscopy mainly focused on Frank Condon Principle where he suggested the rapidity of electronic transitions phenomenon and it's internuclear distance. In his theory, it is clear that the molecules participated during vibration does not change their inter-nuclear distance. When the sample is undergone UV experiment, the promotion of electrons from the ground state to excited state takes place and two types of transition occur i.e. spin-forbidden and symmetry forbidden transition. Spin forbidden

transitions are mainly based on the spin of electrons and symmetry forbidden transitions are mainly dependent on symmetry of molecules present in the samples.

2.8.3.5. Laser Confocal Scanning Microscopy (LCSM)

To overcome traditional microscopes, in 1975 Marvin and his team invented confocal microscopy images with better visualization of sample loaded with drugs, dye and infected cell lines. This is an advanced design of simple wide field fluorescence microscopy. Confocal Microscopy Laser imaging of polymeric nanoparticles was performed using a confocal microscope with model no Zeiss LSM 700. When a **laser** beam is allowed to pass through a light source and focused the samples by an objective lens into a small area, the required image is produced by the emitted photons of fluorophores [266].

2.8.3.6. MTT Assay (Biocompatibility against human carcinoma cell)

Multimode microplate reader can be used to study physical, chemical and biological behaviour of nanomaterials. The methyl thiazolyltetrazolium (MTT) assay was used for the bio-compatibility test of the above polymeric samples using the human breast carcinoma cell of MDA-MB231 cells. Cells were cultured in Dulbecco's Modified Eagle medium (DMEM) supplemented with 10% heat-inactivated fetal bovine serum (FBS), 100 units/ml penicillin, 100μg/ml streptomycin and cultured at 37°C, 5% CO₂ humidified incubator. The insertion of prepared cells placed in 96 well microplates with a uniform volume added to each block. After the preparation of samples, there are allowed under a specific wavelength light source.

For this dissertation work, we have used Multimode reader with model no iMarkTM Microplate Absorbance Reader, Bio-Red.

2.8.3.7. Antibacterial Susceptibility test (Killing Efficiency Bacteria)

Antibacterial Susceptibility test was performed by using Infinite 200 PRO NanoQuant, TECAN spectrometer. *In vitro* antibacterial susceptibilities of polymeric nanomaterials were investigated by easily available broth micro dilution method using two microorganism *gram negative ATCC bacterial strains of Escherichia coli (ATCC-25922)* as well as with *gram positive Staphylococcus aureus (ATCC-25923)*. The bacterial strains were taken and maintained at 4°C. Briefly, 5µl of the bacterial culture in each segment of 96-well plate followed by 150µl of broth containing 50µl different concentrations (1.25mg/ml with serial dilution up to 0.0048 mg/ml) of samples [PEG-*b*-PBLG-*b*-PBLA], [PEG-*b*-PBLG5-*b*-

PBLA₁₈], [PEG-*b*-(PBLA)₇-*b*-(PBLG)₁₇] and [PEG-*b*-(PBLA)₇] incubated for 24hr at a physiological temperature 37°C for both the bacterial strains. The last segment was the tenth segment consisting of bacterial strains but without any sample medium.

Other techniques and instruments have been used for the development of morphologically varying organic-inorganic solids and amino acid based block copolymeric nanomaterials.

CHAPTER-3

RESULTS AND DISCUSSION

Part I. Dielectric study on the Organic-inorganic nanoparticles

3.1 Results and Discussion: Part IA

A detailed study on the dielectric properties of CCTO@SiO₂ core-shell nanoparticles: Role of SiO₂ shell over CCTO core surface

3.2 Results and Discussion: Part IB

Dielectrics of graphene oxide sheets decorated with nanocomposite silica-coated calcium copper titanate (CCTO) nanoparticles

Part II. The biological study of the amino acid based block copolymeric nanoparticles

3.3 Results and Discussion: Part IIA

Stimuli responsive biocompatible synthetic polypetidic nano micelles: Novel approaches towards antibacterial & therapeutic applications

3.4 Results and Discussion: Part IIB

Designing of new triblock polypepto vesicle sized nanobiomaterials and its action upon antibacterial activity

RESULTS AND DISCUSSION

Part I. Dielectric study on the Organic-inorganic nanoparticles

Part IA: A detailed study on the dielectric properties of CCTO@SiO₂core-shell nanoparticles: Role of SiO₂ shell over CCTO core surface

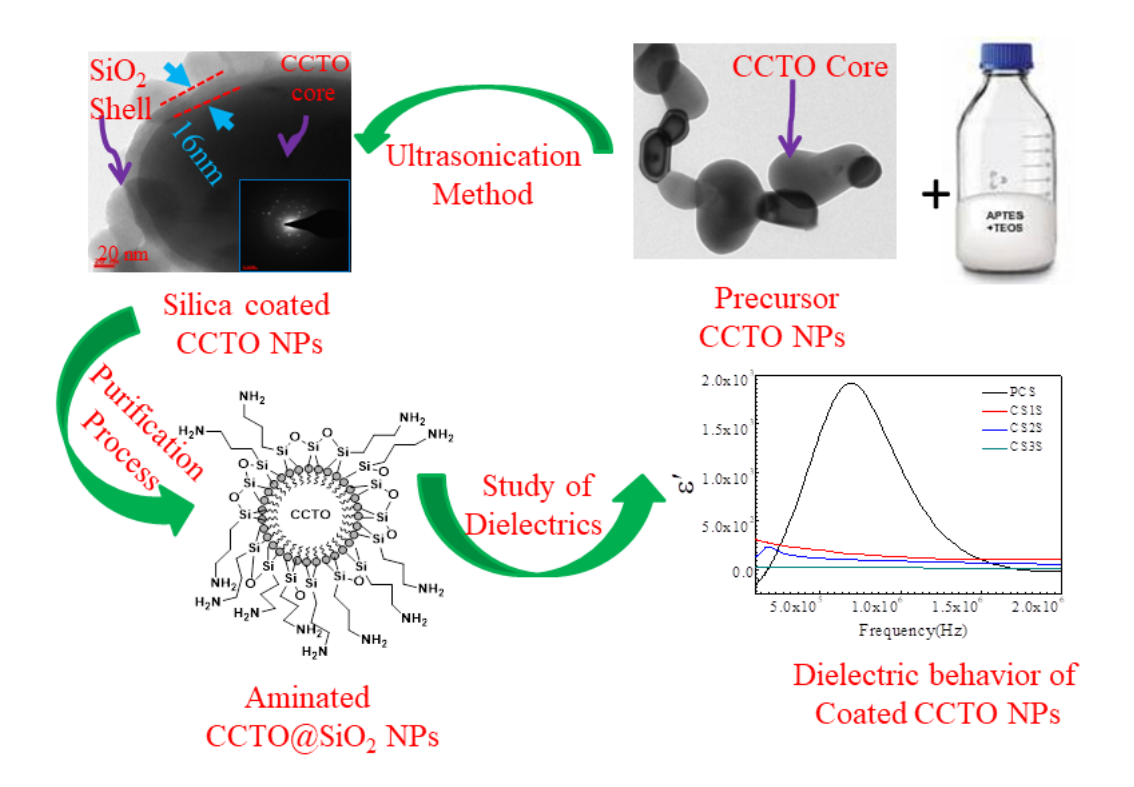


Table of Content for Part IA: CCTO@SiO₂core-shell nanoparticles synthesis, its dielectric behaviour and the role of SiO₂-NH₂ shell over CCTO core surface

Outcome from this part

1. <u>Bharatiya Debasrita</u>, Kumar K Santhosh, S Raghunandan & Paik Pradip. (2019). A detailed study on the dielectric properties of CCTO@SiO₂ core-shell nanoparticles: Role of SiO₂-NH₂ shell over CCTO core surface. **Journal of Solid State Chemistry**. 10.1016/j.jssc.2019.06.023

Objectives of this Part IA

Part IA (**Objective 1**): To synthesize CCTO@SiO₂ nanoparticles and design the respective NPs in core-shell aclimates of variant shell thickness range.

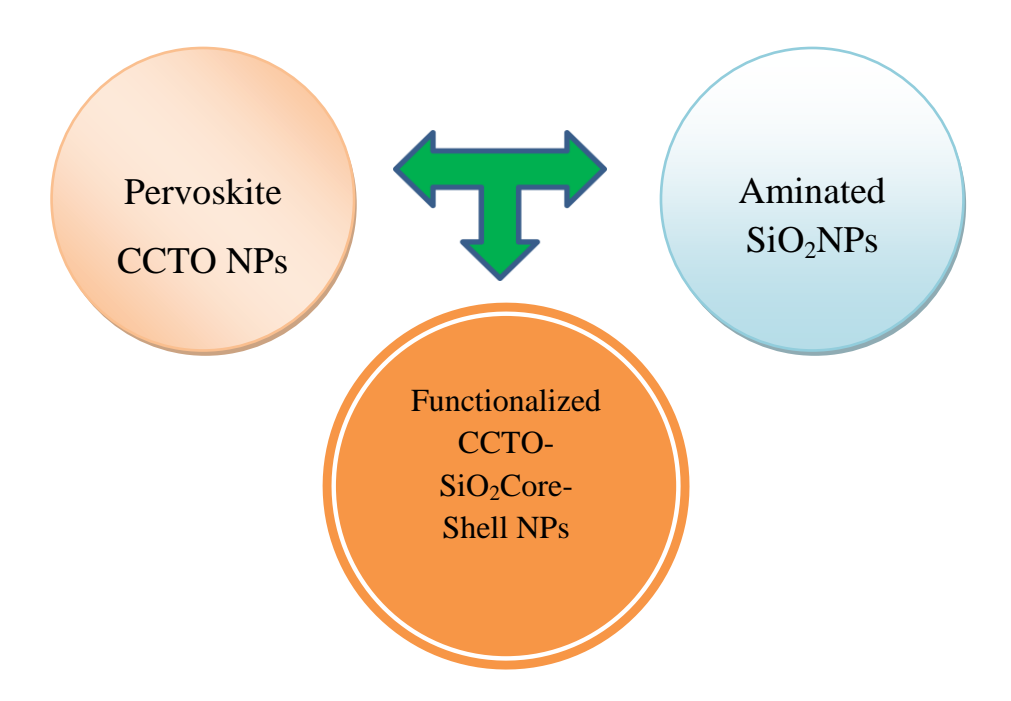


Figure 3.1.A. Objective diagram of CCTO@SiO2core-shell nanoparticles synthesis.

3.1.1. Abstract for This Part

In this part, an attachment strategy of an organic group –NH₂ has been developed with smart silica nanoparticles via sol-gel method. The inorganic metallic group of calcium copper titanate (CCTO) developed an electrostatic interaction with the amine functionalized silica to form a new core-shell type nanostructure. This approach of attachment is between an organic and inorganic part resulted in a high dielectric solid phase which further can be used for the electrical application purposes with its high dielectric constant and low loss. The morphology of CCTO@SiO₂ core-shell NPs consists of CCTO as core (dia. 100 nm - 300 nm), and silica as a shell of thickness from 5 nm - 20 nm with the increase in a weight percentage ratio of APTES: TEOS during chemical reactions. CCTO@SiO₂core-shell NPs were characterized with suitable characterization tools and the dielectric behaviours were measured through impedance measurement. The dielectric study confirmed that CCTO@SiO₂ core-shell NPs prepared at sintered temperature 1000°C (6h) has shown significantly high dielectric properties than nonsintered samples prepared at room temperature (RT). Further, with the increase in the shell thickness of coated SiO₂ on CCTO core, the dielectric constant ε', as well

as the dielectric loss ϵ'' values decreased at respective frequencies, ranges between 10^2 Hz and 2 MHz and vice versa. The study also suggests that at the lowest frequency of 10^2 Hz, CCTO@SiO₂ NPs with a thickness of ~15 nm shows a very low ϵ' value (1.39×10^2) whereas for shell thickness of ~5nm shows a maximum ϵ' value of 1.39×10^3 . However, with a change in the thickness of SiO₂ the values of ϵ' and ϵ'' varied with a regular trend $(10^2$ Hz to 2 MHz). The thinner and thicker coated SiO₂ on CCTO NPs exhibited ϵ'' of (0.39, 0.3) and (0.65, 4.49) at 1 kHz and 2 MHz, respectively. Looking at the very low tangent values of less coated CS1S, CCTO@SiO₂-NH₂ core-shell NPs, it is confirmed that the material is appropriate to use for electrical storage material. The values of ϵ' as a function of frequency for CCTO@SiO₂ core/shell NPs at different temperature range between RT to 300°C signifies that when coated sample undergoes heat treatment, it leads to the removal of some organic group before 150°C which contributes to the increase of ϵ' due to the property showing by CCTO surface towards the externally applied field. Finally, it can conclude that this series of CCTO@SiO₂ with a different dielectric constant can be used for designing various electronic devices.

3.1.2. Introduction and Motivation

Concentrating on the above facts, in this work we have designed a series of core-shell materials of CCTO and SiO2-NH2 NPs where CCTO has been used as precursor core and SiO₂-NH₂ as a shell so that with a change in the shell thickness, the properties of charge storage devices/ microelectronic devices can be tuned. The important factors like chemical functionalization on the surface, the microstructure of composite and nano or microparticles of CCTO strongly control the dielectric property as well as impedance properties of the nanocomposites. We have targeted for the development of these core-shell materials as better dielectrics than few other lanthanide series perovskite materials such as ACu₃M₄O₁₂ (M=La, Nd, Sm, Gd and Y) at 100K Hz and found to be succeeded [59]. Previously it is elucidated about perovskite oxides as excellent dielectrics material [76, 78]. This reason attracted us to focus CCTO as a base material for the development of this dielectric material. Due to the capability of forming uniform shell thickness, change of charge polarization and dipole moment due to presence of various polar groups, we consider SiO₂ as a shell material which further could help the CCTO to improve its stability even after sintering at a very high temperature (e.g. above 1000°C) with a long time heating. The other reasons why we choose silica as our shell nanomaterial are the absence of organic functional group, less chance of group lost after sintering at high temperature, and low dielectric loss. Few functionalizations of organic/inorganic groups on CCTO have been reported previously [167, 169], but no research has been done with amine functionalization of silica on CCTO. We aimed for a unique modification of amine coated silica on CCTO NPs and found to be effective for dielectric study. Herein, we have functionalized silica with an amine by using (3-Aminopropyl) triethoxysilane (ATPES) with tetraethyl orthosilicate (TEOS) for the better core-shell interaction to generate the required shell thickness along with covalent interaction and synthesized by the modified Stober method [187]. The impedance study was performed in the frequency range of 10^2 Hz and 10^6 Hz to find out the role of shell thickness in tuning the dielectric properties (real and imaginary) [267]. Further, the impedance studies also were performed at a very low frequency (at 20-100 Hz) to check how the interfacial polarization change with shell thickness [268, 269]. The studies were performed for both the sintered and non-sintered materials. Here, in this study, the role of -NH₂ and the chemistry behind the core-shell CCTO @SiO₂-NH₂ NPs have also been investigated in both the non-sintered and sintered materials. Again, the surface chemistry, dipolar polarization, thermal vibrations of involved groups which prove the variation of dielectric constant $\varepsilon'/\varepsilon''$ at different temperatures has also been studied. Adding to the exception, the non-sintered pure CCTO was showing better dielectrics than sintered, but choosing of sintered CCTO@SiO₂-NH₂ NPs core-shell material over non-sintered material for dielectric study as-sintered coated samples showing better dielectric behaviour than non-sintered NPs.

In conclusion, the remarkably new core-shell materials make it as new competing materials and allow the use as colossal permittivity materials which permit scaling advances in electronic devices with shell thickness.

In this chapter, the discussion of short synthesis method, characterization and application of $CCTO@SiO_2-NH_2$ core-shell like NPs have been represented.

3.1.2. Brief Synthesis Procedures of CCTO@SiO₂-NH₂ NPs

Detailed synthesis procedure for CCTO@SiO₂-NH₂ NPs has been described in the **chapter-2** and **section** 2.3.2. In short, core-shell CCTO@SiO₂-NH₂ NPs have been successfully synthesized by an improved sol-gel method. Pure CCTO was synthesized by solid-state reaction method [179]. Pure CCTO NPs along with cyclohexane were allowed for stirring following to the ultrasonication. The addition of surfactant Igepal 50 and

conc.NH₄OH was added to the above solution dropwise and sonicated. The reaction mixtures were separated into a few sets of the reaction medium with different concentrations of TEOS and APTES (1:2:3) and added to each solution of mixture set. The solution sets were allowed on an orbital shaker. The synthesized materials were collected by repeated centrifugation and washing processes. The purified materials were collected and dried at 100°C. All the samples were characterized by standard methods.

3.1.4. Reaction Pathway of prepared core-shell NPs

The proposed mechanism for CCTO@SiO₂-NH₂ NPs was followed by sol-gel method, hydrolysis, dehydrolysis, evaporation, centrifugation methods. The bonding interaction after the third step between aminated silica and CCTO NPs arises due to the electronic interaction of the lone pair of nitrogen present on the surface of silica led to the successful synthesis of CCTO@SiO₂-NH₂ NPs.

Schematic 3.1.1. Schematic illustration of the formation of core-shell CCTO@SiO₂-NH₂ NPs with a stepwise mechanism via sol-gel method.

3.1.5. Morphological Characterization of core-shell NPs by HRTEM

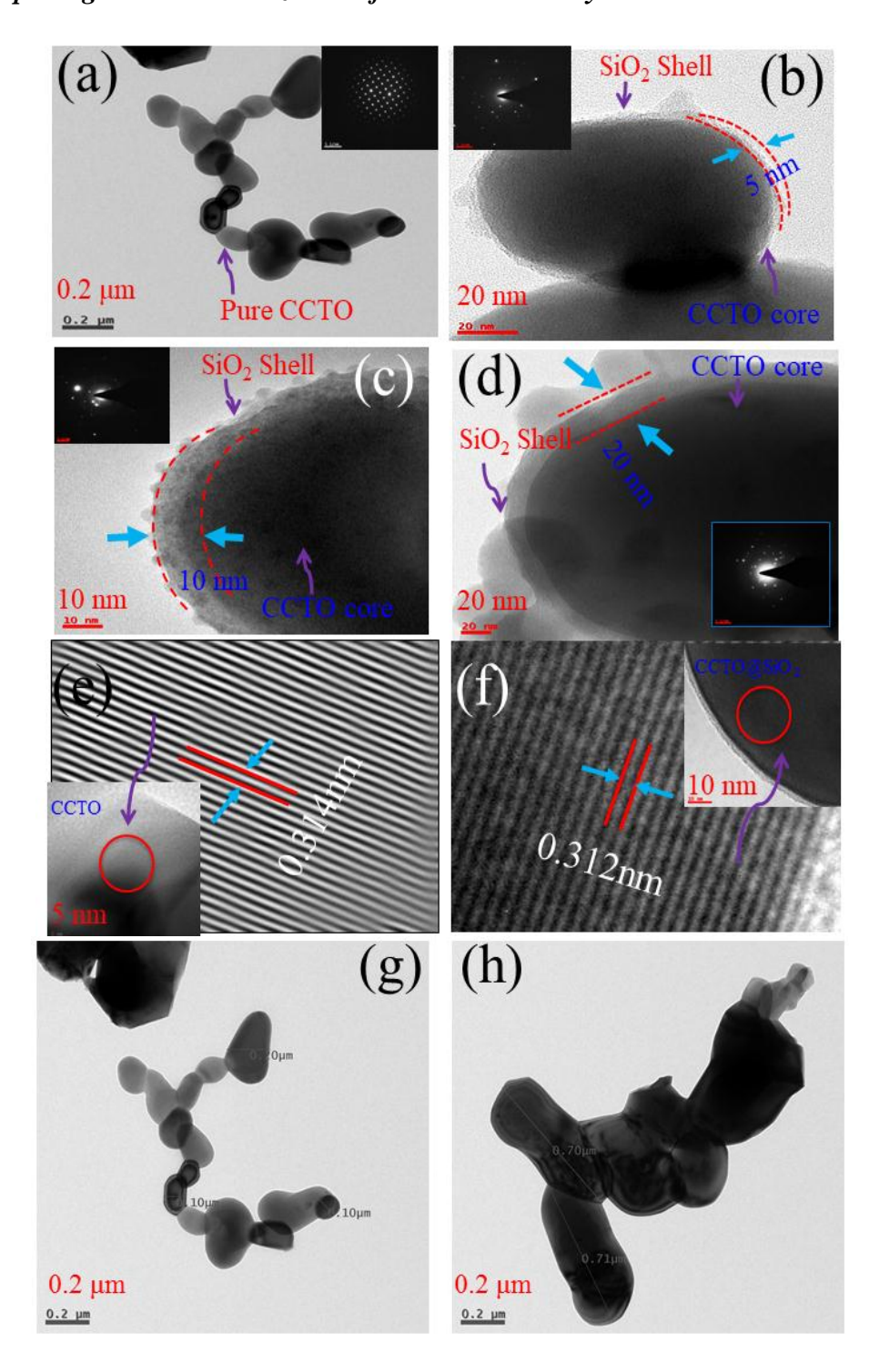
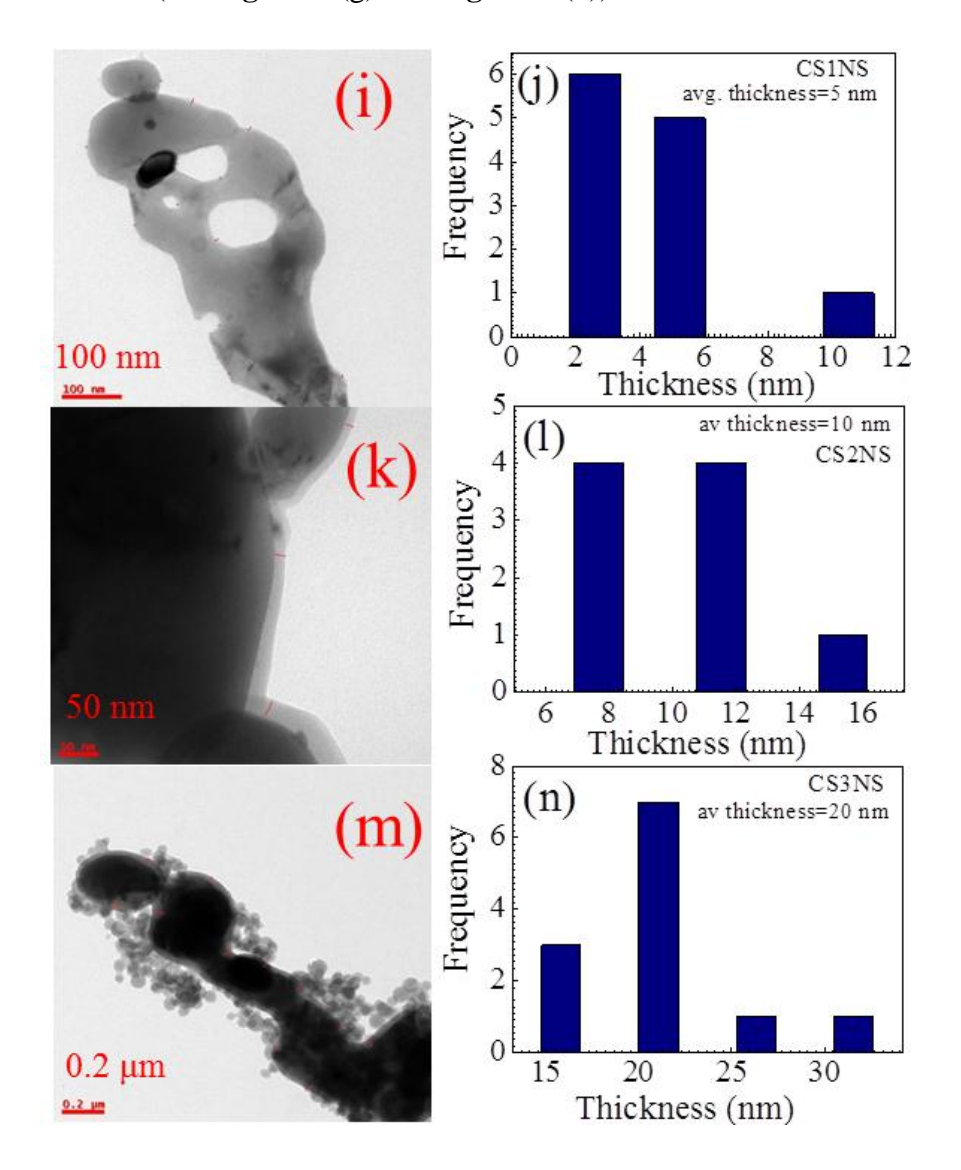


Figure 3.1.1. High resolution TEM images with varying shell thickness of aminated SiO₂ on CCTO core (a) PCNS (uncoated CCTO) (b) CS1NS NPs, 3-4 nm (c) CS2NS NPs, 7-10 nm (d) CS3NS NPs, 15-20 nm (e) IFTT image of PCNS and (f) IFTT image of coated CCTO@SiO₂-NH₂ NPs, (g) and (h) illustrate the length and diameter of uncoated PCNS NPs of 500 nm-700 nm and (h) 100-200 nm, respectively.

TEM micrograph of **Fig**. 3.1.1(a), showed the formation of bare uncoated CCTO NPs and the particle size are found to be average of 150-200 nm in diameter and length ranges from 500 nm-700 nm (see **Fig**. 3.1.1(g) and **Fig**. 3.1.1(h)).



Figures 3.1.1. (i)-(n) showed the HRTEM images with a varying shell thickness of aminated SiO₂ on CCTO core NPs. **Figs.** 3.1.1(i) CS1NS NPs (5 nm) 3.1.1(k) CS2NS NPs (10 nm) 3.1.1(m) CS3NS NPs (20 nm), respectively. **Figs.** 3.1.1(j), (l) and (m) have shown the average coating thickness of CS1NS, CS2NS and CS3NS, respectively.

The core-shell CCTO@SiO₂-NH₂ NPs are in **Figs**. 3.1.1. (b), (c) and (d) for different SiO₂-NH₂ thickness samples, respectively. From **Figs**. 3.1.1. (b), (c) and (d), it is seen that the thickness of SiO₂-NH₂ on CCTO is increasing from 5 nm to 20 nm, which includes CS1NS NPs (5 nm), CS2NS NPs (10 nm) and CS3NS NPs (20 nm), respectively. The average thickness of the SiO₂ shell of each sample has been confirmed by considering HRTEM image

consisting of more number of particles (statistical analysis) and the corresponding images and plots have been shown in the **Figs.** 3.1.1. (i) - 3.1.1. (n). The thickness of the silica layer coated on the CCTO particles was about 5 nm to 20 nm depending on the increase of silica ratio (APTES: TEOS) weight percentage during the chemical reaction which concludes to the increase of the shell thickness surrounded by CCTO core.

Here in above, we observed the CCTO NPs are surrounded by some shadows showing the presence of the SiO₂-NH₂ shell on the CCTO core and the difference in shadow thickness signifies to the coating of SiO₂-NH₂ NPs. The shadow of SiO₂ around CCTO is amorphous as the scattered light of TEM is allowed to pass through it [270, 172]. It is estimated that the average thickness of the SiO₂-NH₂ shell NPs are in between 5nm to 20nm and successfully coated on the surface of CCTO for the dielectric applications. The formation of a SiO₂shell of the CCTO core can be explained in three steps. In step-1, CCTO dispersed in cyclohexane in presence of Igepal-50. In the second step, in the presence of APTS and TEOS, the addition of NH₄OH forms sol-gel which contained amine functionalized SiO₂. In the third step, nucleates of SiO₂-NH₂ deposited on the surface of CCTO in such a way that the shell has grown with a uniform thickness. However, with a change in the content of APTES and TEOS the shell thickness can be varied as shown in **Figs**. 3.1.1. (b) - (d). From TEM (**Fig**. 3.1.1.), it is seen that the SiO₂-NH₂ shell is quite transparent to the electrons and the transparency of SiO₂ decreases with the increase in thickness from 5 nm to 20 nm **Figs**. 3.1.1. (b)-(d).

Figs. 3.1.1. (e) and (f) represent the IFTT images with a d-spacing value of 0.314 nm and 0.312 nm for PCNS and CCTO@SiO₂-NH₂ core-shell NPs respectively. The decrease of d spacing value in case of silica coated CCTO NPs is due to rearrangement of lattice positions from a CCTO NPs to CCTO@SiO₂-NH₂ core-shell structure. PCNS has shown the highest d values of 0.314 nm while other is showing a low value compared to it. The newly formed SiO₂-NH₂ shell on CCTO may have led to the decrease in the free atomic radii of Cu, Ti and O ions in CCTO upon external forces like covalent bonding.

3.1.6. Crystalline nature and Thermal stability performance studied by XRD and Thermal Analysis

Performing physical characterizations like XRD and TG-DTA, we have preferred nonsintered CCTO@SiO₂-NH₂ NPs over sintered to attain the aminated silica behaviour towards CCTO NPs. The crystalline nature of the samples was confirmed by XRD technique.

XRD was done in 2θ between 10° - 80° . XRD results exhibited the peaks of CCTO NPs which are cubic perovskite structure in nature.

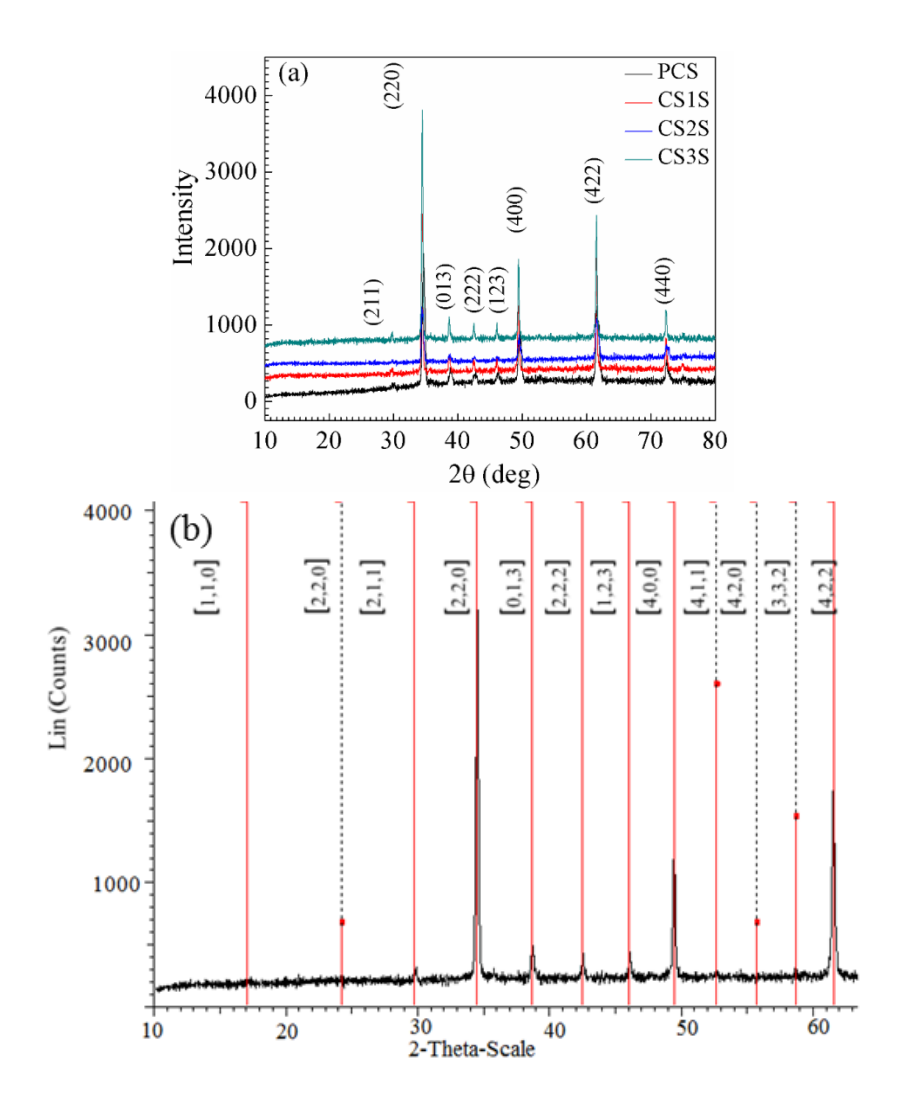
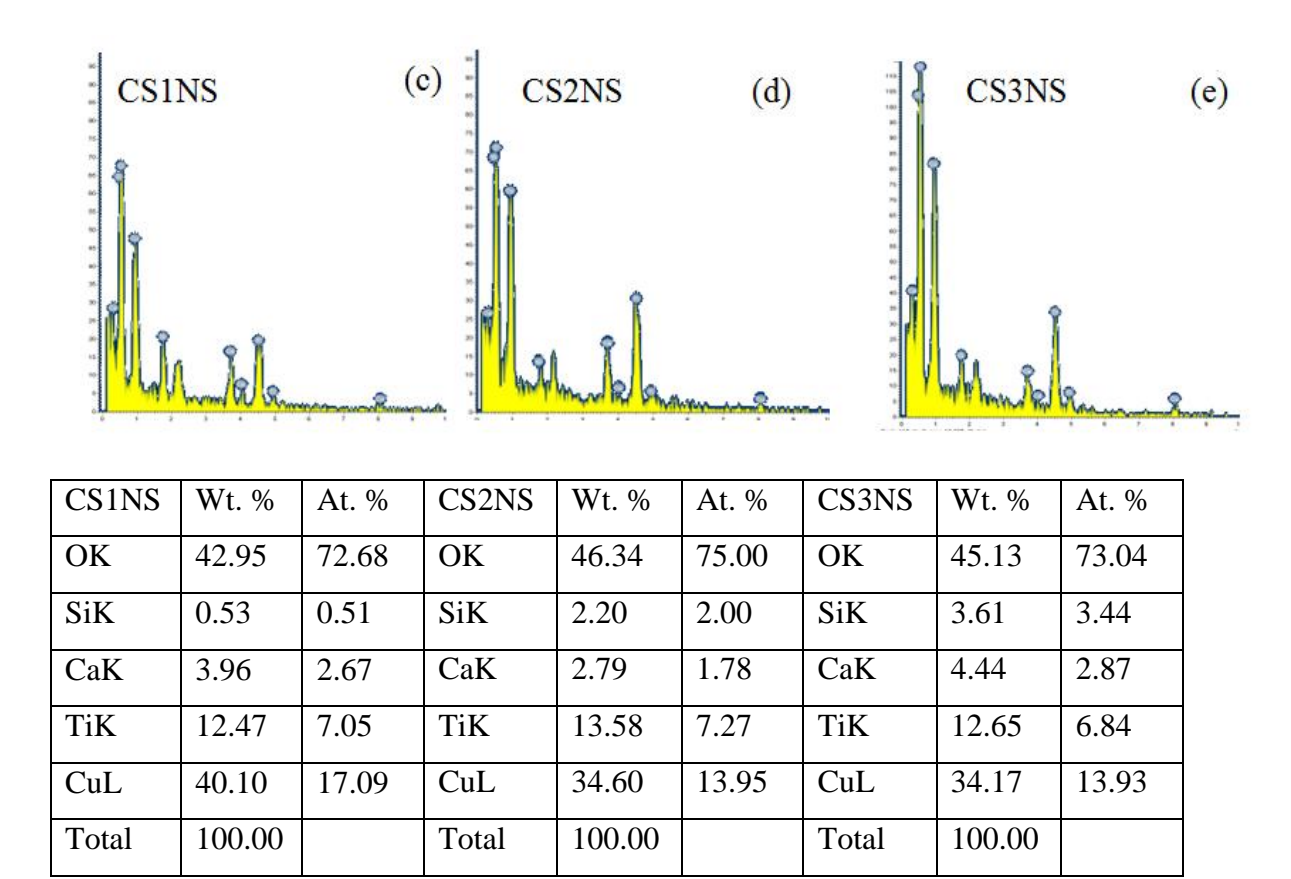


Figure 3.1.2. (a) X-Ray Diffractrogram pattern for nonsintered uncoated PCNS and coated CCTO@SiO₂-NH₂ NPs and **Fig.** 3.1.2. (b) represents JCPDS file number 01-070-0609 for CS3NS NPs.

From **Fig**. 3.1.2. (a), the XRD diffraction peaks are appeared at $2\theta = 31.1^{\circ}$, 34.3° , 38.2° , 43.7° , 46.5° , 49.8° , 63.8° and 74.2° for diffraction plane of (211), (220), (310), (222), (321), (400), (422) and (440), respectively [171, 187]. The prominent peak with plane 220 at 34.3° indicated the presence of precursor CCTO NPs. Since the extent of SiO₂ is very less, therefore, the peak positions for CCTO NPs and CCTO@SiO₂-NH₂ NPs remained unaltered due to the amorphous nature of SiO₂ shell. The JCPDS card number 01-070-0609 of CS3NS NPs has been attached on **Fig** 3.1.2. (b).



Figures 3.1.2. (c), (d) and (e) EDX graph and table obtained from FESEM of CS1NS, CS2NS and CS3NS NPs respectively.

From EDAX images **Figs**. 3.1.2. (c) - (e), it is observed the presence of very less amount of amorphous SiO₂-NH₂ along with oxygen in coated CS1NS, CS2NS, and CS3NS NPs.

The thermal analysis of nonsintered PCNS and CCTO@SiO₂-NH₂ NPs are shown in **Fig.** 3.1.2 (f). TGA graph showed a weight loss of PCNS NPs up to a maximum of 3% and CS1NS, CS2NS and CS3NS up to 1%, 3% and 14%, respectively. The least aminated silica coating on CCTO caused a lower weight loss than precursor CCTO proving the synthesized material more thermally stable. The highest percentage of weight loss occurs in case of CS3S NPs and it may be due to the presence of a high amount of functionalized silica groups along with organic amine component attached to the core surface which has been lost due to heating at 1000°C.

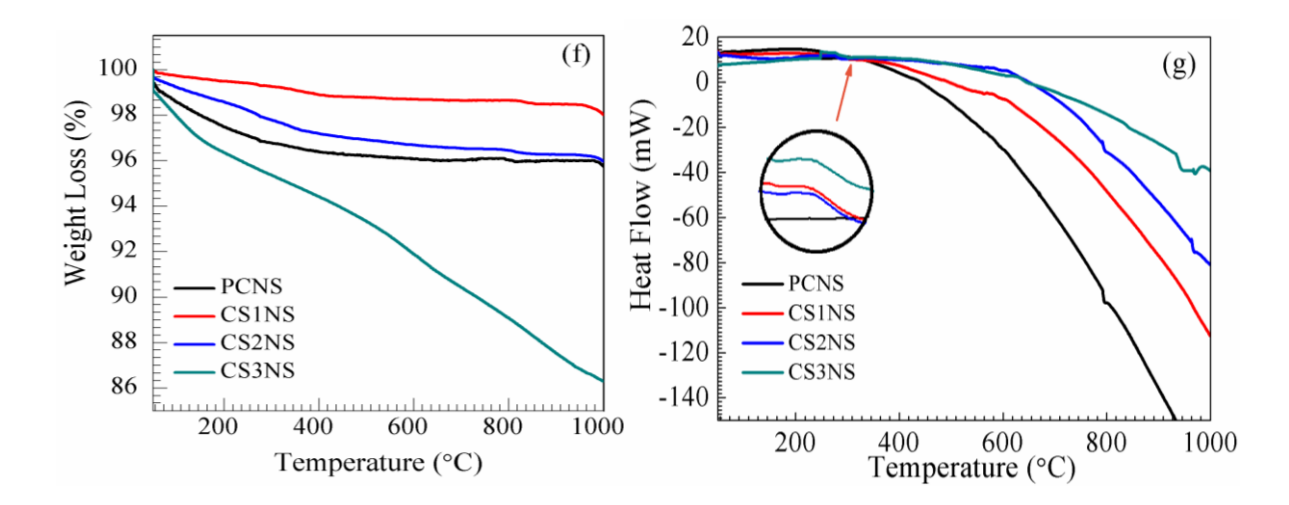


Figure 3.1.2. (f) and 3.1.2. (g) represents TGA and DTA thermogram for nonsintered uncoated PCNS and coated CCTO@SiO₂-NH₂ NPs with a heating rate of 10° C per minute in N₂ atmosphere respectively.

Fig. 3.1.2. (g) explained the DTA curve exhibits one endothermic peak and two exothermic peaks for all the sample of uncoated PCNS and coated CS1NS, CS2NS, and CS3NS NPs. The presence of an exothermic peak at 276°C is concerned with the decomposition of many organic functional groups associated in the NPs. In the meantime, a significant weight loss due to the evaporation of water and decomposition of the organic compound is observed in the TGA plot around 280°C. The first endothermic peak was observed around 600°C for all the coated NPs except PCNS may be due to the melting of organic functional groups. The second endothermic peak at 795°C in the DTA curve is related due to the secondary phase formation of perovskite CCTO and CCTO@SiO₂-NH₂ [271, 272].

The sharp endothermic peak at 795 °C also led to the crystalline change of the CCTO@SiO₂-NH₂ NPs. Previous reports have verified the weight loss of precursor CCTO around 10% [187, 273] whereas our work has shown the loss up to a minimum 1% in lowest amine coated silica CCTO NPs. Silica with organic functionalization have shown its loss up to 50% previously reported [274, 275] after 500°C, but exception happened when loss decreased to only 1% at 1000°C after coated with CCTO NPs. Hence, all the synthesized coated samples are thermally quite stable up to 1000°C. The CS1NS is the most effective material for thermal application which is also confirmed from the dielectric study in the below discussion.

3.1.7. Functional group identification by FTIR experiment

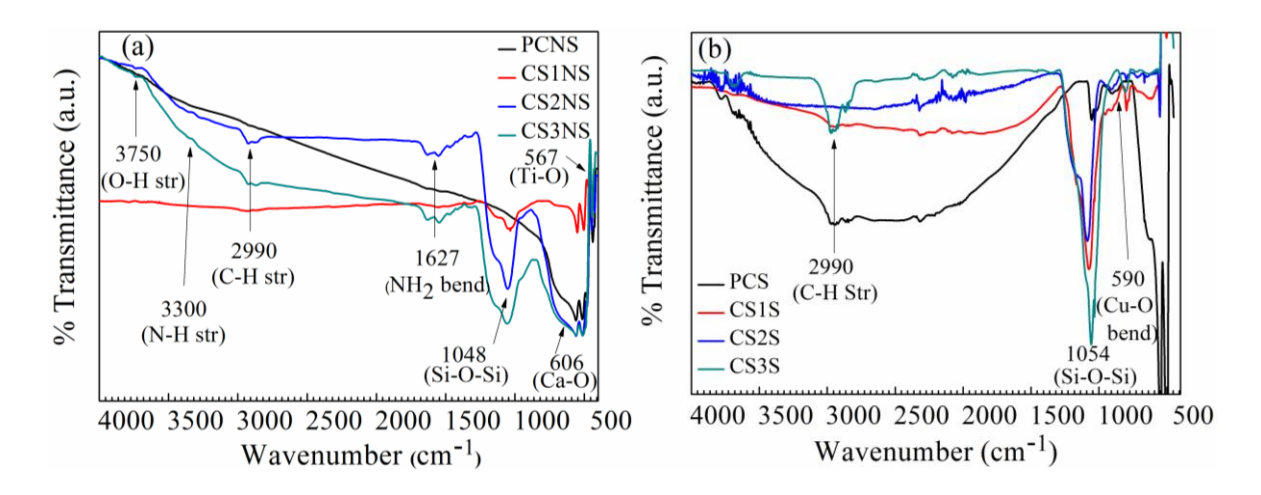


Figure 3.1.3. Comparison between FTIR spectrums for (a) non-sintered PCNS, CS1NS, CS2NS and CS3NS NPs (b) sintered PCS, CS1S, CS2S and CS3S NPs, respectively.

We performed FTIR experiments for non-sintered and sintered CCTO@SiO₂-NH₂ NPs to check the functionality and chemical groups present in the composites at room temperature and high temperature i.e. 1000°C, 6 hr. This difference will help us to make easy distinguish of chemical functionality at various temperatures like RT and 1000°C. Figure 3.1.3. (a) has shown the characteristic absorption bands at 1048 cm⁻¹ appeared due to asymmetric stretching vibration of Si-O-Si. The peaks at 3300 cm⁻¹ and 1627 cm⁻¹ are corresponding to the N-H stretching and bending modes of amine molecules present in nonsintered CCTO@SiO₂-NH₂ NPs but absent in sintered CCTO@SiO₂ NPs (see Fig. 3.1.3. (b)). The sharp band at 3000 cm⁻¹ and 1376 cm⁻¹ are corresponding to C-H stretching and bending mode. But in this case, the hump formed shows the presence of the SiO₂ group. Fig. 3.1.3. (b) showed the FTIR spectrum for samples sintered at 1000°C temperature, where all the organic contents (amine,-CH₂, -OH etc.) are removed (see TGA results, Fig. 3.1.2. (f)) whose functional groups usually show the FTIR bands at 3500 cm⁻¹ and 1635 cm⁻¹. Both sintered and non-sintered NPs show a peak at 3750 cm⁻¹ which may be due to the presence of free O-H bonds. For all the samples, the vibrational mode of Ti-O-Ti showed a peak at 470 cm⁻¹, Ca-O showed at 606 cm⁻¹, whereas the bending mode of Cu-O showed a peak at 590 cm⁻¹ [276]. It is worth mentioning that all the samples are containing CCTO with Ca-O, Cu-O and Ti-O-Ti bond.

3.1.8. Comparative Raman Study between sintered and nonsintered samples

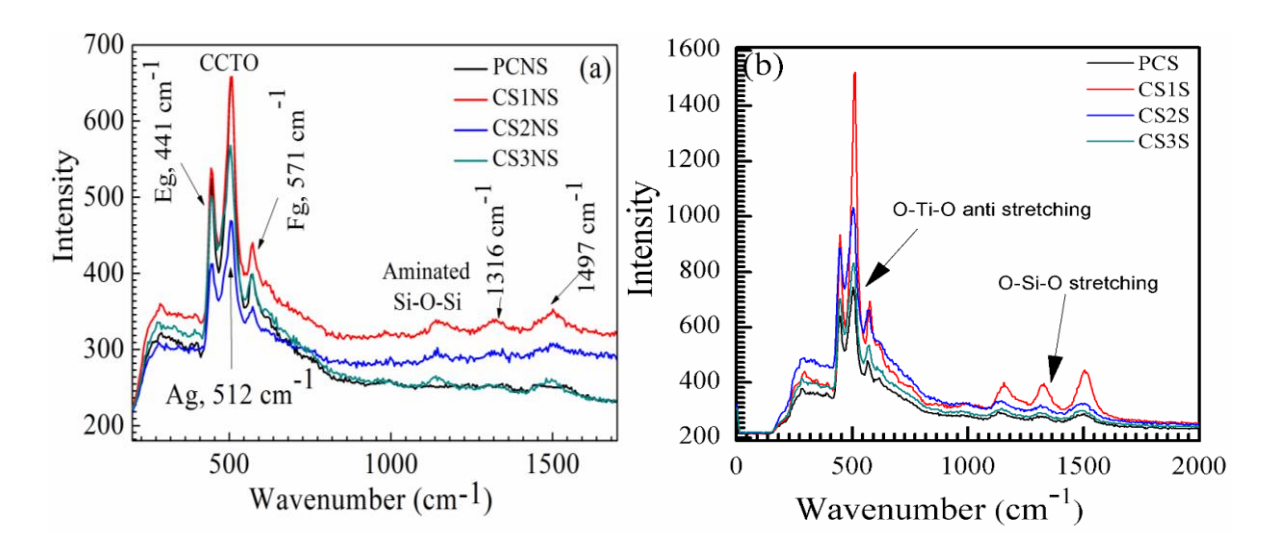


Figure 3.1.4. Comparative study of RAMAN spectrums for (a) non-sintered PCNS, CS1NS, CS2NS and CS3NS NPs (b) sintered PCS, CS1S, CS2S and CSNS) NPs, respectively.

Further, the CCTO and CCTO@SiO₂-NH₂core-shell NPs were characterized to see the Raman activity. It is found that the pure CCTO and CCTO@SiO2core/shell NPs (sintered or non-sintered) are Raman active in nature (Fig. 3.1.4). The band associated with heavy atoms like bonds of CCTO showed low Raman shift, whereas bands associated with light atoms like Si-O-Si showed high Raman shifts and it was described based on molecular weight. The significant intensity bands of pure CCTO (PCS and PCNS) NPs falls in the region of 200 to 500 cm⁻¹, whereas important bands related to silica are falling under the region from 1100 to 1500 cm⁻¹. The perovskite structure like CCTO possessing high dielectric constants mainly caused by the atomic displacement within a non-centre symmetrical structure and the Raman spectra of CCTO bands are assigned due to the phonon modes in various scattering intensities. Fig 3.1.4. (a) and (b) has shown expected Raman active modes for CCTO structure were observed at 295cm⁻¹ (E_g), 444cm⁻¹ and 503 cm⁻¹(A_g Sym, TiO₆), 567cm⁻¹ (F_g sym, O-Ti-O anti stretching) and 1147cm⁻¹ (CCTO) [277, 278]. The charge redistribution or Ti-shift within the TiO₆ octahedral affects the frequency of modes involving Ti-O stretching lesser extent than TiO₆ rotations. The rotation modes, however, would be more sensitive to changes of the TiO₆ tilts [173]. The peak at 1316 cm⁻¹ and 1497 cm⁻¹ indicated the bond stretching vibration of Si-O-Si bridging group [279, 280] functionalized with organic amine groups.

The experiments were performed in RT so that the molecules possess low values of kinetic energies which lead to stokes lines to be more intense. Due to increase in SiO₂ shell thickness on CCTO, some stretching frequencies are formed around 1316 cm⁻¹ and 1497 cm⁻¹ and it may cause more number of SiO₂ molecules along with amine groups which helps in more polarization of molecules [281] (see **Fig.** 3.1.4). At room temperature, the number of molecules possessing low energy is more but after sintering at 1000°C, the kinetic energy of the molecules increases and number of molecules are raised to higher energy state, due to which the intensity of the material observed to be high. The Raman spectra show sharp peaks which represent the crystalline nature of CCTO and the broad/diffused peaks show the amorphous nature of aminated SiO₂ coated over the CCTO NPs. Finally, CCTO@SiO₂ is Raman active showing rotational, as well as the vibrational motion of the molecules due to which it affects the change of polarizability. This leads to the change in dipole moment for which it is an easy way to calculate the impedance and dielectric parameters.

3.1.9. Investigation of the absorption behaviour through UV-Visible Measurement

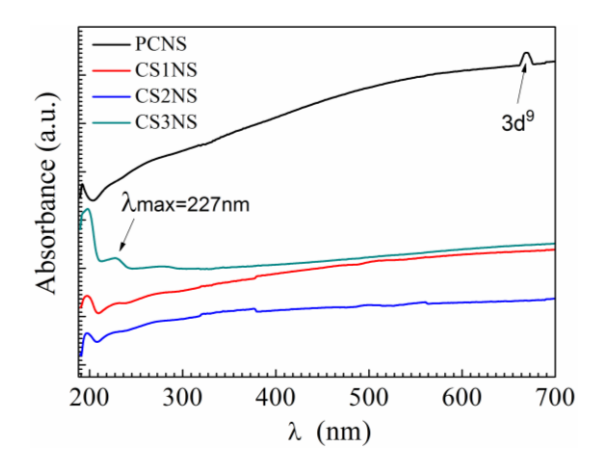


Figure 3.1.5. Ultra-Violet measurement of non-sintered PCNS, CS1NS, CS2NS and CS3NS NPs from 180-700 nm, respectively.

The study has confirmed the excitation of electrons from the ground to excited state via bonding and antibonding orbitals in the electronic transition of CCTO@SiO₂ complex system. **Fig.** 3.1.5 suggested two different types of excitation occur at lower λ 210 nm and higher λ 670 nm due to the excitation of $n\rightarrow\pi^*$ and d-d transition effect. The former excitation is mainly found due to the organic groups attached on the shell area where the latter transition is mainly observed with the presence of d⁹ orbital state of Cu in CCTO core surface.

3.1.10. Dielectric analysis for non sintered and sintered sample of CCTO@SiO₂NPs

3.1.10.1. Frequency-dependent dielectric study of nonsintered samples

The dielectric study of sintered PCS, CS1S, CS2S, and CS3S provide the information about the orientation adjustment of dipoles and translational motion of mobile charges present in it, in response with the application of the external electrical field [282-284]. The study also explained about the relaxation time or exponential decay, behaviour of dipoles or charges with respect to a different temperature from RT to 250°C and frequencies from 20 Hz to 2 MHz at which the experiments were conducted. The reason why we choose the sintered samples over non-sintered NPs is due to the better dielectric constant values of sintered samples without amine groups (see in the later section of 3.1.10.2).

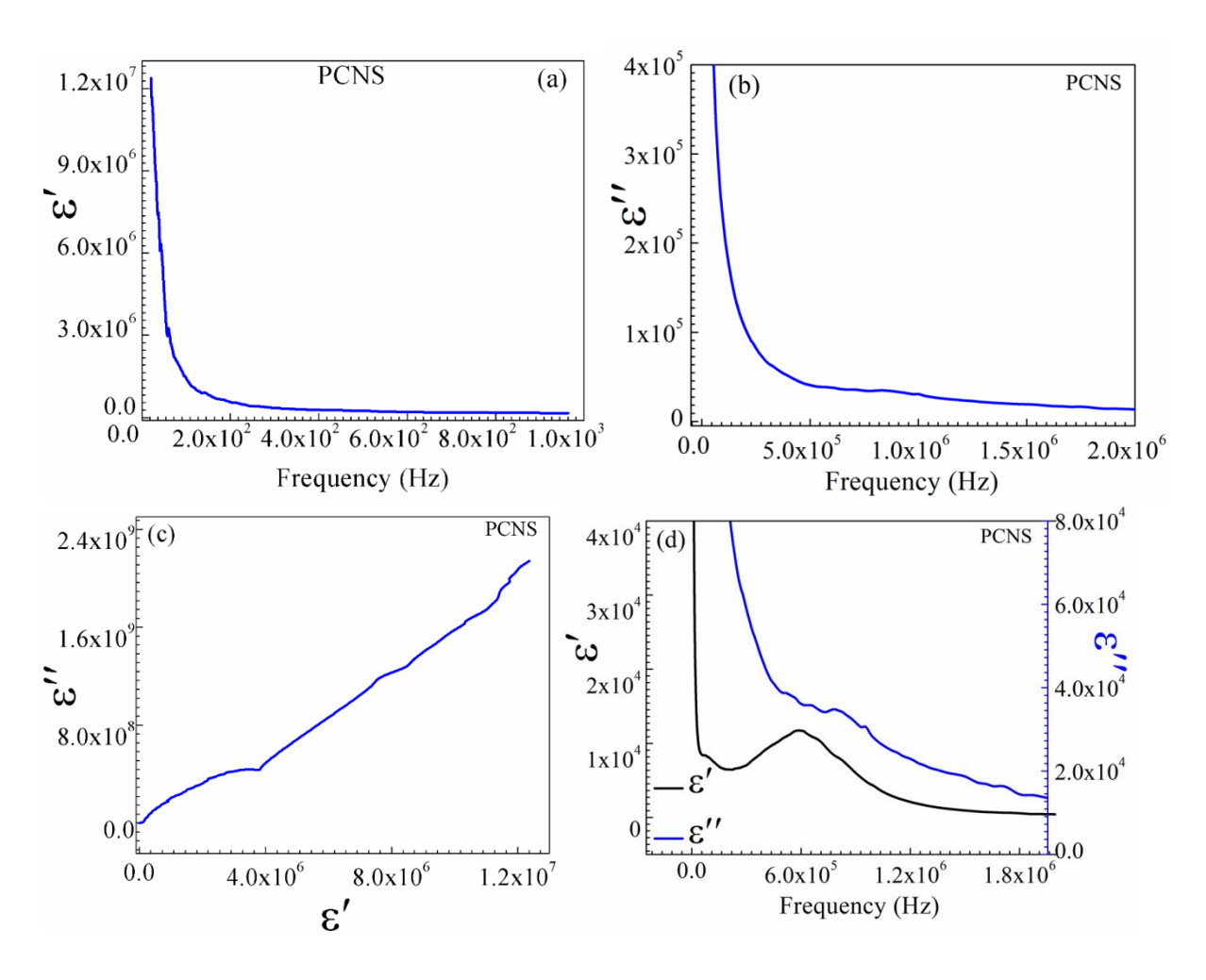


Figure 3.1.6. (a), (b), (c) and (d) represent the variation of the real part of dielectric constant (ε') and imaginary part of dielectric constant (ε'') with respect to frequency (20 Hz to 2 MHz) for PCNS NPs.

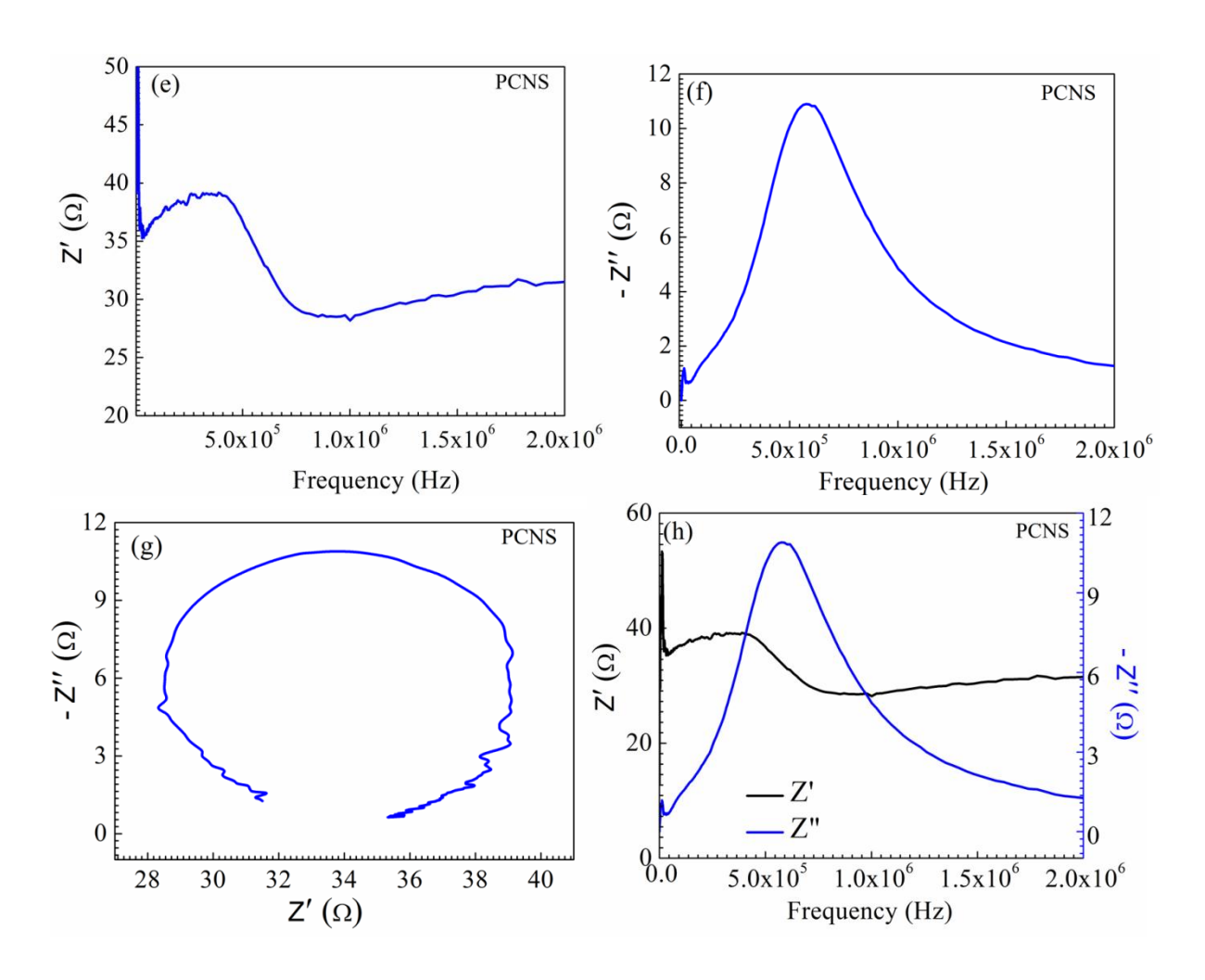


Figure 3.1.6. (e), (f), (g) and (h) represent the variation of impedance constant (Z') and impedance loss (Z") loss with respect to frequency (20 Hz to 2 MHz) for nonsintered PCNS NPs.

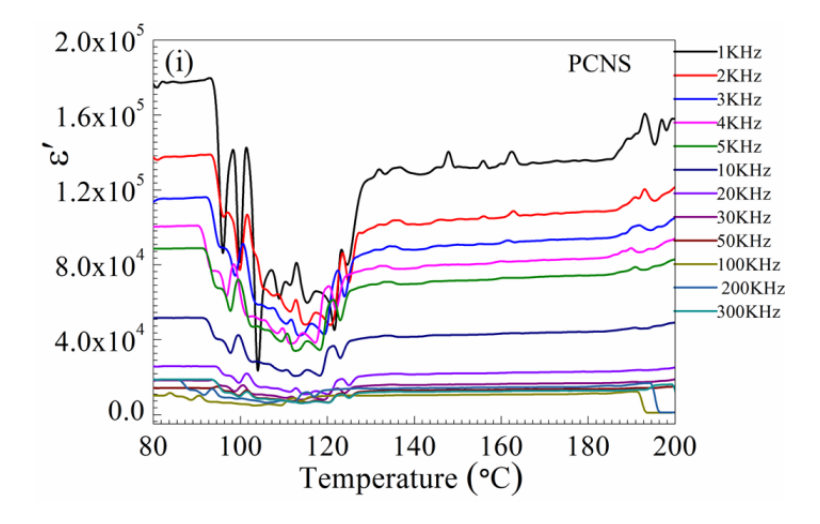


Figure 3.1.6. (i) ε'as a function of the frequency of PCNS NPs at different temperature range between RT to 200 °C.

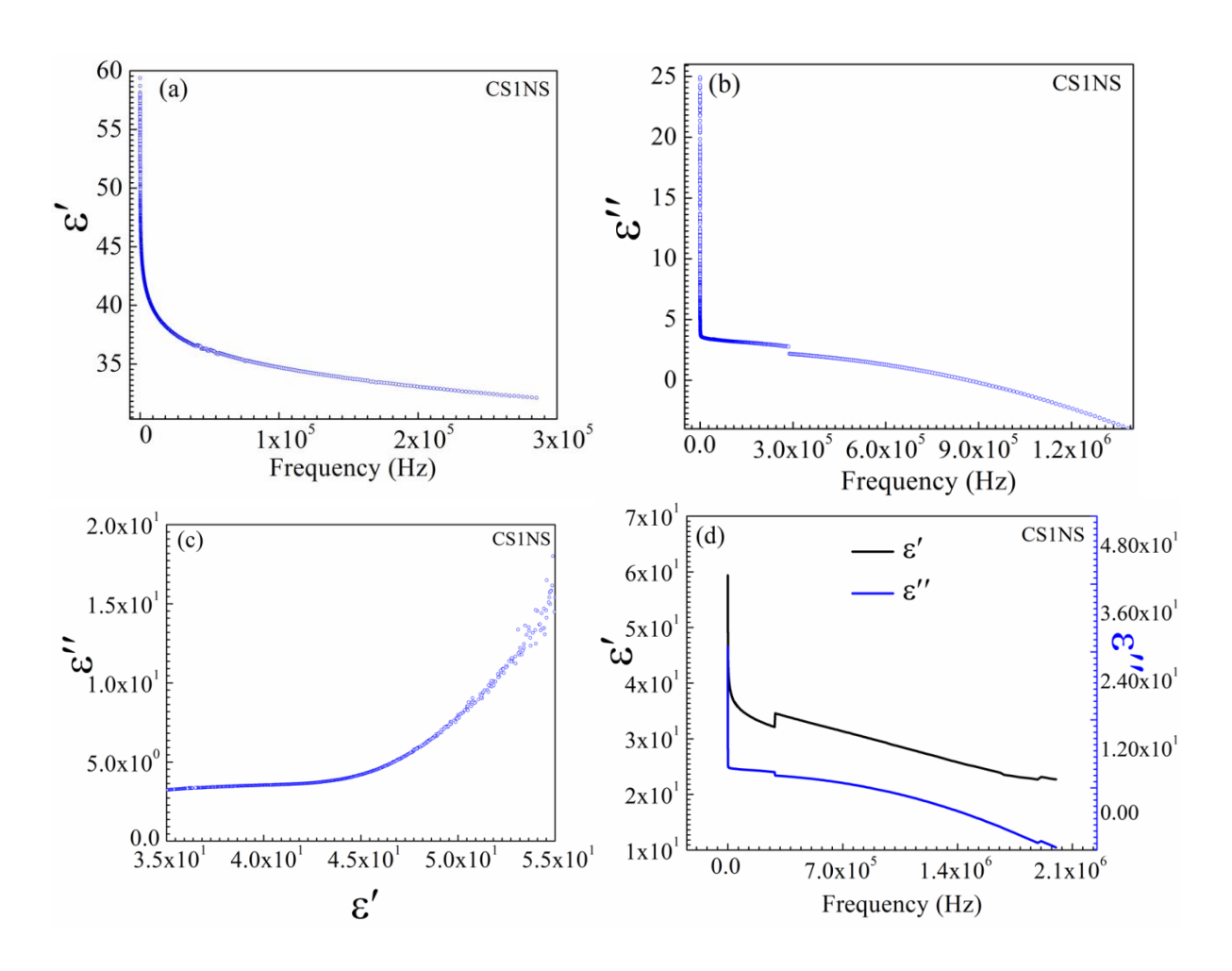


Figure 3.1.7. (a), (b), (c) and (d) represent the variation of the real part of dielectric constant (ε') and imaginary part of dielectric constant (ε'') with respect to frequency (20 Hz to 2 MHz) for PCNS NPs.

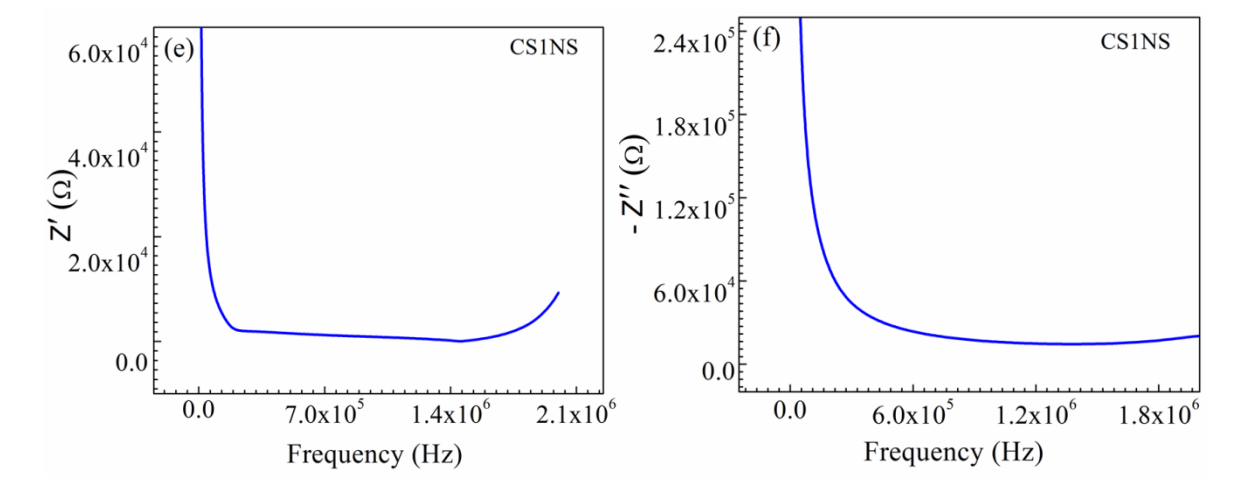


Figure 3.1.7. (e) and (f) represents the variation of impedance constant (Z') and impedance loss (Z") loss with respect to frequency (20 Hz to 2 MHz) for nonsintered CS1NS NPs.

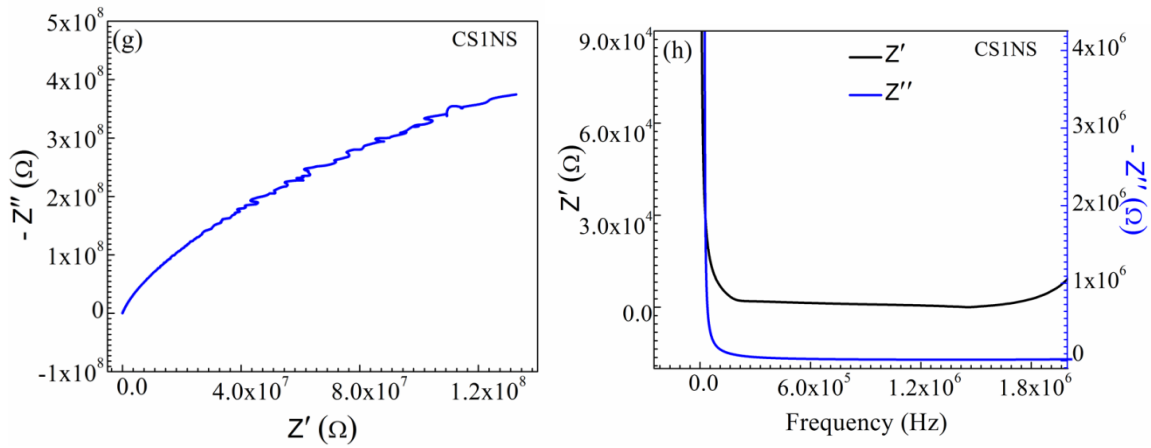


Figure 3.1.7. (g) and (h) represent the variation of impedance constant (Z') and impedance loss (Z") loss with respect to frequency (20 Hz to 2 MHz) for nonsintered CS1NS NPs.

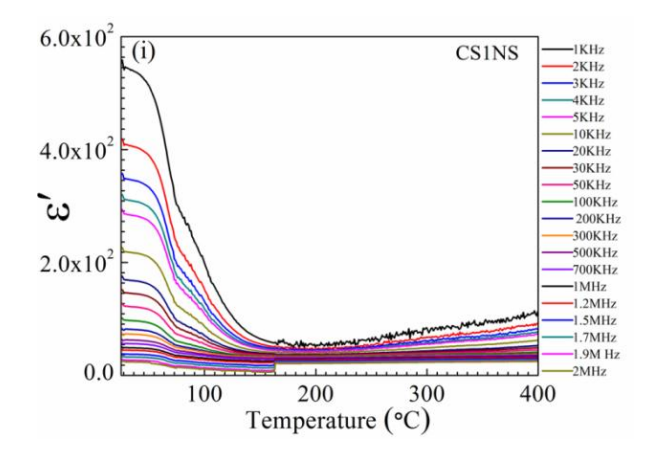


Figure 3.1.7. (i) ε' as a function of frequency of CS1NS NPs at different temperature range between RT to 400 °C.

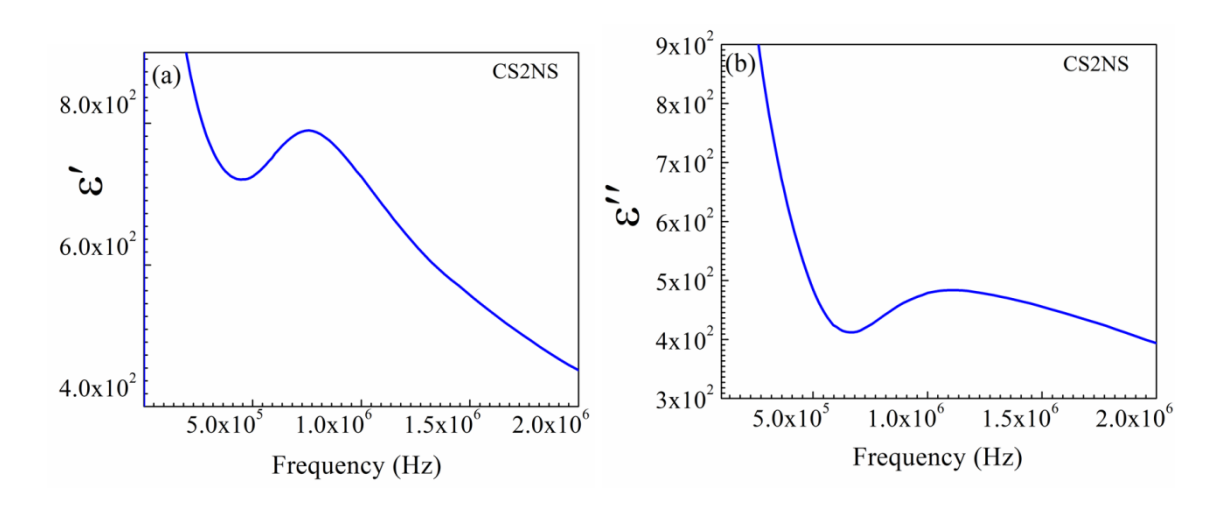


Figure 3.1.8. (a) and (b) represent the variation of the real part of dielectric constant (ϵ') and imaginary part of dielectric constant (ϵ'') with respect to frequency (20 Hz to 2 MHz) for CS2NS NPs.

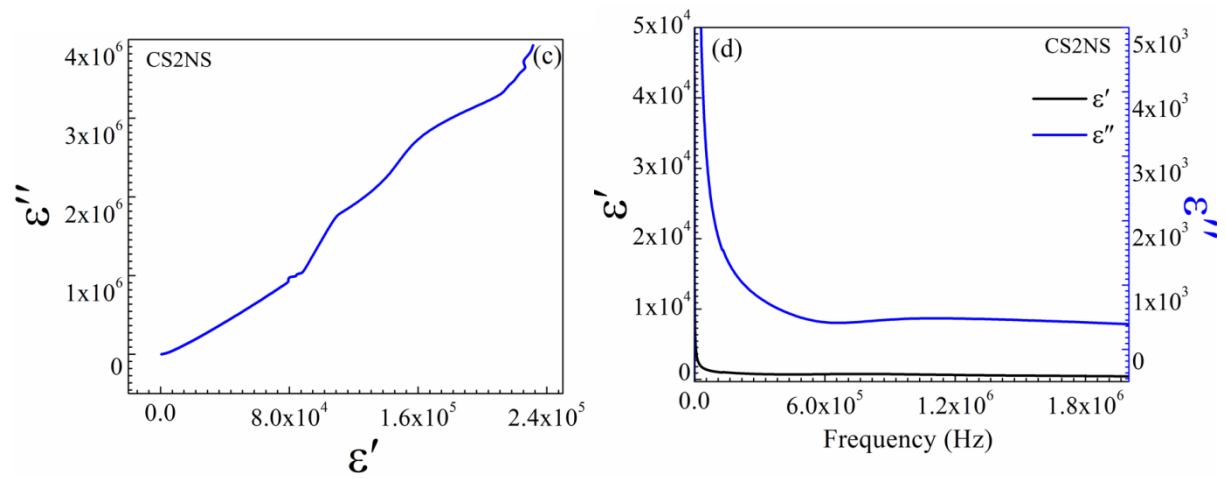


Figure 3.1.8. (c) and (d) represent the variation of the real part of dielectric constant (ϵ') and imaginary part of dielectric constant (ϵ'') with respect to frequency (20 Hz to 2 MHz) for CS2NS NPs.

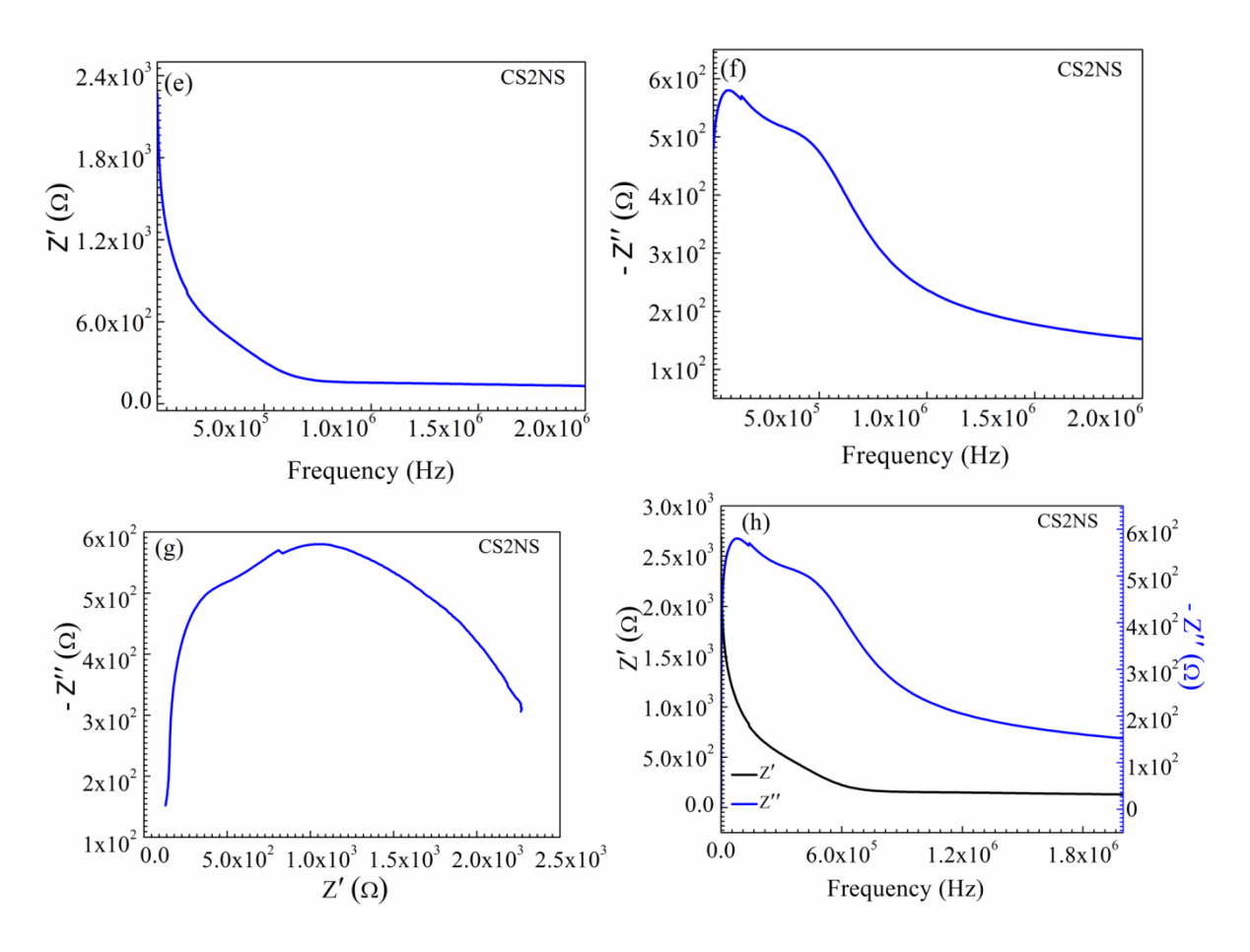


Figure 3.1.8. (e), (f), (g) and (h) represent the variation of impedance constant (Z') and impedance loss (Z") loss with respect to frequency (20 Hz to 2 MHz) for nonsintered CS3NS NPs.

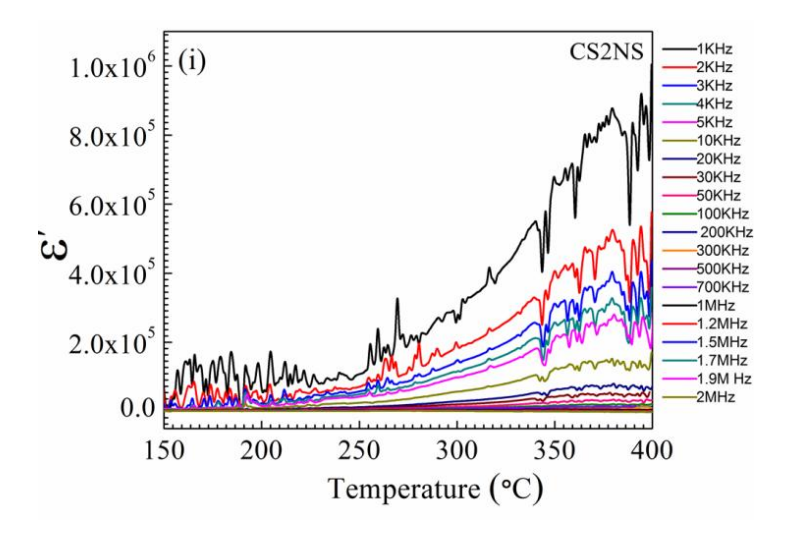


Figure 3.1.8. (i) ε' as a function of frequency of CS2NS NPs at different temperature range between RT to 400 °C.

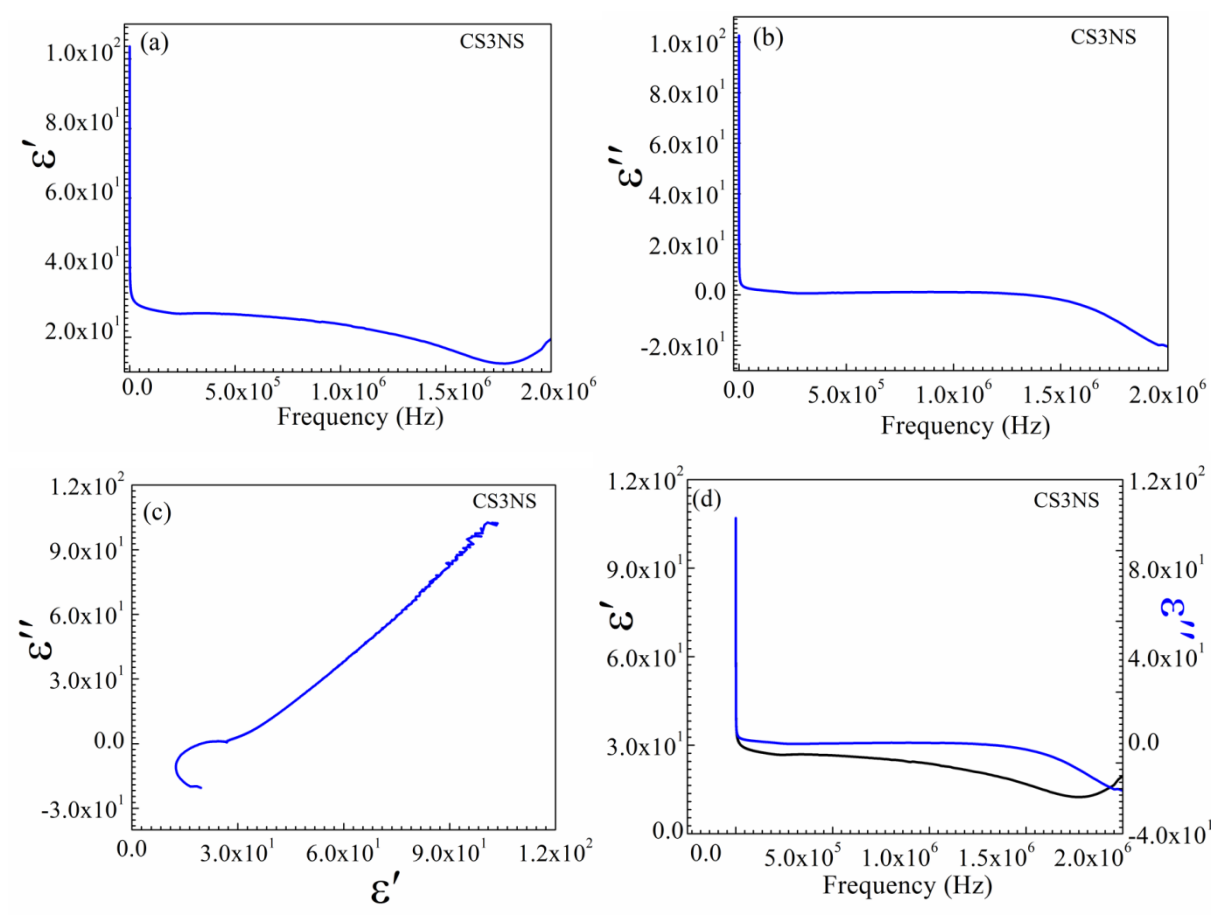


Figure 3.1.9. (a), (b), (c) and (d) represent the variation of the real part of dielectric constant (ϵ') and imaginary part of dielectric constant (ϵ'') with respect to frequency (20 Hz to 2 MHz) for CS3NS NPs.

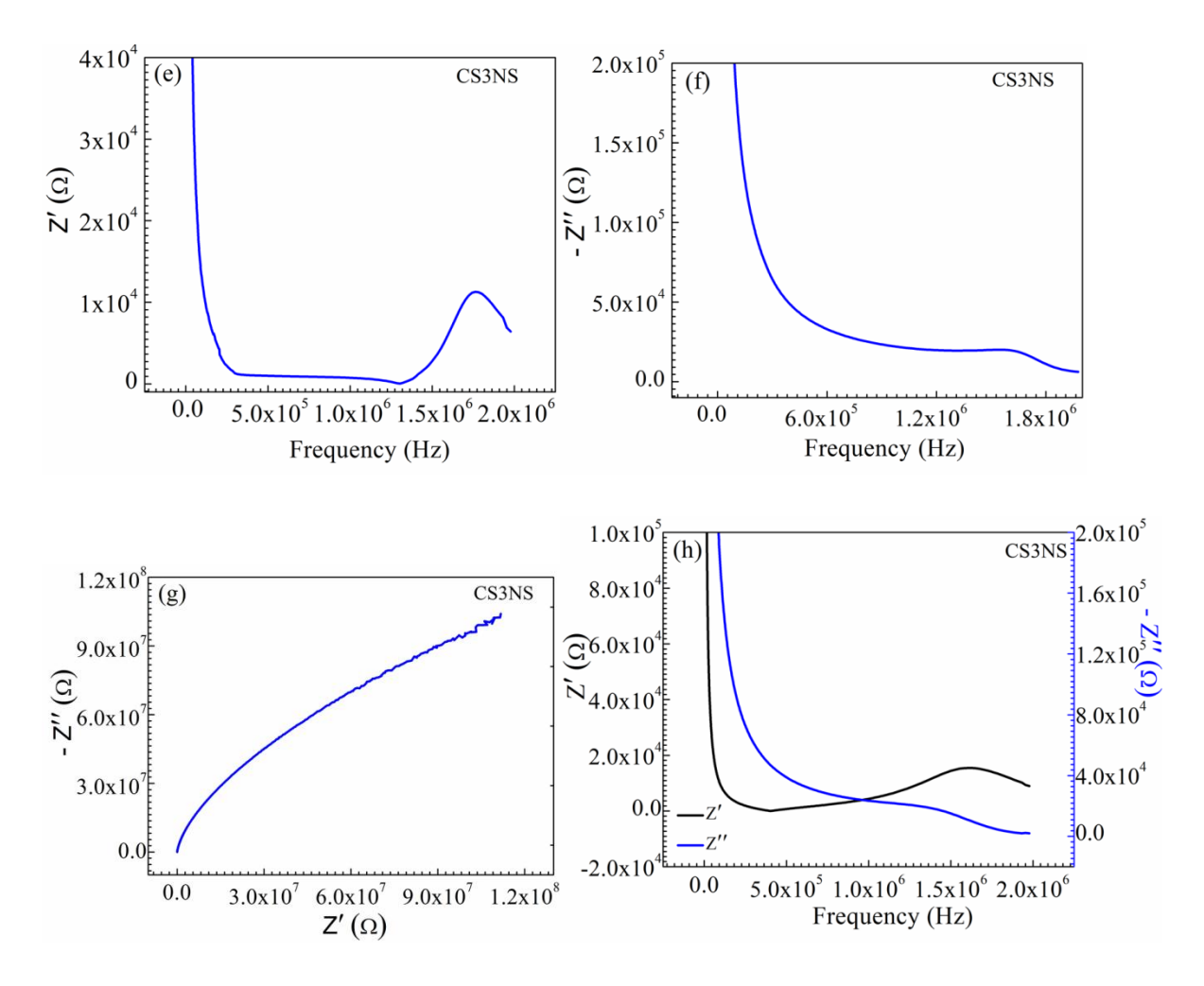


Figure 3.1.9. (e), (f), (g) and (h) represent the variation of impedance constant (Z') and impedance loss (Z") loss with respect to frequency (20 Hz to 2 MHz) for nonsintered CS3NS NPs.

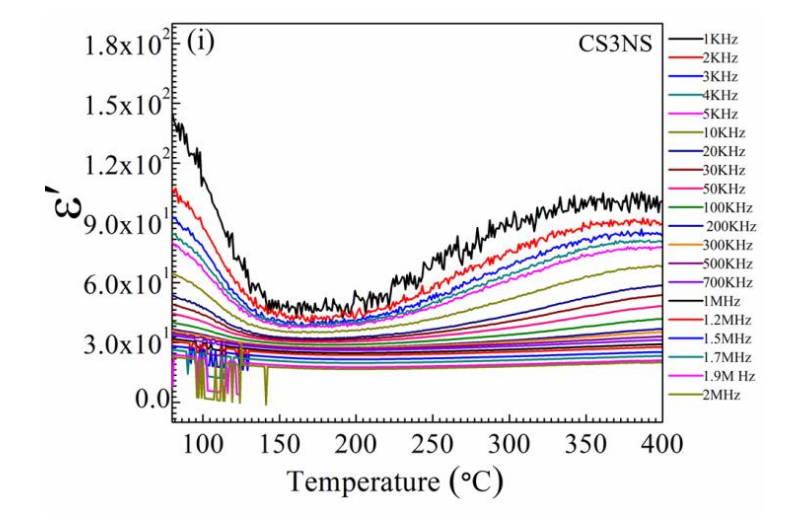


Figure 3.1.9. (i) ε' as a function of the frequency of CS3NS NPs at different temperature range between RT to 400 °C.

The **Figures**. 3.1.6. (a)-3.1.6. (i), 3.1.7. (a)-3.1.7. (i), 3.1.8. (a)-3.1.8. (i), 3.1.9. (a)-3.1.9. (i) explained about the variation in the frequency and temperature dependent study of the real and imaginary part of dielectric constant, impedance study of non-sintered PCNS ,CS1NS,CS2NS and CS3NS NPs respectively.

PCNS is showing highest ε' value 1.2×10^7 at 50Hz among synthesized materials. The coated sintered samples are showing better ε' and the factor may depend on various factors like synthesis method, group interaction, absence of dipolar groups and micropores containing oxygen [276]. **Figs.** 3.1.6 (e-h), **Figs.** 3.1.7 (e-h), **Figs.** 3.1.8 (e-h) and **Figs.** 3.1.9 (e-h) represent the impedance data of nonsintered samples, where it is found that PCNS, CS1NS, CS2NS, and CS3NS have Z' of 73, 17300, 1.83×10^6 and 2.93×10^6 , respectively within the temperature range 25°C to 250°C for 1kHz (constant frequency).

3.1.10.2. Frequency-dependent dielectric study of sintered samples

Previous reports have mentioned the CCTO impedance at a very low value [129, 285, 286] but our study is showing higher value for all the sintered samples. This may be affected by the different synthesis parameter along with the groups present on the surface of CCTO NPs. The impedance study was done for non-sintered and a sintered sample of both bare CCTO and CCTO@SiO₂ NPs which shows very similar behaviour to ε' with respect to frequency from 20Hz to 2×10^6 Hz for each sample. But with an increase in the thickness of shell diameter, the Impedance is also increasing at the respective frequency in the applied field. We found that sintered PCS, CS1S, CS2S and CS3 NPs possessing a uniform graph in increasing order of Z' 73, $1.7 \times 10^6 .1.18 \times 10^6$ and 2.93×10^6 at 1×10^3 Hz and 63.4, 1.01×10^3 , 2.7×10^3 and 9.3×10^3 at 2×10^6 Hz, respectively. But Z' is increasing with frequency leading to the increase in the ac conductivity of the material. The impedance loss is showing a regular trend in all the coated NPs, whereas the constant is showing a different trend for all NPs. Figs. 3.1.10 (c) and (d) revealed that with an increase in shell thickness, the real part of impedance constant and imaginary part of impedance loss increases and vice-versa. Silica ceramics has shown previously impedance constant up to 10³ but our work is showing the development of impedance up to 10⁶ [211]. This increased value of impedance results to a major contribution from this work in ac conductivity of the material. However, beyond 5 kHz, it is showing a gradual fall in its values up to 2 MHz.

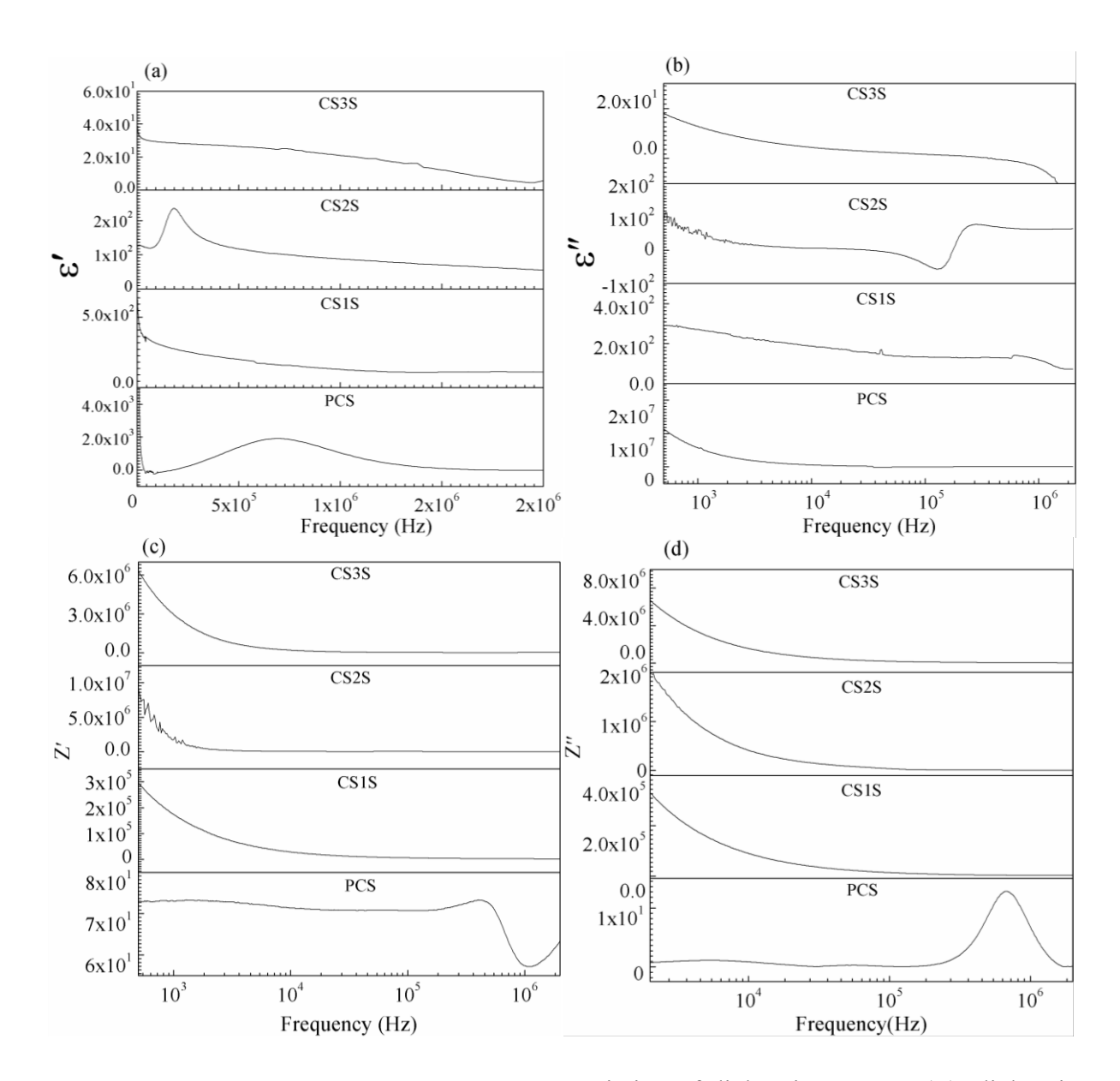


Figure 3.1.10. (a), (b), (c) and (d) shown the variation of dielectric constant (ε'), dielectric loss (ε"), impedance constant and impedance loss with respect to frequency (20Hz to 2MHz) for sintered uncoated (PCS) and coated CCTO@SiO₂ (CS1S, CS2S and CS3S) NPs, respectively at 25° C.

Figure 3.1.10. (a) showed the variation of the dielectric constant with frequency ranges from 20 Hz - 2 MHz for the following samples PCS, CS1S, CS2S, and CS3S NPs. At lowest frequency (20 Hz), sintered PCS NPs possess ε' is obtained to be ~2.49×10⁶. But with an increase in frequency from 20 to 200 Hz there was a sudden fall of ε' of pure CCTO is due to the space charge polarization and interfacial polarization [267, 272]. With the increase in frequency, there is a gradual decrease of ε' from 20 Hz to 5×10^3 Hz due to the absence of ionic or orientation polarization. A sudden hump has been observed between 3.5×10^3 Hz to

 1×10^6 Hz caused by immediate ionic interaction with the external field and space charge mechanism [233].

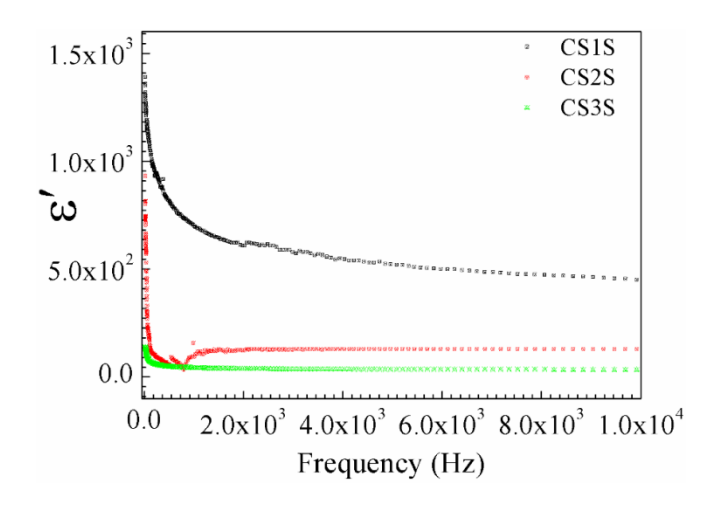


Figure 3.1.11. Represents frequency dependence ε' for PCS NPs from 20Hz to 1×10^4 Hz.

From Fig. 3.1.10. (a), it has been observed that with an increase in the thickness of the SiO_2 shell on CCTO core, there is a clear decrease in dielectric constant ε' at a particular frequency. At 20 Hz, highest coated CS3S showed less ϵ' value of 1.39×10^2 , whereas least coated CS1S showed maximum ε' value of 1.390×10³ and CS2S showed an intermediate value 9.7×10^2 (see Fig. 3.1.11). Fig 3.1.11 also represented ε' that at 1×10^3 Hz, CS1S, CS2S and CS3S NPs showing a uniform plot in the decreased order of ε' 700, 94.1 and 42.7, respectively. The decrease of ε' with the increase in shell thickness is due to the absence of interfacial polarization in lower frequency region contributing to less space charge in the interface region at the core and shell barrier of CCTO@SiO2 NPs. Sintered PCS, CS1S, CS2S, and CS3S have shown ε' values -14.7, 1.11×10², 55.2 and 6, respectively at a maximum frequency 2×10^6 Hz. From the results, it can be explained that with an increase in the frequency from 20Hz to 2×10^6 Hz, the ε' values are in decreasing trend. This happens may be due to the ceasing of various polarizations in case of PCS NPs, or maybe due to the circumscription of the CCTO in SiO2 shell which leads to the presence of few extents of charge at the interface of core and shell of the core-shell nanostructure [287, 288]. Table **3.1.1** has information about the difference between dielectric constant values for non-sintered and sintered samples.

Table 3.1.1: The dielectric constant (ϵ ') values for nonsintered samples (PCNS, CS1NS, CS2NS and CS3NS) core-shell NPs and sintered samples (PCS, CS1S, CS2S and CS3S) core-shell NPs with varying frequency at RT have been elucidated in a tabulated form.

Frequency(Hz)	PCNS	C S1NS	CS2NS	CS3NS	PCS	CS1S	CS2S	CS3S
$2 \times 10^1 \mathrm{Hz}$	5.1703E6	56.9	966.52	101.98	2.49E6	1390	971	139
$1 \times 10^3 \mathrm{Hz}$	160175.2	44.56	93.28	39.84	27300	700	94.1	42.7
$5 \times 10^3 \mathrm{Hz}$	83884.7	41.06	119.55	33.60	13100	521	129	34.9
$1 \times 10^4 \mathrm{Hz}$	45597	39.53	103.16	31.89	4770	450	129	33
$5 \times 10^4 \mathrm{Hz}$	8567.6	36.19	81.10	28.99	-111	349	120	30.1
$1 \times 10^5 \mathrm{Hz}$	7927.2	34.69	68.87	27.98	-166	310	134	29.1
$5 \times 10^5 \mathrm{Hz}$	10705.4	32.90	200.4	26.59	1390	200	117	26.3
$1 \times 10^6 \mathrm{Hz}$	4267.8	29.04	124.82	23.83	1050	129	87.7	21
$2 \times 10^6 \mathrm{Hz}$	420.8162	22.80	-175.6	18.44	-14.7	111	55.2	5.74

Figure 3.1.10. (b) showed with the increase in the thickness of the SiO₂ shell on CCTO core there is a gradual decrease in dielectric loss ε" as similar behaviour like real part dielectrics variation. At 1×10^3 Hz, the imaginary part of dielectric ε" for PCS NPs was observed to be 5.65×10^6 and with an increase in frequency, ε" seems to decrease slowly and reaches to a negative value of -3.5×10^3 at 2MHz. The reason of PCS nanomaterial to possess a negative value of ε" is due to the absence of different polarisations which may be useful for the absorbance of microwaves generation and used for electronic devices [187, 289]. The study also revealed that, at low and high frequency (1×10³ Hz and 2M Hz), CS3S, CS2S and CS1S possessed ε" value of 1.3×10^1 , 6.2×10^1 , 2.7×10^2 and -25, 64 and 72, respectively. But with an increase of frequency from 1×10^3 Hz to 2×10^6 Hz, the imaginary part of dielectric constant is decreasing and following a regular decrease trend. Further, it has been observed that with an increase in the SiO₂ thickness the negative loss has become more prominent as SiO₂ does not allow the applied field to interact/penetrate with the CCTO NPs [134]. **Table**

3.1.2 has also further clarified that the non-sintered possessed higher dielectric loss than corresponding sintered NPs. The dielectric losses for the sintered samples are very less compared to constant ε' for respective samples at particular frequencies, which will be helpful to use them for better applications for designing the charge storage devices, sensors etc.

Table 3.1.2: The dielectric loss ε'' values for nonsintered samples (PCNS, CS1NS, CS2NS and CS3NS) core-shell NPs and sintered samples (PCS, CS1S, CS2S and CS3S) core-shell NPs with varying frequency have been elucidated.

Frequency(Hz)	PCNS	CS1NS	CS2NS	CS3NS	PCS	CS1S	CS2S	CS3S
$2 \times 10^1 \mathrm{Hz}$	1.3334E9	24.05	13306.9	102.49	2.86E8	960	6060	159
$1 \times 10^3 \mathrm{Hz}$	2.27164E7	4.04	136.95	12.08	5.65E6	270	62.3	12.8
$5 \times 10^3 \mathrm{Hz}$	4.3991E6	3.58	60.74	5.64	1.11E6	207	9.69	5.98
$1 \times 10^4 \mathrm{Hz}$	2.2591E6	3.5	43.78	4.3	549000	187	5.45	4.4
$5 \times 10^4 \mathrm{Hz}$	429808.2	3.33	36.11	2.43	-10200	139	-8.06	2.3
$1 \times 10^5 \mathrm{Hz}$	215752.2	3.2	49.68	1.88	-60700	132	-43.7	1.63
$5 \times 10^5 \mathrm{Hz}$	40680.3	1.64	147.32	0.8	12000	128	67.2	0.526
$1 \times 10^6 \mathrm{Hz}$	31125.6	-0.76	130.08	1.04	7590	119	62.7	-3.68
$2 \times 10^6 \mathrm{Hz}$	13541.6	-10.25	-66.68	-19.	-3570	72.4	64	-25.8

Figs. 3.1.6. (e-h), **Figs.** 3.1.7. (e-h), **Figs.** 3.1.8. (e-h) and **Figs.** 3.1.9. (e-h) represent the impedance data of nonsintered samples, where it is found that PCNS, CS1NS, CS2NS, and CS3NS have Z' of 73, 17300, 1.83×10⁶ and 2.93×10⁶, respectively within the temperature range 25°C to 250°C for 1kHz (constant frequency). **Tables 3.1.3** and **3.1.4** have given a clear idea of the nonsintered NPs possessing higher impedance constant and loss value than their sintered NPs at respective frequencies.

Table 3.1.3: Frequency with respect Z' for nonsintered samples (PCNS, CS1NS, CS2NS and CS3NS) core-shell NPs and sintered samples (PCS, CS1S, CS2S and CS3S) core-shell NPs with varying frequency have been elucidated.

Frequency(Hz)	PCNS	CS1NS	CS2NS	CS3NS	PCS	CS1S	CS2S	CS3S
$2 \times 10^1 \text{Hz}$	12.9	1.32751E8	1.4255E6	1.11754E8	76	5.31E6	4.48E6	1.02E8
$1 \times 10^3 \mathrm{Hz}$	31.421	954200	810616.6	3.7369E6	73	173000	1.83E6	2.93E6
$5 \times 10^3 \mathrm{Hz}$	39.47	162974.6	90764.6	526080.7	72.2	48800	63100	417000
$1 \times 10^4 \mathrm{Hz}$	46.10	83469.2	37271.4	223409.6	71.3	28000	18300	175000
$5 \times 10^4 \mathrm{Hz}$	35.75	16614	1663.8	30315.5	70.8	8520	5870	23300
$1 \times 10^5 \mathrm{Hz}$	37.03	7623.8	2636.9	12431.1	70.7	5420	11600	9040
$5 \times 10^5 \mathrm{Hz}$	36.69	1555.4	2485.7	990.3	72.4	2280	3970	690
$1 \times 10^6 \mathrm{Hz}$	28.18	850.3	2088.7	748.4	57.4	1740	2900	4280
$2 \times 10^6 \mathrm{Hz}$	31.50	8031.1	1773.9	6861.1	63.4	1010	2410	9380

Table 3.1.4: Frequency with respect to Z" for nonsintered samples (PCNS, CS1NS, CS2NS and CS3NS) core-shell NPs and sintered samples (PCS, CS1S, CS2S and CS3S) core-shell NPs with varying frequency have been elucidated.

Freq(Hz)	PCNS	CS1NS	CS2NS	CS3NS	PCS	CS1S	CS2S	CS3S
$2 \times 10^1 \mathrm{Hz}$	0.02394	3.74499	210207.9	1.04021	0.0423	1.57E7	55000	2.04E
		E8		E8			0	8
$1 \times 10^3 \mathrm{Hz}$	0.29854	1.04169	1.1751E6	1.15073	0.42	57800	4.61E	1.2E7
		E7		E7		0	6	
$5 \times 10^3 \mathrm{Hz}$	0.86816	2.2011E	315267.6	2.9536E	1.06	15600	81400	2.91E
		6		6		0	0	6
$1 \times 10^4 \mathrm{Hz}$	1.0563	1.1382E	175783.1	1.5813E	0.81	88800	40600	1.54E
		6		6			0	6

$5 \times 10^4 \mathrm{Hz}$	0.7722	244754.8	42072.3	352104.	0.24	23200	87300	3340
				4				00
$1 \times 10^5 \mathrm{Hz}$	1.4352	127067.5	19225.9	183294.	0.04	13000	35100	1720
				9				00
$5 \times 10^5 \mathrm{Hz}$	10.1091	27712.3	3368.4	39373.1	8.63	3220	6880	3910
								0
$1 \times 10^6 \mathrm{Hz}$	4.8454	16219.5	2013.9	21876.9	6.8	2030	4050	2360
								0
$2 \times 10^6 \mathrm{Hz}$	1.2637	20052.2	1143.8	6479.6	0.12	1560	2060	2210

3.1.11. Temperature-dependent dielectric behaviour of CCTO@SiO₂ NPs core-shell NPs

Figures 3.1.6. (i), 3.1.7. (i), 3.1.8. (i) and 3.1.9. (i) represent the temperature dependence of dielectric constants for the non-sintered samples, where it is found that PCNS, CS1NS, CS2NS, and CS3NS have ε' of 6×10^5 , 1×10^2 , 4×10^6 and 3.9×10^2 , respectively within the temperature range 25°C to 250°C. The dipoles of SiO₂ and amine act as important factors in the explanation of the dielectric behaviours of the non-sintered coated CCTO@SiO₂ NPs. The permanent dipole moments of amine group in CS1NS, CS2NS and CS3NS are randomly oriented in the absence of electric field. However, once amine functionalized CCTO@SiO₂NPs are placed in the electric field, the permanent dipole moments of the molecule gets oriented in the direction of the electric field [268]. Due to orientation polarization of the polar groups like amine –NH₂ helps in the increment of dielectric strength of non-sintered coated CCTO NPs. For materials that possess permanent dipoles, there is a significant variation of the ε' values with variation in temperature. This is due to the effects of thermal vibration and orientation polarization [286, 291]. The reason for such a high ε' is still unknown, and to describe we choose sintered samples for further study. For most of the sintered material after a certain range of frequency, it is showing low dielectric properties. Due to more loss in the synthesized non-sintered CCTO@SiO2NPs which leads to more heating can be used for microwave heating purpose [168].

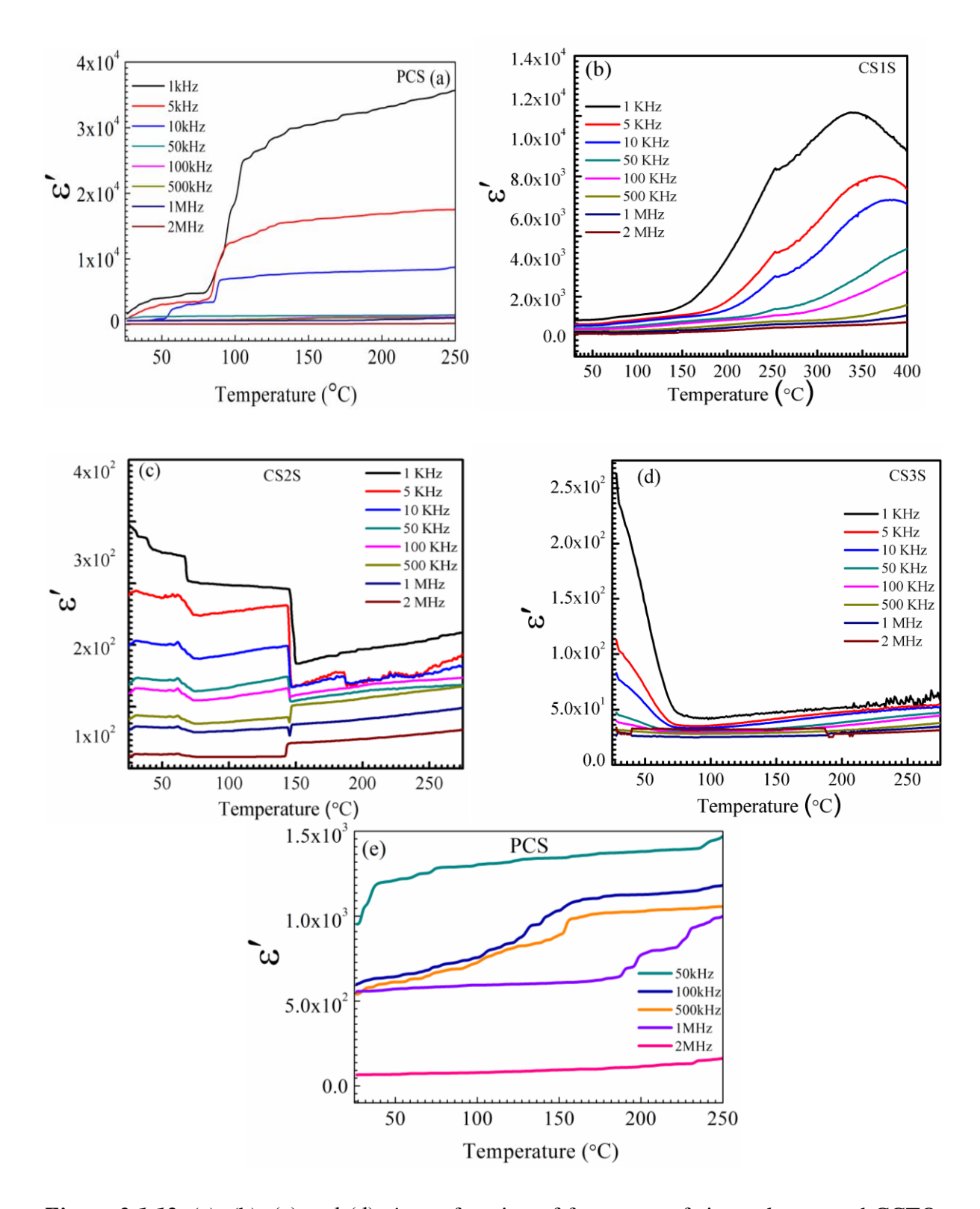


Figure 3.1.12. (a), (b), (c) and (d) ε' as a function of frequency of sintered uncoated CCTO, coated CS1S, coated CS2S and coated CS3S at different temperature range between RT to 250°C, respectively. **Figure** 3.1.12. (e) represents the temperature-dependent ε' for PCS NPs at higher frequency region.

It is known that SiO_2 possess $\varepsilon' \sim 100$ and for pure CCTO shows ε' value is 1×10^6 [179, 187]. The temperature dependence of dielectric constant has been studied for the samples PCS, CS1S, CS2S and CS3S NPs within the temperature range RT to 250 °C at different frequencies and shown in **Figs.** 3.1.12. (a-d). It was found that ε' is showing an interesting variation in the temperature range with frequency from 1kHz to 2MHz. Coated sintered NPs already lost most of the organic groups were present in it, and due to which they show more dielectric constant (ε') as compared to non-sintered samples. The above study revealed that the ε' for CS1S, CS2S, and CS3S are quite less than PCS NPs. This is occurred due to the presence of inorganic insulator silica. But the ε' for coated functionalized silica is showing better dielectric behaviour than other polyimides as well as inorganic dielectric [267,292, 293]. It has been shown that PCS is showing an increase in ε' of 4.9×10^3 at 100° C, but suddenly it increased up to 3.8×10^4 at 1×10^3 Hz, 250° C. In the former case, it happened due to moisture and other impurities lost at 100° C and after that base CCTO material is showing the interface polarization more effectively by increasing ε' .

PCS is showing minimum ϵ' at 2×10^6 Hz and showing similar trends with an increase in temperature from RT to 250°C as at high frequency region polarization does not occur for CCTO (see **Fig.** 3.1.12. (e)). It is also observed that with an increase in the frequency from 1×10^3 Hz to 2×10^6 Hz, the ϵ' of sintered coated CS1S, CS2S, and CS3S NPs decreases at a particular temperature range from RT to 150°C, but after 150°C it gradually increases up to 250°C. The reason for the increase of ϵ' after 150°C is may be due to the number of surface charges activation on CCTO@SiO₂ NPs occurred helps them to interact with the applied field causing to various polarisation. Thicker coated CS3S and thinner coated CS1S are having ϵ' of 2.5×10^2 and 1.2×10^4 for frequency 1×10^3 Hz respectively. But for pure bare CCTO at RT and 1×10^3 Hz ϵ' found to be 2×10^4 . The sudden decrease in ϵ' is more significant in the low-frequency range and at a low temperature is may be due to the ionic or dipolar migration occurred in coated materials before 150°C and structural disturbance occurred in CCTO NPs [239, 267].

Another reason for sudden drop also occurred due to the degradation of material resulting in the rearrangement of molecular moieties which affect the polarization. it is noticed that the dipolar and interfacial polarization is mainly responsible for the development of dielectric property of a material. So why it involves the perturbation of thermal motion of ions or groups present in the material. It is observed that a single polarisation with low loss is

present. Another reason for the coated sintered samples to show such type of decrease in ε' may be due to the average alignments of dipoles with a decrease in the field strength and as a result polarisation decreases which further resulted to the low dielectric constant which is analysed that from RT to 150°C. From **Fig**. 3.1.12. (b - d) it has been revealed that once the temperature increases beyond 150°C the ε' gradually increases with increase in temperature and this phenomenon is observed mainly due to the contribution of ionic groups present in all coated CCTO@SiO₂NPs. At this temperature range, most of the organic groups like –NH₂, C-H and H₂O are degraded out along with few SiO₂ molecules. Further, after the removal of the organic moieties from the CCTO@SiO₂NPs some microporosity generated also leads to the enhancement of dielectric constant ε' .

3.1.13. Analysis of COLE-COLE plots for CCTO@SiO2NPs

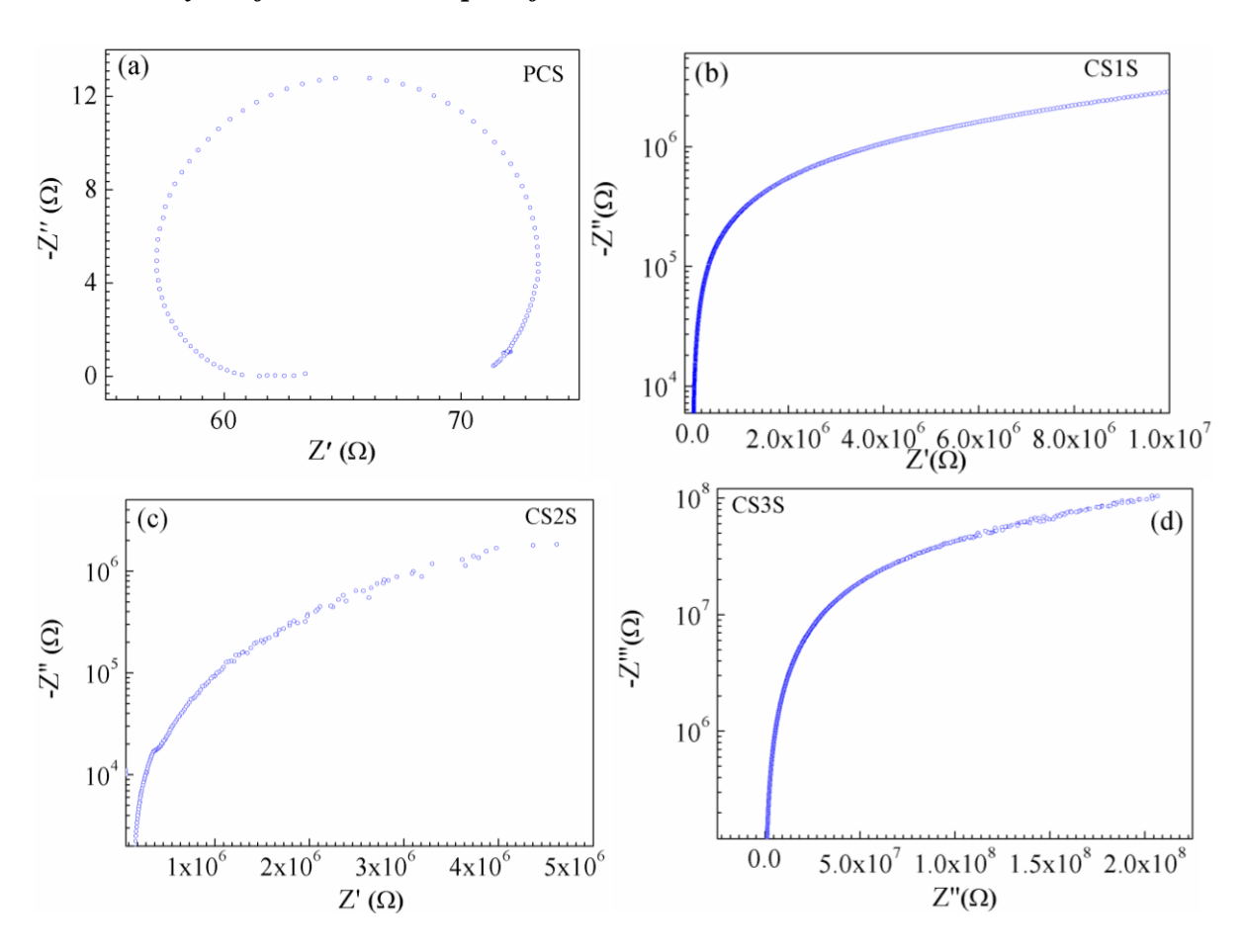


Figure 3.1.13. (a), (b), (c) and (d)—The Cole-Cole plot of sintered uncoated PCSNPs, coated CS1S, coated CS2S and coated CS3S NPs, respectively.

The impedance measurements have been done and the plots between the real and imaginary parts of the impedance possessing different relaxation behaviour. The width of the

distribution of relaxation frequency is explained by the Cole-Cole plot. **Fig.** 3.1.13. represents the Cole-Cole plot of the pure CCTO NPs and it is evident in support that synthesized sintered CCTO NPs acts as a very good dielectric material as it is a perfect semicircle [168]. From **Figs.** 3.1.13(a) – (d), it is clear that uncoated sintered CCTO NPs possesses higher dielectrics than silica coated CCTO@SiO₂ NPs. It is established that CCTO has the best dielectric property from room temperature to 600°C without any structural distortion due to relaxation [161, 294]. In **Fig.** 3.1.13. (a) the origin of the circular Cole-Cole plot is (0, 0). For a better visibility, the plot has been magnified and showed in the manuscript. However, the exact figure with (0, 0) origin has been incorporated below.

The ac conductivity of the samples can be calculated from the diameter of the semicircle in the cole-cole plot. We observed Cole-Cole plots for coated samples, it is clear that the impedance values are changed enormously when compared to bare CCTO sample. Further, within the measured range of frequency, the plots are not showing full circles and contributions from various species. Though contributions from two different species exist, to see the effect of various contributions, the measured frequency range is not sufficient. The three plots we obtained show a straight line which is in fact a small part of a half circle Although the coated NPs (CS1S, CS2S, and CS3S) are not showing perfect semi-circles, but the ac conductivity can be estimated as all these plots are partially semi-circle in nature. The presence of arc-like straight line in **Fig.** 3.1.13. (b) - (d) mainly represents the contribution from the grain boundary.

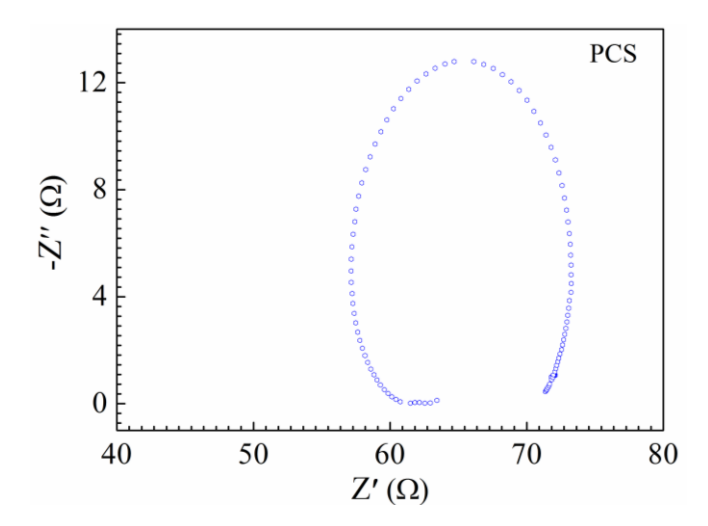


Figure 3.1.14. represents the Cole-Cole plot for PCS.

But **Fig.** 3.1.13. (c) is showing a similar nature of Cole-Cole plot to the pure CCTO NPs comparative to CS1S and CS3S. It is observed that beyond 5×10^6 Hz frequency the

dielectric property is diminished and the loss property is becoming prominent in these coated materials which can be used for microwave heating purpose. The straight-line Cole-Cole plot confirmed due to the interface and dipolar contribution from space charge and dipoles from the interface of synthesized material became the ε 'is low at high frequency region.

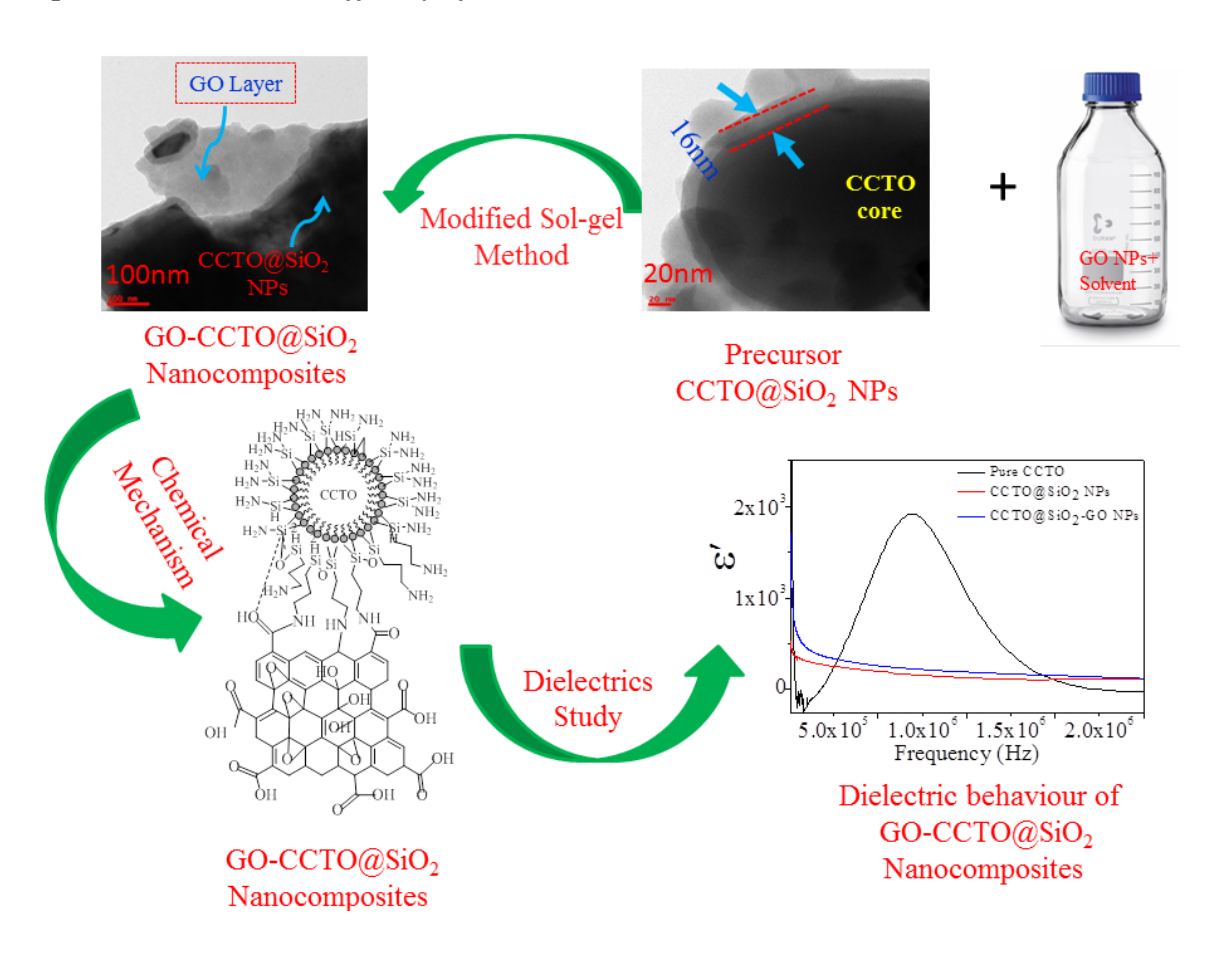
3.1.14. Conclusions for Part IA

In this work, a series of the core-shell nanostructure of CCTO and amine functionalized SiO₂ with a shell thickness from 5 nm to 20 nm have been prepared and their dielectric properties have been studied. The amine functionalized silica-coated CCTO NPs are showing better dielectric than bare silica NPs, few metal oxide composites along with CCTO polymeric composites. It is confirmed from the impedance studies that sintered coreshell CCTO@SiO₂ NPs exhibited better dielectric properties than other dielectric nanocomposites like organic polymer, barium titanates and other perovskite oxides including non-sintered CCTO@SiO₂-NH₂ NPs. The synthesis procedure and surface chemistry have a great impact on the dielectric study of CCTO@SiO2-NH2 NPs. With the dielectric loss, we can use the material for microwave heating purposes. This type of core-shell nanoparticles can be used for polymer composite materials due to the organic amine groups present on the surface of CCTO core shell. The attachment can be possible with the control of various external parameters during the experiment process. The results further suggest that using these core-shell materials microelectronic and energy storage devices with variable dielectric properties can be designed due to its high loss compared to bare CCTO NPs and other related materials reported. This novel work is on the basis of thickness, hence showed that with minimum coating can increase the dielectrics behaviour to a high level and for better charge storage device application in future.

RESULTS AND DISCUSSION

Part I. Dielectric study on the Organic-inorganic nanoparticles

Part IB. Dielectrics of the noble synthesized nanocomposite silica coated CCTO over Graphene oxide with the efficacy of CCTO@SiO₂ NPs decoration.



Schematic TOC for Dielectrics of the noble synthesized nanocomposite silica coated CCTO over Graphene oxide with the efficacy of CCTO@SiO₂ NPs decoration.

Outcomes from this part

- 1. <u>Bharatiya</u>, <u>Debasrita</u>& Kumar, K Santhosh & Raghunandan, S & Paik, Pradip. (2019). Dielectrics of graphene oxide decorated with nanocomposite silica-coated calcium copper titanate (CCTO) nanoparticles. **Journal of Materials Science.** 54. 10.1007/s10853-019-03336-8
- 2.<u>Debasrita Bharatiya</u>, K santhosh Kumar, Raghunandan S, Pradip Paik (**Short invited** talk/ Oral Presentation) Synthesis and dielectrics of GO-CCTO-SiO₂ nanocomposite. April

12-14, 2019, Mahatma Gandhi University, Kerala, 4th International Conference on Nanomaterials-2019

3.<u>Debasrita Bharatiya</u>, K santhosh Kumar, Raghunandan S, Pradip Paik (**Poster Presentation**) Study of dielectrics of GO-CCTO-SiO₂ nanocomposite. **January 6th-8th** 2020, IIT Kharagpur, WB, ICFM-2020.

Part IB (Objective 2): To design CCTO@SiO₂-GO sheet based nanocomposite

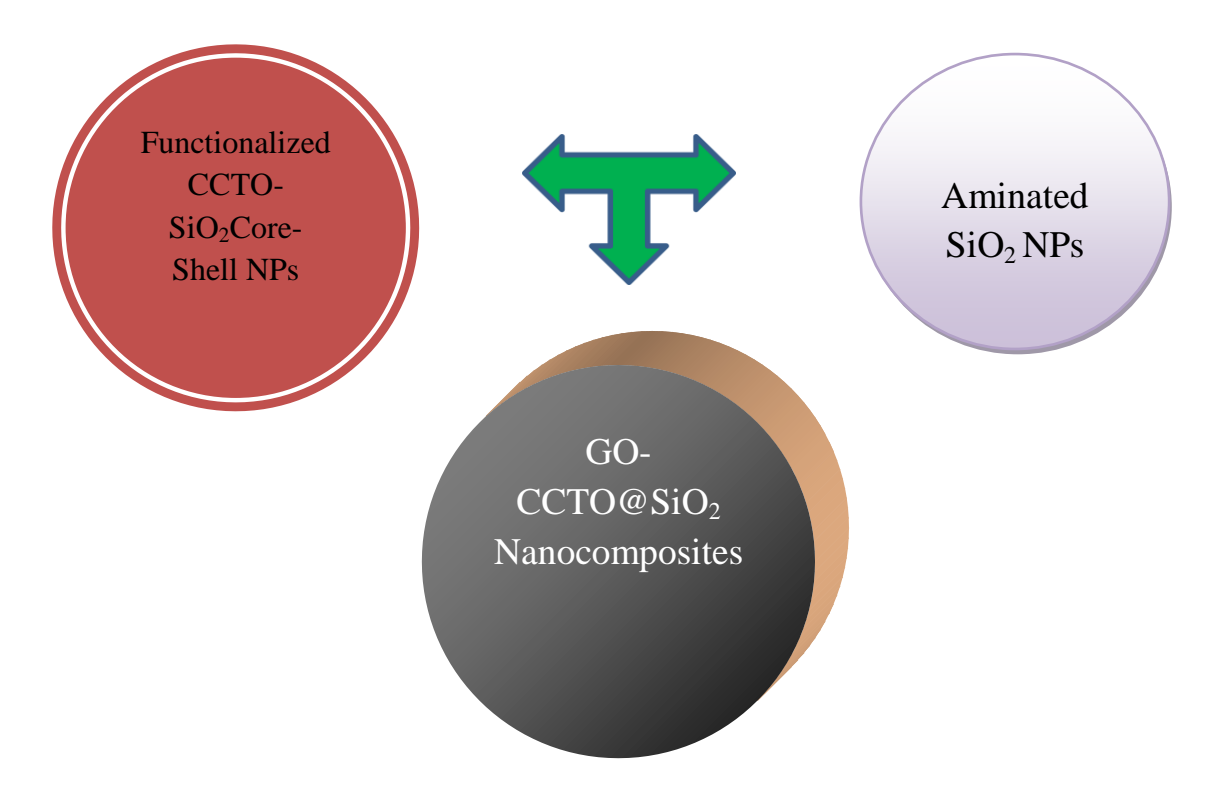


Figure 3.2.A. Objective Diagram for Dielectrics of the noble synthesized nanocomposite silica coated CCTO over Graphene oxide with the efficacy of CCTO@SiO₂ NPs decoration.

3.2.1. Abstract for this part IB

This work presents the synthesis of the noble nanocomposites of Silica Coated Calcium Copper Titanate-Graphene (GO-CCTO@aminated-SiO₂) by the established Sol-gel method. This work showed the decoration of CCTO@SiO₂ NPs on the surface of Graphene oxide and how the decoration/attachment depends on various environmental along with the instrumental factors like sonication time, stirring rate, centrifugation rpm and the thickness of

silica shell coated on CCTO NPs. The prepared CCTO@SiO₂-GO composites were characterized by suitable characterization techniques. FESEM and TEM techniques confirmed the morphological study of nanocomposites and how the CCTO@SiO₂ NPs are attached to the surface of GO sheet. FTIR has shown the presence of O-H, N-C groups which helps in the formation of types of bonds between CCTO@SiO₂ NPs and GO. This work further revealed an excellent result of a dielectric study indicating the best-decorated CCTO@SiO₂ NPs over the surface of the GO sheet causes the increment of dielectric constant ϵ' from 10^2 up to 10^5 . Meanwhile, this study also suggested high loss ϵ'' up to 10^6 at a lower frequency, i.e. 20 Hz at RT which can be useful for microelectronic devices. This variance of dielectrics is due to the effect of polarization and decoration of CCTO@SiO₂ NPs over the GO sheets. As the frequency increases from 20 Hz to 2 MHz, the dielectric constant ϵ' , as well as the loss of ϵ'' , reached up to 10^2 values for the highest decorated material. Our study also clearly explained a uniform variation of dielectric constant ranges from 1×10^2 to 1.5×10^4 at a different temperature range from room temperature to 560° C with a frequency range of 3×10^4 Hz to 2×10^6 Hz and the value varies accordingly with the synthesis method.

3.2.2. Introduction and Motivations

From the literature, it is clear that with an increase in shell thickness over CCTO NPs leads to the gradual decrease of dielectric constant ϵ' and loss ϵ'' [46, 47]. In contrary to the silica thickness over dielectric constant [86], our work has revealed an interesting fact that the effect of silica shell thickness is unable to cease the real part of dielectrics ϵ' , whereas the effect of spreading of core-shell NPs on the GO sheet becomes prominent. The effect of the decoration of CCTO@SiO2 NPs with the best positioning causes the nanocomposite material to increase the dielectric constant ϵ' and loss ϵ'' within the frequency range of 20 Hz - 2MHz. The study of temperature dependence dielectrics with respect to variable frequency showed exceptional behaviour towards the effect of spreading which is not clear in this case. This might be either due to the charge polarization effect with a change in dipole moment. Various characterization techniques help in the analysis of synthesized silica coated calcium copper titanate on graphene oxide (CCTO@SiO2-GO) nanocomposite to confirm its several chemical properties and physical behaviour. The dielectric study of these nanocomposites reveals a very different and significant study of the decorated CCTO@SiO2-GO nanocomposites.

3.2.3. Preparation of sheet like CCTO@SiO₂-GO Nanocomposites

The detailed synthesis method for the development of CCTO@SiO₂-GO has been explained earlier in chapter 2 and section 2.4.3. CCTO@SiO₂-GO nanocomposites were synthesized using the modified sol-gel method in which, CCTO@SiO₂ NPs and GO act as precursor materials which are previously synthesized by Hummer's method and sol-gel process respectively. The mixture is allowed under hydrolysis process and sonication. These solutions are poured into a reagent bottle and allowed for sonication. Several decoration types of CCTO@SiO₂-GO nanocomposites is mainly depended on a few environmental parameters given in the below-attached **Table 3.2.1**. With the completion of 3days, the composite material was continuously centrifuged with distilled water at high rpm and very low temperature. Once the centrifugation is over, the material was allowed for drying at 100°C and the grey colour material was collected. Various steps of the sol-gel synthesis method of CCTO@SiO₂ NPs are shown in **Schematic 3.1.1**. The pellet preparation method is the same as available in our previous work [268].

Table 3.2.1: Synthesis of CCTO@SiO₂-GO nanocomposites with different parameters

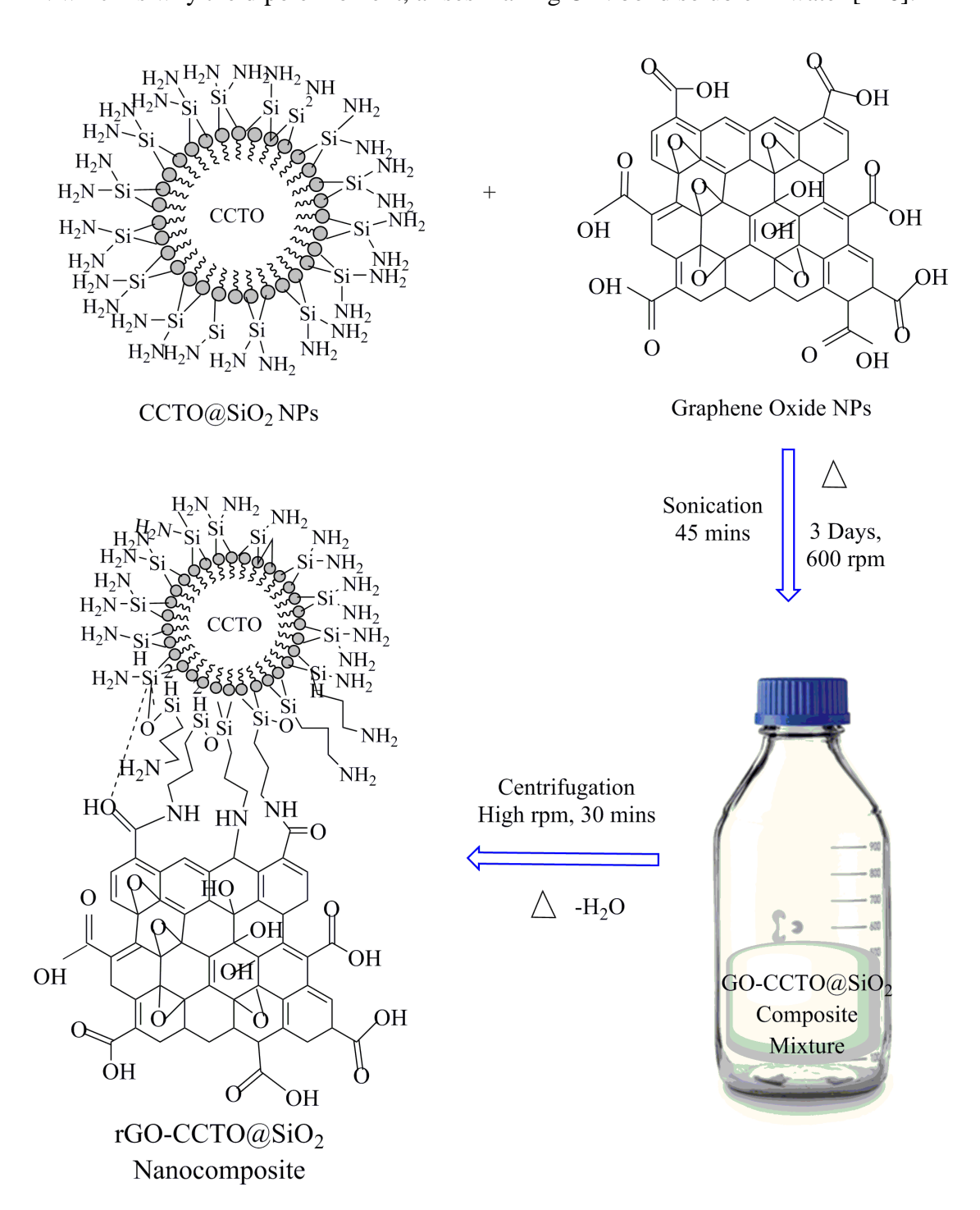
Sample Name	Shell thickness	Sonication Time	RPM
CSG1	3 nm	45 mints	14000
CSG2	5-7 nm	3 hrs	14000
CSG3	15-20 nm	3 hrs	12000

We did several experiments but among all the synthesis procedure it is confirmed that at higher rpm of the centrifugation process helps in better extraction of water like solvent along with unnecessary surfactant from the final product of the composite material. This method also signifies that more time of shaking also enhances the spreading/decorating capability of silica coated CCTO on the surface of GO.

3.2.4. Reaction Mechanism for CCTO@SiO₂-GONanocmposites

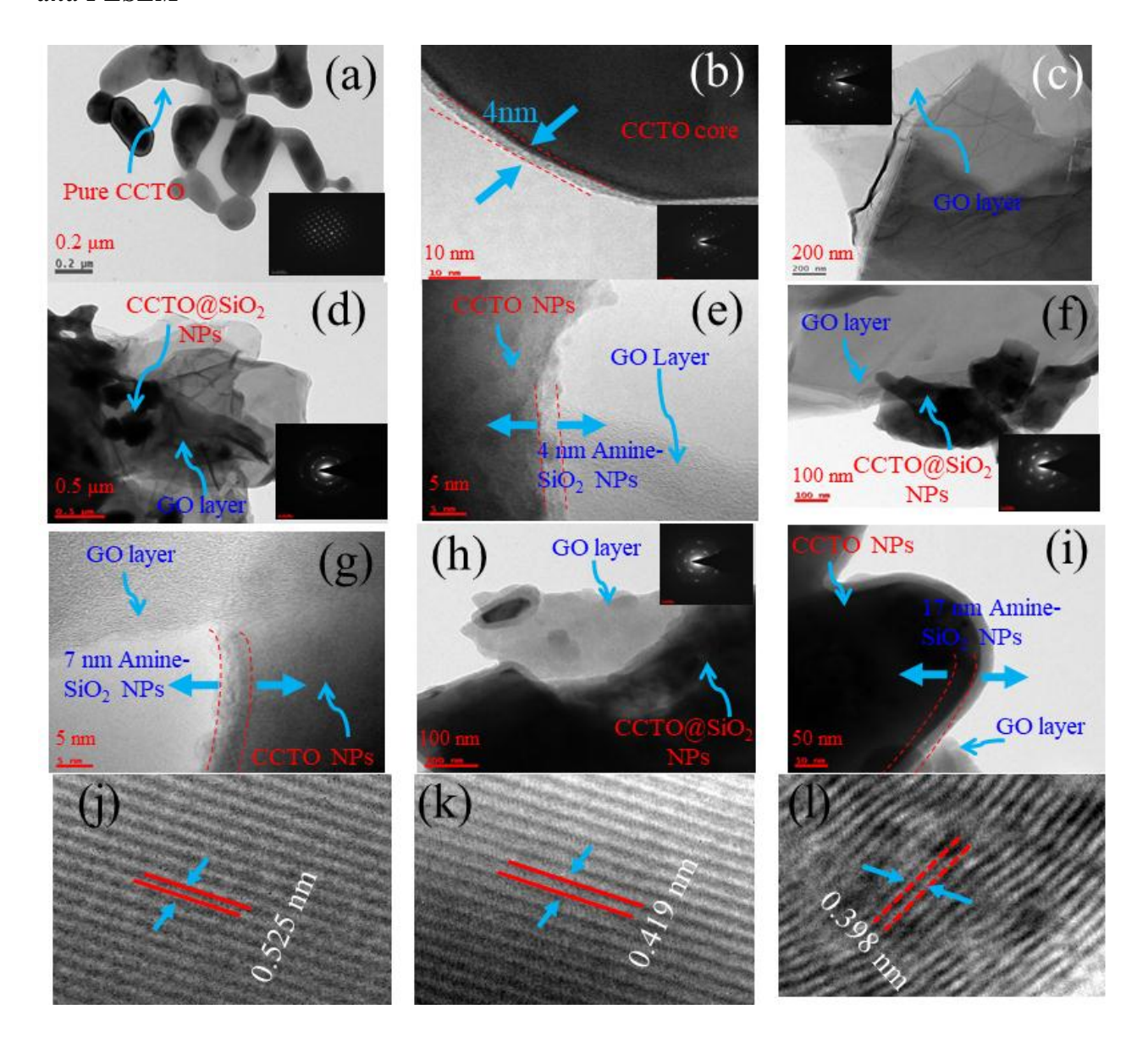
The reaction mechanism follows the concept of covalent bonding of silica and GO or amide bonds may play the role for the synthesis of CCTO@SiO₂ NPs on the surface GO sheet. The reasons of choosing water as the suitable solvent as FTIR study has shown a clear image of C-N bond present in the composites which may arise due to the interaction between carboxylic -COOH, hydroxyl (-OH) or ether (-O-) of GO and -NH₂ or SiO₂ groups of

CCTO@SiO₂ NPs. C-N bond is strongly polarized towards N due to the presence of lone pair in N which is why the dipole moment, arises making C-N bond soluble in water [216].



Schematic 3.2.1. Schematic steps of the sol-gel synthesis method of CCTO@SiO₂ NPs

3.2.5. Investigation of Shape and Morphology of sheet like nanocomposites via HRTEM and FESEM



Figures 3.2.1. (a), (b) and (c) are the HRTEM images of pure CCTO NPs, coated CCTO@SiO₂NPs and GO, respectively. Figs. 3.2.1 (d), (f) and (h) illustrate the coating CCTO@SiO₂ NPs GO named as CSG1, CSG2 and CSG3, respectively. Figs. 3.2.1. (e), (g) and (i) show the shell thickness of silica coated on CCTO NPs which are attached on the surface of GO layers of thickness 2-4 nm, 5-7 nm and 15-17 nm, respectively. Figs. 3.2.1. (j), (k) and (l) illustrates IFTT images with d-spacing values of pure CCTO NPs, CCTO@SiO₂ core-shell NPs and CCTO@SiO₂ NPs over GO, respectively.

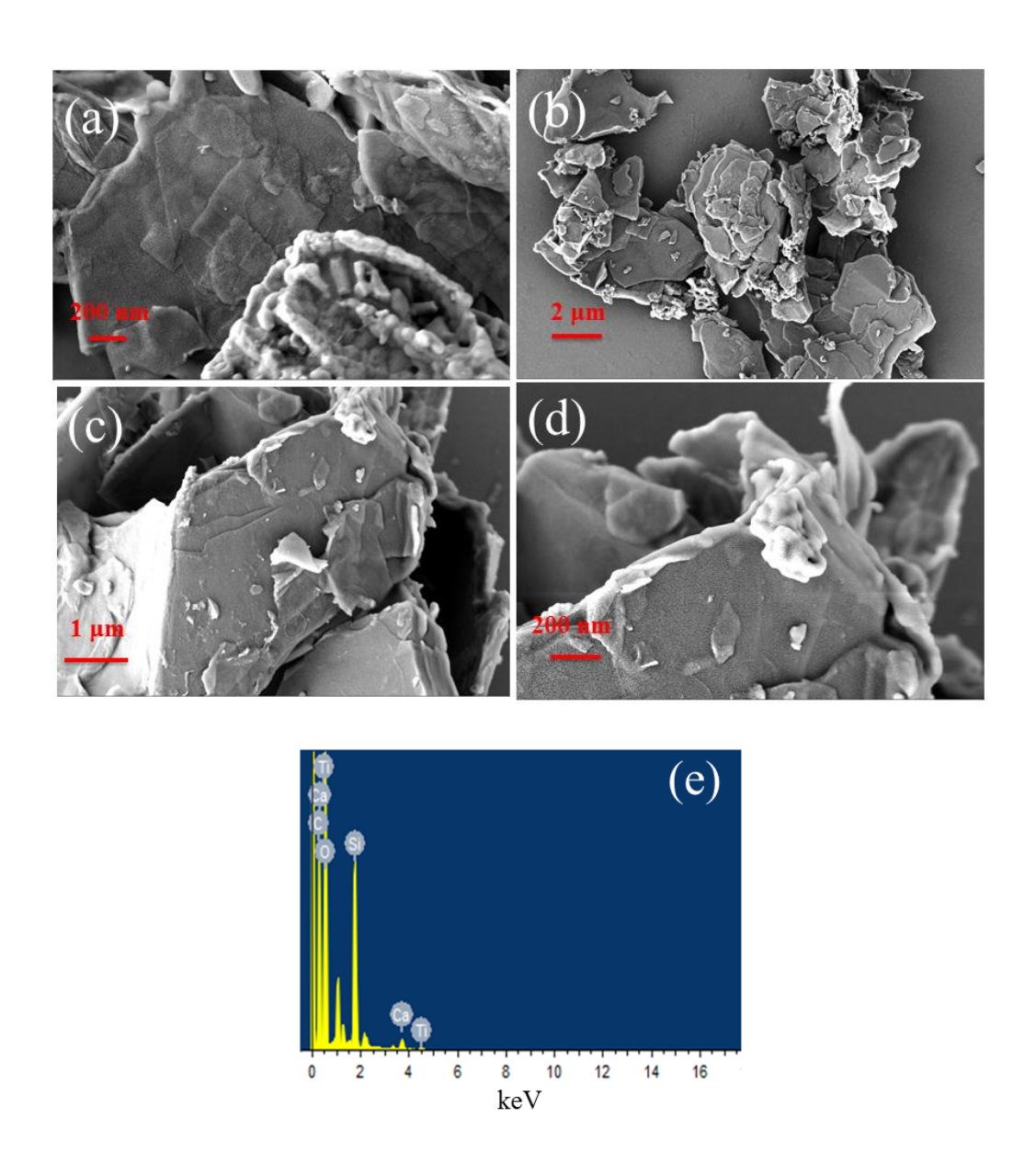


Figure 3.2.2. (a), (b), (c) and (d) illustrates FESEM images of CSG1, CSG2 and CSG3 derived nanocomposites synthesized from 2-4 nm, 5-7 nm and 15 nm CCTO@SiO₂ core-shell NPs. *Fig.* 3.2.2. (e) 2 represents EDX data for CSG 2 nanocomposites.

Table 3.2.2 represents EDX data for CSG 2 nanocomposite.

CS1NS	Wt. %	At. %
CK	35.90	46.15
OK	46.05	44.15
SiK	15.10	8.30
CaK	2.39	0.32
TiK	0.56	0.18
Total	100.00	

In **Fig**. 3.2.1(a), the HRTEM image suggests that uncoated pure CCTO has been successfully synthesized with a diameter range of 200 nm and length 500 nm. **Fig**. 3.2.1. (b), HRTEM micrograph has confirmed the formation of silica-coated CCTO (CCTO@SiO₂) NPs, bearing silica shell thickness of 2-3 nm. GO sheet has been observed clearly in **Fig**. 3.2.1(c) with the transparent pattern and layers which is alike reported earlier and further confirmed by FESEM images of (**Figs**. 3.2.2 (a) and (b)).

These layers like shapes are modified to folded like sheets in (**Figs.** 3.2.2 (c) and (d)), due to the interaction of the functional groups present on the GO sheets and experimental factors. From these images, it is also noticed that several random unshaped particles are attached to the layer of GO which may indicate the presence of CCTO@SiO₂ core-shell particles. HRTEM images in **Fig.** 3.2.1(d) (low magnification) and **Fig.** 3.2.1(e) (high magnification) confirm the attachment/decoration of 2-3 nm thick silica-coated CCTO (CCTO@SiO₂) core-shell NPs over GO surface. This could be possible only by the formation of enormous covalent bonding between GO and CCTO@SiO₂ NPs which further have been confirmed through FTIR results. There are numerous possibilities of bonding which may include hydrogen molecular bonding due to the presence of secondary amine group of CCTO@SiO₂ core-shell NPs,-COOH groups of GO, C-N covalent bond attached to the Si-O-GO surface [268]. Composites were synthesized in the water medium to facilitate the formation of C-N bonds between -COOH, -OH or -O- of GO and -NH₂ or SiO₂ groups of CCTO@SiO₂ NPs. C-N bond is strongly polarized towards N due to the presence of lone pairs in N so why the dipole moment arises making C-N bond soluble in water [210].

From **Fig.** 3.2.2(e) and **Table** 3.2.2., the EDS spectra of CCTO@SiO₂-GO-2 (CSG2), confirmed that all the precursor materials i.e.SiO₂, CCTO, CCTO@SiO₂ including Cu, Ti, O, C and Si are present. GO property helps itself to undergo the formation of sheets which enhances the surface area of GO so its weight percentage is more compared to Cu, Ti, and Si whereas we have taken the same amount of CCTO@SiO₂: GO (1:1) [295]. The dark colour particles represent Si coated CCTO and the brighter parts represent for the GO sheet NPs. Here many particles attached to the surface are seen to be less and not effectively coated all over the surface of the GO sheet. In the latter study, we will discuss the better coating of CCTO@SiO₂ NPs on the GO sheet. **Fig.** 3.2.1. (e) gives a better idea of how CCTO@SiO₂

NPs attached to the GO sheet. **Figs**. 3.2.1. (e), (g) and (i) clearly show the transparent nature of GO for single or few layers is due to GO impermeable property [296].

Fig. 3.2.1. (a) and **Fig.** 3.2.3. (b) represent the 15-20 nm coated silica (CCTO@SiO₂) NPs are attached to the surface as well as it is shown that the excess of silica whatever attached to CCTO NPs has come out from the core-shell and formed agglomerations in few places. It may be due to the effect of excess sonication time or else increased rpm of the centrifugation process. **Figs.** 3.2.1(j), (k) and (l) illustrate the IFTT images with a d-spacing value of 0.525 nm, 0.419 nm and 0.398 nm for pure CCTO NPs, CCTO@SiO₂ NPs and CCTO@SiO₂ NPs over GO, respectively.

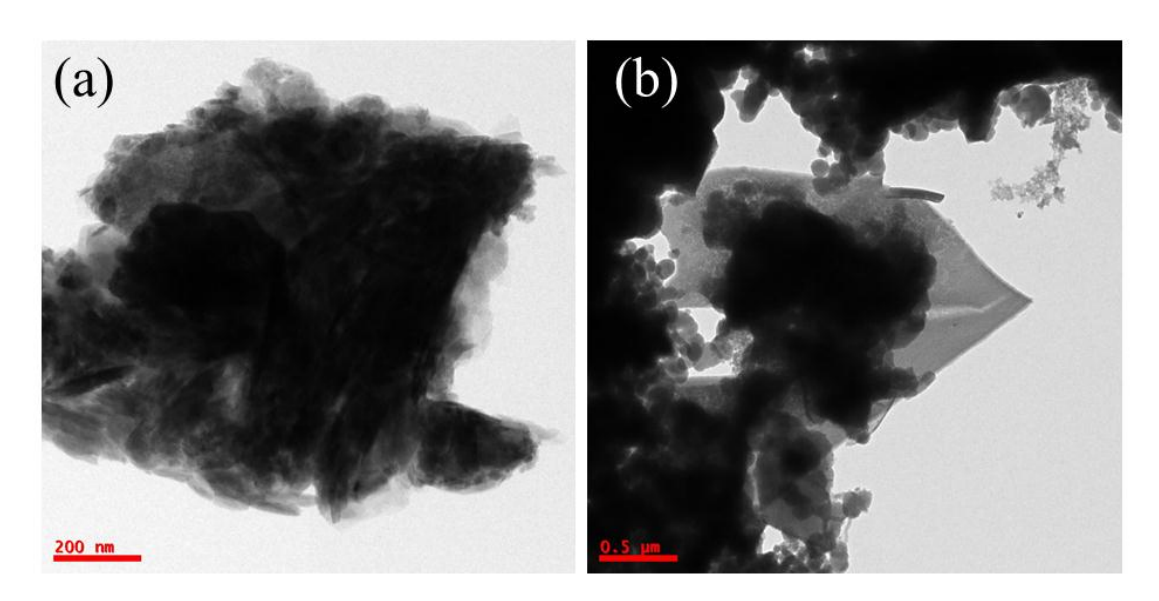


Figure 3.2.3. (a) and (b) represents well spread silica-CCTO over GO for CSG2 and CSG3 nanocomposites respectively.

Figure 3.2.3. (a) shows an effective coating of CCTO@SiO₂ on GO sheet as the dark coloured material is well spread over the brighter material. This is why in other images it is shown the brighter particles clearly but not in this image. It is a well-occupied material and may be due to the effect of stirring time which helps CCTO@SiO₂ to absorb all over the GO sheet. The concept of adsorption signifies the morphology of CCTO@SiO₂-GO composites that CCTO@SiO₂ molecule acts as an adsorbate on the surface of GO sheet as an adsorbent. **Fig.** 3.2.1. (f) shows a near view of **Fig.** 3.2.3. (a) which helps us to see the particles very clearly.

3.2.6. Crystalline nature and Thermal Stability Study by XRD and TGA

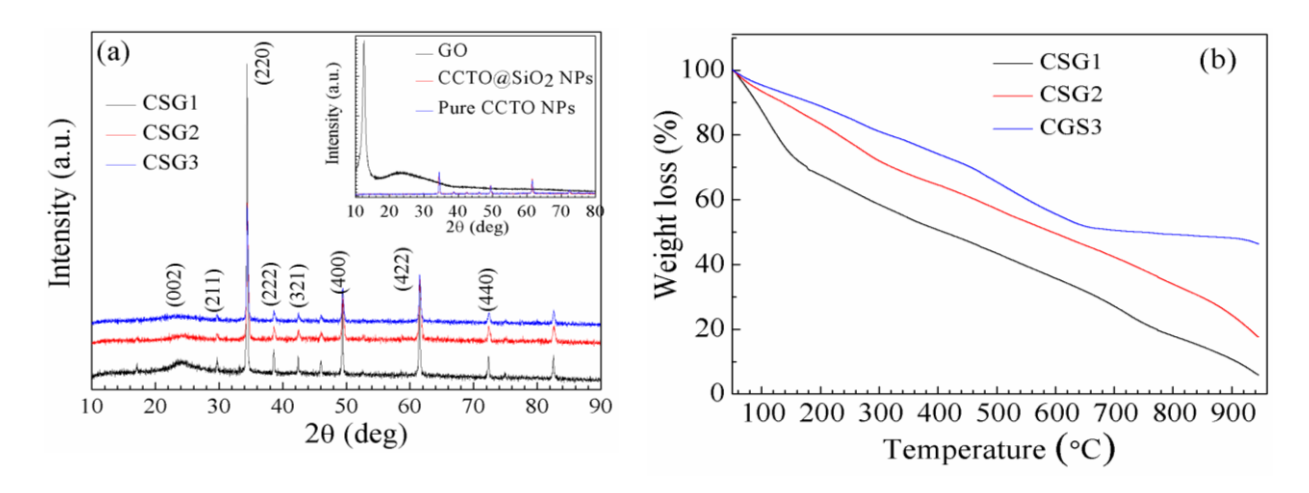


Figure 3.2.4 (a) and (b) illustrates XRD Pattern and TGA Thermogram of CSG1, CSG2 and CSG3 nanocomposites synthesized from 2-4 nm, 5-7 nm and 15-17 nm Si coated CCTO NPs, respectively.

The crystalline structure of the nanocomposite was confirmed by XRD. GO shows its peak in the range of 7-10° 2θ with Cu Kα radiation [297]. Inset Figure of Fig 3.2.4.(a) found to be very similar peaks for GO, pure CCTO and silica-coated CCTO NPs [125,191]. But after the reduced synthesis of CCTO@SiO₂ -GO nanocomposites, GO is showing its peak at 25.2° with Cu $K\alpha$ radiation. It may be due to GO is reduced with water or maybe with other precursor material of CCTO@SiO₂ NPs. Earlier we discussed the bonding between CCTO@SiO₂ and GO surface and here we conclude that GO converted to r-GO showing the peak range at 25.2 ° (2θ) with Cu Kα radiation which confirms the crystallinity of GO NPs or it may happen that shifting causes may be due to the decrease of spacing between the layers of GO shown in Fig. 3.2.1. (j), (k) and (l) on reduction helps in the broad peak of GO at the peak value of 9 at 20 shifted towards 25 making it more diffused i.e. small hump like a peak. Meanwhile, Fig. 3.2.4. (a) represents the other 2 theta values of 30.3°, 35.4°, 38.3°, 43.7°, 46.4°, 49.1°, 63.2° and 74.2° like (211), (220), (310), (222), (321), (400), (422), and (440) shows the presence of CCTO patterns[150]. But it is not showing any peaks for silica. It may be due to very less weight percentage of Si is present in the material but the presence of silica is already confirmed from earlier EDX analysis in Fig. 3.2.2. (e).

Fig. 3.2.4. (b) represents the TGA thermogram of CSG1, CSG2 and CSG3 nanocomposites synthesized from 2-4 nm, 5-7 nm and 15-17 nm Si coated CCTO NPs respectively at inert atmosphere, heating rate 10°C/min. It is clear that GO shows thermal

instability between RT to 1000°C. The factor of the highest percentage of coating or well spreading of material over the surface shows an exceptional behaviour as compared to another disturbed coating. It is mentioned earlier that a significant weight loss occurs in GO NPs [298]. The total weight loss % of CSG1and CSG2 is showing ~80%, 92% whereas CSG3 has shown only 50%. The less weight loss in the highest thickness coated CCTO@SiO2 is due to the presence of silica which has higher thermal stability. In the former case weight loss is showing mainly in between 150°C to 250°C and the loss % is ~25% and it may be due to the presence of some by-product gases like H2O, CO2 etc.CSG1 shows a gradual decrease in weight loss from 250°C to 900°C without any significant changes and its weight loss finally reaches 80%. But in the case of CSG2, the weight loss has been remarkably occurred in between 300°C to 500°C and the loss% is 92 %.

3.2.7. Chemical Functionality through FTIR Spectra

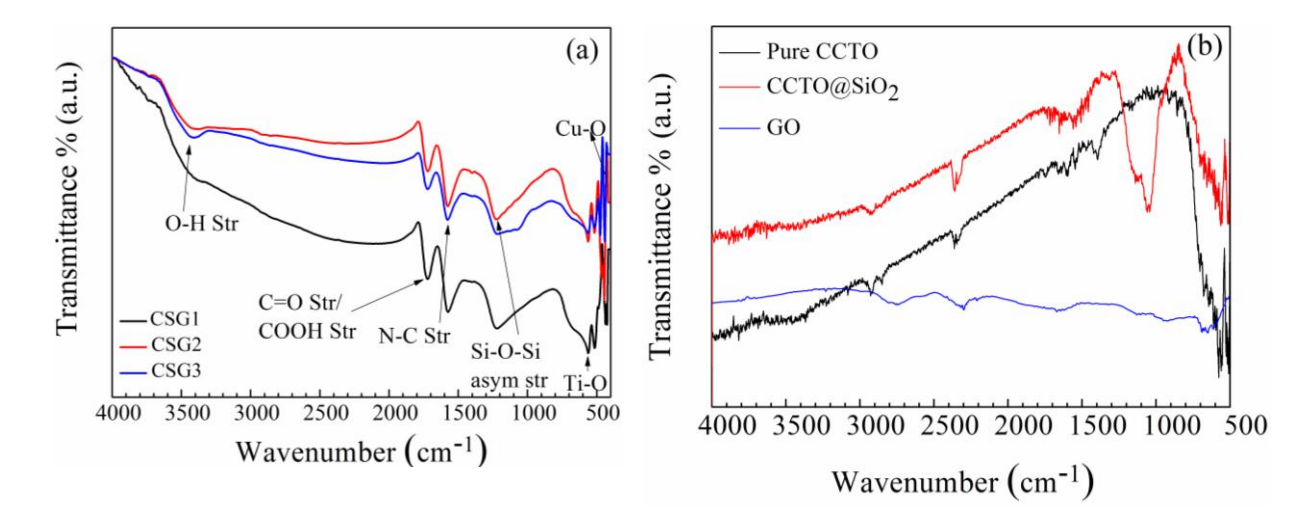


Figure 3.2.5. (a) Illustrates the FTIR spectra of CSG1, CSG2 and CSG3 nanocomposites synthesized from 2-4 nm, 5-7 nm and 15-17 nm Si coated CCTO NPs, respectively. **Fig.** 3.2.5. (b) represented FTIR Spectra for precursor materials.

Hence it is proved that the highest silica decorated CCTO core-shell NPs on the GO sheet is not thermally stable in nature. Contradict to both CSG1 and CSG2, the highest silica coated CCTO over GO i.e. CSG3 is showing the lowest 50 % of weight loss with maximum stability at high temperature 1000°C. The sudden weight loss may occur due to the breaking of the covalent bond between the amine group of silica and carboxylic acid (-COOH)/hydroxyl (-OH) group of GO or other functional groups attached to the silica-coated CCTO have been decomposed between this range.

Figure 3.2.5. (b) represents FTIR spectra for GO, Pure CCTO NPs and CCTO@SiO₂ NPs, which resembles peaks like CCTO NPs at 560 cm⁻¹,590 cm⁻¹ and 450 cm⁻¹ for Ti-O and Cu-O str while GO has shown peak near 1643 cm⁻¹, 1095 cm⁻¹ and 1198 cm⁻¹ for aromatic C=C, C-O alkoxy group and C-O epoxy groups confirming the precursor for synthesized nanocomposites. Figure 3.2.5. (a) suggests the chemical functionality of the decorated CCTO@SiO2-GO composite. In this plot, it is clearly shown that the schematic diagram (Scheme 3.2.1.) of CCTO@SiO₂-GO composite exists with the group functionality proof. The OH bond of the GO can be observed at 3413 cm⁻¹. The stretching vibration band has seen at 1724cm⁻¹ was associated with the stretching of the free -C=O or -COOH band which is arisen due to the unreacted carbonyl groups in GO with core-shell NPs. The characteristic peak of the silica can be seen at 1235 cm⁻¹ (Si–O–Si, asymmetric stretching). 1570 cm⁻¹ peak has been observed and is responsible for the formation N-C asymmetric stretching mode, it may be arisen due to the bonding interaction of amine group of CCTO@SiO2 NPs and hydroxyl of carboxylic group of GO NPs. The peaks of 563 cm⁻¹, 557 cm⁻¹ and 447 cm⁻¹ show the presence of precursor material Ti-O, Cu-O and Ca-O bending modes respectively. GO has epoxy groups before the experimental synthesis procedure but after the required process, the nucleophilic O of the epoxy group may be converted to a hydroxyl group and electrophilic C-H group attached to the nucleophilic part of the Si-coated CCTO NPs [298, 299]. CCTO is a perovskite material [283] and it does not have any organic functional group in the material so why coated Silica bearing functionalized amine group is helping in the fabrication of this nanomaterial composite.CSG-2 is showing the highest percentage of transmittance that means maximum frequency passed straight through this material without being absorbed as it is well spread over the surface of GO so why it is showing the highest value of transmittance.

3.2.8. Raman Spectra analysis of CCTO@SiO₂-GO nanocomposites

After going through the literature of Raman spectra for CCTO, silica coated CCTO NPs and GO we have observed a very similar vibrational mode result for the precursors of nanocomposites of CCTO@SiO₂-GO. **Figure** 3.2.6. (b) confirmed the peaks at 1353 cm⁻¹ (D-band) and 1593 cm⁻¹ (G-band) for GO whereas very similar peaks were observed at 444 cm⁻¹,503 cm⁻¹,572 cm⁻¹,1122 cm⁻¹ and 1324 cm⁻¹ for CCTO as well as core-shell CCTO@SiO₂ NPs. **Figure** 3.2.6 (b) suggest the Raman spectrum of the synthesized nanocomposite as it is a non-invasive method to give huge information about the randomness of atoms, the thermal conductivity of a nanocomposite material [300].

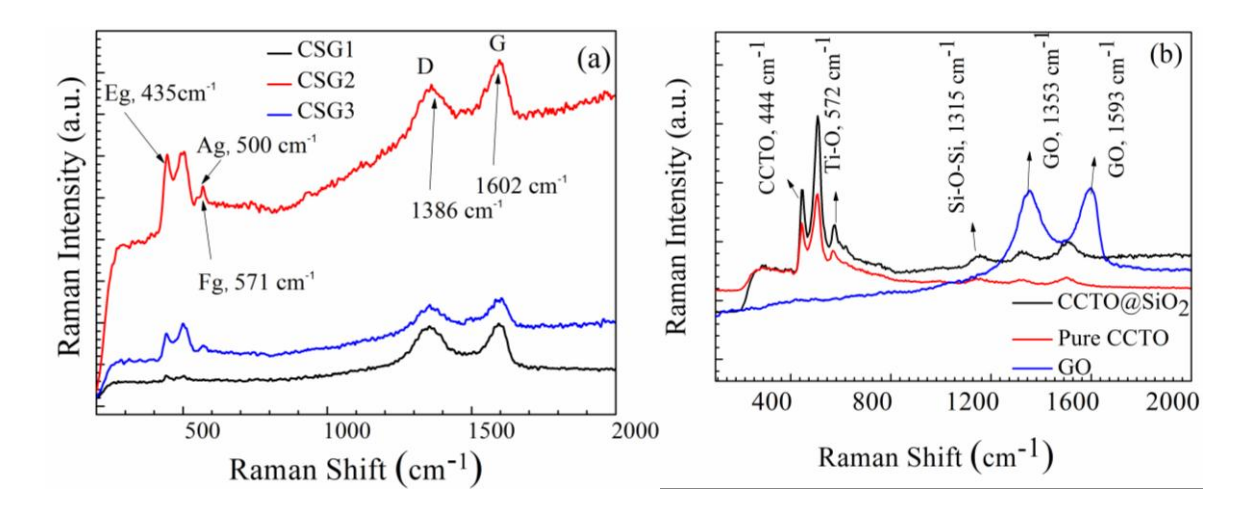


Figure 3.2.6. (a) Illustrates the Raman Spectra of CSG1, CSG2 and CSG3 nanocomposites synthesized from 2-4 nm, 5-7 nm and 15-17 nm Si coated CCTO NPs, respectively. **Fig.** 3.2.6. (b) represented Raman spectra for precursor materials.

The CCTO@SiO₂-GO composite shows two important bands of Raman spectrum irradiated by an laser beam, showing significant and strong D peaks at 1386 cm⁻¹, 1394 cm⁻¹ and 1353 cm⁻¹ and G peaks at 1586 cm⁻¹, 1602 cm⁻¹ and 1602cm⁻¹ for CSG1, CSG2 and CSG 3 which is very similar to D band at 1350 cm⁻¹ and G band at 1580 cm⁻¹ of GO sheet [301]. TEM images of the material suggested the presence of multilayer of the prepared nanocomposite. As the number of graphene oxide layers increases the shift of spectrum occurs and it mainly depends on the polarization of atoms through various angles [302].

Here it has seen that G band and D band for GO at 1602 cm⁻¹ and 1394 cm⁻¹ whereas TiO₆ rotation like and O-Ti-O anti stretching show their peak at 439 cm⁻¹ and 494 cm⁻¹ for highest coated CCTO@SiO₂-GO-3. Its intensity is very high as compared to other decorated material is shown in below **Table** 3.2.2. The G band is shifted to 1602 cm⁻¹ may be due to the presence of isolated organic unsaturated bonds in the material [303] which resonates at a higher frequency. To understand easily the concept of Raman modes of vibration of synthesized nanocomposites of CCTO@SiO₂-GO, **Table** 3.2.2 has been attached below.

As the disorder randomness increases, Raman intensity increases with separate disorder peaks. It is proved that longitudinal optical phonon mode is active near the armchair edge, where transverse optical phonon mode is active near the zig-zag edge. So this the reason leads the G-band intensity is enhanced from 1580 cm⁻¹ to 1602 cm⁻¹. Hence, it is concluded that the polarization of the excitation layer is parallel to the armchair edge and perpendicular to the zig-zag edge.

Table 3.2.2.: Raman modes of vibration of newly synthesized nanocomposites of CCTO@SiO₂-GO

Name of the	D-Band(cm ⁻¹)	G-Band (cm ⁻¹)	D-Band(intensity)	G-Band(intensity)
composite				
CSG1	1386	1586	371	391
CSG2	1394	1602	953	1033
CSG3	1353	1602	443	461

3.2.9. UV-Visible analysis for sheet like decorated CCTO@SiO₂-GO nanocomposites

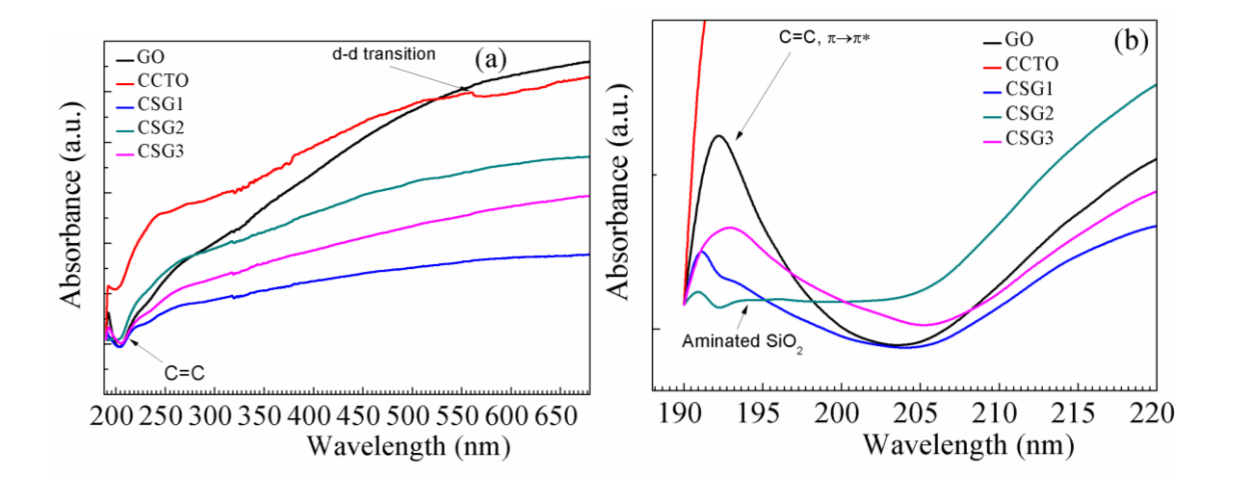


Figure 3.2.7. (a) and (b) illustrate UV-Vis NIR Spectrums of pure CCTO NPs, GO NPS, CSG1, CSG2 and CSG3 nanocomposites synthesized from 2-4nm, 5-7 nm and 15-17 nm Si coated CCTO NPs, respectively.

Figure 3.2.7. (a) shows the UV-Visible spectra in which GO is showing the highest intensity peak whereas other coated CSG1, CSG2 and CSG3 nanocomposites, as well as pure CCTO, shown a very less intensity. The effect of coating on GO is not allowing to occur the excitation of electrons from the surface in addition to the absence of high-intensity peaks. This above figure clearly shows the absence of π - π interactions of graphene oxide with any of the CCTO@SiO₂-GO nanocomposites where PGO is showing a clear excitation near 570 nm [212, 304].

3.2.10. Study on frequency and temperature dependence dielectrics of CCTO@SiO₂-GO nanocomposite: Dielectrics behaviour with respect to change in frequency

Table 3.2.3: Indicating the relative ϵ' and ϵ'' of CCTO@SiO₂-GO sheet like Nanocomposites at various frequency region

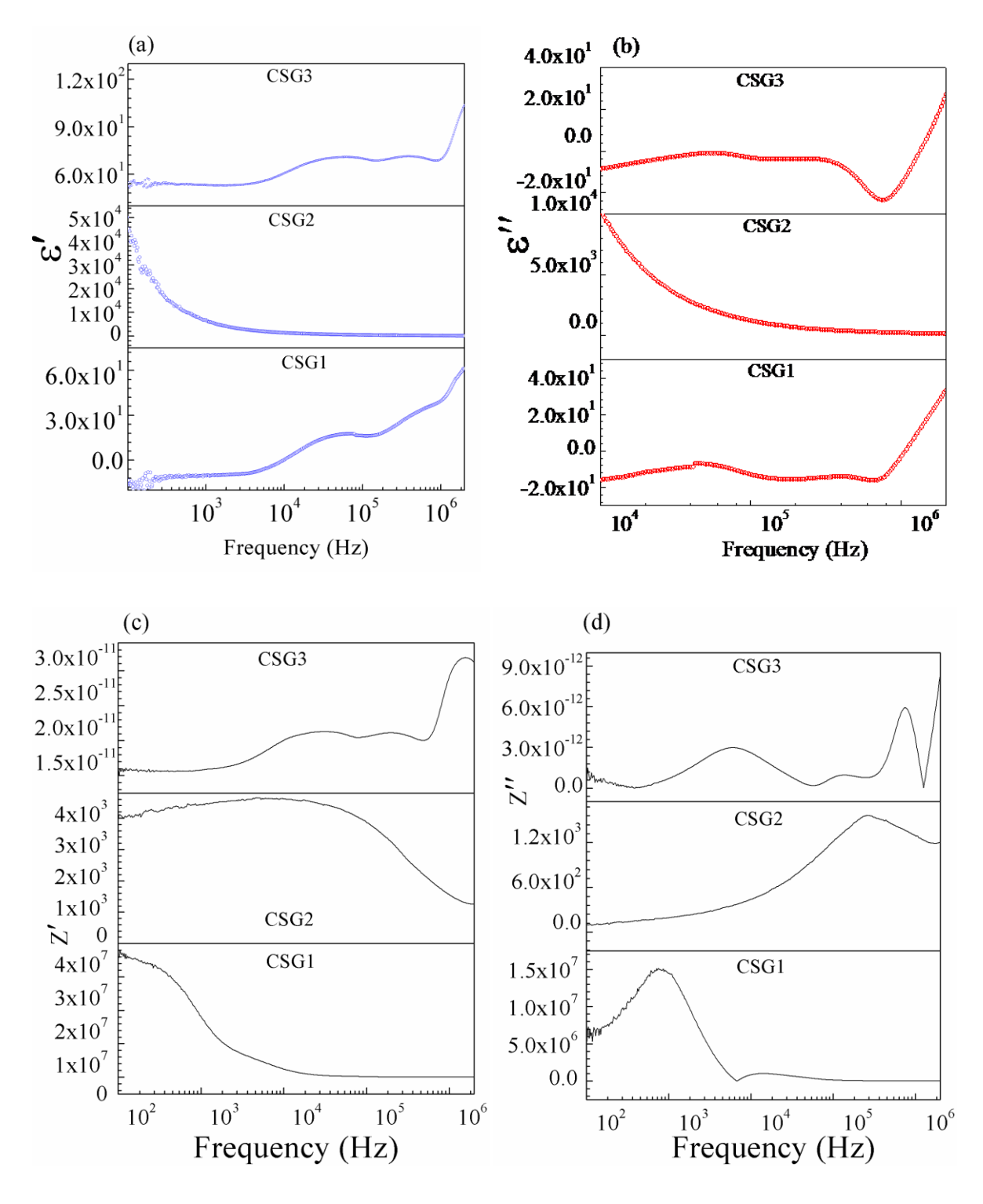
Frequency	CSG1(ε')	CSG2(ε')	CSG3(ε')	CSG1(ε")	CSG2(ε")	CSG3(ε")
(Hz)						
2×10 ² Hz	15.03	79873.9	66.55	397.88	6.2434E6	5.07
$1 \times 10^3 \mathrm{Hz}$	-9.65	4921.3	53.04	15.03	105888.5	-2.47
$5 \times 10^3 \mathrm{Hz}$	0.04	1674.9	60.3	-16.4	20350.8	-9.68
$1 \times 10^4 \mathrm{Hz}$	9.5	1149.5	66.78	-15.77	10059.6	-8.5
$5 \times 10^4 \mathrm{Hz}$	16.44	572.8	70.07	-7.15	2239.4	-0.96
$1 \times 10^5 \mathrm{Hz}$	19.22	448.23	69.29	-13.03	1199.9	-3.26
$5 \times 10^5 \mathrm{Hz}$	39.04	259.67	69	-14.55	338.37	-12.41
$1 \times 10^6 \mathrm{Hz}$	61.03	192.73	102.2	-3.38	208.98	-16.2
$2 \times 10^6 \mathrm{Hz}$	52.89	122.05	117.09	33.1	116.36	26.92

Table 3.2.4: Indicating the relative impedance constant and loss data of CCTO@SiO₂-GO Nanocomposites at various frequency region

Frequency	CSG1(Z')	CSG2(CSG3(Z')	CSG1(Z")	CSG2(Z"	CSG3(Z")
(Hz)		Z'))	
$2 \times 10^1 \mathrm{Hz}$	4.77569E	2953.2	1.55391E-	2.9788E6	33.49	5.1888E-
	7		11			12
$1 \times 10^3 \mathrm{Hz}$	1.79215E	4433.1	1.58087E-	1.44526E	192.17	7.20277E-
	7		11	7		13
$5 \times 10^3 \mathrm{Hz}$	4.9876E6	4642.7	1.80118E-	1.247E6	338.89	2.928E-12
			11			
$1 \times 10^4 \mathrm{Hz}$	2.3954E6	4608.3	2.00809E-	868213	441.6	2.594E-12
			11			
$5 \times 10^4 \mathrm{Hz}$	275739.3	4269.5	2.10168E-	428790	919.27	2.13612E-
			11			13
$1 \times 10^5 \mathrm{Hz}$	120973.1	3859.4	2.05731E-	131754.6	1223	8.04998E-

			11			13
$5 \times 10^5 \mathrm{Hz}$	7568.3	2176	2.0031E-11	17500.5	1459.5	2.9909E- 12
$1 \times 10^6 \mathrm{Hz}$	553.98	1558.8	2.92046E- 11	6234.5	1292.7	3.6693E- 12
$2 \times 10^6 \mathrm{Hz}$	1566.6	1254.5	3.1197E-11	2519	1205.2	8.354E-12

Fig. 3.2.8. (a) represents the plot for the variation of dielectric constant, with respect to frequency, range from 1×10^3 Hz to 1×10^6 Hz for of CSG1, CSG2 and CSG3 nanocomposites synthesized from 2-4nm, 5-7nm and 15-17 nm SiO₂ coated CCTO coreshell NPs respectively. Although the experiment was started at 20Hz as lowest frequency, due to an instrumental error we have avoided the data from 20Hz and have shown from 1×10^3 to 2×10^6 Hz. Complete data including dielectric along with impedance constant have been attached in Table 3.2.3. and Table 3.2.4. Fig. 3.2.8. (a) and 3.2.8. (b) have clearly shown about CSG2 which is showing the highest dielectric constant ϵ' of ~3×10⁵ and loss of ϵ'' $\sim 1 \times 10^6$ at 1×10^3 as due to the highest decoration property. The HRTEM image of **Fig**. 3.2.3(a) includes CSG2 nanocomposite and the coated CCTO NPs is well-spread all over the GO sheet. In the bearing of high dielectric constant nature of CCTO NPs over GO enhances the dielectric values as compared to other CSG1 and CSG3 nanocomposites. But the same composite is remarkably showing a giant value of constant ε' and loss ε'' of 7.9×10^5 and 6.2×10⁶ at 20 Hz. In comparison to CSG2, the other two composites i.e. CSG1 and CSG3 show dielectric constant ε' of 9 and 53 with loss ε'' of 15 and -2 at the same frequency. Dielectric values are very low, due to surface area covered by the CCTO@SiO2 core-shell NPs over GO NPs, which helps in a net polarization of dipoles or atoms present in both the material in the presence of an applied electric field. When an electric field is applied to the material of CSG1 and CSG3 it is not capable to show atomic polarisation effectively so why it shows very low dielectric constant ε' as compared to CSG2, wherein CSG2 core-shell NPs helps in the atomic polarisation.



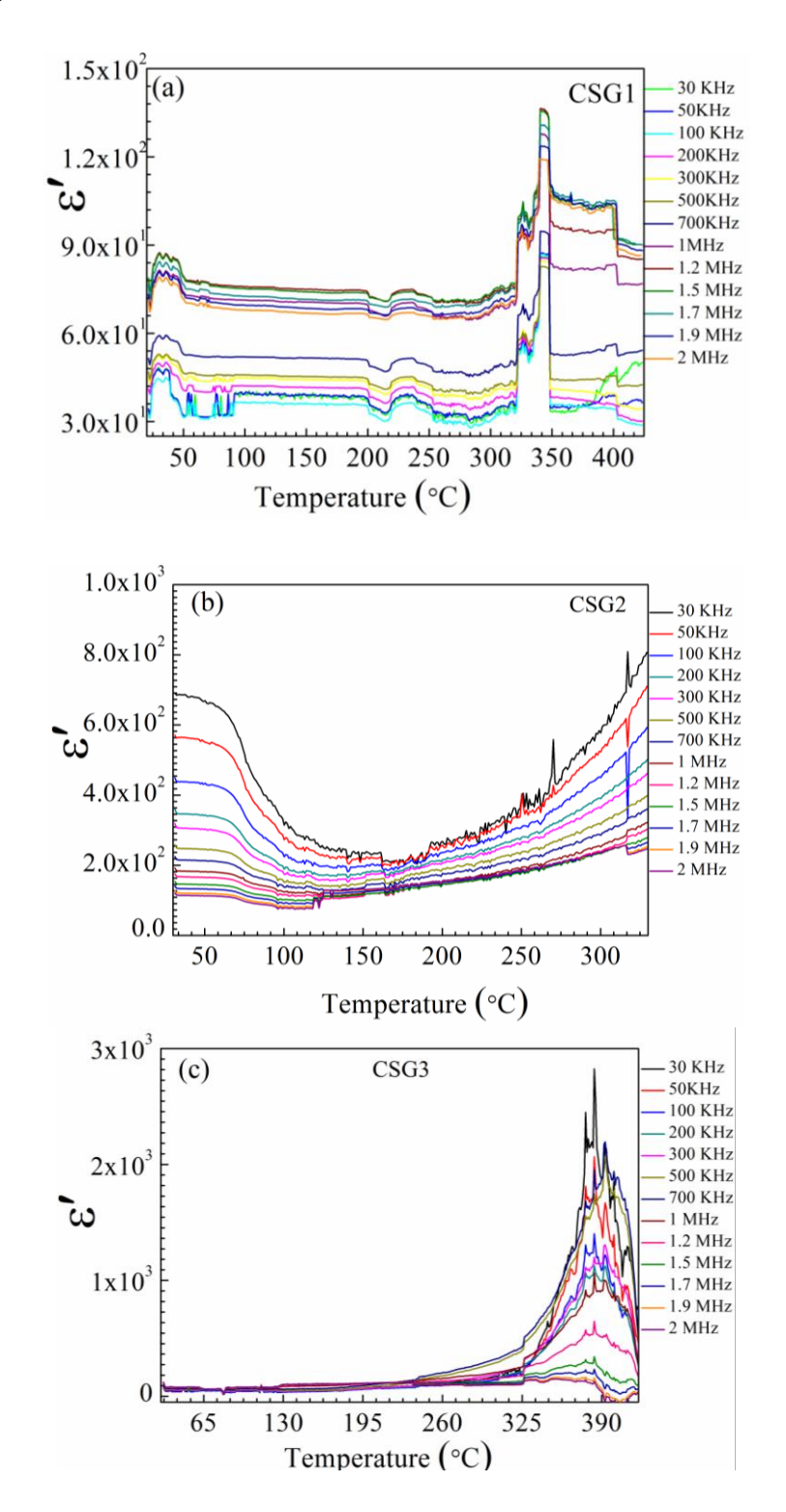
Figures 3.2.8.(a), (b), (c) and (d) Illustrate the Variation of dielectric constant (ϵ'), dielectric loss (ϵ''), impedance constant (Z') and impedance loss (Z'') with respect to frequency of CSG1, CSG2 and CSG3 nanocomposites synthesized from 2-4 nm, 5-7 nm and 15-17 nm Si coated CCTO NPs, respectively.

Another reason can be attributed for the high constant and loss of CSG2 once the frequency reached up to 1×10^4 Hz may be due to the dropping of dipole motion of dipole active atoms [282]. The dipoles present in the less decorated material i.e. CSG1 and CSG3 are dropping with an increase in frequency is due to less and more number of dipole active atoms respectively. As the number of dipoles is less the friction between dipoles against the surface of the precursor sheet will be less and contributes to the decrement of charge polarization attached to the material helping in the increment of dielectric constant ε' . But in the case of CSG2, the number of dipoles are more, leads to less polarization of charges hence dielectric constant ε' decreases. The higher the dielectric loss ε'' of silica coated CCTO-GO nanomaterial than the constant ε' CSG2 can be used in microwave technology as it may be due to the microwave property shown by the CCTO or Silica. This phenomenon can be used for application in microwave appliances [276]. CSG1 and CSG3 are showing a variable property which is not common in the dielectric study. The explanation for why the dielectric property shows a significant variation with the increase in frequency at constant room temperature is that it may be due to the dipoles like silica, ammine or CO₂ present in the material arises friction which goes against dipole motion and helps in dropping of constant [268].

Another significant variation of this nanocomposite may be due to the forces of attraction present in the material. We have already discussed a study about the presence of permanent dipoles inside the material, which may be affected by electronic polarization that leads to the electron shifting within the molecules. In a few cases, it is showing a negative dielectric constant and it may be due to the contribution of restoring force present in the isotropic sheet-like the structure of GO NPs [213].

From the above discussion, it is clear that only CSG2 is showing the best result of dielectric constant as compared to other coated nanocomposite. **Fig.** 3.2.8.(c) and (d) confirm that CSG2 nanocomposite is giving the lowest impedance value of $\sim 10^3$ whereas another composite is giving the value up to $\sim 10^7$. It confirms that CSG2 has a lower conductivity of electrons compared to other composites [211].

3.2.11. The temperature dependence of the dielectric properties of silica coated CCTO-GO nanocomposite



Figures 3.2.9. (a), (b) and (c) Illustrate the Variation of dielectric constant with different temperature from RT to 400°C at variable frequency region of CSG1, CSG2 and CSG3 nanocomposites synthesized from 2-4 nm, 5-7 nm and 15-17 nm Si coated CCTO respectively.

The temperature dependence of the dielectric behaviour of silica coated CCTO-GO composite shows a variable observation. As from earlier studies, it is clear that there can be a variation of dielectric constant with increase in temperature and it may be due to the crystallinity of the material or atomic arrangement or some other physical behaviour like the presence of permanent dipoles like secondary amines. The presence of secondary amine groups in the material shows the presence of H- bonding attached to the N- atom which leads to the permanent dipole effect, slightly less, but still, it behaves like a permanent dipole (See scheme 3.2.1 for bonding interaction).

Earlier studies give the information that the presence of permanent dipole inside material will contribute to the significant variation of dielectric constant ε' with temperature which can be explained in our study. The CSG2 material shows the best dielectric flow as we see in Fig. 3.2.9 (b). Fig. 3.2.9 (b) shows an explanatory image of temperature dependence dielectric behaviour. It shows the decrease of ε' from 7×10^2 to 3×10^2 with the temperature range from RT to 175°C may be due to the loss of organic groups like hydroxyl or amine groups, which have reached their respective boiling points and ceases the charge polarization. But after reaching 175°C, ε' started to increase till it reaches up to a higher temperature and can be explained based on the occurrence of structural disturbance. The structural disturbance may occur due to the vanishing of hydroxyl /COO- groups in GO to form numerous bonding interactions with the amine or silica group of core-shell CCTO@SiO2 NPs and make it as defective structure. The formation of covalent C-N or VanderWaals O-Si -H may also play the variation of dielectric constant. Fig. 3.2.9 (a) and (c) images of CSG1 and CSG3 have given an idea that with an increase in shell thickness of silica coated CCTO on GO sheet the dielectric constant is also increasing. Here CSG3 gives highest ε' of ~ 1.3×10⁴ (Fig. 3.2.10.) while CSG1 and CSG2 are giving around 1×10^3 and 1×10^2 . These two composites have shown an irregular dielectric behaviour as compared to CSG2. Fig. 3.2.9. (a) shows that at high-temperature, ε' is slightly decreasing may be due to the polarity effect. The polar groups present in the material like SiO₂ affects the disturbance to the alignment of dipoles like leftover substituted amine for which it causes to decrease of ε' at high temperature [198, 305].

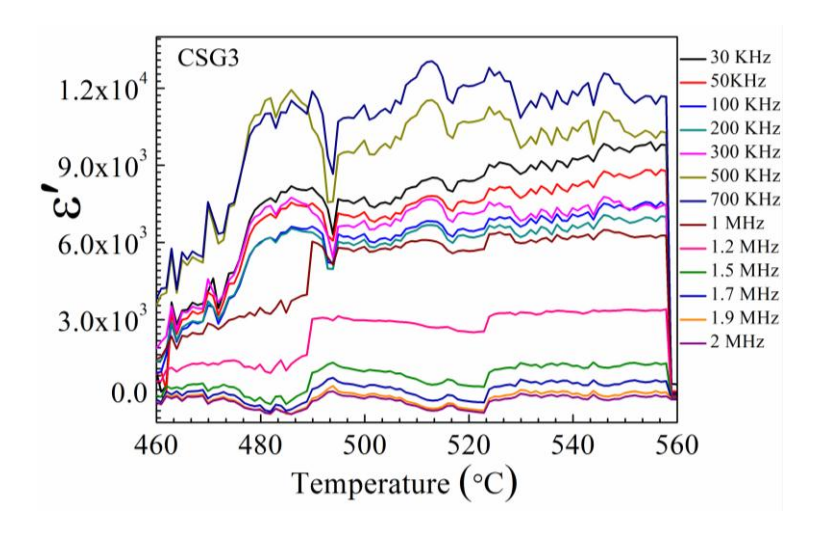
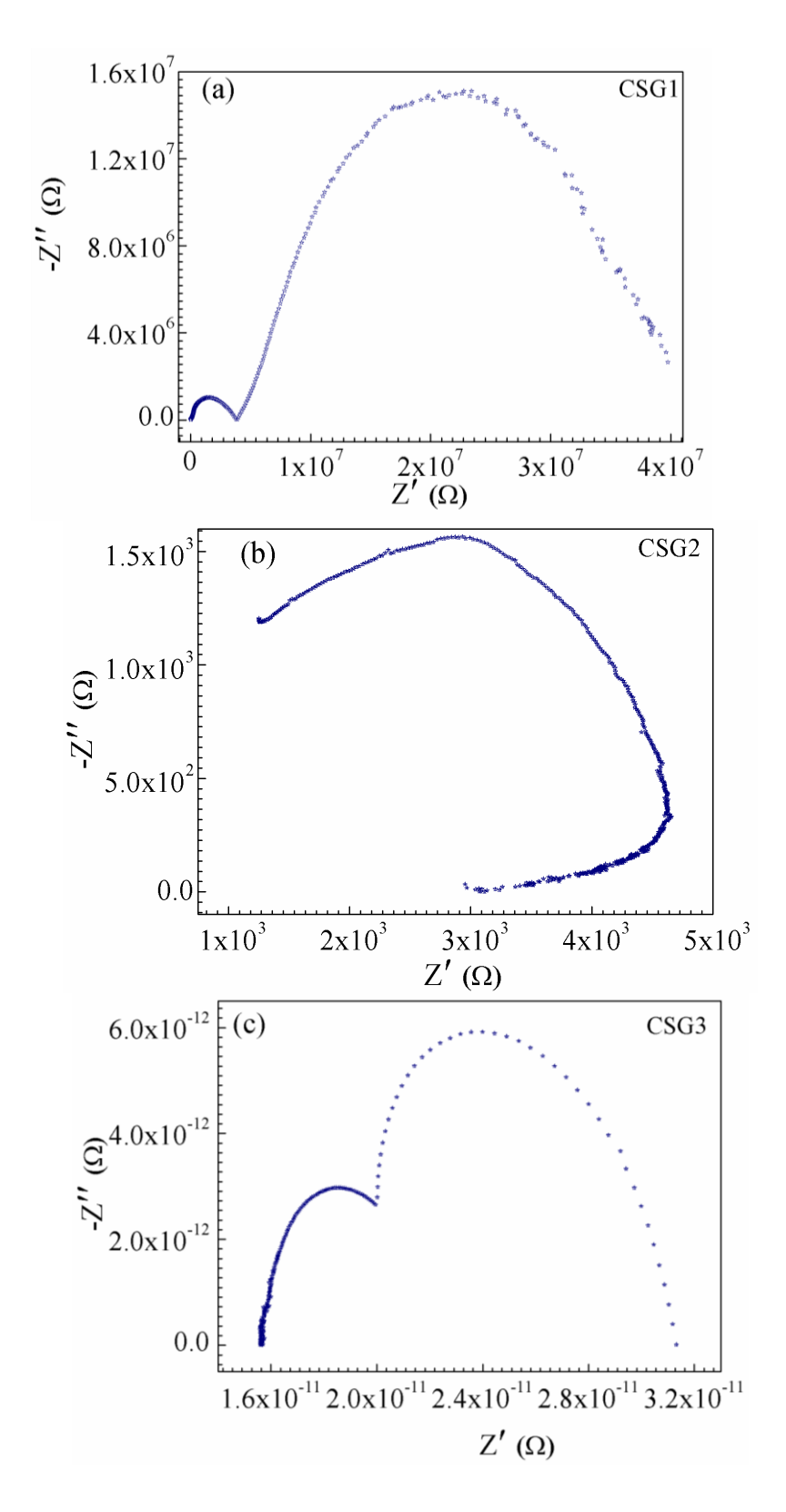


Figure 3.2.10. represents temperature dependent plot with variable frequency of highest thickness coated silica-CCTO over GO for CSG3 nanocomposite.

Hence, CSG3 composite possessed a high dielectric constant up 10^4 value is due to the more amount of silica present in the material (**Figs.** 3.2.3 (a)) and 3.2.10. also confirmed that this composite is even stable up to 550° C possessing constant up to $\epsilon' \sim 1.15 \times 10^4 \sim 1.3 \times 10^4$ for 500 kHz and 700 kHz respectively with all other frequency in descending order.

3.2.12. Cole-Cole plot for sheet like nanocomposites

These three synthesized nanocomposites of GO-CCTO@SiO₂ are showing a very dissimilar type of Cole-Cole plot among, ranges in low as well as the high-frequency region. Fig. 3.2.11.(a) CSG1 and (c) CSG3 represent two semicircle segment proving the presence of two types of dielectric relaxation for decorated material as the dipoles present in them have relaxed twice [202]. This type of two semi-circles have taken place due to the interaction of basal plane and functional groups like epoxy (-O-), carboxyl (-COOH)or hydroxyl (-OH) groups present in GO with applied field or may be due to interfacial polarization occurred due to decoration between GO and core-shell NPs which is mentioned in our previous work [268]. CSG2 with the highest decoration has shown a distorted semicircle may be due to relaxation caused by loss of conductivity in CCTO NPs.In the case of CSG2, all dipoles have relaxed in a single phase of time wherein the case of CSG1 and CSG3 have accomplished with two relaxation time resulting in them to two semicircles. Hence highest decorated material has shown a perfect Cole-Cole plot than other synthesized composites.



Figures 3.2.11. (a), (b) and (c) represent the Cole-Cole plot in the low and high-frequency region for of CSG1, CSG2 and CSG3 nanocomposites, respectively.

3.2.13. Part IB-Conclusion of CCTO@SiO₂-GO nanocomposites

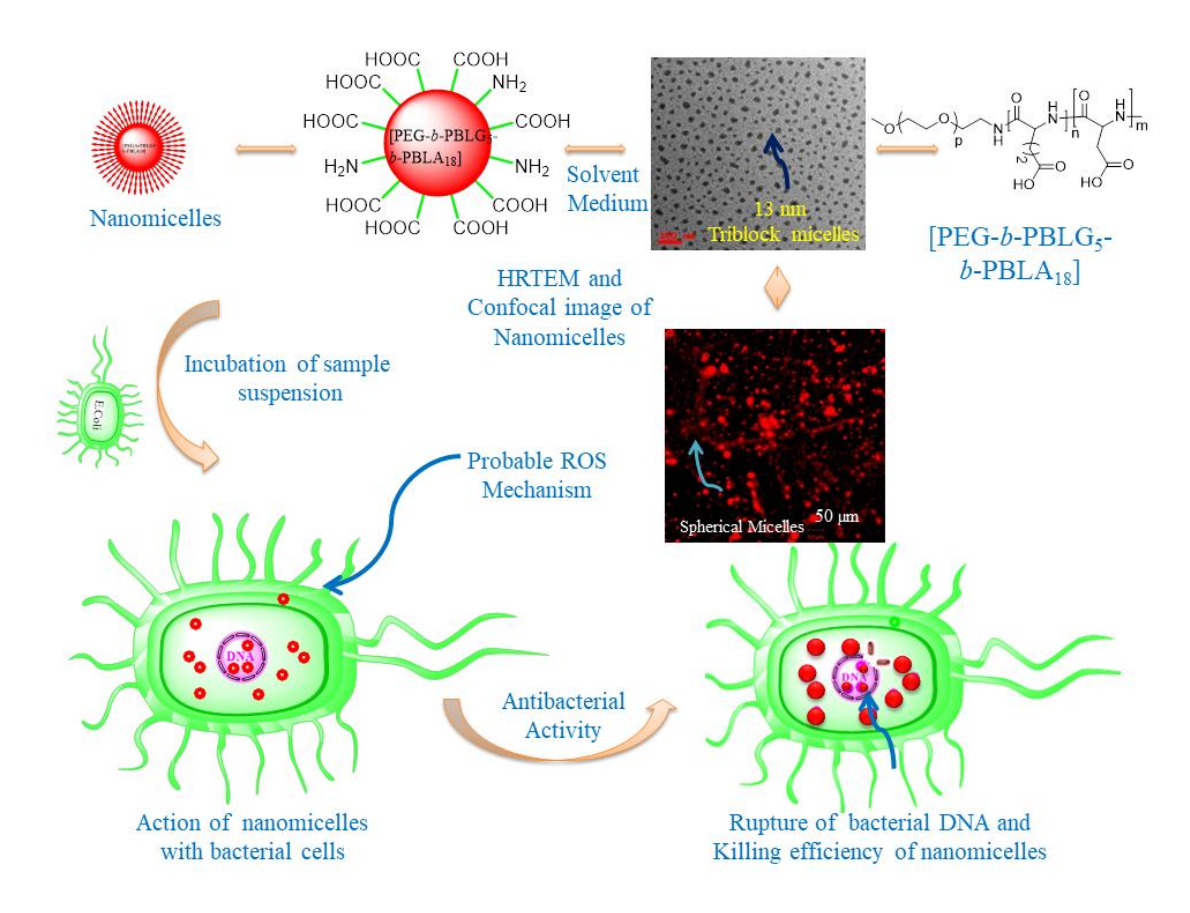
In this work, a series of CCTO@SiO₂-GO nanocomposites have been prepared through a novel synthesis method. Silica-coated CCTO NPs decoration over the surface of GO plays the vital for the successful synthesis which mainly considers few environmental conditions like balanced atmospheric condition, Stirring and centrifugation rpm, sonication time duration and amount of solute. It shows a variable study of dielectrics with respect to the different temperature and frequencies. The material shows a high ϵ' of 1.5×10^4 after 500°C which can be used as a good dielectric material for the electronics device use as sensors, charge storage devices etc. But a high loss was also observed more than constant at corresponding frequencies lead to its use in the microwave electronics device industry. Concluding to this chapter, the prepared nanocomposite can be used as a good dielectric material with the variation in the thickness of silica decoration over CCTO NPs and GO sheet. Even though many reports have given an idea about being used in wide areas, however, our work has established new nanocomposites which can be used in designing new functional electronic devices and electrochemistry.

RESULTS AND DISCUSSION

Part II. Amino acid Based Polymeric Nanobiomaterials

Part II A. Stimuli responsive biocompatible synthetic polypetidic nano micelles: Novel approaches towards antibacterial & therapeutic applications

Graphical Abstract:



TOC of Part IIA: Stimuli responsive biocompatible synthetic polypetidicnano micelles: Novel approaches towards antibacterial & therapeutic applications

Outcomes of this Part

- **1. <u>Debasrita Bharatiya</u>**, Biswajit Parhi, Khumukcham Saratchandra Singh, Bramanandam Manavathi, Pradip Paik (Manuscript under Communication)
- 2. <u>Debasrita Bharatiya</u>, Pradip Paik. The synthesis and study of AB, BC and ABC types of Bio-Compatible amino acids based block copolymers for biomedical application. (**Poster Presentation**). **November 08-10, 2017**, Panjab University, Chandigarh, India, **International Conference Nano Sci Tech 2017**

Part IIA (*Objective 3*): Target to develop biocompatible synthetic polypeptidicnano micelles of [PEG-b-PBLG₅-b-PBLA₁₈]

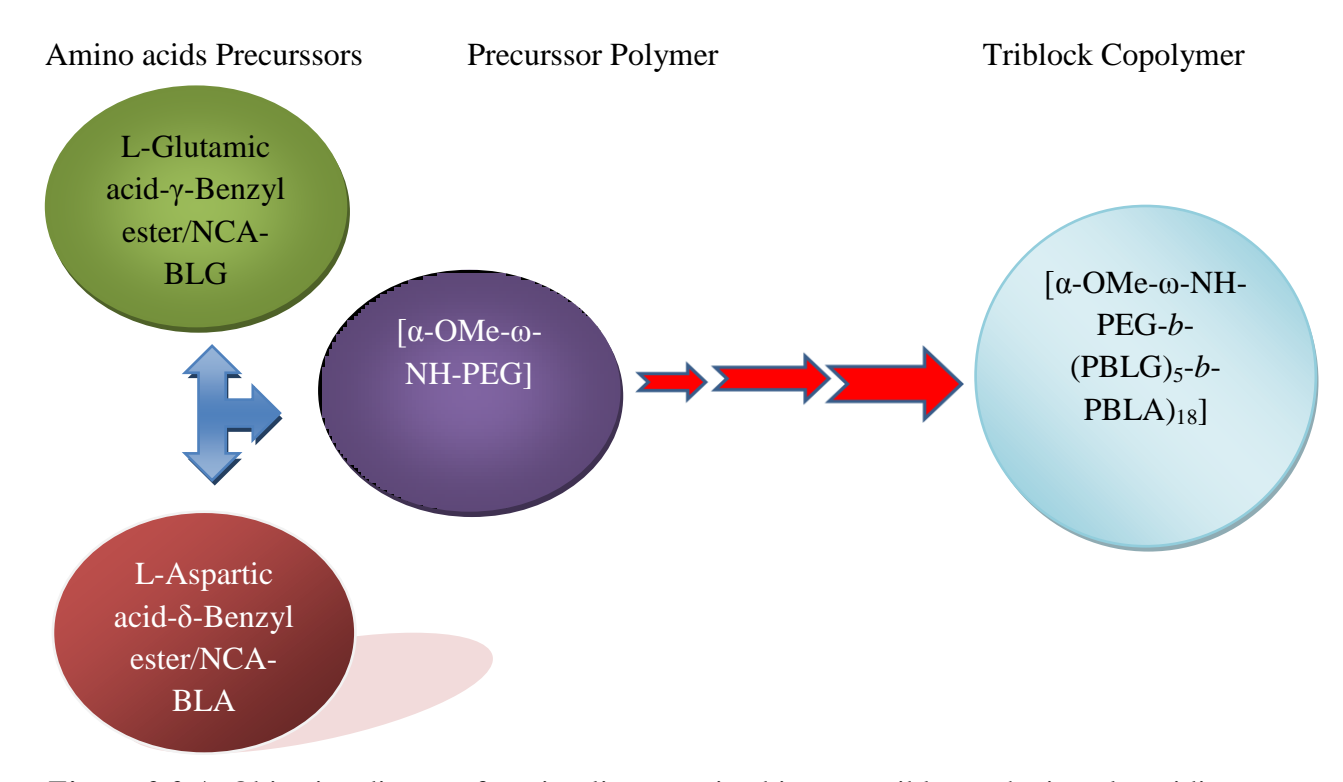


Figure 3.3.A. Objective diagram for stimuli responsive biocompatible synthetic polypetidic nano micelles [α-OMe- ω -NH-PEG-b-(PBLG)₅-b-PBLA)₁₈]

3.3.1 Abstract

This work represents the successful synthesis of self-assembled nano micelles of triblock copolymer of α -methoxy- ω -amino Poly(ethylene Glycol)-L-Glutamate-L-Aspartate [MeO-PEG-NH-b-(L-GluA)5-b-(L-AspA)18]/[PEG-b-PBLG-b-PBLG] through modified ring-opening polymerization approach of NCAs L-Glutamic acid- γ -benzyl ester and L-aspartic acid- δ -benzyl ester. HRTEM have confirmed the average sizes of micelles range of ~13 nm and ~22 nm for triblock [PEG-b-PBLG-b-PBLA] and diblock [PEG-b-PBLG] copolymers, respectively. The Laser Confocal study has given the concrete evidence on the formation of micelles in the presence of the solvent medium. The folding, unfolding behaviour with several stimuli action was investigated detailed through dynamic light scattering, Zeta potential and Circular dichroism studies. The synthetic polypeptides exhibited self-assembly behaviour and finally formed a stage of denatured protein due to the change in temperature and pH ranges. It is revealed that at pH 8 and 35°C, polymers exhibited the highest percentage of β -sheets and random coils. These polymers exhibited a significant protein folding behaviour with more percentage of random coils and antiparallel β -sheets

formation due to the presence of active -COO and -NH₃⁺ groups on the surface of the micelles. Zeta potential analysis result supports the highly colloidal stability of polymer micelles with ζ value of - 45 mV. Biocompatibility of the block copolymeric micelles was confirmed using against MDA-MB231 cell lines through MTT assay. Finally, the antibacterial activities for both the polymeric micelles were studied through the broth microdilution method and found to be effective both for *gram* (-) *E.coli* and *gram* (+) *Staphylococcus aureus*. It is revealed that the triblock copolymeric micelles inhibited the growth of the *gram* (-) *E.coli* at a very minimum concentration of 0.0048mg/ml. Thus the present work directed that the synthesized di-/tri-block-polymers and their micelles could have potential uses in biomedical and for therapeutic applications.

3.3.2. Introduction and Motivations

Herein, we have synthesized ABC type triblock copolymer of α -methoxy- ω -amino-(poly ethylene glycol)-L-glutamic acid-L-aspartic acid, i.e. [MeO-PEG-NH]-b-(PBLG)₅-b-(PBLA)₁₈] by ring-opening polymerization method of NCAs and studied various biomedical applications including antibacterial activity due to its colloidal properties like self-assemble nature with temperature and pH responsive behaviour for biological activities inside the body, very minute sized micellar morphology, and thermal stability. We have earlier reports on diblock copolymer [PEG-b-PBLG] with its characteristic properties. However, the detailed study on folding, morphology, versatile biological application scope and size variation with the adverse effects such as pH and temperature have not reported yet [241]. We have considered amino acid chain as our primary backbone of the polymer due to its associative nature [242], unique colloidal properties [243], and biocompatible nature [244] which further can be used for various pharmaceutical and medical applications [245]. Morphology of numerous shapes of these type polymers can also exhibit significant results in physio-chemical behaviour[246-248] Very small polymeric micelles (d ~10nm) can be used as a drug delivery vehicle for targeted therapy and other biomedical applications. Present work is extended on the protein folding nature with changing the pH from 4 to 10 and varying the temperature from 20°C- 50°C using Circular dichroism of our polymeric micelles. Further, we have studied the biocompatibility of the synthesized polymers through MTT assay. Finally, the antibacterial susceptibility for polymer micelles was investigated using gram (+) staphylococcus aureus and gram (-) E.coli at a very minimum dilution of polymers. The antibacterial study provides information for the future applications of our triblock-copolymers.

3.3.3. Synthesis of a triblock copolymer of [PEG-b-PBLG-b-PBLA]

The detailed synthesis method has been discussed elaborately in chapter 2 and section 2.3. This method involves the conversion of acid to anhydride with the help of a reducing agent triphosgene which is highly hygroscopic. Few gm of PEG was added to a solution of NCA BLG and allowed for few days hrs of reaction till it produced a shiny pale yellow solid. After the intermediate reaction is completed, we have added the dissolved solution of NCA BLA with dry THF to the [PEG-b-BLG] solution. The reaction mixture turned into a transparent solution after the addition of NCA BLA. The reaction mixture was again allowed to stirrer maintaining optimized environmental parameters. After the completion of the reaction, the mixture was evaporated and purified through recrystallization method (hexane and THF, 1:1). Then hydrogenation was performed using Pd-C, H₂/THF to obtain the final block copolymer. The synthesized product was collected and allowed for freeze-drying.

3.3.2.1. Cell Viability Study and MTT assay

The standard methyl thiazolyltetrazolium (MTT) assay was used for the biocompatibility test of the above polymeric micelles using MDA-MB231 cells (obtained from National Centre for Cell Science (NCCS), Pune, India). Cells were cultured in Dulbecco's Modified Eagle medium (DMEM) supplemented with 10% heat-inactivated fetal bovine serum (FBS), 100 units/ml penicillin, 100µg/ml streptomycin and cultured at 37°C, 5% CO₂ humidified incubator. Details of the methods have been discussed in our previous reports [174].

3.3.2.2. Antibacterial activities Studies against different bacterial models

In vitro antibacterial susceptibilities of polymeric micelles were investigated by broth dilution method using two microorganism gram negative ATCC bacterial strains of Escherichia coli (ATCC-25922) as well as with gram positive Staphylococcus aureus (ATCC-25923). The bacterial strains were taken and maintained at 4°C. Briefly, 5μl of the bacterial culture in each segment of 96-well plate followed by 150μl of broth containing 50μl different concentrations (1.25mg/ml with serial dilution up to 0.0048 mg/ml) of samples [PEG-b-PBLG-b-PBLA] and [PEG-b-PBLG₅-b-PBLA₁₈], and incubated for 24hr at a physiological temperature 37°C for both the bacterial strains. The last segment was the tenth segment consisting of bacterial strains but without any sample medium. We have studied the antibacterial activities of polymeric micelles with different types of bacteria and have found

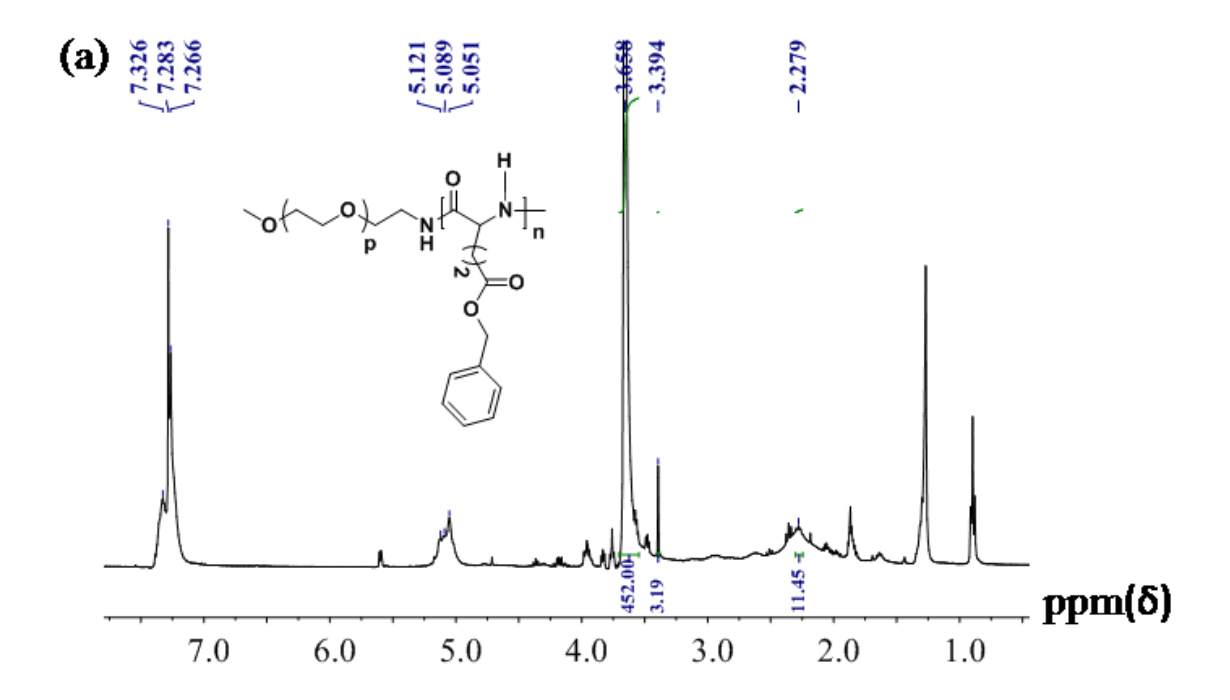
the effectiveness of our materials for further biomedical applications. All the samples were characterized by suitable methods.

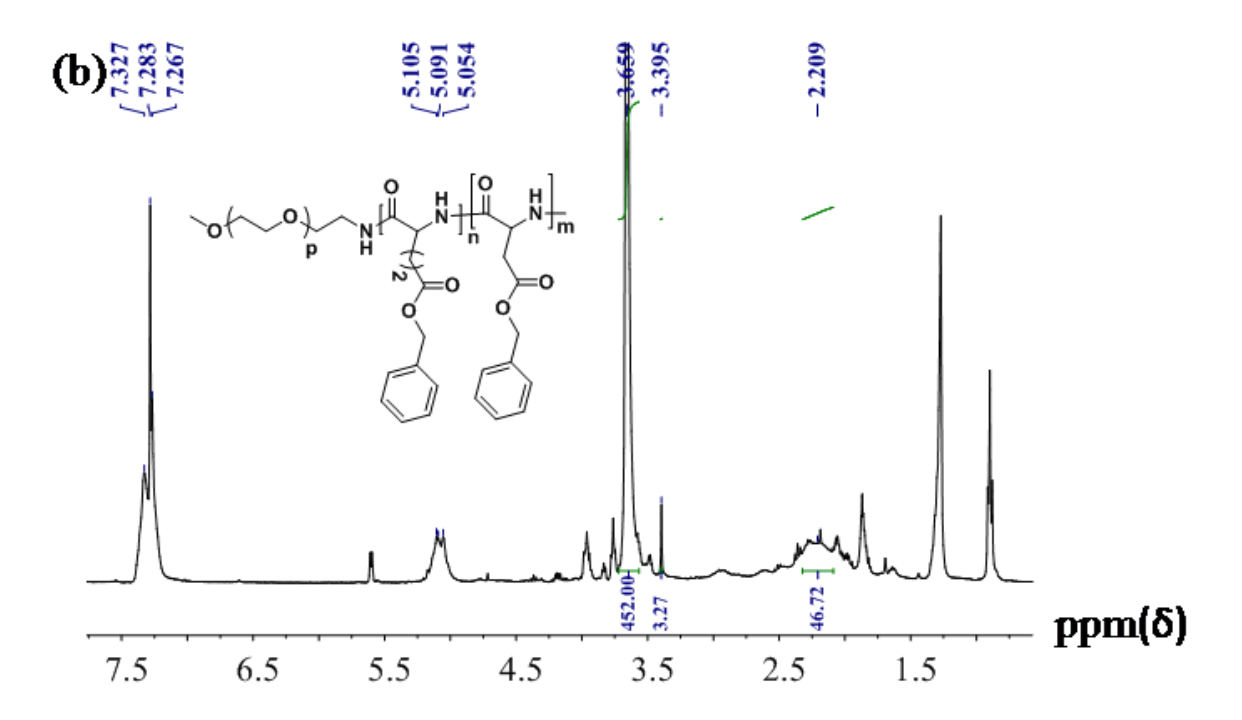
3.3.4. Reaction Pathway for the formation of [PEG-b-PBLG-b-PBLA] block copolymer

Schematic 3.3.1: The mechanistic pathway involved in the synthesis approach of polymers through ring-opening polymerization of [PEG-b-PBLG-b-PBLA].

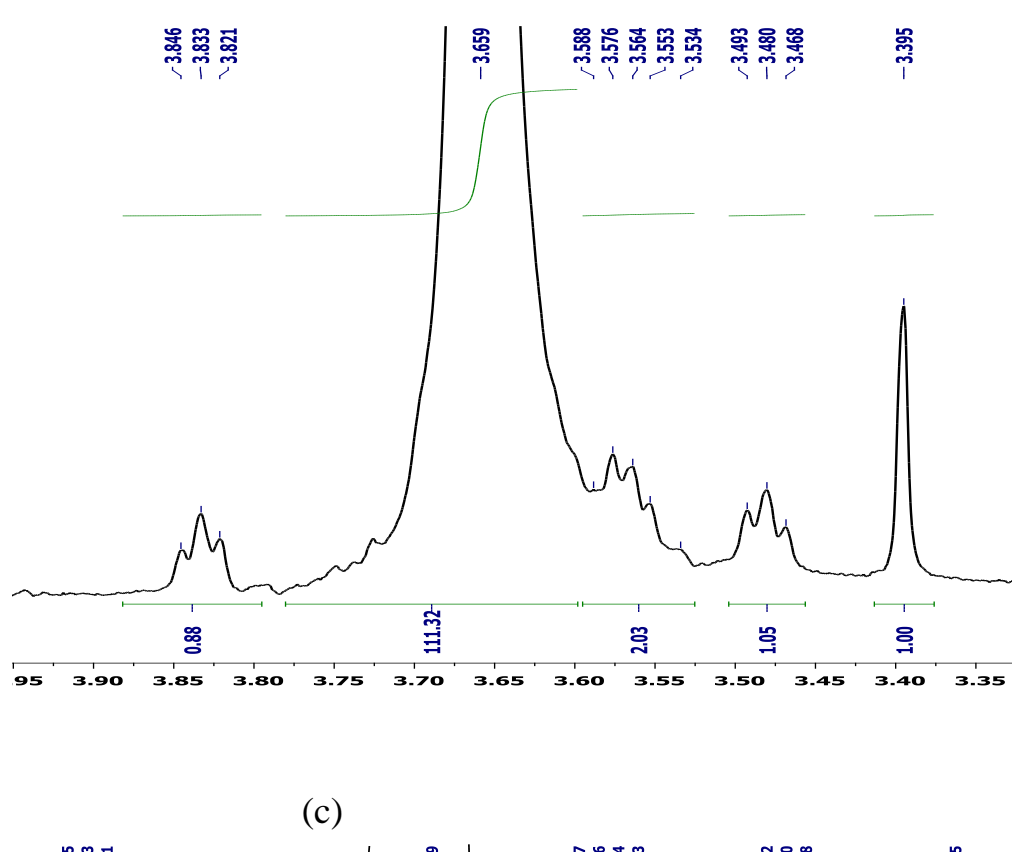
In short, the AB diblock copolymer of PEG-b-BLG has been synthesized first then the new block of NCA BLA has been attached to the electron-rich N-terminal of glutamate forming an amide -(C=O)-NH₂ bond. For better understanding, we have designated prepared samples as diblock [PEG-b-BLG] polymeric micelles and triblock [PEG-b-BLG-b-BLA] polymeric micelles before catalytic hydrogenation method. The mechanism followed the ring-opening polymerization method to develop di and triblock copolymer following dehydrogenation method.

3.3.5. Structural Confirmation through ¹H NMR Analysis





Figures 3.3.1. (a) and (b) represent the ¹HNMR results of diblock copolymer [PEG-*b*-BLG] and triblock copolymer of [PEG-*b*-BLG₅-*b*-BLA₁₈] before catalytic hydrogenation, respectively. Where p= no. of CH₂ units of PEG, n= no. of CH₂ units of glutamate and m= no. of CH₂ units of aspartate, (See **Scheme** 3.3.1).



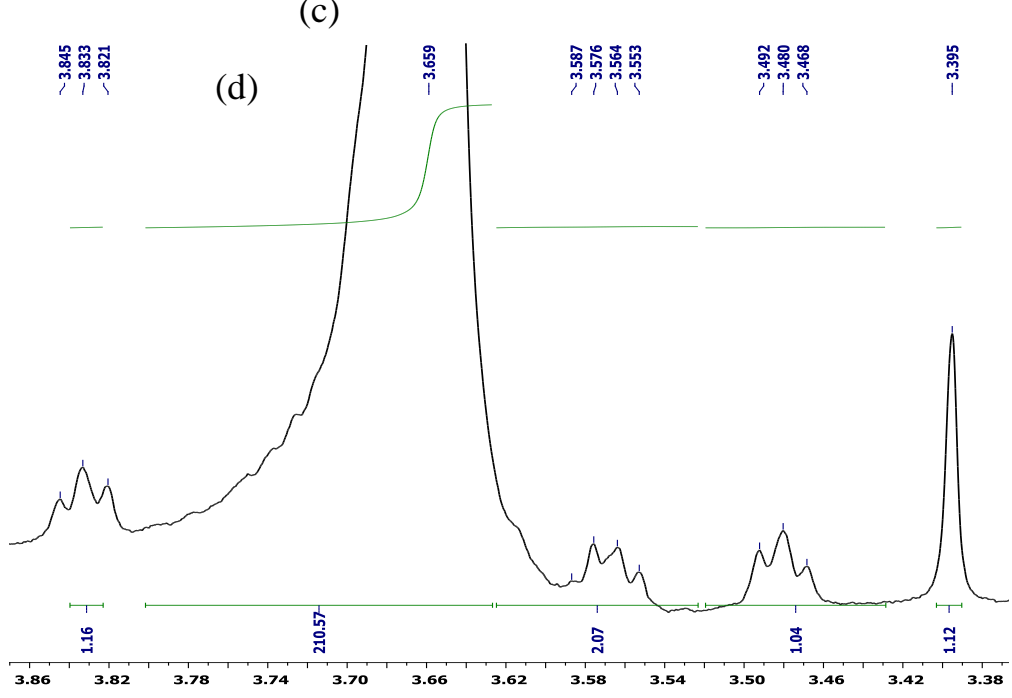
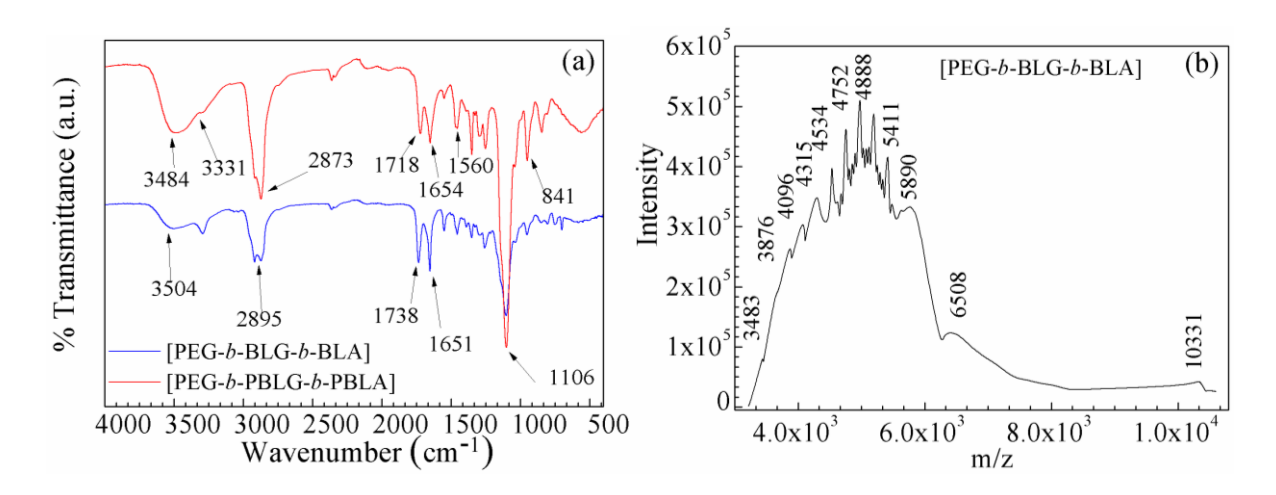


Figure 3.3.1. (c) and (d) represent the cross-sectional H¹NMR data of diblock copolymer of [PEG-b-PBLG] and triblock copolymer of [PEG-b-PBLG-b-PBLA] after catalytic hydrogenation respectively. Where n= no. of CH₂ units of glutamate and m= no. of CH₂ units of aspartate.

Figure 3.3.1. (a) represents the ¹HNMR results of [PEG-b-BLG₅] diblock copolymer before catalytic hydrogenation which confirms the presence of n = 5 number of glutamic – CH₂- units attached to the linear backbone of (MeO-PEG-NH₂). This also confirmed from the number of -CH₂ units in below MALDI results [241, 306]. ¹HNMR results confirm the presence of $\delta = (7.20, 5H, \text{ an aromatic proton of (BLG)}_5, \delta = (7.0, CDCl_3), \delta = (5.21, Ar-$ CH₂-), $\delta = (3.36, 452H, CH_2 \text{ group of MEO-PEG-NH}_2)$, $\delta = (3.4, -OCH_3) \delta = (3.1, CH_2 \text{ alpha}_2)$ to C-N bond), $\delta = (2.26,11\text{H}, \text{CH}_2 \text{ group (BLG)}_5 \text{ and } \delta = (1.9, 3\text{H}, -\text{CH}_3)$. Whereas after addition of third block i.e, NCA BLA to diblock of [PEG-b-BLG], it has been calculated the presence of n = 18 number of $-CH_2$ units, showing 46 units of around δ 2.3 (see in **Fig.** 3.3.1. (b)). Fig. 3.3.1(b) shows that additional n = 10 number of $-CH_2$ units have been attached to the amide backbone of diblock and the other proton active bands present at $\delta = (7.33, 12H,$ an aromatic proton of glutamic acid and aspartic acid with CDCl₃), $\delta = (5.603, 3H, a)$ benzylic proton), $\delta = (3.7, 452H, -a CH_2 \text{ group of MEO-PEG-NH}_2)$ and $\delta = (2.261, 46H, -a CH_2 \text{ group of MEO-PEG-NH}_2)$ CH₂ group of glutamic acid, and aspartic acid). The synthesized benzylated triblock polymer [PEG-b-BLG₅-b-BLA₁₈] has shown the shifting of methylene group from $\delta = 2.279$ to $\delta =$ 2.209 due to the shielding effect caused by the more number of proton signals towards TMS.

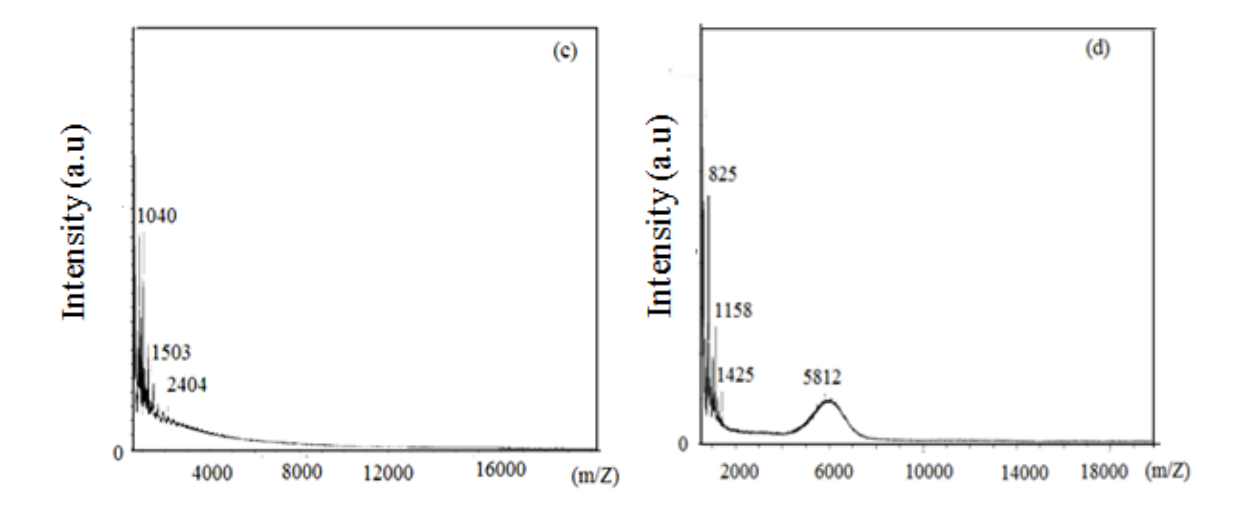
Fig. 3.3.1. (c) represents the near view cross sectional NMR data of [PEG-b-PBLG] diblock copolymer of after catalytic hydrogenation and very similar peaks to [PEG-b-BLG], however, there is the absence of benzyl protons. **Fig.** 3.3.1. (a) and (b) have shown the diastereoselective nature of polymer with 1:2 ratio. These figures confirmed the more diastereoselective property of the diblock and triblock copolymer before catalytic hydrogenation than after hydrogenation (1:1.2). The diastereoselective data for [PEG-b-PBLG]: [PEG-b-PBLG-b-PBLA] explained the lower intense peak was integrated into one and the higher intense band was calculated with respect to the lower which shows 2:1 diastereoselectivity after hydrogenation. Thus, ¹HNMR study confirmed that the amino acid based NCA BLA groups are attached to the backbone of di-block polymer [PEG-b-BLG] successfully and the polymeric micelles are diastereoselective in nature. This result is promising in controlling the folding behaviour of the synthesized copolymers that have been explained in the subsequent section through the CD study.

3.3.6. Chemical Functionality and Molecular Weight Confirmation by FTIR and MALDI-TOF Analysis



Figures 3.3.2. (a) represents the FTIR spectra of type triblock copolymer of [PEG-*b*-PBLG-*b*-PBLA], before [PEG-*b*-BLG-*b*-BLA] and after catalytic hydrogenation [PEG-*b*-PBLG-*b*-PBLA], respectively and (b) MALDI-TOF of triblock copolymer of [PEG-*b*-BLG₅-*b*-BLA₁₈] before catalytic hydrogenation.

Figure 3.3.2. (a) shows the FTIR spectra of [PEG-b-PBLG₅-b-PBLA₁₈] triblock copolymer before and after catalytic hydrogenation of ABC copolymer. The characteristic bands appeared at 3484 cm⁻¹ (O-H str. of terminal acid), 3331 cm⁻¹ (N-H str), 2873 cm⁻¹ (C-H str of –CH₂ units), 1718 cm⁻¹ (α-NH Carboxylic acid group), 1654 (amide, C=O), 1560 cm⁻¹ ¹ (2° amide), 1466 cm⁻¹ (C-H def) in methylene group and 841 cm⁻¹ (-CH₂ rocking). For triblock b-ABC bands appeared at 1651 cm⁻¹ (for amide I, -CONH₂), 1545 cm⁻¹ (for amide II, -CONH-), 1738 cm⁻¹ (for benzyl ester, C=O). The bands for benzyl ester at 1738 cm⁻¹ (-C-O of MeO-PEG-NH₂) have disappeared due to the catalytic hydrogenation. Presence of absorption band at 1651 cm⁻¹ is due to the α-helical structure which further has been confirmed through CD spectroscopy study [266]. Thus FTIR results exhibited that benzyl ester group gas been removed successfully by hydrogenation using H₂/C/Pd from [PEG-b-BLG-b-BLA] polymer [306-309]. Due to the removal of the benzyl group from the polymeric chain increases the biocompatibility of the synthesized polymers. The newly synthesized triblock copolymer of [PEG-b-PBLG-b-PBLA] after catalytic hydrogenation exhibited more intense band in FTIR spectra than [PEG-b-BLG-b-BLA] polymer, which happened due to the introduction of the additional number of functional groups as the new block produces several transmissions causing factors. Further, the FTIR spectra confirmed the presence of pure triblock copolymer with targeted functional groups like amide, carboxylic, hydroxyl and C-N groups for targeted delivery to the human cell.

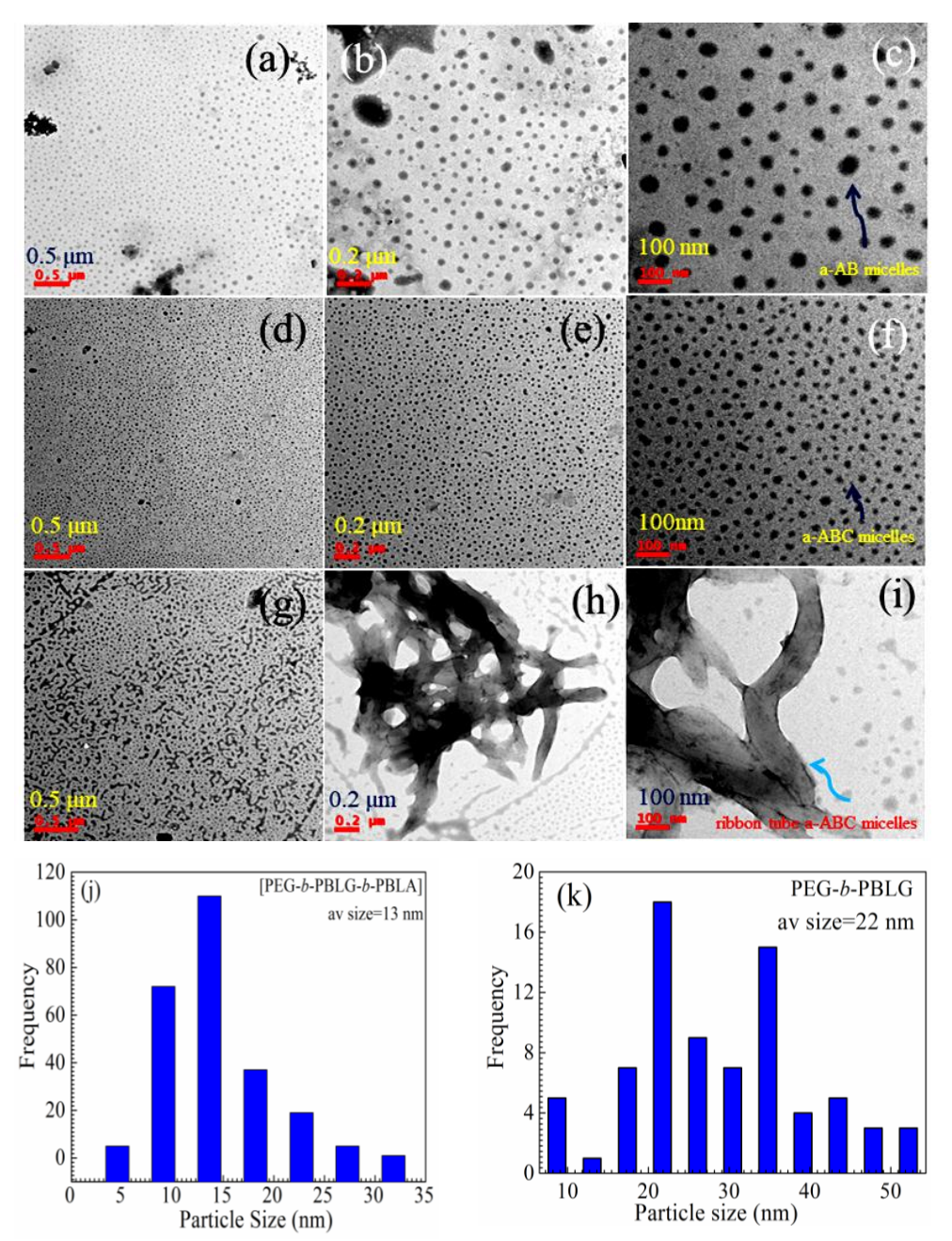


Figures 3.3.2. (c) and (d) represent the MALDI data of NCA BLG which is a precursor for the synthesis of diblock copolymer [PEG-b-PBLG-b-PBLA], before catalytic hydrogenation respectively.

Figure 3.3.2. (c) and (d) represent the molecular weight measurement results acquired from MALDI-TOF of NCA-BLG which has been used as a precursor for the synthesis of triblock copolymer [PEG-b-BLG₅-b-BLA₁₈]. The results clearly revealed the molecular weight increases from ~ 4900 Dalton to 5890 Dalton after the polymerization to form diblock [PEG-b-BLG₅]. **Fig.** 3.3.2. (b) further shows the stepwise addition of monomers and the increment of the molecular weight with respect to the band intensity of the starting material. Previous reports have explained that with the addition of new blocks, the molecular weight of the new polymer can be increased in many ways [310-312]. **Fig.** 3.3.2. (b) exhibited a band at 10331 Dalton confirming the successful synthesis of [PEG-b-PBLG₅-b-PBLA₁₈] triblock copolymer with an attachment of n=18 number of –CH₂- units of a new block named "C" block of NCA BLA attached to the backbone of AB-type diblock (see **Schematic** 3.2.1).

3.3.7. Morphology and Size Analysis by using TEM

The HRTEM micrographs (**Fig.** 3.3.3. (a)-(c)) revealed the morphology of the di-block polymers synthesized in this work. From HRTEM it is observed that the triblock copolymer micelles of [PEG-b-PBLG] are distorted spheroid in shape which is mainly due to the self-assembly behaviour of charged ions in the solvent medium [313, 314].



Figures 3.3.3. (a-c) represent the HRTEM micrographs of diblock copolymer micelles of [PEG-b-PBLG] from lower to higher resolution. **Figs.** 3.3.3(d), (e) and (f) illustrate the distorted shape of the triblock copolymer micelles of [PEG-b-PBLG-b-PBLA]. **Figs.** 3.3.3(g), (h) and (i) show the ribbon type triblock copolymer of [PEG-b-PBLG-b-PBLA] at various ranges of 100 nm-200 nm. **Figs.** 3.3.3. (j) and (k) are the particle size distribution of [PEG-b-PBLG-b-PBLA] triblock copolymer and [PEG-b-PBLG] diblock copolymer, respectively

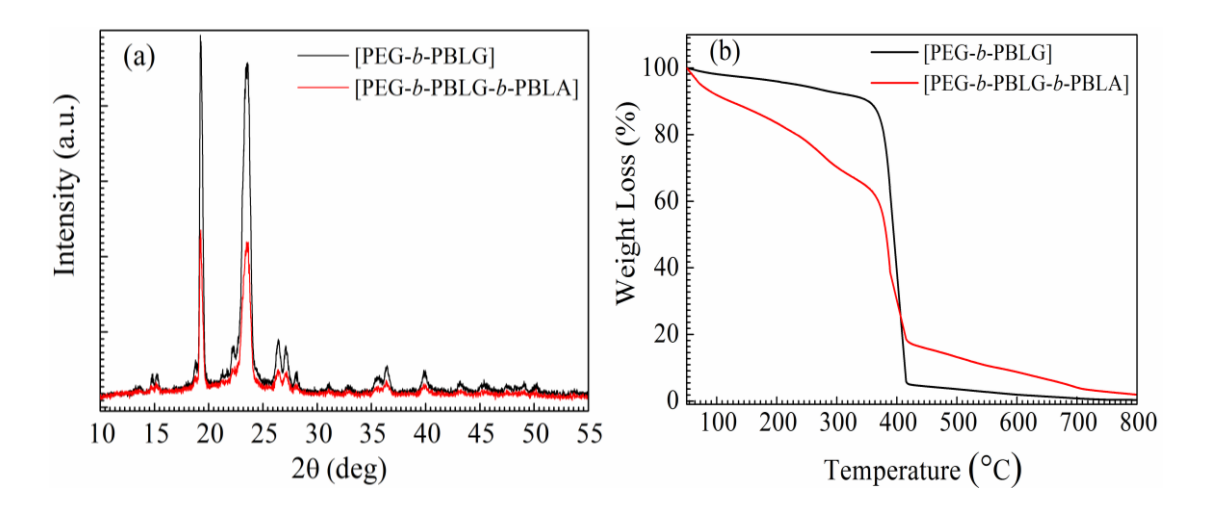
From **Figs**. 3.3.3(d), (e) and (f) we observed the distorted shape of the triblock [PEG-b-PBLG-b-PBLA] micelles. From HRTEM it is observed that the tri-block copolymer micelles are seen to be less distorted spheroid in shape than the di-block copolymer, which is

observed due to the self-assembly behaviour of charged ions of more number of hydrophobic groups in a solvent medium. The average size of the micelles has been calculated to the range of 10-60 nm (see size distribution profile **Figs.** 3.3.3. (j) and (k)). The calculated average sizes of [PEG-b-PBLG-b-PBLA] and [PEG-b-PBLG] polymeric micelles are found to be 13 nm and 22 nm, respectively. Although [PEG-b-PBLG-b-PBLA] polymer is having higher molecular weight than the [PEG-b-PBLG] copolymer, the [PEG-b-PBLG-b-PBLA] copolymer micelles exhibit smaller size in comparison to [PEG-b-PBLG-b-PBLA] polymer due to the association and interaction with the solvent (water) and intermolecular chains medium. Another reason for low radii of triblock copolymer micelles is due to hydrophobic part –O– ether groups are removed with hydrogenolysis.

Figs. 3.3.3. (g) shows the cross-linked mosaic pattern of size in the order of 1μm. **Figs.** 3.3.3. (h) and (i) are showing the ribbon shaped for [PEG-*b*-PBLG-*b*-PBLA]copolymer micelles/ fibrils of size in the diameter of the order of 100nm. The variation of morphology for tri-block polymers is observed due to the change in the sample preparation method and parameters using deionized H₂O under ultra-sonication for a few minutes. There may be chances of electrostatic forces of attraction caused by the solvent on the surface of polymer attracted positive and negative charged ions like -COO and -NH₃⁺ groups leading to the formation of fibril like structure [315, 316].

3.3.8. XRD and TGA Analysis for the crystallinity and thermal stability of block copolymer

Earlier it has been reported that block-co-polymers are mostly semicrystalline in nature [306]. From XRD (**Fig.** 3.3.4. (a)), it is observed that di- and triblock polymers synthesized in this work are semicrystalline in nature. From XRD the diffraction peaks appeared at 2θ = 19.3°, 23.2°, 26.7°, 27.9°, 36.4° and 40.5°, respectively for the presence of smaller domain of the crystalline region of the polymeric matrix of di- and tri-block copolymers. The intensity of the XRD peaks for di-block copolymer [PEG-*b*-PBLG] is more compared to the triblock [PEG-*b*-PBLG-*b*-PBLA] copolymers. Therefore, with the addition of the third block to the di-block copolymer results in the decrease in the crystallinity. Less crystalline triblock copolymer [PEG-*b*-PBLG-*b*-PBLA] is more useful in biomedical science as it can be degraded easily compared to the di-block copolymers [317].

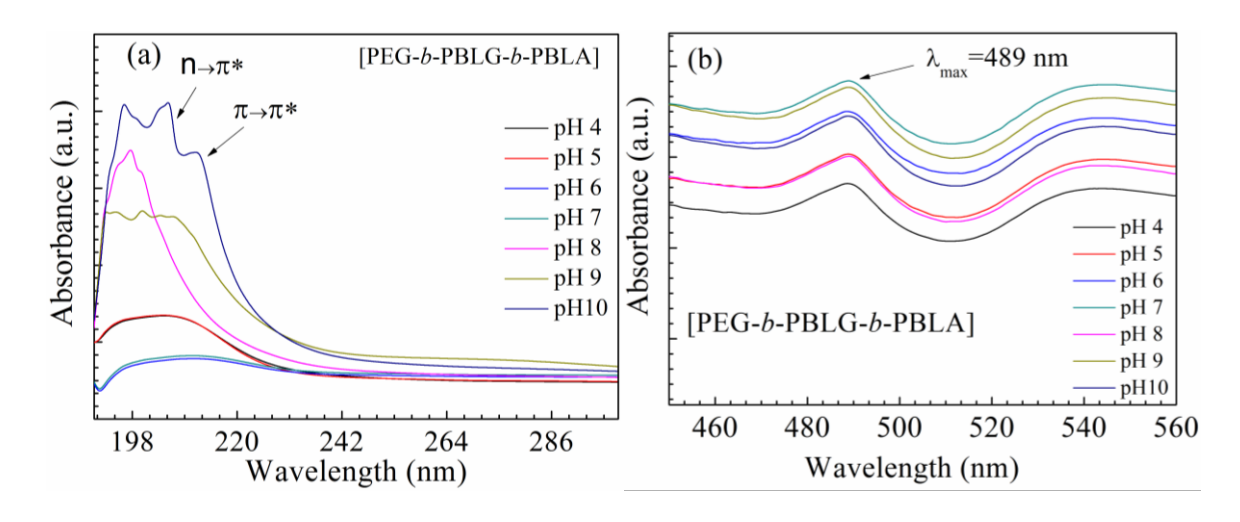


Figures 3.3.4. (a) and (b) represent XRD plots and TGA thermogram of [PEG-b-PBLG-b-PBLA] triblock copolymer and a-AB diblock copolymer of [PEG-b-PBLG], respectively.

Thermal stability of the different block copolymers has been studied through TGA (**Fig.** 3.3.4. (b)) and found that the triblock copolymer [PEG-b-PBLG-b-PBLA] is more stable compared to the di-block copolymers [PEG-b-PBLG]. Degradation of [PEG-b-PBLG-b-PBLA] polymers has occurred only at a higher temperature (say at 400°C) compared to the di-block copolymers. For di-block copolymer a continuous weight loss is observed before 200°C. However, for [PEG-b-PBLG-b-PBLA] polymer the weight loss before 400°C is occurred mostly due to the loss of volatile components present along with more number of organic groups attached to the backbone of polymer in the sample. But after 400°C, [PEG-b-PBLG-b-PBLA] is showing comparative less weightless till 800°C due to the covalent bonding associated in the polymer. Thus the synthesized tri-block copolymer [PEG-b-PBLG-b-PBLA] is thermally more stable compared to the di-block copolymer [PEG-b-PBLG], owing to the possible uses at a relatively higher temperature in the solid phase [251].

3.3.9. Electronic excitation Study through UV-Visible Spectroscopy

The broad absorption band appeared in UV-Vis spectra indicates the presence of chromophoric groups such as -(C=O)-NH₂ and (-C=O) (at 220 nm and 206 nm, respectively). These bands appeared due to the free electron transfer from nonbonding to π antibonding orbital causing $n\rightarrow\pi^*$ and $\pi\rightarrow\pi^*$ transitions for carbonyl and amide bonding. We have scanned the UV-Vis absorption of [PEG-*b*-PBLG-*b*-PBLA] triblock copolymer at room temperature (RT) by varying pH from 4-10.



Figures 3.3.5. (a) and (b) represent the UV-Vis spectra for triblock copolymer of [PEG-*b*-PBLG-*b*-PBLA] at the range 190-300 nm and 450-550 nm, respectively.

From **Fig.** 3.3.5., it is obvious that with the decrease in pH the intensity of absorption bands decreases as the number of active acid chromospheres in the solution medium increases and lead to the broadening of the absorption bands. However, the number of active amine chromospheres increases at pH 10 resulting in a sharp and intense absorption band. A very small absorption band at 489 nm appeared indicating the presence of protein (-NH₂) and –OH groups [318]. **Figure** 3.3.5. (c) is also showing absorption due to the occurrence of a similar mechanism of the copolymer of [PEG-*b*-PBLG] with a wavelength of maximum at 196 nm causing by carbonyl groups associated in them.

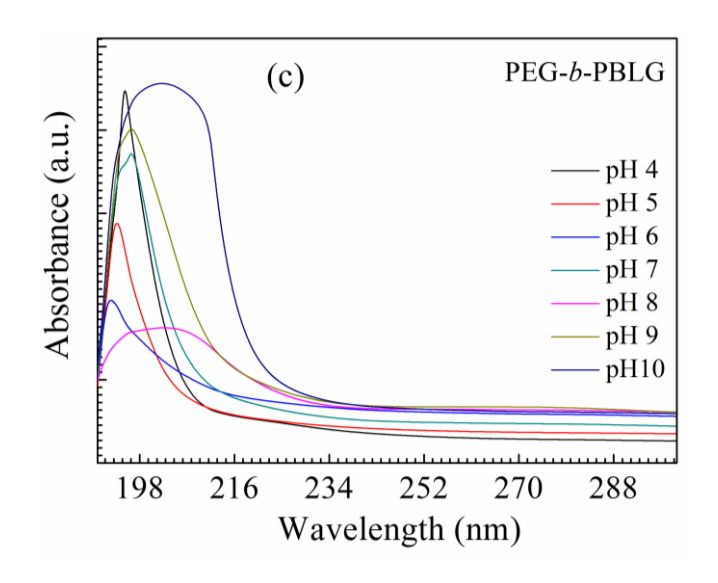


Figure 3.3.5. (c) illustrates UV graph of a-AB diblock copolymer of [PEG-b-PBLG]

3.3.10. Morphological and biological shape through Laser Confocal Scanning Microscopy

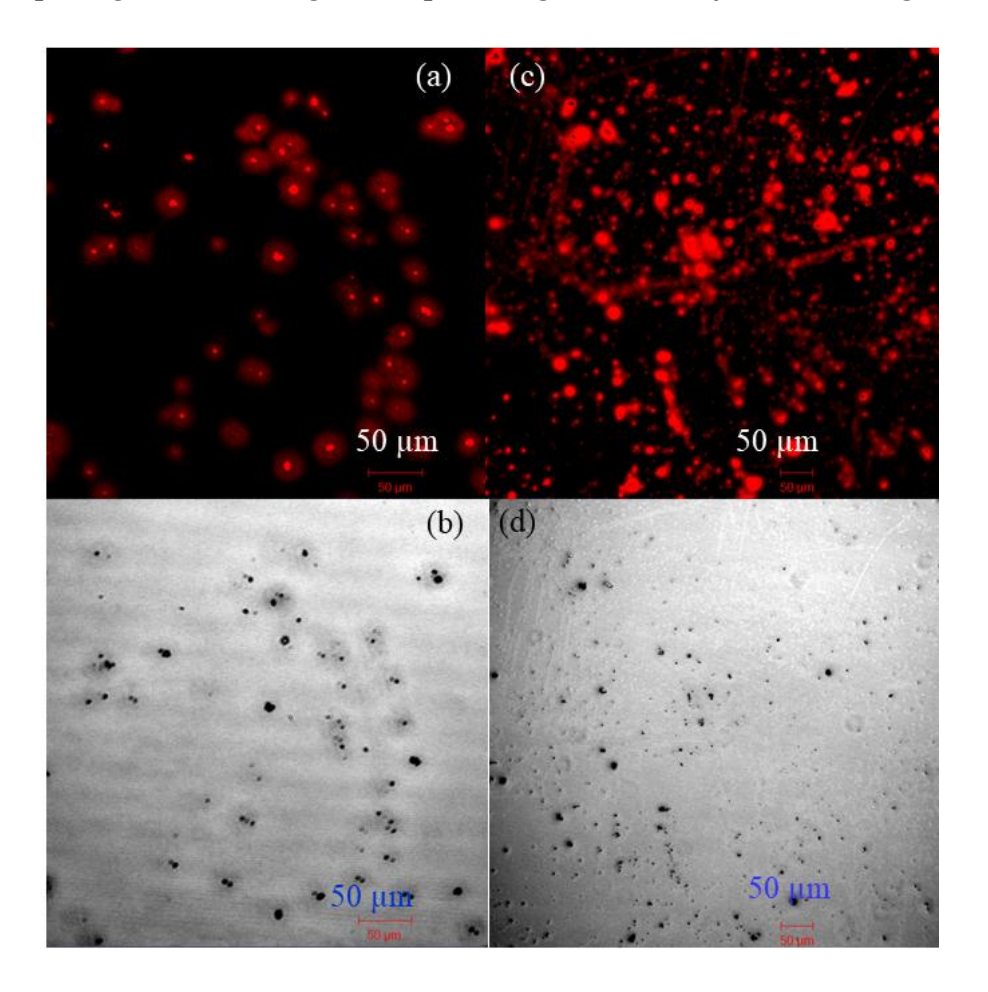


Figure 3.3.6. (a) and (b) illustrate Laser Confocal images of diblock [PEG-b-PBLG], and **Figs.** 3.3.6. (c) and (d) represent triblock copolymer [PEG-b-PBLG-b-PBLA] for laser and bright field images, respectively.

Laser Scanning confocal experiment was performed to give the concrete evidence about the formation of amino-acid based triblock copolymeric micelles in the presence of laser light. The polymers were loaded with Rhodamine 6G molecules along with several times washing. **Figs.** 3.3.6. (a) and (b) showed the presence of spherical particulate like structure indicating the presence of [PEG-b-PBLG] whereas the **Figs.** 3.3.6. (c) and (d) are representing the number of micellar like red coloured spherical structures are due to the higher MW polymeric materials of [PEG-b-PBLG-b-PBLA] respectively. Comparing the above microscopy data with HRTEM images, it is clear that the [PEG-b-PBLG-b-PBLA] are spherical micelles in shape. Hydrophilicity behaviour and the amphiphilic nature of the diblock and triblock polymer micelles led to the formation of micelles with the reluctance of solvation property of the hydrophobic group which caused particle size to decrease sharply

[235,319-324]. The self-association property along with intermolecular hydrogen bonding between cationic and anionic groups of [PEG-b-PBLG] and [PEG-b-PBLG-b-PBLA] triblock copolymer in a suitable solvent leads to the formation of micelles [325-328].

3.3.11. Electro Kinetic Potential Measurements by Zeta Experiment

The solubility of triblock copolymer was checked in a various solvent medium, e.g., in THF, acetone, ethanol, 1, 2-dioxane, DMSO, cyclohexane, chloroform, DMF, toluene, water and ether. In this work, we have chosen DDI water as our solvent due to the suitability of water for biological applicability. For the sample for Zeta measurement, we have prepared dispersion at 0.5mg/ml conc. at 25°C. **Fig.** 3.3.7. (a) and 3.3.7. (b) represented the stability of colloidal dispersion of [PEG-b-PBLG-b-PBLA] triblock and [PEG-b-PBLG] di-block copolymers, respectively at different pH range.

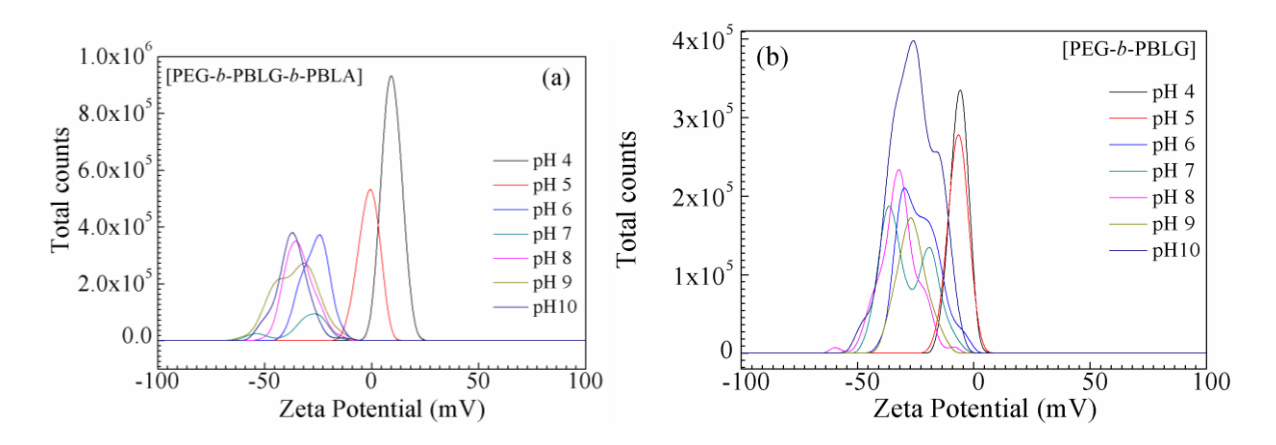


Figure 3.3.7. (a) and (b) show the profile for Zeta potential for triblock copolymer [PEG-*b*-PBLG] and di-block copolymer [PEG-*b*-PBLG], respectively at different pH (pH 4 to 10) and 25°C.

Results exhibited that [PEG-*b*-PBLG-*b*-PBLA] triblock copolymer has much more ζ potential values than diblock copolymers due to the presence of more number of hydrophilic as well as hydrophobic groups present in it [329, 330]. From **Fig.** 3.3.7. it is further noticed that at all the pH from 4 to 10, both types of polymers are coagulated and responsive towards the colloidal particle formation. The ζ potential of [PEG-*b*-PBLG-*b*-PBLA] copolymer micelles with having a maximum value of -44.6 mV at pH 10, whereas for di-block copolymer micelles it is -34 mV at pH 8. The minimum ζ potential possessed by [PEG-*b*-PBLG-*b*-PBLA] copolymer micelles was approximately 1 mV at pH 4. Synthesized triblock copolymers have exhibited two peaks in **Fig.** 3.3.7. (a), which may due to the

presence of two different pKa values (pKa1 and pKa2) produced by available dissociated ions in the medium and due to the distribution of particles size. The inter-ionic, as well as hydrogen bonding interactions on the micelle's surface of [PEG-b-PBLG-b-PBLA] block copolymers, leads to the increase in the ζ potential value. This value seems to be more in the basic medium (up to $\zeta = -45$ mV) compared to the values obtained in acidic medium (-9 mV). In addition to the solvent effects, the basic OH groups also influence the surface activation (properties) indirectly providing H-interactions among the polymeric micellar solution. The reversal of the positive charge on the carboxylic group tends to the electronic delocalization and leads to the formation of neutral (charge) environment. The surface charge of the micelles of triblock copolymer has consisted of -COOH groups. On addition of NH₄OH solution to the medium, it was immediately converted to -COO ions which repel the adjacent -COO groups of [PEG-b-PBLG-b-PBLA] copolymer resulting to an increase in ζ values. However, on the addition of acid to the polymer solution, it hinders the formation of the cations at the surface of the micelles of the block copolymer. The reason for the increasing ζ value is the reversibility nature of -COOH groups and the act of -COO- as counter ions in salvation [324,331, 332]. The highest ζ potential value for [PEG-b-PBLG] micelles is -30 mV at pH 8 which showed the highest stability whereas the ζ value of triblock polymer solution is stable at all the pH values ranging from 6 to 10 at 25°C (see **Table** 3.3.1.). The detail ζ potential values for di-block [PEG-b-PBLG] and tri-block [PEG-b-PBLG-*b*-PBLA] copolymer solutions have been shown in **Table** 3.3.1.

Table 3.3.1: (Data Obtained from Zeta exp.)

Diblock copolymer [PEG-b-PBLG]	Zeta potential	Triblock copolymer [PEG-b-PBLG-b-PBLA]	Zeta potential
pH 4	-6.79	pH 4	-1.10
pH 5	-1.65	pH 5	-8.14
pH 6	-26.36	pH 6	-34.43
pH 7	-22.8	pH 7	-38.6
pH 8	-31.66	pH 8	-37.76
pH 9	-23.46	pH 9	-32.93
pH 10	-23.2	pH 10	-41.13

3.3.12. CD analysis for amino-acid based polymeric proteins with varying pH and temperature

The configuration of synthesized block copolymers are a mixture of both helical and random coil configuration(see CD band results **Fig.** 3.3.8.). From **Fig.** 3.3.8. it is calculated that the triblock copolymer of [PEG-b-PBLG-b-PBLA] consists of 6.00% α -helix, 49.00% antiparallel β -sheets, 3.70% parallel β -sheets, 16.60% Beta-Turns, and 29.20% random coils at 35° C. The antiparallel β -sheets are calculated to be up to 50% for tri-block block copolymers synthesized in this work and they are exhibiting protein like structure in pH 4 to 10.

The higher percentage of the anti-parallel β -sheet structure is observed due to the presence of more number of peptide bonds (-C=O-NH-) associated with each other through hydrogen bonding in the solvent medium. Its variation has been observed more distinctly with the increase in temperature from 20°C to 50°C. Although the difference in the percentage of α -helix, β -sheets, and random coils are obtained at numerous temperature and pressure,, there is no significant change in values compared to the values obtained at 35 °C and pH 8. The synthesized block copolymers exhibit bands with low intensity at 220 and 190 nm when experiments were performed at 35 °C. The band at 220 nm is attributable to the $n\rightarrow\pi^*$ transition of the peptide bonds in the block copolymer chain. Major bands appeared at 208 nm (less intense) and 193 nm (maximum intensity) attributable to the parallel and perpendicular excitations of the $\pi\rightarrow\pi^*$ transition of the [PEG-*b*-PBLG-*b*-PBLA] triblock polymer peptide due to the more percentage of antiparallel β -sheets in the solution.

However, the CD band intensities are not acting in the same way among the three sets of reference proteins including ours (CDNN) since the nature of the spectrum of CD components depend on the reference proteins used for the deconvolution [336-338]. **Fig.** 3.3.9. illustrates CD analysis for [PEG-b-PBLG] diblock copolymer of [PEG-b-PBLG] obtained at 20 °C to 50 °C with varying pH, exhibiting less ellipticity than triblock copolymers. The folding of chain for [PEG-b-PBLG] diblock copolymers are less due to the less number of interaction acting between peptide bond which ceases its ellipticity compared to the [PEG-b-PBLG-b-PBLA] triblock polymers.

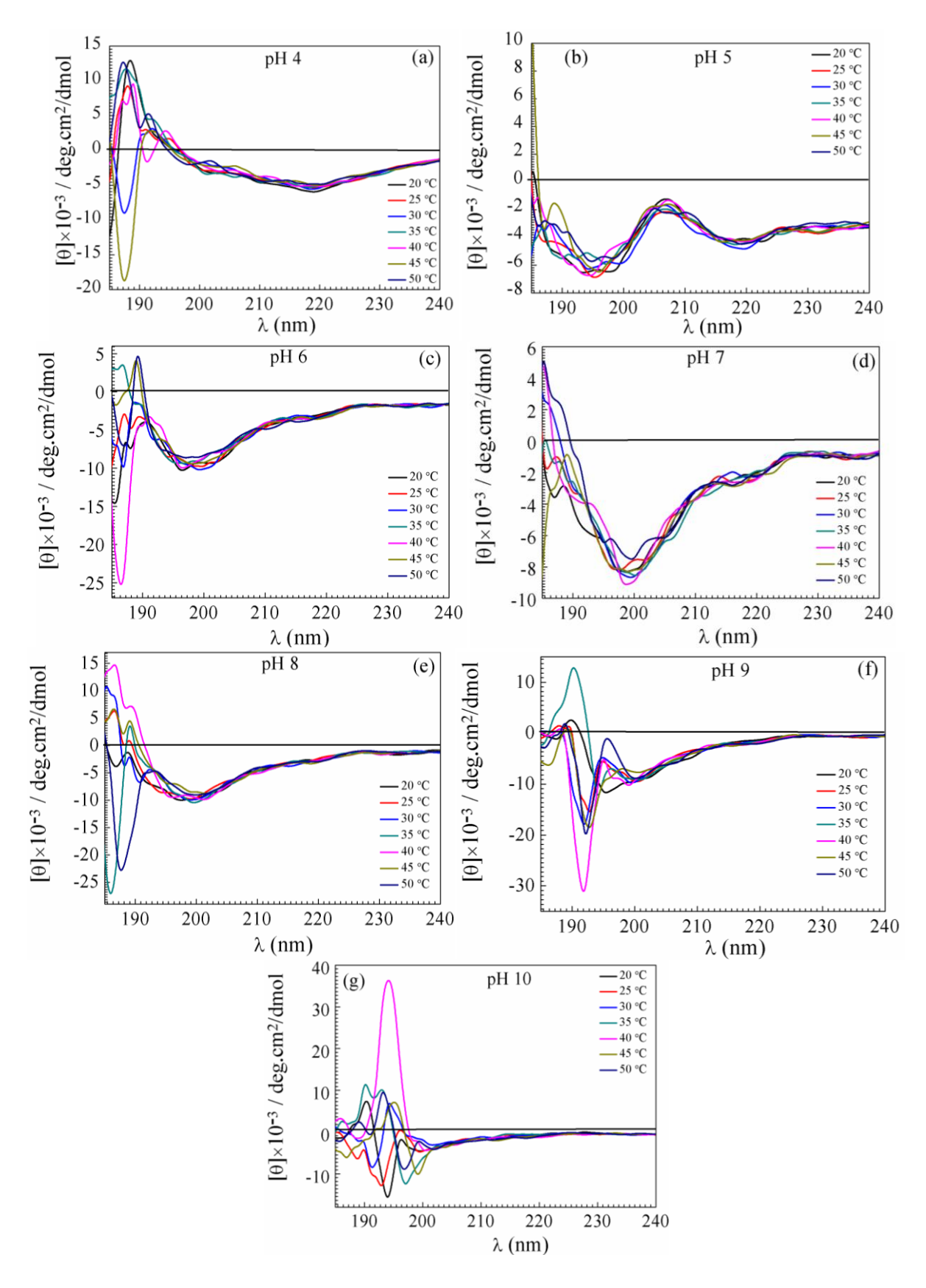


Figure 3.3.8. illustrates CD results for triblock copolymer of [PEG-*b*-PBLG-*b*-PBLA] at 20 to 50 °C with different pH (a) pH 4, (b) pH 5, (c) pH 6, (d) pH 7, (e) pH 8, (f) pH 9 and (g) pH 10, respectively.

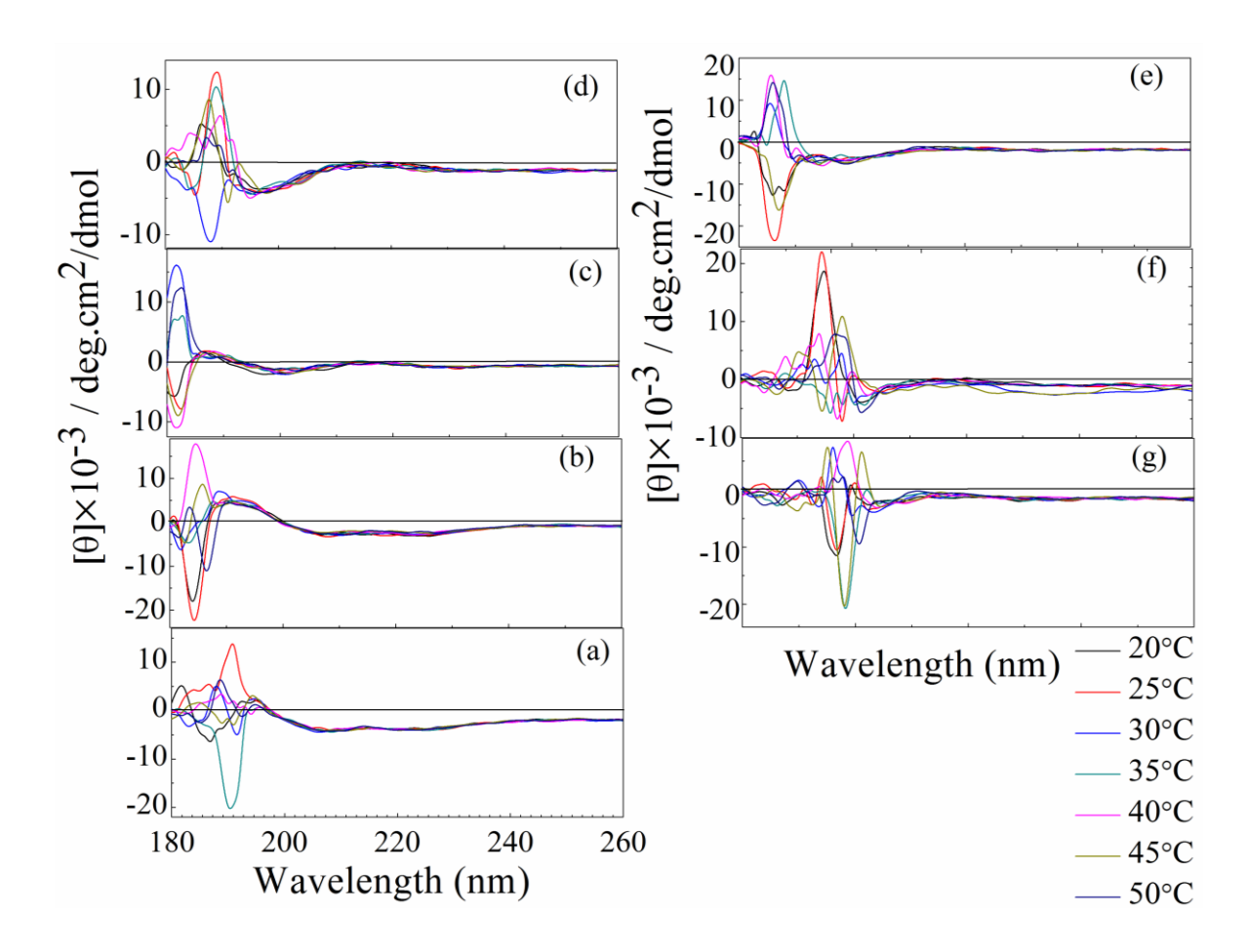


Figure 3.3.9. illustrates Circular Dichroism analysis for a-AB diblock copolymer of [PEG-*b*-PBLG] over a change of temperature range 20°C to 50°C with respect to different pH conditions (a) pH 4, (b) pH 5, (c) pH 6, (d) pH 7, (e) pH 8, (f) pH 9 and (g) pH 10 respectively.

3.3.13. In vitro cytotoxicity assay of polymeric micelles

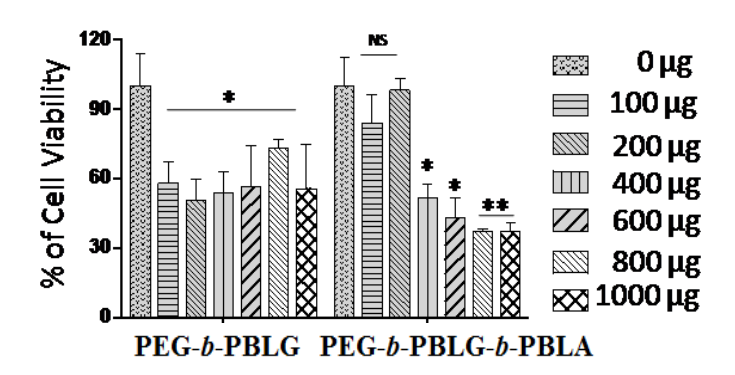


Figure 3.3.10. Cell viability results for diblock copolymer of [PEG-b-PBLG] and triblockcopolymer[PEG-b-PBLG-b-PBLA], respectively.

We have reported the dielectric composites with a significant dielectric behaviour with respect to both frequency and temperature-dependent method [338, 339]. Here in this work, we wanted to develop a method with biological applications. Cell viability assay was performed according to the method reported earlier [340]. In brief, compounds [PEG-b-PBLG] and [PEG-b-PBLG-b-PBLA] were dissolved in DMEM medium with mild sonication and treated with MDA-MB231 cell lines (human carcinoma cells), taking 5x10³ cells/well for 24 hr incubation in 96-well plates with different concentrations of polymers. The viability of cells was assessed by adding 10 µL of MTT solution (stock solution 5 mg/ml) per well and incubated at 37 °C for 3 h. The medium was discarded, and the formazan blue, which formed in the cells, was dissolved in 100 µl of DMSO. The intensity of colour formation was measured at 570 nm (background 665 nm) in a spectrophotometer (iMarkTM Microplate Absorbance Reader, Bio-Red). The percentage of cell viability was calculated concerning the control values (without test compound). Cell viability assay was performed for both the sets of micelles in DMEM medium treated against MDA-MB231 cells for 24 hr resulting to purely cell viable up to 200µg/ml of concentration. The cell viability % was gradually decreased with increase in concentration and significantly reduced to 88%, 95%, 53% and 46% at 100, 200, 400 and 600µg/ml. The cells in the presence of triblock polymer (see Fig. 3.3.10.) are viable more than 95% up to 200µg/ml whereas [PEG-b-PBLG], showing cell viability only up to 50%. At higher concentration, the cell viability decreases indicating that at a lower concentration of the sample, the synthesized material can be used for various medical purposes. MTT assay test of [PEG-b-PBLG₅-b-PBLA₁₈] polymeric nano micelles against MDA-MB231 cells has shown a remarkable result than [PEG-b-PBLG], the polymer which is also discussed effectively in an antimicrobial study in the subsequent section. All these results reveal that the synthesized polymer can be used for a range of biomedical applications [340]. The toxicity of [PEG-b-PBLG-b-PBLA] polymer is found to be very less. Bearing low toxic conduct, this polymer can be used as a very good drug carrier for several therapeutic applications.

3.3.14. In vitro antibacterial activity of polymeric micelles

Previous works report that the polymeric materials associated with the quaternary ammonium salts directly can be used for the antibacterial activities [341]. The presence of quaternary ammonium salts has increased the antimicrobial activity of the prepared material which attracted us to perform the samples for antimicrobial profile test against bacterial strains. **Fig.** 3.3.11. (a) is showing the effective killing efficiency of bacteria at 0.156, 0.3125,

0.625 and 1.25 mg/ml with the lowest MIC and OD of 60%, 57%, 50% and 40% respectively [342]. The low OD value for triblock copolymers [PEG-b-PBLG₅-b-PBLA₁₈] against positive strain is far better than diblock copolymer [PEG-b-PBLG₅] micelles due to the presence of more number of quaternary ammonium salts in the medium ceases bacterial survival effectively.

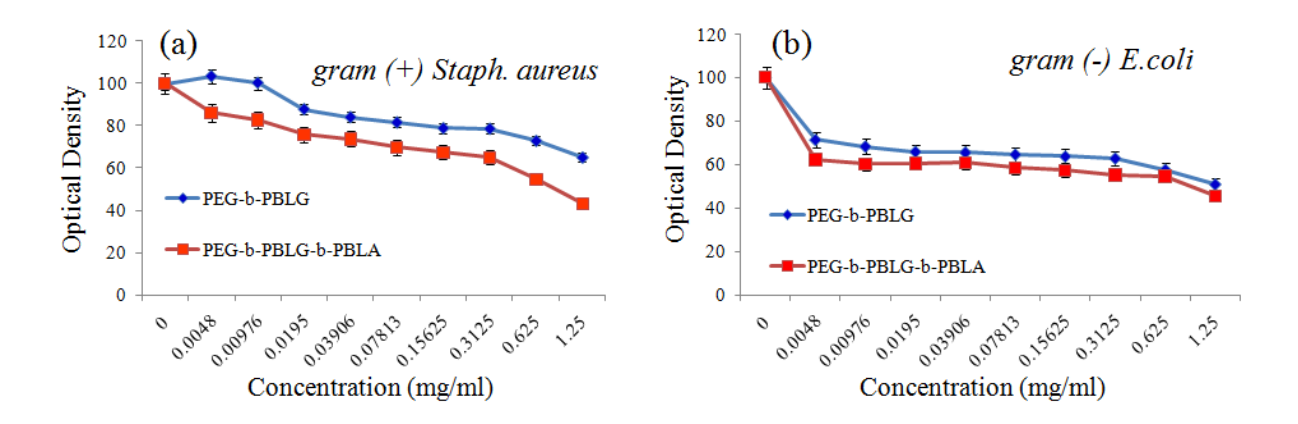
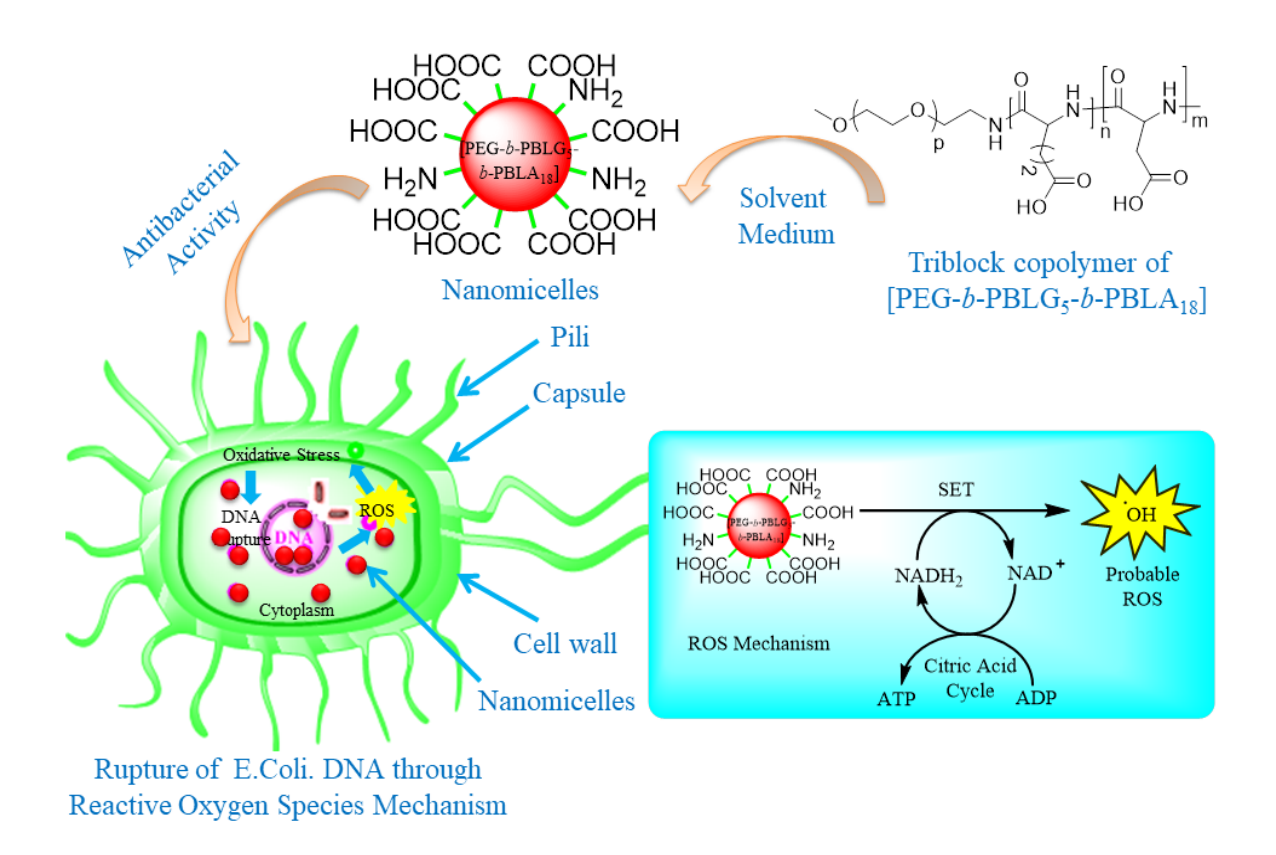


Figure 3.3.11. (a) and (b) show the *in vitro* antimicrobial activity results for diblock copolymer of [PEG-b-PBLG] and triblock copolymer of [PEG-b-PBLG-b-PBLA] for *Gram* (+) *Staphylococcus aureus* and *Gram* (-) *E.Coli*, respectively.

Figure 3.3.11(b) is also showing an excellent low OD synthesized [PEG-b-PBLG-b-PBLA] polymeric micelles than [PEG-b-PBLG] micelles, indicating the effective killing efficiency of bacterial cells at a concentration of 1.25mg/ml for both the strains. With the decrease of polymeric micelles concentration up to the lowest value of 0.0048mg/ml, the bacterial killing efficiency of [PEG-b-PBLG-b-PBLA] polymeric micelles remained around the same in gram (-) bacterial strain of *E.coli*. If we compare the antibacterial susceptibility test, [PEG-b-PBLG-b-PBLA] has shown a very good antibacterial effect in case of gram (-) *E.coli*. at very minimum dilution than *gram(+)* staph aureus bacterium. But when the serial dilution increased above 0.07813mg/ml, in the [PEG-b-PBLG-b-PBLA] polymer micelles, the cells have shown a very low difference of percentage of survival than [PEG-b-PBLG] polymer indicating better use for inhibition of the growth of microbial at a negative strain. It followed the probable reactive oxygen species (ROS) mechanism to destroy the bacteria. As the polymeric micelles enter inside the cell-wall of bacterium they led to the formation of reactive free radicals due to the ions in the solution medium causing the oxidation with the rupture of DNAs, lipids and folding of proteins by single electron mechanism process. Thus it is observed that these two polymeric nano micelles are capable of antimicrobial activity and can be used for further detailed study of medical therapy. The entire process is shown in the

schematic-3.3.2., which follows the reactive oxygen species mechanism pathway to damage the bacterial DNAs.



Schematic 3.3.2: Probable schematic representation for Reactive Oxygen Species Pathway (ROS) mechanism for the killing of bacteria by tri-block-copolymers.

3.3.15. Conclusion for Part IIA

Herein, we have summarized our work with the noble synthesized biocompatible triblock copolymer [PEG-b-PBLG₅-b-PBLA₁₈] which showed greater relevance in UV-Vis absorbance, DLS, and ZETA potential with compared to the diblock copolymer [PEG-b-PBLG]. The controlled surface morphology with the response to temperature and pH of this copolymers became the main reason of the micelles to behave as a most interesting structure than other low molecular weight polymers. Biocompatibility, the zeta potential of -45mV and CD results of the various secondary structure have revealed the synthesized block polymeric materials are effective for in vitro biomedical applications. Due to host-guest inclusion complex formation activity, our synthesized polymers can form complexes with various proteins, peptides, metal complexes and other biocompatible materials. MTT assay test of polymer against human breast carcinoma found to be active and low cytotoxic. Further, the triblock copolymer is very efficient for the killing of gram (-) E.Coli than gram (+) Staph aureus bacteria. It can be used for further applications such as drug delivery (HRTEM images, 13 nm) and other biomedical application as a nano vehicle, antiseptic agent, antibacterial therapy element. Path of polymer science is growing very fast in everyday life and hopefully, we will able to implicate these block copolymers for further applications in microbiology and related biotechnology.

RESULTS AND DISCUSSION

Part IIB: Amino acid Based Polymeric Nanobiomaterials

Part IIB. Designing of a new polypepto based nanovesicles sized macromolecular triblock biomaterials and its action against bacterial resistance

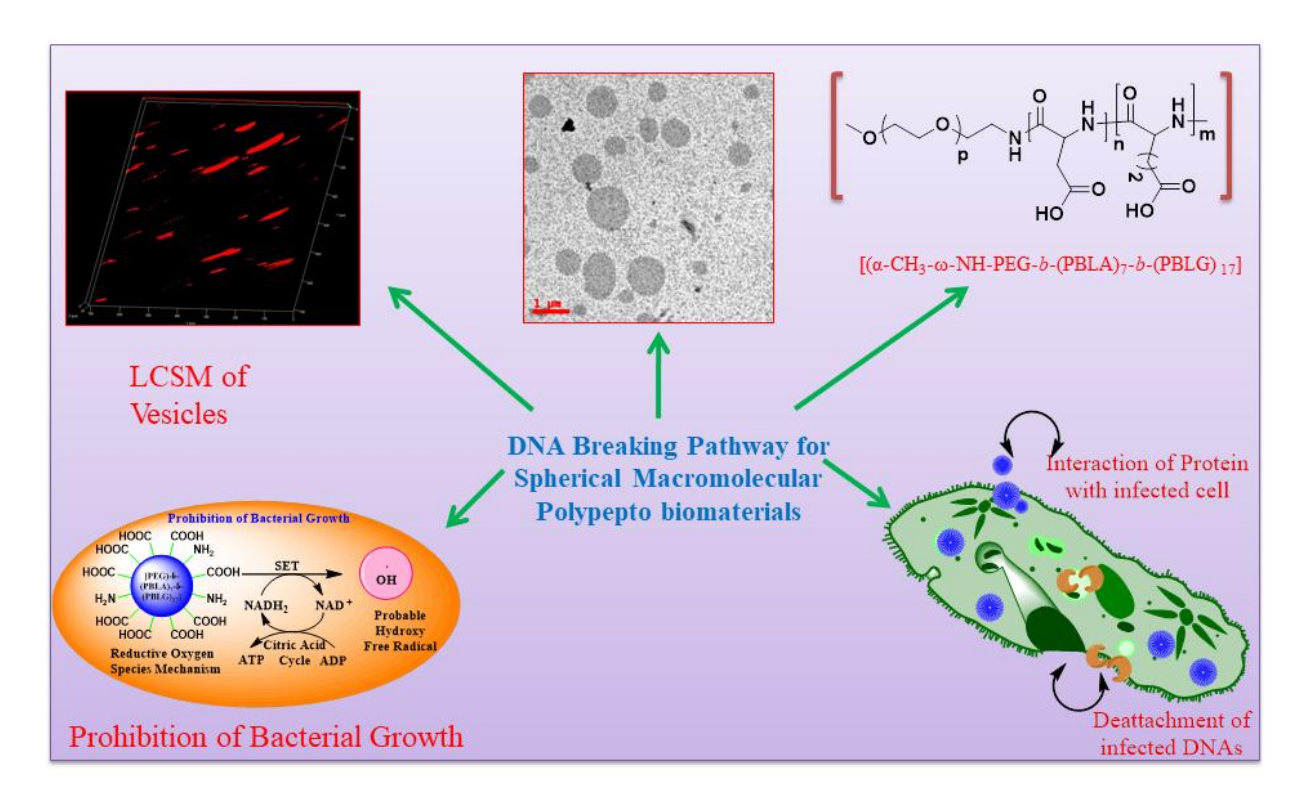


Table of content of this chapter: Designing of a new polypepto based nanovesicles sized macromolecular triblock biomaterials and its action against bacterial resistance.

Outcome of this Part

1. Debasrita Bharatiya, Pradip Paik (Designing of a new polypepto based nanovesicles sized macromolecular triblock biomaterials and its action against bacterial resistance) (Manuscript Prepared)

2.Debasrita Bharatiya, Pradip Paik. Study of AB and ABC types of Bio-compatible Amino Acids based nano micro block copolymer vesicles for biomedical applications.(ISBN:978-81-924726-4-5). October- 04-06, 2018 Jawaharlal Nehru Technical University, Hyderabad, India, 2nd International Conference on Nano & Science and Engineering Applications-2018 (Poster Presentation)

Part IIB (*Objective 4*): Designing of new triblock polypepto vesicle sized [(α-OCH₃-ω-NH-PEG)-b-(PBLA)₇-b-(PBLG)₁₇] nanobiomaterials

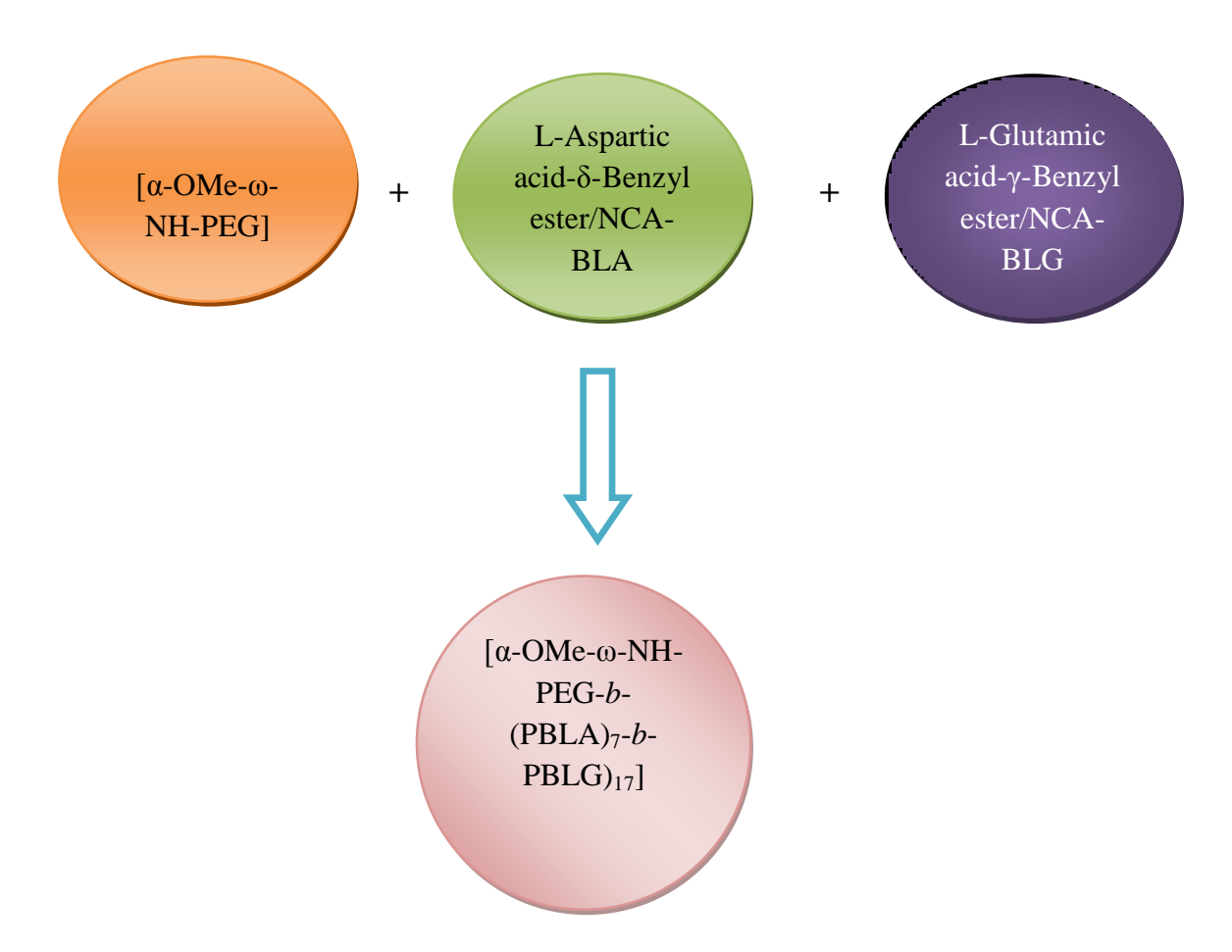


Figure 3.4.A. Objective diagram for Designing of a new polypepto based nanovesicles sized macromolecular triblock biomaterials.

3.4.1 Abstract

This work aims to design a triblock polymer of α -methoxy- ω -amino-Poly Ethylene Glycol)-L-aspartic acid-L-Glutamic acid [(α -OCH₃- ω -NH-PEG)-b-(L-AspA)₇-b-(L GluA)₁₇]/[PEG-b-(PBLA)₇-b-(PBLG)₁₇]. The evidence of nanovesicle sized [PEG-b-(PBLA)₇-b-(PBLG)₁₇] polymer has been synthesized by improved ring-opening polymerization method of NCA of BLA and BLG. In this part, we have performed physical, chemical and biological study of the designed polymers. The antibacterial resistive response of triblock nanovesicles against two different bacterial strains of *Gram* (+) *bacteria Staphylococcus aureus and Gram* (-) bacterial strain *of E.coli respectively* is found to be more significant than the diblock nano micelles at the similar environment and low concentration (<1mg/ml). The antibacterial inhibition for vesicles is found to be more

effective for conventional microorganisms *E.coli* than *staph aureus*. *In vitro* cytotoxicity was performed using MTT assay against cancerous Human Caucasian breast adenocarcinoma MDA-MB231 cells and viability percentage was found to be nearly 95% at $800\mu g/ml$. We have performed series of experimental methods to know the morphological study through HRTEM and LCSM showing the size of the vesicles as 600 nm spherical shaped and to confirm the formation of synthesized triblock copolymer via -C=O-NH₂- bonding formation (interaction of carbonyl with an amine). The molecular weight of the vesicle sized polymer is found to be 10360 Dalton. The stimuli responsive block polymeric nanovesicles have been analyzed with the change of pH from acidic to basic and temperature change from RT to 50° C and observed to be embedded with more percentage of antiparallel β -sheets. The ζ potential study of zwitterionic colloidal solution of this macromolecule has a regular trend of increase of ζ potential value of -40 mV, RT.

3.4.2. Introduction and Motivations

The aim is the synthesis of noble vesicle sized macromolecular polymeric nanobio compounds for the biomedical applications depending on enormous properties. Previous reports by Arijit et. al. have mentioned that amino acid based polymers are biocompatible and easily metabolised by the human system [240]. It is also reported that the biopolymers are degraded upon hydrolysis. The bio-chemical behaviour of polypepto vesicles include of the self assembly nature in presence of the solvent medium, biocompatibility with human carcinoma cells, antibacterial active agent, possessed of helical proteins, responsive experimental parameter and possessed of chirality. Due to the multipurpose behaviour of macromolecule, it can be defined as a smart material. Earlier reports based on smart materials have been include above behaviour but few reports only published with few of the above factors [328, 343]. We have focused the modified synthesis of newly designed macromolecule through ring-opening polymerization and succeded with the application in vitro biotechnology process. Due to the spherical vesicular property, it can be used for drug delivery process and tissue engineering application [344]. Previous reports like [244, 345] have shown PEG as a very biocompatible backbone of any macromolecule due to its amphiphilicity which attracted our team to work on it with other essential amino acids. The manuscript has a very detailed discussion about all the physio-chemical-biological behaviour of these smart polymeric vesicles in the later section.

3.4.3. Synthesis of a triblock copolymer of [PEG-b-(PBLA)₇-b-(PBLG)₁₇]

We have followed the previously reported method for the synthesis of AB type [PEG-b-(PBLA)₇] [170]. After the synthesis of [PEG-b-(BLA)], following the same method we have added NCA GluA to the solution mixture of [PEG-b-(BLA)] and allowed for 72 hrs at 600 rpm and 45°C with an inert atmosphere condition so that the polymerization would take place completely. The Di-PA block copolymer of [PEG-b-(BLA)] has been synthesized first then the new block of NCA-BLG has been attached to the N-atom of aspartate forming an amide -(C=O)-NH₂ bond. The functional groups like carboxy (-COOH) and amine (-NH₂) helps for further condensation polymerization. The benzylic deprotection method of block copolymer with the help of Pd/C catalyst has led to the formation of benzene free block copolymer of [PEG-b-(PBLA)₇-b-(PBLG)₁₇]. The purified polymeric particles were collected and allowed for freeze-drying at a low temperature, -20°C.

3.4.4. Reaction Mechanism

Scheme 3.4.1: Mechanistic pathway for [PEG-b-(PBLA)₇-b-(PBLG)₁₇] via modified ring-opening polymerization where p= no of –CH₂ units for α -CH₃- ω -NH₂-PEG, n= no of –CH₂ units for NCA-BLA and m= no of –CH₂ units for NCA-BLG respectively.

3.4.5. Morphological Study of Polymer via HRTEM

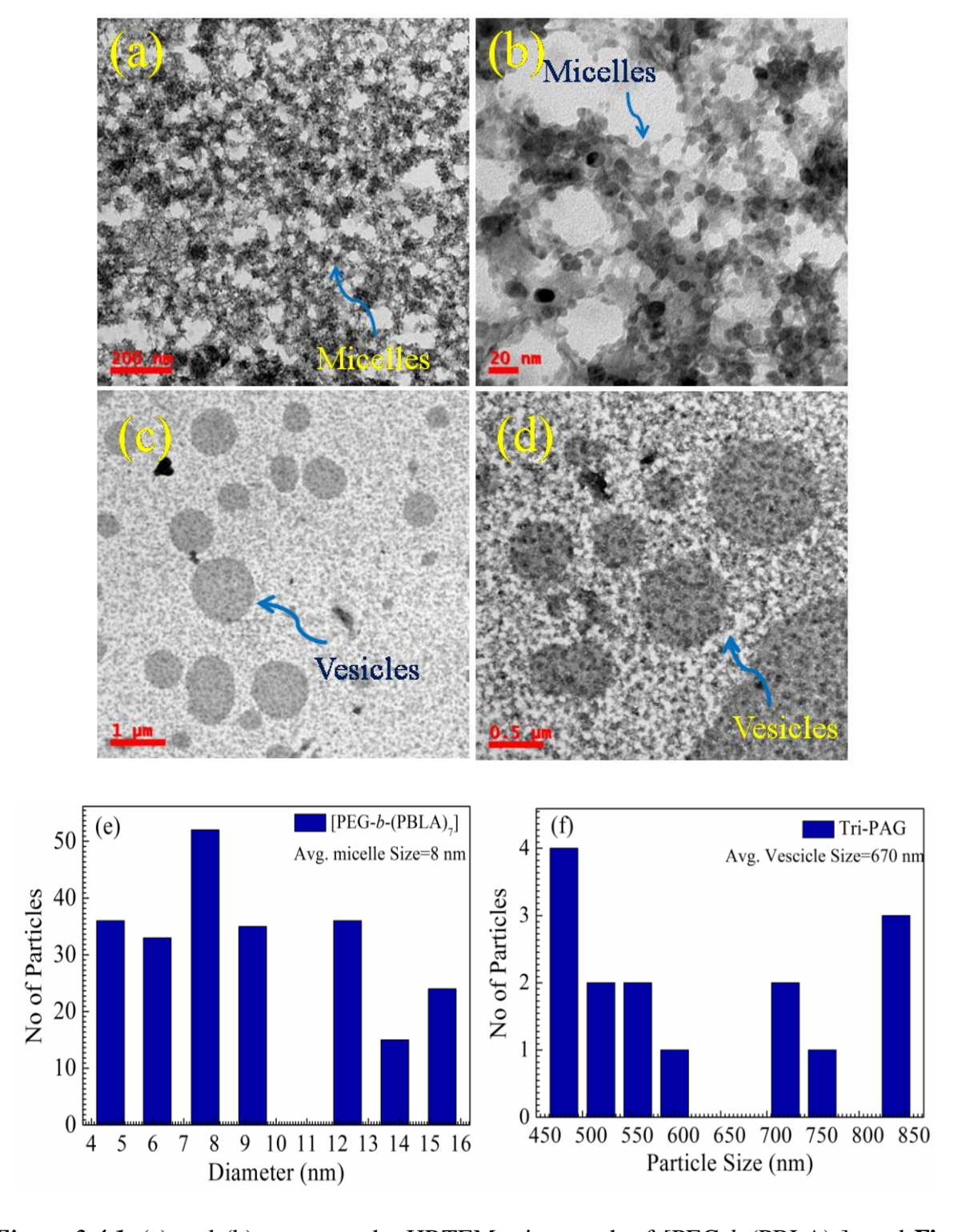


Figure 3.4.1. (a) and (b) represent the HRTEM micrograph of $[PEG-b-(PBLA)_7]$ and **Fig.** 3.4.1(c) and (d) show for $[PEG-b-(PBLA)_7-b-(PBLG)_{17}]$, respectively. **Figs** .3.4.1. (e) and 1(f) illustrates the average size for $[PEG-b-(PBLA)_7]$ nano micelles of average size 8 nm and $[PEG-b-(PBLA)_7-b-(PBLG)_{17}]$ nanovesicles of average size 670 nm respectively.

TEM samples have been prepared in deionised H₂O as a standard solvent with the concentration of 0.5mg/ml. HRTEM micrographs for **Figs**. 3.4.1. (a), (b), (c) and (d) are showing a clear picture of spherical shapes for both the synthesized diblock micelles and triblock vesicle sized copolymers via modified ring-opening polymerization method. **Figs**. 3.4.1. (a) and (b) are showing very minute spherical micelles of [PEG-*b*-(PBLA)₇], AB type block copolymer. **Fig**. 3.4.1. (e) has shown an average size of 8 nm leading the formation of diblock polymers as nano micelles in a particular solvent at a fixed temperature [346]. The small nano micelles formed due to the involvement of interionic interaction among COO and NH₄⁺ ions among themselves with H and OH ions of given solvent. The phenomenon of ionic interaction reduces the size of spherical diblock nanomicellic copolymers below 10 nm which is an excellent pathway for the drug delivery carrier response.

Figures 3.4.1. (c) and (d) have shown a clear image of small spherical vesicles for [PEG-*b*-(PBLA)₇-*b*-(PBLG)₁₇] [347]. The interaction of numerous ions along with the covalent interaction between different types of [a-(α-OCH₃-ω-NH-PEG)], [b-(NCA-BLA)₇] and [b-(NCA-BLG)₁₇] blocks among themselves causes many molecules of AB to come together with each other in the presence of a solvent. The vesicles are consisted of many micelles together via covalent and hydrogen bonding caused by polymer and solvent behaviour. The factors like chemical bonding, zwitterionic effect and amphiphilic nature of polymer caused micelles in agglomerated position to form bigger size vesicles. **Fig.** 3.4.1. (f) illustrated the average size for [PEG-*b*-(PBLA)₇-*b*-(PBLG)₁₇] nanovesicles is 670 nm. **Fig.** 3.4.1. (f) helped to calculate the size of vesicles so that in future during the use of biomedical application it can be used as a drug carrier in the human cell line. **Fig.** 3.4.1. (g) and **Table** 3.4.1. showed the elemental composition of [PEG-*b*-(PBLA)₇-*b*-(PBLG)₁₇] block copolymer via EDX plot.

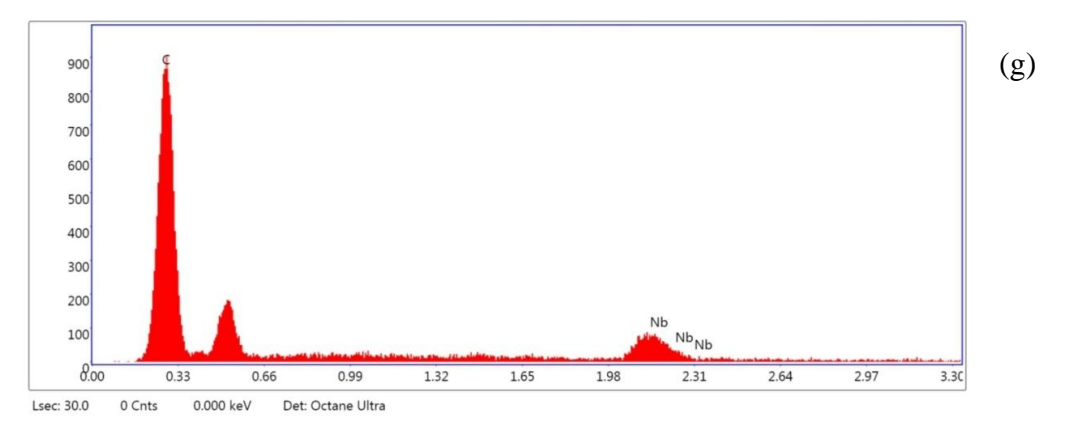


Figure 3.4.1.(g) EDAX analysis for [PEG-b-(PBLA)₇-b-(PBLG)₁₇] block copolymer

Table 3.4.1: {EDAX analysis for [PEG-b-(PBLA)₇-b-(PBLG)₁₇]}

Element	Weight %	Atomic %	Net Int.	Error %	Kratio	Z	A	F
C K	64.29	93.30	484.09	8.34	0.4841	1.1873	0.6342	1.0000
0	35.71	6.70	63.11	13.93	0.2408	0.6588	1.0235	1.0000

3.4.6. LCSM analysis of copolymer [PEG-b-(PBLA)₇-b-(PBLG)₁₇

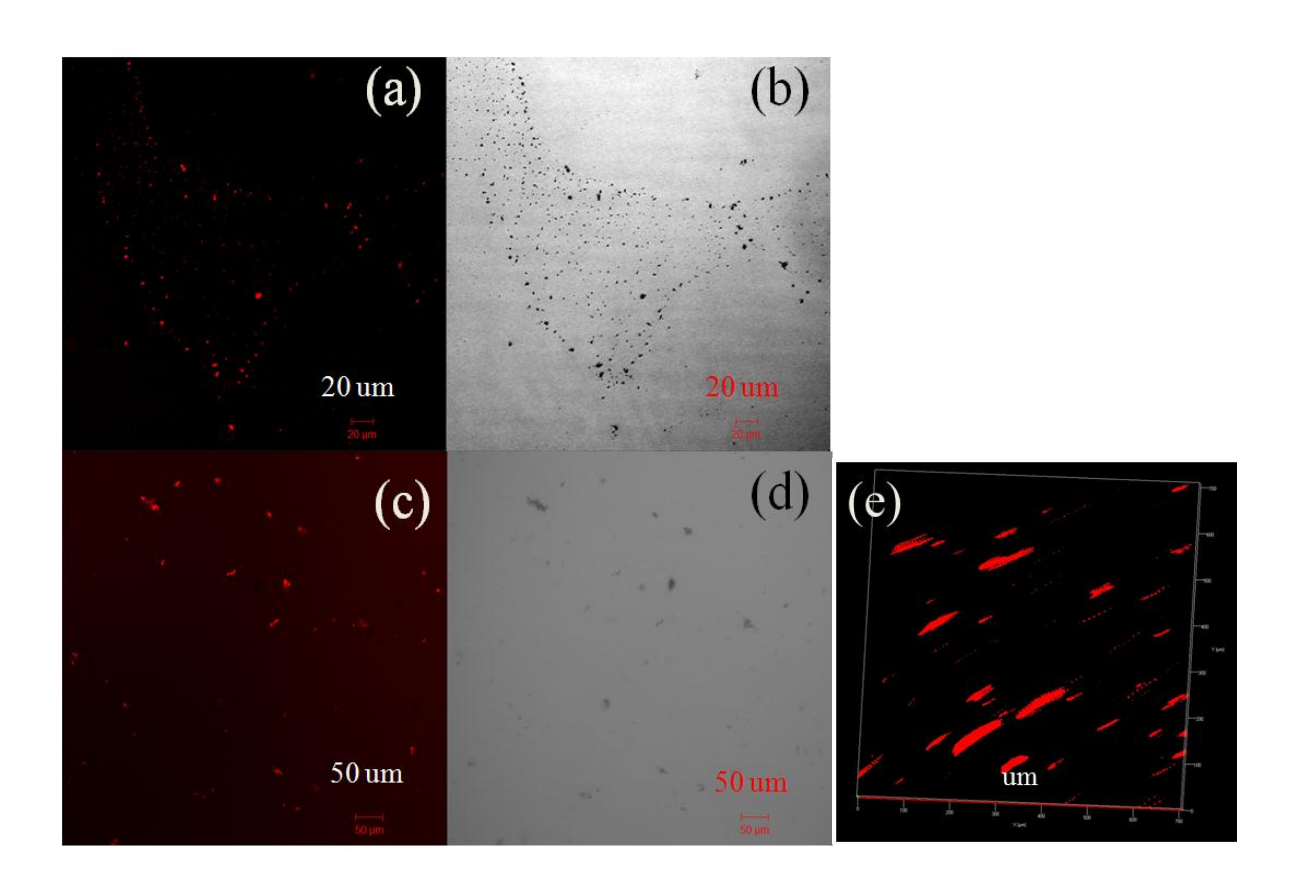


Figure 3.4.2. (a) and (b) represented LCSM images for of [PEG-*b*-(PBLA)₇] whereas **Fig.** 3.4.2. (c) and (d) indicated the LCSM images for [PEG-*b*-(PBLA)₇-*b*-(PBLG)₁₇], respectively. **Fig.** 3.4.2(e) represents the axial view of [PEG-*b*-(PBLA)₇-*b*-(PBLG)₁₇] at magnification of 50μm.

To verify the structural behaviour of synthesized [PEG-b-(PBLA)₇-b-(PBLG)₁₇] polymer, LCSM method was followed. Rhodamine 6G was used as a fluorescent dye as the polymer itself is not fluorescent active. From **Fig.** 3.4.2 (a) and (b) particles are observed to be like very small-sized whereas the **Fig.** 3.4.2 (c) and (d) show that particle is comparatively larger. If we take a close look at **Fig.** 3.4.2 (e), it can be observed the attachment of micelles via numerous chemical forces to form larger vesicles. This provides an anomalous structural determination to the developed polymer.

3.4.7. Position of Hydrogens by ¹HNMR

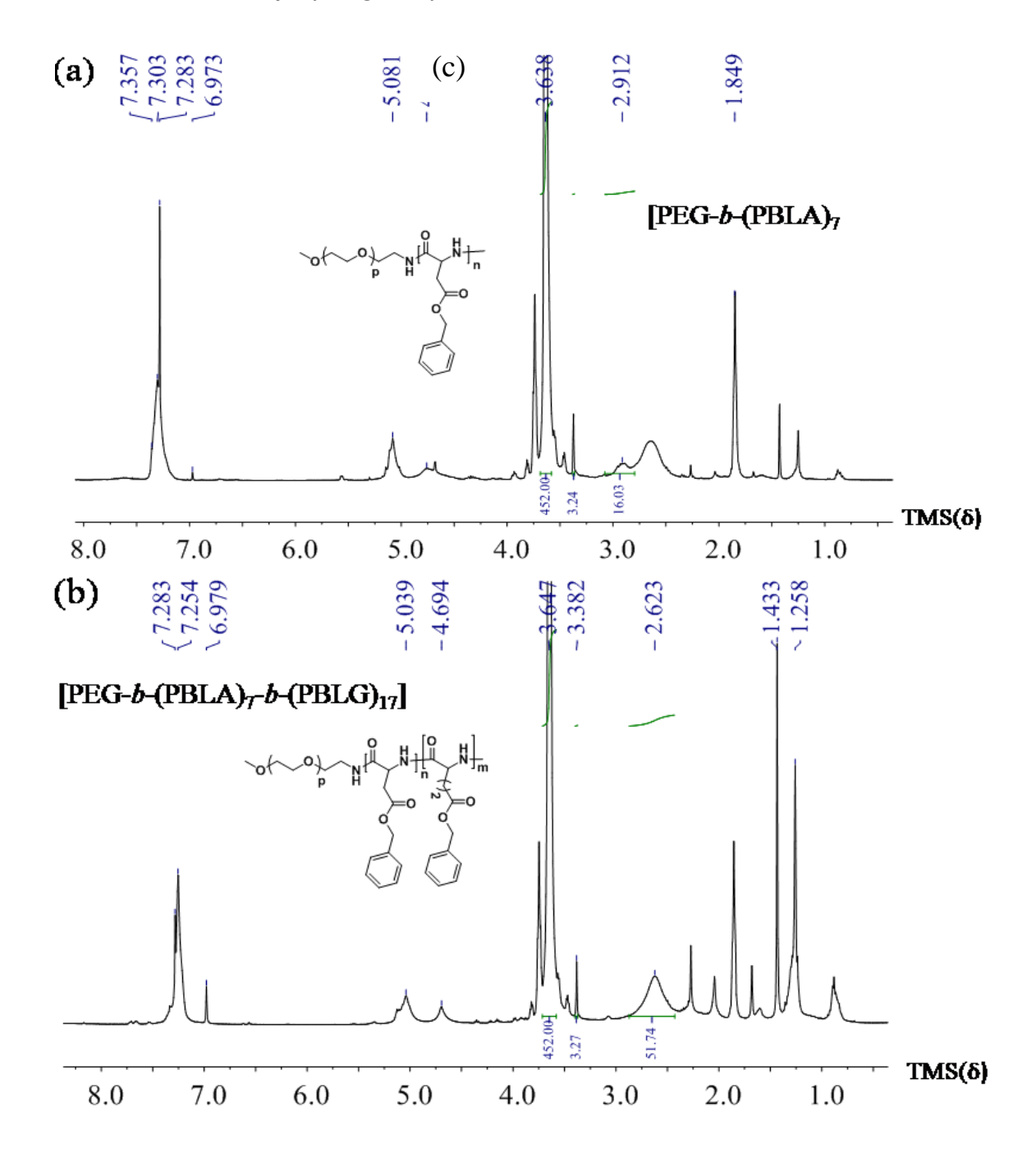


Figure 3.4.3. (a) and (b) represent the H¹NMR spectra for diblock [PEG-b-(PBLA)₇], triblock [PEG-b-(PBLA)₇-b-(PBLG)₁₇] and precursor [α-OCH₃-ω-NH-PEG] respectively with CDCl₃ as solvent and tetramethylsilane (TMS) as an internal reference. Where p=no. of CH₂ units in a-MeO-PEG-NH₂, n= no. of CH₂ units in b-(BLA)₇ and m= no. of CH₂ units in b-(NCA-BLG)₁₇.

Figure 3.4.3. (a) represents the NMR data of diblock [PEG-b-(PBLA)₇] with the various position of the hydrogen in the polymeric chain. The peaks are at $\delta = (7.3, 35H,$

aromatic proton), $\delta = (5.22, 2H, benzylic proton)$, $\delta = (3.75, 452H, -CH_2 group of a-PEG, (H^1NMR spectra for precursor PEG (<math>\alpha$ -OCH₃- ω -NH₂-PEG)), $\delta = (4.34, 1H, -CH_-)$, and $\delta = (2.60, 16H for -CH₂ for aspartate)$ and with few other peaks may represent impurities. **Fig.** 3.4.3(b) is showing NMR data triblock [PEG-b-(PBLA)₇-b-(PBLG)₁₇] which is very similar to the diblock copolymer and chirality by diastereoselectivity at δ =(4.7, 1H). The hydrogen positions are at $\delta = (7.35, 35H, aromatic proton due to unprotected polymeric chain), <math>\delta = (5.3, 2H, benzylic proton)$, $\delta = (3.7, 452H, -CH_2 group of a-PEG)$, $\delta = (4.34, 1H, -CH_-)$, and $\delta = (2.60, 51H for -CH₂ for <math>b$ -NCA BLA and b-NCA BLG). The deshielding of -CH₂ group of a-PEG is due to the presence of linked -O- group of PEG have shifted to the left of the standard TMS line. But the presence of amine group causes shielding of polymeric chain causing shifting towards low δ in the TMS standard [306]. Increased numbers of -CH₂ units showed the attachment of new 17 NCA BLG to the diblock copolymer backbone.

3.4.8. Chemical nature and Weight of the block copolymer study by FTIR and MALDI-TOF Analysis

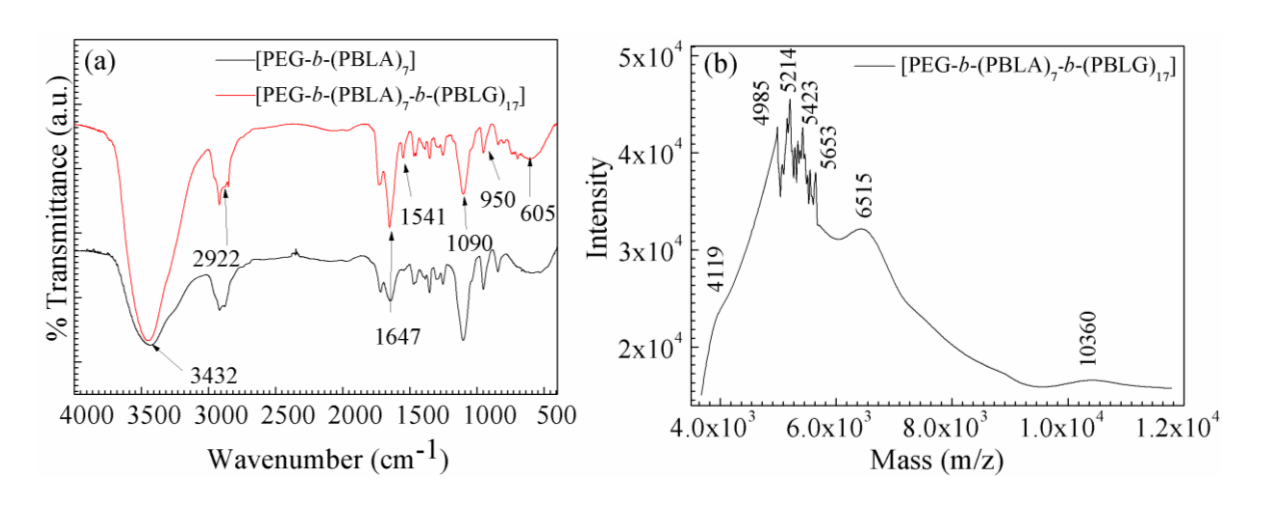


Figure 3.4.4 (a) and 3.4.4 (b) illustrates the FT-IR spectra and MALDI-TOF data for [PEG-b-(PBLA)₇] and [PEG-b-(PBLA)₇-b-(PBLG)₁₇] respectively with DCM and CHCl₃ as the standard soluble solvent.

Figure 3.4.4. (a) has given a clear data of various stretching and bending modes of functional groups present in the triblock [PEG-b-(PBLA)₇-b-(PBLG)₁₇], respectively nanovesicles as well as diblock [PEG-b-(PBLA)₇], nano micelles. The important peaks at 3473 cm⁻¹ (O-H str of terminal acid in the polymeric chain, see **scheme** 3.4.1.) and 1718 cm⁻¹ (α -NH to the acid group) are the measure peaks as the % of transmittance for both the stretching modes are high compared to other functional groups present in the polymeric

vesicles. Other peaks are at 2896 cm⁻¹ (C-H str of –CH₂ units), 1651 (amide, C=O), 1555 cm⁻¹ (amide II, N-H) and 954 cm⁻¹ (-CH₂ rocking). The absence of peaks at benzyl ester at 1733 cm⁻¹ and 1259 cm⁻¹ (C=O of MeO-PEG-NH₂) confirmed the formation of deprotected benzyl polymeric nanovesicles [307-309]. The presence of 1651 cm⁻¹ peak has indicated the presence of α-helix structure of peptides which have been confirmed in CD spectra in later section [244]. This peak is more prominent in [PEG-*b*-(PBLA)₇-*b*-(PBLG)₁₇], due to the high intensity of micelles in the vesicles resulting in the formation of more number of the peptide bond.

Molecular weight determination has performed under an advance process of MALDI-TOF using chloroform as standard solvent. **Fig.** 3.4.4. (b) represents the MALDI data of [PEG-*b*-(PBLA)₇-*b*-(PBLG)₁₇] triblock copolymer bearing a hump-like structure of molecular weight around 10360D, whereas [PEG-*b*-(PBLA)₇] bore its weight to 6515D. **Fig.** 3.4.3 (b) is showing the stepwise addition of each block to each other concerning the intensity versus molecular weight (Dalton) [240,242]. We have calculated the MW of [PEG-*b*-(PBLA)₇-*b*-(PBLG)₁₇] and correlated the given data with NMR (see **Fig.** 3.4.3.) and confirmed the attachment new 17glutamate units to the diblock [PEG-*b*-(PBLA)₇].

3.4.9. Crystalline behaviour and thermal stability study by XRD and TGA analysis of vesicle sized polymers.

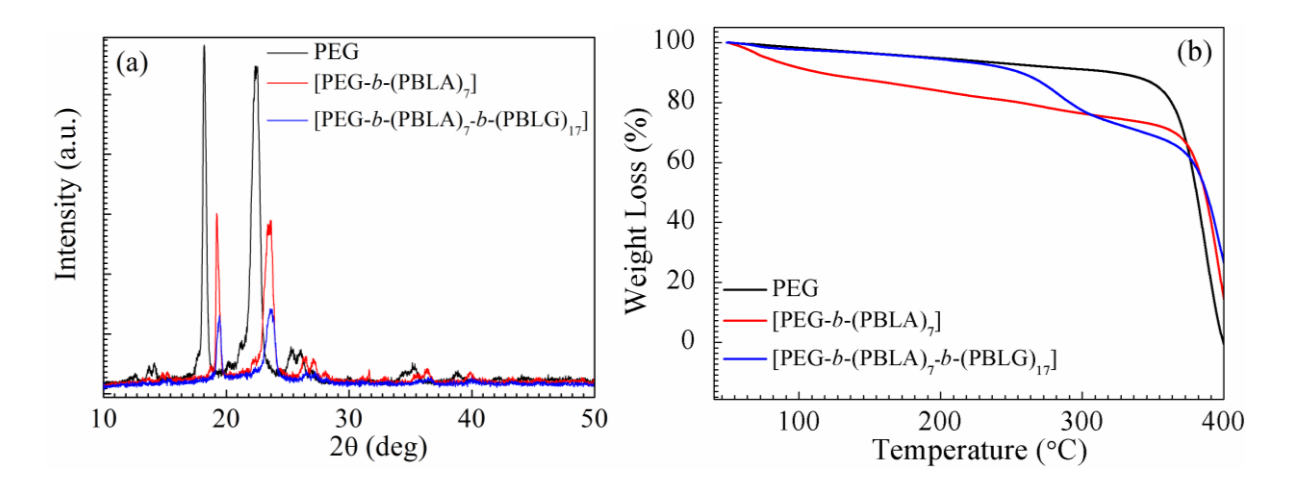


Figure 3.4.5. (a) and (b) illustrates the XRD and TGA data for $[PEG-b-(PBLA)_7]$ and $[PEG-b-(PBLA)_7-b-(PBLG)_{17}]$, respectively.

The crystalline nature of [PEG-*b*-(PBLA)₇] nano micelles and [PEG-*b*-(PBLA)₇-*b*-(PBLG)₁₇] nano vesicle is confirmed from **Fig**. 3.4.5. (a). **Fig**. 3.4.5 (a) has shown diffraction peaks at 15.2°, 19.2°, 24.7°, 26.3°, 36.8° and 39.2° for all the samples including PEG. Previous

reports have shown the peaks for PEG are 13.1°, 19.3°, 23.4° and 27.8° [306]. However, in the present case, the peaks of polymer vesicles samples have shifted due to the atomic and molecular rearrangement of ions depending upon the chemical functional groups present, Diffraction peaks at 36.8° and 39.2° are new to the XRD study for [PEG-b-(PBLA)₇-b-(PBLG)₁₇] polymeric nanovesicles. These peaks may occur due to the various functional groups present in the polypeptide polymeric chain

Fig. 3.4.5. (b) shown the phase change behaviour of all the polymeric samples including PEG. This Figure has given a clear idea that [PEG-*b*-(PBLA)₇-*b*-(PBLG)₁₇] nanovesicle is thermally more stable than [PEG-*b*-(PBLA)₇] nano micelle up to 300°C. The bigger size of vesicle may help the polymer to bind each other with covalent bond due to more number of molecules present in [PEG-*b*-(PBLA)₇-*b*-(PBLG)₁₇]. The degradation of [PEG-*b*-(PBLA)₇-*b*-(PBLG)₁₇] occurs after 400°C while [PEG-*b*-(PBLA)₇] occurred after only 100°C. The weight loss % of [PEG-*b*-(PBLA)₇] and [PEG-*b*-(PBLA)₇-*b*-(PBLG)₁₇] are 27% and 14% when it reached up to 300°C respectively. [PEG-*b*-(PBLA)₇-*b*-(PBLG)₁₇] is showing almost similar weight loss trend compared to base PEG precursor. Hence from this experiment, it is clear that [PEG-*b*-(PBLA)₇-*b*-(PBLG)₁₇] can be used for better use in *in vivo* biomedical application due to its synthesis temperature as well as in high temperature daily use products [251, 313].

3.4.10. Zeta Potential measurement at different pH of polymer vesicles

Figure 3.4.6. (a) showed an excellent ζ value for PEG-*b*-(PBLA)₇] and [PEG-*b*-(PBLA)₇-*b*-(PBLG)₁₇], respectively with DDI H₂O as the standard soluble solvent. The ζ potential value for [PEG-*b*-(PBLA)₇-*b*-(PBLG)₁₇] nanovesicles has been observed to be more as compared to [PEG-*b*-(PBLA)₇] micelles. Deprotonated α-COOH group and protonated NH₄⁺of amino acids in the vesicular solvent system caused the increase in surface interaction potential value. The maximum value of ζ potential -45.6 mV is for [PEG-*b*-(PBLA)₇-*b*-(PBLG)₁₇] at pH 8, RT. The more ζ value at pH 8 it is more favourable for biological application as it is very nearer to human body pH 7.4. The more ζ potential has arisen due to more number of ions at the interface of the colloidal solution of polymeric nanovesicles. Even at pH 7 also [PEG-*b*-(PBLA)₇-*b*-(PBLG)₁₇] is showing ζ value of -36.7. The same analysis was also done for [PEG-*b*-(PBLA)₇] showing highest ζ value of -41.4 at pH 8 medium in RT.

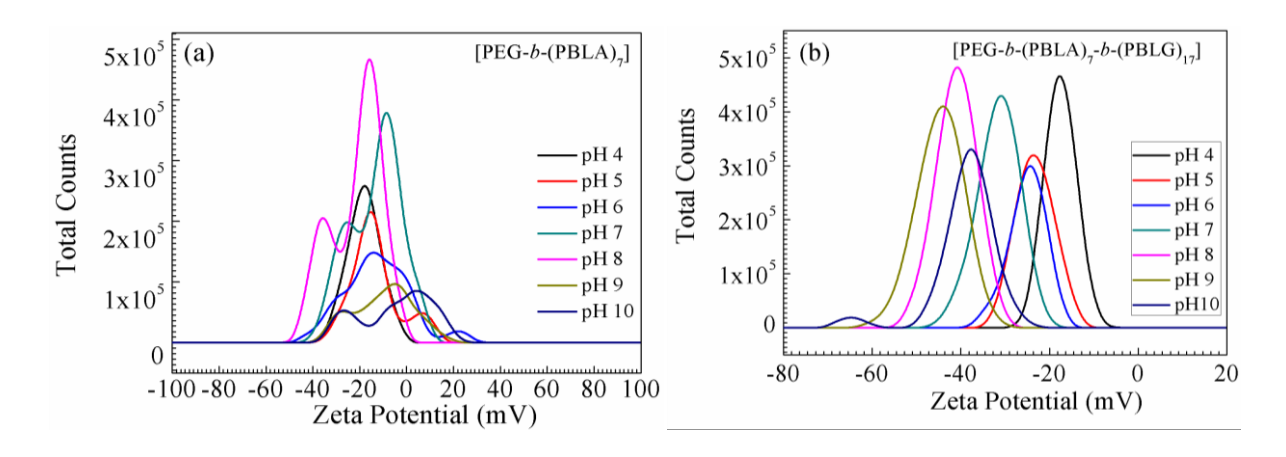


Figure 3.4.6. (a) and (b) show the ζ potential value for [PEG-*b*-(PBLA)₇] and [PEG-*b*-(PBLA)₇-*b*-(PBLG)₁₇], respectively with DDI H₂O as the standard soluble solvent.

Important plausible mechanisms of high ζ potential are shown in **scheme** 3.4.2. In the basic medium, (i) on the dissociation of NH₄OH with the solvent medium it released NH₄⁺ and OH⁻ ions, Type I showed OH⁻ deprotonated the hydrogen of acidic part of polymer and type II caused the deprotonation of hydrogen from amide N occurred. In acidic medium donation of an electron to the hydrogen from O. N, primary amine and amide O respectively showed in type I, II, III and IV [348, 349]. However, among these six types of mechanisms, only four seem to happen in the colloidal solution. Total of six anions and four cations have been produced in basic and acidic medium respectively. This is the reason why ζ potential is more in basic medium as the larger number of anions at the outer surface of Tri-PAG are formed and less in the acidic medium due to the less number of cations compared to anions in the colloidal dispersion medium.

Scheme 3.4.2: Plausible acid-base interaction in the colloidal solution in of nanovesicular [PEG-*b*-(PBLA)₇-*b*-(PBLG)₁₇].

3.4.11. UV-Visible Measurement of vesicle sized block copolymer at different stimuli pH

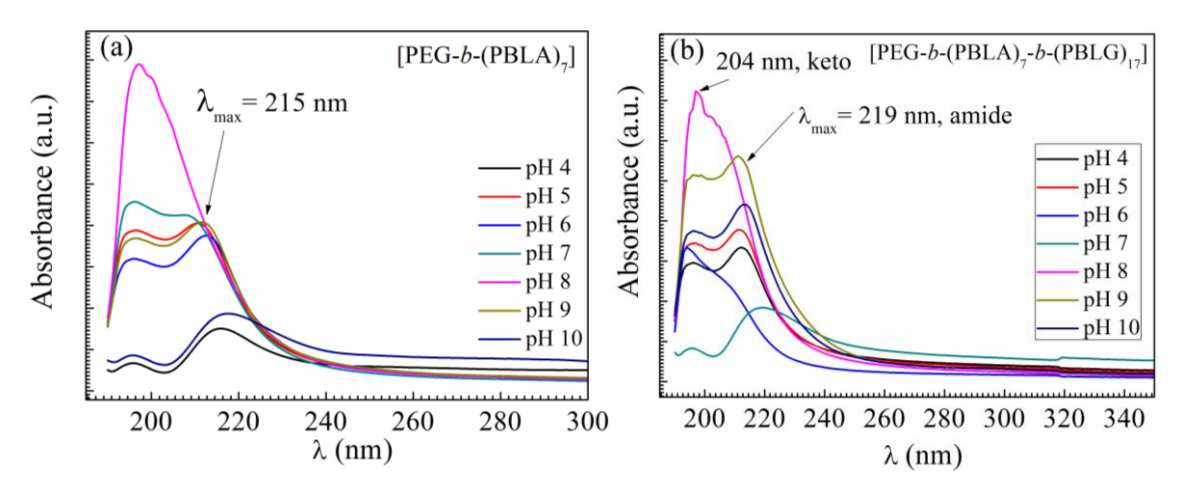


Figure 3.4.7. (a) and (b) represent the UV spectra for [PEG-b-(PBLA)₇] and [PEG-b-(PBLA)₇-b-(PBLG)₁₇], respectively at room temperature with variation of pH from 4 to 10.

Ultraviolet measurements were performed using UV-Vis NIR LAMDA 750 spectrometer (PerkinElmer) at 300 nm. The presence of 220 nm and 206 nm peaks in the UV range have indicated the availability of chromophores such as amide [-(C=O)-NH₂] and keto (-C=O) functional groups, respectively. The transfer of electrons $n\rightarrow\pi^*$ transition takes place in the polymeric vesicles as well in micelles. From **Fig.** 3.4.7, it is represented that the absorption peaks are more prominent in [PEG-*b*-(PBLA)₇-*b*-(PBLG)₁₇] than [PEG-*b*-(PBLA)₇] due to more number of functional groups present in triblock compared to diblock copolymer [248].

3.4.12. CD Spectra for polymer vesicles at different pH medium and temperature range

Circular Dichroism analysis explained the behaviour towards the change in the secondary structure of proteins at various pH and temperature. After 45°C, acidic pH formed an agglomerated particle due to the degradation of polymer particles as the synthesis parameters have been changed. Synthesized block copolymers are helical well as random which is confirmed from all the graphs of CD data. CD exhibited 7.1% of α -helix, +5% of parallel β -sheets, +44% of β anti-parallel-sheets, +18% of β -turns and 32% of random coils for Tri-PAG at pH 8 and 25 °C (see **Fig.** 3.4.8). CDNN software has been used for the CD analysis of block copolymers. The α -helices spectra exhibited two negative peaks at 227nm and 241nm whereas β -sheets confirmed two positive peaks at 203nm and 188nm respectively. The spectra exhibited a high percentage of β anti-parallel-sheets and random coils in the vesicular solution.

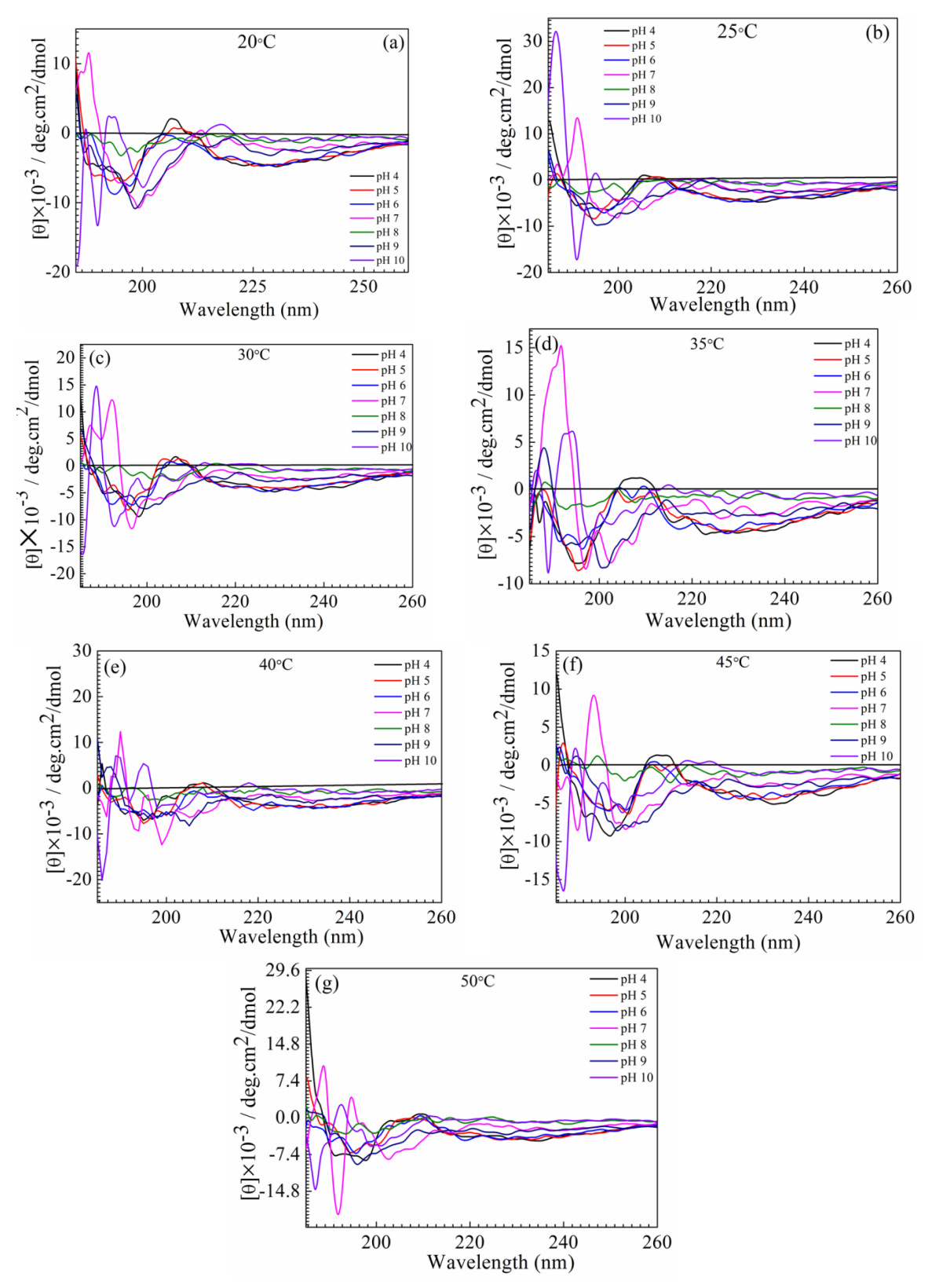


Figure 3.4.8. illustrates the CD component spectra showing deconvoluted protein folding behaviour of [PEG-*b*-(PBLA)₇-*b*-(PBLG)₁₇], the concentration of solution 0.5mg/ml with the variation of pH 4 to 10 and temperature from 20°C to 50°C with 23 reference proteins.

The factors behind this increment depends on (i) transition of micelles to vesicles, (ii) the mixing of two oppositely charged ions (see **scheme** 3.4.2.) and (iii) change of an external parameter of temperature and pH and (iv) the possibility of lateral overlapping of two peptide chains via hydrogen bonding [333-337].

Previous reports have mentioned the stability of peptides is due to α -helix and β antiparallel-sheets. Hence it is proved that, although the polymer is low in α -helix percentage, planar β anti-parallel-sheets made the polymer more stable in the solution medium via H bonding. The random coils are also effectively found in the polymer may be due to numerous chemical interactions between amino acid side chains. The change in polymer structure is induced by both temperature and pH which is seen in Fig. 3.4.8. Fig. 3.4.9. represent the CD spectra showing protein folding behaviour of [PEG-b-(PBLA)₇] at acidic pH 4, neutral pH 7 and basic pH 8 with the temperature ranged from 20°C to 45°C. It had shown less random coils than [PEG-b-(PBLA)₇-b-(PBLG)₁₇], as less number of peptide bond formation occur in the former case. Acidic pH showed a low percentage of α -helix, β -sheets, β -turns and random coils due to the repulsion between the amino acid residues and protonation effect caused in the [PEG-b-(PBLA)₁-b-(PBLG)₁₇] medium (see **scheme** 3.4.2) [321-324, 326]. Hence CD spectra for self-assembled [PEG-b-(PBLA)₇-b-(PBLG)₁₇] vesicular system confirmed the sheets and random coils due to the presence of peptide bonds in the various medium at different temperature. Fig. 3.4.9. illustrates the CD spectra showing protein folding behaviour of [PEG-b-(PBLA)₇] at acidic pH 4, neutral pH 7 and basic pH 8 with the temperature ranged from 20°C to 45°C.

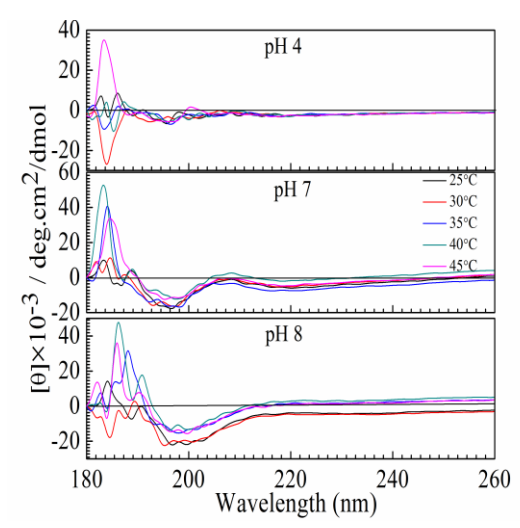


Figure 3.4.9. illustrates the CD spectra showing protein folding behaviour of [PEG-*b*-(PBLA)₇] at acidic pH 4, neutral pH 7 and basic pH 8 with the temperature ranged from 20°C to 45°C.

3.4.13. Antimicrobial Resistance of [PEG-b-(PBLA)₇-b-(PBLG)₁₇] nanovesicles

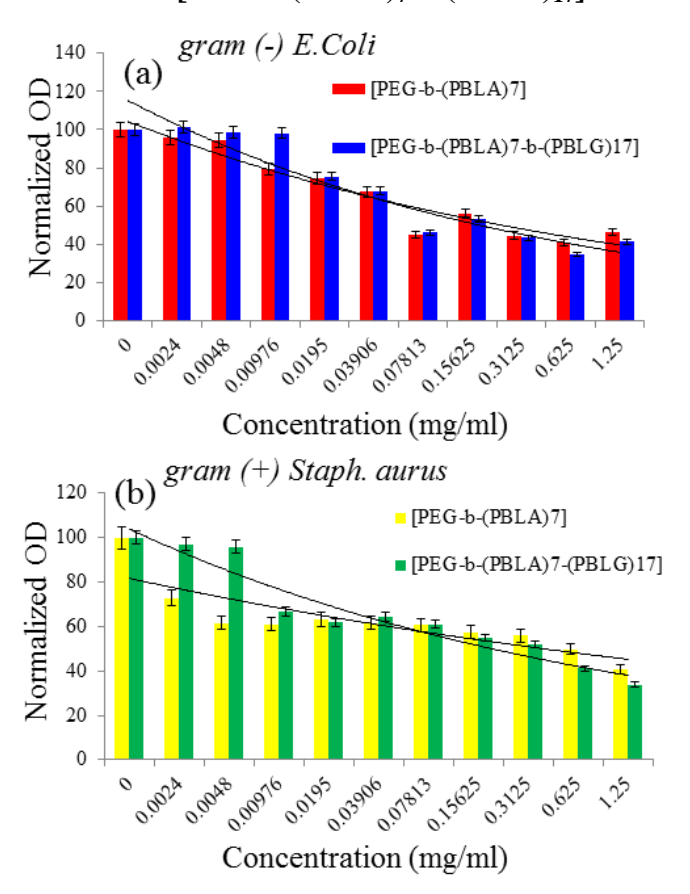


Figure 3.4.10. (a) and (b) represents the antibacterial susceptibility test showing the inhibition of growth for [PEG-b-(PBLA)₇] and [PEG-b-(PBLA)₇-b-(PBLG)₁₇] at room temperature with two different bacterial strains of gram (-) bacterial strain of E.coli and gram (+) bacteria Staphylococcus aureus respectively.

Figure 3.4.10. (a) and (b) is showing the optical density of bacteria death for [PEG-b-(PBLA)₇] nano micelles and [PEG-b-(PBLA)₇-b-(PBLG)₁₇] nanovesicles against two types of bacterial strains i.e. *gram* (+) *bacteria Staphylococcus aureus and gram* (-) bacterial strain of *E.coli* for better assessment of our polymeric samples. [PEG-b-(PBLA)₇-b-(PBLG)₁₇] has indicated an excellent bacteria killing efficiency at concentration 1.25mg/ml for *gram* (-) *E.coli* than *gram* (+) *staph aureus*. With the increase in concentration from 0.07813, 0.1562, 0.3125, 0.625 and 1.25 mg/ml, the gradual decrease in normalized OD 52%, 53%, 43%, 34% and 41% prohibited the growth of *staph aureus* bacteria in the medium, proving the polymer as a very effective antibacterial agent. With the increase of concentration from the lowest value to 0.0048mg/ml, the bacterial killing efficiency remained around the same in *gram* (-)

bacterial strain of *E.coli*, but the survival efficiency decreased after 0.00976mg/ml to 1.25mg/ml due to more number of acidic anions present in the medium.

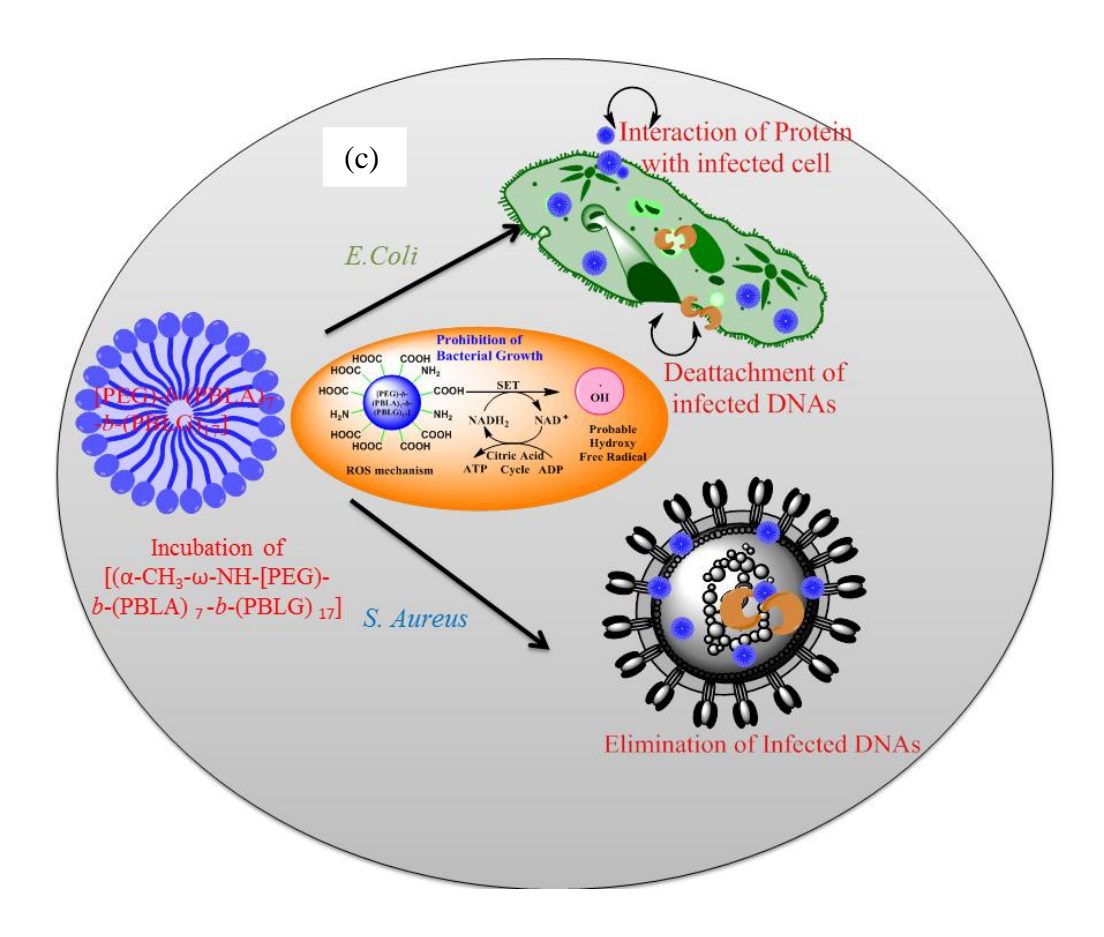


Figure. 3.4.10. (c): Probable Reductive Oxygen-Free radical mechanism against antibacterial infection.

Polymer [PEG-b-(PBLA)₇-b-(PBLG)₁₇] is showing better killing efficiency than [PEG-b-(PBLA)₇] for both the bacterial strains from 1.25mg/ml up to 0.00976mg/ml. So from the above experiment, it is observed that these two polymeric nano micelles and nanovesicles are eligible for *in vivo* antibacterial activity [341-342, 278, 350]. The established ROS mechanism helps the polymer pathway to kill the pathogenic bacteria via a single electron transfer mechanism. (See **Fig.** 3.4.10. (c)). We have observed the performance of polymeric micelles with different bacteria and found to be effective for further biomedical activity and applications.

3.4.14. In vitro MTT assay test for [PEG-b-(PBLA)₇-b-(PBLG)₁₇] nanovesicles

The human breast carcinoma cell MDA-MB231 cells were cultured for 24 hours in DMEM medium. *In vitro* Cytotoxicity assay was performed for both [PEG-*b*-(PBLA)₇] nano micelles and [PEG-*b*-(PBLA)₇-*b*-(PBLG)₁₇] nanovesicles (see **Fig**. 3.4.11.). Both the polymeric samples were dissolved in DMEM medium with mild sonication process separately. Then polymeric samples were allowed to treat with human breast carcinoma cell MDA-MB231 cells seeded on 96-well plates with different test concentrations and cell density of 5000 cells/well. The cell viability was assessed by adding 10 μL of MTT solution (stock solution 5000 μg/ml) per well and incubated at 37°C for 3 h. The medium was removed, and the formazon blue, which formed in the cells, was dissolved in 100 μl of DMSO.

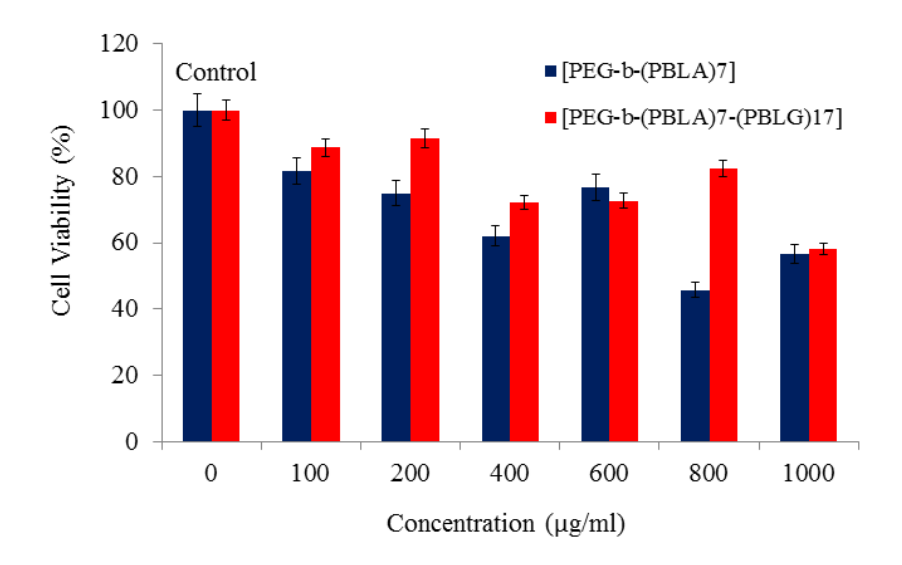


Figure 3.4.11. Cytotoxicity MTT assay test of $[PEG-b-(PBLA)_7]$ and $[PEG-b-(PBLA)_7-b-(PBLG)_{17}]$ solution in solvent medium towards MDA-MB231after 24 h incubation.

The colour formation intensity was measured at 570 nm. [PEG-*b*-(PBLA)₇-*b*-(PBLG)₁₇] vesicular solution has shown consistency in high cell viability % up to 800 μg/ml and low cytotoxicity with more than 70% cell viable whereas [PEG-*b*-(PBLA)₇] has shown up to 200 μg/ml. But the excellent result for [PEG-*b*-(PBLA)₇-*b*-(PBLG)₁₇] is due to a high amount of acidic anions released in the solvent medium which helps to kill the cancerous cell. From CD and Zeta analysis, we can correlate, the formation of more number of active ions in the colloidal solution helps to kill of carcinoma cell at acidic pH [338-340].

3.4.15. Conclusion for Part IIB

Here, in summary, we synthesized and characterized noble triblock copolymer [PEG-b-(PBLA)₇-b-(PBLG)₁₇] which showed morphologically as well as a physio-chemie variation to other polymers. Compared to other self-assembled polymers, our polymer is showing greater impact in CD, Zeta and thermal stability performance. Polymer with higher thermal stability (up to 300°C) in solid phase can be used for the thermal instrument in the medical technology. The giant ζ potential leads to the stability of block copolymers and adoption of the double helix as well as β -sheets found in the solvent medium. The well-defined diameter of the polymeric vesicles ranges 100 nm-670 nm polymer has shown its effective action against human carcinoma cell along with various infected pathogenic bacteria. Polypeptide-based vesicles acting as an interesting structure and may offer many advantages compared to low molar mass vesicles, in particular for applications in drug delivery, as nanocarrier with some other anticancer causing material. The other biological application of this triblock copolymer is in progress and hopefully can be used in advanced medical therapy.

CHAPTER 4

SUMMARY AND CONCLUSION

4.1 Summary

The fourth chapter of this dissertation concludes to the different nanosized designed nanomaterials and its exceptional application features in electrical nanodevices and biotechnology area. Here we have discussed the beneficial and useful of morphologically varied synthesized nanomaterial with concrete proofs for our future generation development.

This dissertation includes of following chapters

Chapter-1: In detail, the introduction, important terminology, literature study for both the organic-inorganic dielectric solids and Amino-acid based biocompatible block copolymers has been discussed. Moreover, a systematic literature review on both the abovementioned materials for electronic and biomedical applications has been discussed. At the end of this chapter, motivations, challenges and objectives for dielectric and polymeric materials have been discussed elaborately.

Chapter-2: The list of chemicals, chemical and experimental procedures, scientific characterization techniques along with detailed biological and electrical application procedures have been discussed in this chapter. The elaborate synthesis procedures of various morphology based nanomaterials of CCTO@SiO₂ core-shell nanomaterials, GO-CCTO@SiO₂ nanocomposites and amino acid based polymer with PEG as base material have been discussed. In continuation of this chapter, the techniques used to know the structural, physical, chemical and biological behaviour of materials have been discussed thoroughly.

Chapter-3: This dissertation is dedicated to understanding to "Synthesis, Characterization and Application of Morphologically Varying Organic-Inorganic Dielectrics and Amino acid based Biocompatible Copolymeric Nanomaterials". In this chapter, we have discussed the chemical, structural, physical and biological nature of four different morphologically varying nanomaterials i.e. Section A-organic-inorganic dielectrics and Section B-amino acid based copolymers.

4.2. Conclusions

The conclusion chapter has been incorporated with the significant key points of the development of four different types of synthesized nanomaterials for electrical and biological applications.

(*Part-IA*): A detailed study on the dielectric properties of CCTO@SiO₂ core-shell nanoparticles: Role of SiO₂ shell over CCTO core surface

A series of the core-shell nanostructure of CCTO and amine functionalized SiO₂ with a shell thickness from 5 nm to 20 nm have been prepared via a modified sol-gel chemical process. The amine functionalized silica-coated CCTO NPs are showing a far better dielectric than bare silica NPs, few metal oxide composites along with CCTO polymeric composites. The detailed dielectric and impedance properties have been studied for both sintered and nonsintered samples at various frequency ranges from 100Hz to 2MHz. At 20 Hz, least coated CS1S showed maximum ε' value of 1.390×10³, whereas highest coated CS3S showed less ε' value of 1.39×10^2 and CS2S showed an intermediate value 9.7×10^2 . The increase of ε' with the decrease in shell thickness is due to the presence of interfacial polarization in lower frequency region contributing to more space charge in the interface region at the core and shell barrier of CCTO@SiO₂ NPs. The study also revealed that, at low and high frequency $(1\times10^3$ Hz and 2M Hz), CS3S, CS2S and CS1S possessed ϵ'' value of 1.3×10^1 , 6.2×10^1 , 2.7×10² and -25, 64 and 72, respectively. Thicker coated CS3S and thinner coated CS1S are having ε' of 2.5×10^2 and 1.2×10^4 for frequency 1×10^3 Hz respectively with respect to temperature dependence study. It is confirmed from the impedance studies that sintered coreshell CCTO@SiO₂ NPs exhibited better dielectric properties than other dielectric nanocomposites like organic polymer, barium titanates and other perovskite oxides including non-sintered CCTO@SiO₂-NH₂ NPs. This type of core-shell nanoparticles can be used for polymer composite materials due to the organic amine groups present on the surface of CCTO core shell. The attachment can be possible with the control of various external parameters during the experiment process. The results further suggest that using these coreshell materials microelectronic and energy storage devices with variable dielectric properties can be designed due to its high loss compared to bare CCTO and other related materials reported. This novel work is based on thickness, hence showed that with minimum coating can increase the behaviour of the dielectric to a high level and for better charge storage device application in future.

(*Part-IB*): Dielectrics of graphene oxide sheets decorated with nanocomposite silica-coated calcium copper titanate (CCTO) nanoparticles

In this work, a series of CCTO@SiO₂-GO nanocomposites have been prepared through a novel synthesis method. Silica-coated CCTO NPs decoration over the surface of GO plays the vital for the successful synthesis which mainly considers few environmental conditions like balanced atmospheric condition, Stirring and centrifugation rpm, sonication time duration and amount of solute. It shows a variable study of dielectrics concerning the different temperature and frequencies. The material shows a high ε' of 1.5×10⁴ after 500°C which can be used as a good dielectric material for the electronics device use as sensors, charge storage devices etc. But a high loss was also observed more than constant at corresponding frequencies lead to its use in the microwave electronics device industry. Concluding to this manuscript, the prepared nanocomposite can be used as a good dielectric material with the variation in the thickness of silica decoration over CCTO NPs and GO sheet. Even though many reports have given an idea about being used in the wide areas, however, our work has established new nanocomposites which can be used in designing new functional electronic devices and electrochemistry

Part-IIA: Stimuli responsive biocompatible synthetic polypetidic nano micelles: Novel approaches towards antibacterial & therapeutic applications)

Herein, we have summarized our work with the noble synthesized biocompatible triblock copolymer [PEG-b-PBLG₅-b-PBLA₁₈] which showed greater relevance in UV-Vis absorbance, DLS, and ZETA potential with compared to the diblock copolymer [PEG-b-PBLG]. The controlled surface morphology with the response to temperature and pH of this copolymers became the main reason of the micelles to behave as a most interesting structure than other low molecular weight polymers. Biocompatibility, the zeta potential of -45mV and CD results of the various secondary structure have revealed the synthesized block polymeric materials are effective for *in vitro* biomedical applications. Due to host-guest inclusion complex formation activity, our synthesized polymers can form complexes with various proteins, peptides, metal complexes and other biocompatible materials. MTT assay test of polymer against human breast carcinoma found to be active and low cytotoxic. Further, the triblock copolymer is very efficient for the killing of *gram* (-) *E.Coli* than *gram* (+) *Staph aureus bacteria*. It can be used for further applications such as drug delivery (HRTEM

images, 13 nm) and other biomedical application as a nano vehicle, antiseptic agent, antibacterial therapy element. Path of polymer science is growing very fast in everyday life and hopefully, we will able to implicate these block copolymers for further applications in microbiology and related biotechnology.

(*Part-IIB*): Designing of new triblock polypepto vesicle sized nanobiomaterials and its action upon the antibacterial activity

Here in summary, the evidence of noble triblock copolymer [PEG-b-(PBLA)₇-b-(PBLG)₁₇] has been established by trivial ring-opening polymerization method. It has shown morphological as well as physio-chemie variation to other polymers. The well-defined diameter of polymeric vesicles ranges 100nm-670nm polymer has shown its effective action against human carcinoma cell along with various infected pathogenic bacteria. Compared to other self assembled polymers, our polymer is showing greater impact in CD, Zeta and thermal stability performance. Polymer with higher thermal stability (up to 300°C) in solid phase can be used for the thermal instrument in the medical technology. The giant ζ potential leads to the stability of block copolymer and adoption of the double helix as well as β -sheets found in the solvent medium. Polypeptide-based vesicles acting as an interesting structure and may offer many advantages compared to low molar mass vesicles, in particular for applications in drug delivery, as nanocarrier with some other anticancer causing material. The other biological application of this triblock copolymer is in progress and hopefully can be used in advanced medical therapy.

CHAPTER 5

FUTURE SCOPES

The future perspective of this dissertation can be made to understand the application and use in the further growth of science in the following ways:

- 1. Designing of organic dipole based hydroxy, alkyl groups etc. attachment on CCTO@SiO₂ for better dielectric behaviour due to dipole polarization effect and capacitance activity.
- 2. Modification of GO- MO@SiO₂ can be done with lanthanide series oxides like CeO₂, ErO₂, GdO₂ and NbO₂ for better dielectric constant and low loss instead of CCTO NPs.
- 3. Synthesis and application of triblock copolymer of [MeO-PEG-NH-*b*-(L-phenylalanine)-*b*-(L-AspA)] and its effect on mice model for cancer study.
- 4. Synthesis and application of triblock copolymer of [MeO-PEG-NH-*b*-(L-phenylalanine)-*b*-(L-GluA)] and its effect on mice model (SCID) for cancer study.
- 5. Synthesis of the triblock copolymer of [MeO-PEG-NH-*b*-(L-phynylalanine)-*b*-(L-GluA)] and [MeO-PEG-NH-*b*-(L-phynylalanine)*b*-(L-GluA)] with graphene oxide for thermal activity and *InVivo* studies by rats and rabbit.

List of publications from this dissertation

- 1. <u>Bharatiya</u>, <u>Debasrita</u> & Kumar, K Santhosh & Raghunandan, S & Paik, Pradip. (2019). Dielectrics of graphene oxide decorated with nanocomposite silica-coated calcium copper titanate (CCTO) nanoparticles. **Journal of Materials Science**. 54. 10.1007/s10853-019-03336-8.
- **2.**Bharatiya Debasrita, Kumar K Santhosh, S Raghunandan& Paik Pradip. (2019). A detailed study on the dielectric properties of CCTO@SiO2 core-shell nanoparticles: Role of SiO2-NH2 shell over CCTO core surface. **Journal of Solid State Chemistry**. 10.1016/j.jssc.2019.06.023
- **3.**<u>Debasrita Bharatiya</u>, Biswajit Parhi, Khumukcham Saratchandra Singh, Bramanandam Manavathi, Pradip Paik (Manuscript under communication)
- **4.** <u>Debasrita Bharatiya</u>, Biswajit Parhi, Rutuparna Jena and Pradip Paik (Designing of a new polypepto based nanovesicles sized macromolecular triblock biomaterials and its action against bacterial resistance) (Manuscript Prepared)

List of conference presentations based on dissertation work

1. <u>Debasrita Bharatiya</u>, Pradip Paik (**Poster Presentation, International Conference Nano Sci Tech 2017**)

The synthesis and study of AB, BC and ABC types of Bio-Compatible amino acids based block copolymers for biomedical application held from **November 08** th **-10** th, **2017** at Panjab University, Chandigarh, India

2. <u>Debasrita Bharatiya</u>, Pradip Paik (Poster Presentation, 2nd International conference on Nano & Science and Engineering Applications-2018), (ISBN:978-81-924726-4-5)

Study of AB and ABC types of Bio-compatible Amino Acids based nano micro block copolymer vesicles for biomedical applications held from **October 04** th **-06** th, **2018** at Jawaharlal Nehru Technical University, Hyderabad, India.

3.<u>Debasrita Bharatiya</u>, K Santhosh Kumar, Raghunandan S, Pradip Paik (**Short invited talk/ Oral Presentation**, **4**th **International conference on Nanomaterials-2019**)

Synthesis and dielectrics of GO-CCTO-SiO₂ nanocomposite held from **April 12th -14th 2019** atMahatma Gandhi University, Kerala,

4.Debasrita Bharatiya, K Santhosh Kumar, Raghunandan S, Pradip Paik (**Poster Presentation, International Conference on Functional Materials-2020**)

Study of dielectrics of GO-CCTO-SiO₂ nanocomposite. **January 6th-8th 2020**, IIT Kharagpur, West Bengal.

REFERENCES

- [1] M. Ali, A brief history of Indian alchemy covering transitional and tantric periods (circa 800 A.D.-1300 A.D.)., Bull. Indian Inst. Hist. Med. Hyderabad. 26 (1996) 11–38.
- [2] J. Nicholson, Current trends in biomaterials, Mater. Today. 1 (1998) 6–8. https://doi.org/10.1016/s1369-7021(98)80038-2.
- [3] J.F.V. Vincent, Naturally new materials, Mater. Today. 1 (1998) 3–6. https://doi.org/10.1016/s1369-7021(98)80002-3.
- [4] R.R. Mohammed, M.F. Chong, Treatment and decolorization of biologically treated Palm Oil Mill Effluent (POME) using banana peel as novel biosorbent, J. Environ. Manage. 132 (2014) 237–249. https://doi.org/10.1016/j.jenvman.2013.11.031.
- [5] C. Xu, L. Wang, X. Mu, Y. Ding, Nanoporous PtRu alloys for electrocatalysis, Langmuir. 26 (2010) 7437–7443. https://doi.org/10.1021/la9041474.
- [6] F.R. P. There's plenty of room at the bottom of a cell, Eng. Sci. XXIII (1960).
- [7] A.M. Ealias, M.P. Saravanakumar, A review on the classification, characterisation, synthesis of nanoparticles and their application, IOP Conf. Ser. Mater. Sci. Eng. 263 (2017). https://doi.org/10.1088/1757-899X/263/3/032019.
- [8] J.U. Menon, P. Ravikumar, A. Pise, D. Gyawali, C.C.W. Hsia, K.T. Nguyen, Polymeric nanoparticles for pulmonary protein and DNA delivery, Acta Biomater. 10 (2014) 2643–2652. https://doi.org/10.1016/j.actbio.2014.01.033.
- [9] S.M. Moghimi, D. Simberg, Complement activation turnover on surfaces of nanoparticles, Nano Today. 15 (2017) 8–10. https://doi.org/10.1016/j.nantod.2017.03.001.
- [10] S.M. Moghimi, Cancer nanomedicine and the complement system activation paradigm: Anaphylaxis and tumour growth, J. Control. Release. 190 (2014) 556–562. https://doi.org/10.1016/j.jconrel.2014.03.051.
- [11] M. Biesalski, K. Shroff, P. Samyn, Surface-attached, polymerized vesicles exposing adhesive peptide functionalities, ACS Symp. Ser. 1070 (2011) 225–248. https://doi.org/10.1021/bk-2011-1070.ch014.
- [12] M. Bottini, F. Cerignoli, D.M. Mills, F. D'Annibale, M. Leone, N. Rosato, A. Magrini, M. Pellecchia, A. Bergamaschi, T. Mustelin, Luminescent silica nanobeads: Characterization and evaluation as efficient cytoplasmatic transporters for T-lymphocytes, J. Am. Chem. Soc. 129 (2007) 7814–7823. https://doi.org/10.1021/ja070245c.
- [13] C.E. McNamee, M. Nilsson, C. Von Corswant, O. Söderman, Physicochemical

- characterization of PEG1500-12-acyloxy-stearate micelles and liquid crystalline phases, Langmuir. 21 (2005) 8146–8154. https://doi.org/10.1021/la0511539.
- [14] S. Makarov, S. Kudryashov, I. Mukhin, A. Mozharov, V. Milichko, A. Krasnok, P. Belov, Tuning of Magnetic Optical Response in a Dielectric Nanoparticle by Ultrafast Photoexcitation of Dense Electron-Hole Plasma, Nano Lett. 15 (2015) 6187–6192. https://doi.org/10.1021/acs.nanolett.5b02534.
- [15] A.D.T. Marcelo Carmo,† Ryan C. Sekol,† Shiyan Ding,‡ Golden Kumar,‡ Jan Schroers, Bulk Metallic Glass Nanowire Architecture for Electrochemical Applications, ACS Nano. 5 (2011) 2979–2983.
- [16] Y. Chen, Z. Fan, Z. Zhang, W. Niu, C. Li, N. Yang, B. Chen, H. Zhang, Two-Dimensional Metal Nanomaterials: Synthesis, Properties, and Applications, Chem. Rev. 118 (2018) 6409–6455. https://doi.org/10.1021/acs.chemrev.7b00727.
- [17] E.K. Richman, J.E. Hutchison, Bottleneck, 3 (2009) 2441–2446.
- [18] N.H. Hong, Introduction to Nanomaterials: Basic Properties, Synthesis, and Characterization, Elsevier Inc., 2019. https://doi.org/10.1016/b978-0-12-813934-9.00001-3.
- [19] I. Capek, Nanotechnology and nanomaterials, 2019. https://doi.org/10.1016/b978-0-444-63748-2.00001-8.
- [20] B. Zhang, Principles, Methods, Formation Mechanisms, and Structures of Nanomaterials Prepared via Self-Assembly, 2018. https://doi.org/10.1016/b978-0-12-410417-4.00005-8.
- [21] A. Viscido, A. Capannolo, G. Latella, R. Caprilli, G. Frieri, Nanotechnology in the treatment of inflammatory bowel diseases, J. Crohn's Colitis. 8 (2014) 903–918. https://doi.org/10.1016/j.crohns.2014.02.024.
- [22] S. Bhatia, Natural polymer drug delivery systems: Nanoparticles, plants, and algae, 2016. https://doi.org/10.1007/978-3-319-41129-3.
- [23] C.P. Devatha, A.K. Thalla, Green Synthesis of Nanomaterials, Elsevier Ltd., 2018. https://doi.org/10.1016/b978-0-08-101975-7.00007-5.
- [24] P. Innocenzi, L. Malfatti, B. Lasio, A. Pinna, D. Loche, M.F. Casula, V. Alzari, A. Mariani, Sol-gel chemistry for graphene-silica nanocomposite films, New J. Chem. 38 (2014) 3777–3782. https://doi.org/10.1039/c4nj00535j.
- [25] H. Yao, L.P. Wu, G.Q. Chen, Synthesis and Characterization of Electroconductive PHA- graft-Graphene Nanocomposites, 2019. https://doi.org/10.1021/acs.biomac.8b01257.
- [26] Y. Yuan, F. Liu, L. Xue, H. Wang, J. Pan, Y. Cui, H. Chen, L. Yuan, Recyclable

- Escherichia coli-Specific-Killing AuNP-Polymer (ESKAP) Nanocomposites, ACS Appl. Mater. Interfaces. 8 (2016) 11309–11317. https://doi.org/10.1021/acsami.6b02074.
- [27] P.M. Ajayan, Bulk Metal and Ceramics Nanocomposites, 2004. https://doi.org/10.1002/3527602127.ch1.
- [28] W. Wang, K.A.S. Fernando, Y. Lin, M.J. Meziani, L.M. Veca, L. Cao, P. Zhang, M.M. Kimani, Y.P. Sun, Metallic single-walled carbon nanotubes for conductive nanocomposites, J. Am. Chem. Soc. 130 (2008) 1415–1419. https://doi.org/10.1021/ja0768035.
- [29] H. Zhang, D. Liu, M.A. Shahbazi, E. Mäkilä, B. Herranz-Blanco, J. Salonen, J. Hirvonen, H.A. Santos, Fabrication of a multifunctional nano-in-micro drug delivery platform by microfluidic templated encapsulation of porous silicon in polymer matrix, Adv. Mater. 26 (2014) 4497–4503. https://doi.org/10.1002/adma.201400953.
- [30] D. Sitko, W. Bk, B. Garbarz-Glos, A. Budziak, C. Kajtoch, A. Kalvane, Dielectric properties of BaTiO3 based materials with addition of transition metal ions with variable valence, IOP Conf. Ser. Mater. Sci. Eng. 49 (2013). https://doi.org/10.1088/1757-899X/49/1/012050.
- [31] R.K. Pandey, W.A. Stapleton, J. Tate, A.K. Bandyopadhyay, I. Sutanto, S. Sprissler, S. Lin, Applications of CCTO supercapacitor in energy storage and electronics, AIP Adv. 3 (2013) 0–13. https://doi.org/10.1063/1.4812709.
- [32] S. Antohe, N. Tomozeiu, S. Gogonea, Properties of the Organic-on-Inorganic Semiconductor Barrier Contact Diodes In/PTCDI/p-Si and Ag/CuPc/p-Si, Phys. Status Solidi. 125 (1991) 397–408. https://doi.org/10.1002/pssa.2211250138.
- [33] J. Fan, S. Wang, W. Sun, S. Guo, Y. Kang, J. Du, X. Peng, Anticancer drug delivery systems based on inorganic nanocarriers with fluorescent tracers, AIChE J. 64 (2018) 835–859. https://doi.org/10.1002/aic.15976.
- [34] G. Garnweitner, M. Niederberger, Organic chemistry in inorganic nanomaterials synthesis, J. Mater. Chem. 18 (2008) 1171–1182. https://doi.org/10.1039/b713775c.
- [35] L.A. Fredin, Z. Li, M.T. Lanagan, M.A. Ratner, T.J. Marks, Sustainable high capacitance at high frequencies: Metallic aluminum-polypropylene nanocomposites, ACS Nano. 7 (2013) 396–407. https://doi.org/10.1021/nn3044148.
- [36] Y. Ding, M. Chen, J. Erlebacher, Metallic mesoporous nanocomposites for electrocatalysis, J. Am. Chem. Soc. 126 (2004) 6876–6877. https://doi.org/10.1021/ja0320119.
- [37] Q. Mo, N. Chen, M. Deng, L. Yang, Q. Gao, Metallic Cobalt@Nitrogen-Doped Carbon Nanocomposites: Carbon-Shell Regulation toward Efficient Bi-Functional Electrocatalysis, ACS Appl. Mater. Interfaces. 9 (2017) 37721–37730.

- https://doi.org/10.1021/acsami.7b10853.
- [38] C. Xu, X. Wang, J. Zhu, Graphene Metal particle nanocomposites, J. Phys. Chem. C. 112 (2008) 19841–19845. https://doi.org/10.1021/jp807989b.
- [39] J. Kim, H. Yang, P.F. Green, Tailoring the refractive indices of thin film polymer metallic nanoparticle nanocomposites, Langmuir. 28 (2012) 9735–9741. https://doi.org/10.1021/la300374w.
- [40] N. Pazos-Pérez, Y. Gao, M. Hilgendorff, S. Irsen, J. Pérez-Juste, M. Spasova, M. Farle, L.M. Liz-Marzán, M. Giersig, Magnetic Noble metal nanocomposites with morphology-dependent optical response, Chem. Mater. 19 (2007) 4415–4422. https://doi.org/10.1021/cm070248o.
- [41] Z.P. Xu, R. Xu, H.C. Zeng, Sulfate-Functionalized Carbon/ Metal-Oxide Nanocomposites from Hydrotalcite-like Compounds, Nano Lett. 1 (2001) 703–706. https://doi.org/10.1021/nl010045d.
- [42] A.S. Zeraati, M. Arjmand, U. Sundararaj, Silver Nanowire/MnO₂ Nanowire Hybrid Polymer Nanocomposites: Materials with High Dielectric Permittivity and Low Dielectric Loss, ACS Appl. Mater. Interfaces. 9 (2017) 14328–14336. https://doi.org/10.1021/acsami.6b14948.
- [43] B. Luo, X. Wang, E. Tian, H. Gong, Q. Zhao, Z. Shen, Y. Xu, X. Xiao, L. Li, Dielectric Enhancement in Graphene/Barium Titanate Nanocomposites, ACS Appl. Mater. Interfaces. 8 (2016) 3340–3348. https://doi.org/10.1021/acsami.5b11231.
- [44] C. Zhang, S. Guang, X. Zhu, H. Xu, X. Liu, M. Jiang, Mechanism of dielectric constant variation of POSS-based organic-inorganic molecular hybrids, J. Phys. Chem. C. 114 (2010) 22455–22461. https://doi.org/10.1021/jp1080753.
- [45] B. Jiang, X. Pang, B. Li, Z. Lin, Organic-Inorganic Nanocomposites via Placing Monodisperse Ferroelectric Nanocrystals in Direct and Permanent Contact with Ferroelectric Polymers, J. Am. Chem. Soc. 137 (2015) 11760–11767. https://doi.org/10.1021/jacs.5b06736.
- [46] P. Barber, P.J. Pellechia, H.J. Ploehn, H.C. Zur Loye, High-dielectric polymer composite materials from a series of mixed-metal phenylphosphonates, ATi(C6H5PO3)3 for dielectric energy storage, ACS Appl. Mater. Interfaces. 2 (2010) 2553–2559. https://doi.org/10.1021/am1003987.
- [47] Prateek, V.K. Thakur, R.K. Gupta, Recent Progress on Ferroelectric Polymer-Based Nanocomposites for High Energy Density Capacitors: Synthesis, Dielectric Properties, and Future Aspects, Chem. Rev. 116 (2016) 4260–4317. https://doi.org/10.1021/acs.chemrev.5b00495.
- [48] J. Lee, J.W. Chung, G.B. Yoon, M.H. Lee, D.H. Kim, J. Park, J.K. Lee, M.S. Kang, Influence of Dielectric Layers on Charge Transport through Diketopyrrolepyrrole-

- Containing Polymer Films: Dielectric Polarizability vs Capacitance, ACS Appl. Mater. Interfaces. 8 (2016) 30344–30350. https://doi.org/10.1021/acsami.6b09993.
- [49] H. Gao, K. Lian, A comparative study of nano-SiO2 and Nano-TiO2 fillers on proton conductivity and dielectric response of a silicotungstic acid-H3PO4-Poly(vinyl alcohol) polymer electrolyte, ACS Appl. Mater. Interfaces. 6 (2014) 464–472. https://doi.org/10.1021/am4045103.
- [50] Y.Y. Yu, A.H. Jiang, W.Y. Lee, Organic/Inorganic Nano-hybrids with High Dielectric Constant for Organic Thin Film Transistor Applications, Nanoscale Res. Lett. 11 (2016). https://doi.org/10.1186/s11671-016-1710-4.
- [51] D. Misra, Evolution of dielectric Science and Technology for nanoelectronics, Electrochem. Soc. Interface. 20 (2011) 31. https://doi.org/10.1149/2.F02114if.
- [52] B. Brown, D. Hess, V. Desai, M.J. Deen, Dielectric science and technology, Electrochem. Soc. Interface. 15 (2006) 28–31.
- [53] M.Z. Hossain, S.L. Rumyantsev, K.M.F. Shahil, D. Teweldebrhan, M. Shur, A.A. Balandin, Low-frequency current fluctuations in "graphene-like" exfoliated thin-films of bismuth selenide topological insulators, ACS Nano. 5 (2011) 2657–2663. https://doi.org/10.1021/nn102861d.
- [54] S. Takeshita, S. Yoda, Chitosan Aerogels: Transparent, Flexible Thermal Insulators, Chem. Mater. 27 (2015) 7569–7572. https://doi.org/10.1021/acs.chemmater.5b03610.
- [55] L.F. Schneemeyer, R.B. Van Dover, C.K. Madsen, C.L. Claypool, The compositional spread approach to high-dielectric constant materials and materials for integrated optics, ACS Symp. Ser. 814 (2002) 49–64.
- [56] X.Z. Yan, T. Goodson, High dielectric hyperbranched polyaniline materials, J. Phys. Chem. B. 110 (2006) 14667–14672. https://doi.org/10.1021/jp061522p.
- [57] A.R. von Hippel, S.O. Morgan, Dielectric Materials and Applications, J. Electrochem. Soc. 102 (1955) 68C. https://doi.org/10.1149/1.2430014.
- [58] L.R. Radovic, Chemistry and physics of carbon, Chem. Phys. Carbon. 30 (2007) 1– 245. https://doi.org/10.1201/9781420042993.
- [59] H. Tang, Z. Zhou, C.C. Bowland, H.A. Sodano, Synthesis of calcium copper titanate (CaCu<inf>3</inf>Ti<inf>4</inf>O<inf>12</inf>) nanowires with insulating SiO<inf>2</inf> barrier for low loss high dielectric constant nanocomposites, Nano Energy. 17 (2015) 302–307. https://doi.org/10.1016/j.nanoen.2015.09.002.
- [60] J. Świergiel, J. Jadżyn, Electric relaxational effects induced by ionic conductivity in dielectric materials, Ind. Eng. Chem. Res. 50 (2011) 11935–11941. https://doi.org/10.1021/ie201172t.

- [61] Y. Liu, C. Qian, L. Qu, Y. Wu, Y. Zhang, X. Wu, B. Zou, W. Chen, Z. Chen, Z. Chi, S. Liu, X. Chen, J. Xu, A Bulk Dielectric Polymer Film with Intrinsic Ultralow Dielectric Constant and Outstanding Comprehensive Properties, Chem. Mater. 27 (2015) 6543–6549. https://doi.org/10.1021/acs.chemmater.5b01798.
- [62] H. Luo, C. Ma, X. Zhou, S. Chen, D. Zhang, Interfacial Design in Dielectric Nanocomposite Using Liquid-Crystalline Polymers, Macromolecules. 50 (2017) 5132– 5137. https://doi.org/10.1021/acs.macromol.7b00792.
- [63] He seung lee et al., Low dielectric materials for microelectronics, Book. (n.d.) 59–76. https://doi.org/10.1063/1.1567460.
- [64] R. Singh, R.K. Ulrich, High and low dielectric constant materials, Electrochem. Soc. Interface. 8 (1999) 26–30.
- [65] S. Fromille, J. Phillips, Super dielectric materials, Materials (Basel). 7 (2014) 8197–8212. https://doi.org/10.3390/ma7128197.
- [66] L. K. H. VAN BEEK and J. J. HERMANS, Dielectric relaxation in dilute solutions of polar molecules in non-polar solvents, J. Polym. Sci. XXIII (1957) 211–221.
- [67] R.O. Davies, B.K. Scaife, Onsager's theory of the dielectric constant of polar liquids, J. Chem. Phys. 22 (1954) 148–149. https://doi.org/10.1063/1.1739832.
- [68] L. Onsagbr, Electric Moments of Molecules in Liquids, J. Am. Chem. Soc. 58 (1936) 1486–1493. https://doi.org/10.1021/ja01299a050.
- [69] R. Podeszwa, R. Bukowski, K. Szalewicz, Potential energy surface for the benzene dimer and perturbational analysis of π-π interactions, J. Phys. Chem. A. 110 (2006) 10345–10354. https://doi.org/10.1021/jp064095o.
- [70] C.P. Smyth, Dielectric Polarization and Relaxation, Annu. Rev. Phys. Chem. 17 (1966) 433–456. https://doi.org/10.1146/annurev.pc.17.100166.002245.
- [71] M. V. Fedorov, A.A. Kornyshev, Ionic liquids at electrified interfaces, Chem. Rev. 114 (2014) 2978–3036. https://doi.org/10.1021/cr400374x.
- [72] M. Suzuki, J. Shigematsu, T. Kodama, Hydration study of proteins in solution by microwave dielectric analysis, J. Phys. Chem. 100 (1996) 7279–7282. https://doi.org/10.1021/jp953331k.
- [73] H.B. Thompson, The determination of dipole moments in solution, J. Chem. Educ. 43 (1966) 66. https://doi.org/10.1021/ed043p66.
- [74] S. Gao, C.S. Park, S.S. Lee, D.Y. Choi, All-dielectric metasurfaces for simultaneously realizing polarization rotation and wavefront shaping of visible light, Nanoscale. 11 (2019) 3933–3944. https://doi.org/10.1039/c9nr00187e.
- [75] T. Pandirengan, M. Arumugam, M. Durairaj, Development ofhigh dielectric dual

- phase [Bi4Ti3O12]X-[CaCu3Ti4O12]1 X nanocomposite thin films for modern microelectronic device applications, Thin Solid Films. 628 (2017) 117–126. https://doi.org/10.1016/j.tsf.2017.03.021.
- [76] R.J. Cava, Dielectric materials for applications in microwave communications, J. Mater. Chem. 11 (2001) 54–62. https://doi.org/10.1039/b0036811.
- [77] K.S. Cole, R.H. Cole, Dispersion and absorption in dielectrics I. Alternating current characteristics, J. Chem. Phys. 9 (1941) 341–351. https://doi.org/10.1063/1.1750906.
- [78] A.O. Turky, M.M. Rashad, Z.I. Zaki, I.A. Ibrahim, M. Bechelany, Tuning the optical and dielectric properties of calcium copper titanate Ca<inf>x</inf>Cu<inf>3-x</inf>Ti<inf>4</inf>O<inf>12</inf> nanopowders, RSC Adv. 5 (2015) 18767—18772. https://doi.org/10.1039/c4ra15222k.
- [79] Q.G. Chi, J.F. Dong, C.H. Zhang, C.P. Wong, X. Wang, Q.Q. Lei, Nano iron oxide-deposited calcium copper titanate/polyimide hybrid films induced by an external magnetic field: Toward a high dielectric constant and suppressed loss, J. Mater. Chem. C. 4 (2016) 8179–8188. https://doi.org/10.1039/c6tc01655c.
- [80] K.P. Chen, X.W. Zhang, Synthesis of calcium copper titanate ceramics via the molten salts method, Ceram. Int. 36 (2010) 1523–1527. https://doi.org/10.1016/j.ceramint.2010.02.018.
- [81] N. Tripathy, K.C. Das, S.P. Ghosh, G. Bose, J.P. Kar, Fabrication of high-k dielectric Calcium Copper Titanate (CCTO) target by solid state route, IOP Conf. Ser. Mater. Sci. Eng. 115 (2016) 8–12. https://doi.org/10.1088/1757-899X/115/1/012022.
- [82] I. Dakova, P. Vasileva, I. Karadjova, Cysteine modified silica submicrospheres as a new sorbent for preconcentration of Cd (II) and Pb (II), Bulg. Chem. Commun. 43 (2011) 210–216.
- [83] M. Lakhane, K. Bogle, R. Khairnar, S. Dahiwale, R. Sharma, V. Mokale, M. Mahabole, Dielectric properties of zeolite based metal oxide nanocomposites, Nano-Structures and Nano-Objects. 17 (2019) 248–258. https://doi.org/10.1016/j.nanoso.2019.01.008.
- [84] T.I. Yang, R.N.C. Brown, L.C. Kempel, P. Kofinas, Controlled synthesis of core-shell iron-silica nanoparticles and their magneto-dielectric properties in polymer composites, Nanotechnology. 22 (2011). https://doi.org/10.1088/0957-4484/22/10/105601.
- [85] Z.B. Wang, A. Mitra, H.T. Wang, L.M. Huang, Y. Yan, Pure silica zeolite films as low-k dielectrics by spin-on of nanoparticle suspensions, Adv. Mater. 13 (2001) 1463–1466. https://doi.org/10.1002/1521-4095(200110)13:19<1463::AID-ADMA1463>3.0.CO;2-H.
- [86] S. Baskaran, J. Liu, K. Domansky, N. Kohler, X. Li, C. Coyle, G.E. Fryxell, S.

- Thevuthasan, R.E. Williford, Low dielectric constant mesoporous silica films through molecularly templated synthesis, Adv. Mater. 12 (2000) 291–294. https://doi.org/10.1002/(SICI)1521-4095(200002)12:4<291::AID-ADMA291>3.0.CO;2-P.
- [87] P.P. Suttisak Srisuwan, Supakanok Thongyai, Synthesis and Characterization of Low-Dielectric Photosensitive Polyimide/Silica Hybrid Materials Suttisak, J. Appl. Polym. Sci. 116 (2010) 2422–2427. https://doi.org/10.1002/app.
- [88] C.M. Lew, Z. Li, S. Li, S.J. Hwang, Y. Liu, D.I. Medina, M. Sun, J. Wang, M.E. Davis, Y. Yan, Pure-silica-zeolite MFI and MEL low-dielectric-constant films with fluoro-organic functionalization, Adv. Funct. Mater. 18 (2008) 3454–3460. https://doi.org/10.1002/adfm.200800390.
- [89] S. Villa, P. Riani, F. Locardi, F. Canepa, Functionalization of Fe3O4 NPs by silanization: Use of amine (APTES) and thiol (MPTMS) silanes and their physical characterization, Materials (Basel). 9 (2016). https://doi.org/10.3390/ma9100826.
- [90] P. Falcaro, K.M. Nairn, A.J. Hill, D. Buso, Amino functionalized SiO2 nanoparticles for seeding MOF-5, IOP Conf. Ser. Mater. Sci. Eng. 18 (2011) 1–6. https://doi.org/10.1088/1757-899X/18/5/052006.
- [91] A.S. Morris, A. Adamcakova-Dodd, S.E. Lehman, A. Wongrakpanich, P.S. Thorne, S.C. Larsen, A.K. Salem, Amine modification of nonporous silica nanoparticles reduces inflammatory response following intratracheal instillation in murine lungs, Toxicol. Lett. 241 (2016) 207–215. https://doi.org/10.1016/j.toxlet.2015.11.006.
- [92] P. Mélinon, S. Begin-Colin, J.L. Duvail, F. Gauffre, N.H. Boime, G. Ledoux, J. Plain, P. Reiss, F. Silly, B. Warot-Fonrose, Engineered inorganic core/shell nanoparticles, Phys. Rep. 543 (2014) 163–197. https://doi.org/10.1016/j.physrep.2014.05.003.
- [93] S. Kudera, L. Maus, M. Zanella, B. Pelaz, Q. Zhang, W.J. Parak, P. del Pino, W.J. Parak, Inorganic Core–Shell Nanoparticles, Compr. Nanosci. Nanotechnol. (2016) 171–186. https://doi.org/10.1016/b978-0-12-803581-8.00581-6.
- [94] R. Ghosh Chaudhuri, S. Paria, Core/shell nanoparticles: Classes, properties, synthesis mechanisms, characterization, and applications, Chem. Rev. 112 (2012) 2373–2433. https://doi.org/10.1021/cr100449n.
- [95] M.S. Mauter, M. Elimelech, Critical Review Environmental Applications of Carbon-Based Nanomaterials, Am. Chem. Soc. (2008) 5843–5859. https://doi.org/10.1016/j.jvs.2008.11.060.
- [96] A. Holm, J. Park, E.D. Goodman, J. Zhang, R. Sinclair, M. Cargnello, C.W. Frank, Synthesis, Characterization, and Light-Induced Spatial Charge Separation in Janus Graphene Oxide, Chem. Mater. 30 (2018) 2084–2092. https://doi.org/10.1021/acs.chemmater.8b00087.

- [97] V. Srinivasan, M. Asha Jhonsi, M. Kathiresan, A. Kathiravan, Nanostructured Graphene Oxide Dots: Synthesis, Characterization, Photoinduced Electron Transfer Studies, and Detection of Explosives/Biomolecules, ACS Omega. 3 (2018) 9096–9104. https://doi.org/10.1021/acsomega.8b01180.
- [98] M. Ali, T.M. McCoy, I.R. McKinnon, M. Majumder, R.F. Tabor, Synthesis and Characterization of Graphene Oxide-Polystyrene Composite Capsules with Aqueous Cargo via a Water-Oil-Water Multiple Emulsion Templating Route, ACS Appl. Mater. Interfaces. 9 (2017) 18187–18198. https://doi.org/10.1021/acsami.7b02576.
- [99] Y.A. Cheon, J.H. Bae, B.G. Chung, Reduced Graphene Oxide Nanosheet for Chemophotothermal Therapy, Langmuir. 32 (2016) 2731–2736. https://doi.org/10.1021/acs.langmuir.6b00315.
- [100] D.C. Marcano, D. V. Kosynkin, J.M. Berlin, A. Sinitskii, Z. Sun, A. Slesarev, L.B. Alemany, W. Lu, J.M. Tour, Improved synthesis of graphene oxide, ACS Nano. 4 (2010) 4806–4814. https://doi.org/10.1021/nn1006368.
- [101] A.A.F. K. S. Novoselov, A. K. Geim,* S. V. Morozov, D. Jiang, Y. Zhang,1 S. V. Dubonos, I. V. Grigorieva, Enfermedad de Vogt-Koyanagi-Harada, Science (80-.). 306 (2004) 666–669. https://doi.org/10.1016/j.medcli.2015.04.005.
- [102] H.C. Schniepp, J.L. Li, M.J. McAllister, H. Sai, M. Herrera-Alonson, D.H. Adamson, R.K. Prud'homme, R. Car, D.A. Seville, I.A. Aksay, Functionalized single graphene sheets derived from splitting graphite oxide, J. Phys. Chem. B. 110 (2006) 8535–8539. https://doi.org/10.1021/jp060936f.
- [103] M. Zahed, P.S. Parsamehr, M.A. Tofighy, T. Mohammadi, Synthesis and functionalization of graphene oxide (GO) for salty water desalination as adsorbent, Chem. Eng. Res. Des. 138 (2018) 358–365. https://doi.org/10.1016/j.cherd.2018.08.022.
- [104] S. Mallakpour, A. Abdolmaleki, Z. Khalesi, S. Borandeh, Surface functionalization of GO, preparation and characterization of PVA/TRIS-GO nanocomposites, Polymer (Guildf). 81 (2015) 140–150. https://doi.org/10.1016/j.polymer.2015.11.005.
- [105] J.A. Luceño-Sánchez, G. Maties, C. Gonzalez-Arellano, A.M. Diez-Pascual, Synthesis and characterization of graphene oxide derivatives via functionalization reaction with hexamethylene diisocyanate, Nanomaterials. 8 (2018). https://doi.org/10.3390/nano8110870.
- [106] A.M. asiri Anish Khan, Mohammad Jawaid, Bernaurdshaw Neppolian, Graphene Functionalization, n.d. http://surfchem.dk/research/projects/graphene-chemistry/.
- [107] Y. Liu, J. Li, W. Li, Y. Li, Q. Chen, F. Zhan, Nitrogen-doped graphene aerogel-supported spinel CoMn2O4 nanoparticles as an efficient catalyst for oxygen reduction reaction, J. Power Sources. 299 (2015) 492–500.

- https://doi.org/10.1016/j.jpowsour.2015.09.042.
- [108] Y. Gao, D. Ma, C. Wang, J. Guan, X. Bao, Reduced graphene oxide as a catalyst for hydrogenation of nitrobenzene at room temperature, Chem. Commun. 47 (2011) 2432–2434. https://doi.org/10.1039/c0cc04420b.
- [109] E. Istif, J. Hernández-Ferrer, E.P. Urriolabeitia, A. Stergiou, N. Tagmatarchis, G. Fratta, M.J. Large, A.B. Dalton, A.M. Benito, W.K. Maser, Conjugated Polymer Nanoparticle–Graphene Oxide Charge-Transfer Complexes, Adv. Funct. Mater. 28 (2018) 1–10. https://doi.org/10.1002/adfm.201707548.
- [110] B.R. Editor, Ribozymes and RNA catalysis, Choice Rev. Online. 46 (2008) 46-0866-46-0866. https://doi.org/10.5860/choice.46-0866.
- [111] R.A. Vaia, Polymer Nanocomposites: Introduction The 'Nanocomposite 'Concept, Polym. Nanocomposites Introd. (2002) 1–5.
- [112] D.H. Reneker, F. Hao, Polymeric nanofibers: Introduction, ACS Symp. Ser. 918 (2006) 1–6.
- [113] M. Zhang, Y. Hong, W. Chen, C. Wang, Polymers for DNA Vaccine Delivery, ACS Biomater. Sci. Eng. 3 (2017) 108–125. https://doi.org/10.1021/acsbiomaterials.6b00418.
- [114] H. MORAWETZ, HERMAN FRANCIS MARK, nationalacademyofsciences, 1995.
- [115] Tim A. Osswald, Material Science of Polymers for Engineers, 1995.
- [116] J.N. Jakob, R. Winderlich, BERZELIUS, (1852).
- [117] R.O. Ebewele, Polymer science and technology, 2000. https://doi.org/10.1016/0261-3069(95)90127-2.
- [118] P. Flores-Morales, V.H. Campos-Requena, N. Gatica, C. Munoz, M.A. Pérez, B.L. Rivas, S.A. Sánchez, M. Suwalsky, Y. Tapiero, B.F. Urbano, Teaching Polymer Science in the Department of Polymers at the University of Concepción, Chile: A Brief History, J. Chem. Educ. 94 (2017) 1702–1713. https://doi.org/10.1021/acs.jchemed.7b00212.
- [119] J.E. Mark, H.R. Allcock, Inorganic Polymers, Second Edition, 2005.
- [120] R.P. Lattimer, M.J. Vergne, D.M. Hercules, A Developmental History of Polymer Mass Spectrometry, J. Chem. Educ. 84 (2007) 81. https://doi.org/10.1021/ed084p81.
- [121] L. Yang, X. Tan, Z. Wang, X. Zhang, Supramolecular Polymers: Historical Development, Preparation, Characterization, and Functions, Chem. Rev. 115 (2015) 7196–7239. https://doi.org/10.1021/cr500633b.

- [122] J.L. Schultz, E.S. Wilks, Dendritic and star polymers: Classification, nomenclature, structure representation, and registration in the DuPont SCION database, J. Chem. Inf. Comput. Sci. 38 (1998) 85–99. https://doi.org/10.1021/ci9700900.
- [123] R.A. Ramli, Hollow polymer particles: A review, RSC Adv. 7 (2017) 52632–52650. https://doi.org/10.1039/c7ra10358a.
- [124] Y. Tezuka, H. Oike, Topological polymer chemistry: Systematic classification of nonlinear polymer topologies, J. Am. Chem. Soc. 123 (2001) 11570–11576. https://doi.org/10.1021/ja0114409.
- [125] J.L. Schultz, Polymer Nomenclature, Classification, and Retrieval in the Du Pont Central Report Index, J. Chem. Inf. Comput. Sci. 15 (1975) 94–100. https://doi.org/10.1021/ci60002a005.
- [126] D. Wang, T. Zhao, X. Zhu, D. Yan, W. Wang, Bioapplications of hyperbranched polymers, Chem. Soc. Rev. 44 (2015) 4023–4071. https://doi.org/10.1039/c4cs00229f.
- [127] W.-F. Su, Principles of Polymer Design and Synthesis, Extracts. (2013) 19. https://doi.org/10.1007/978-3-642-38730-2.
- [128] L.S. Nair, C.T. Laurencin, Polymers as biomaterials for tissue engineering and controlled drug delivery, Adv. Biochem. Eng. Biotechnol. 102 (2006) 47–90. https://doi.org/10.1007/b137240.
- [129] H.R. KRICHELDORF, Hyperbranched Cyclic and Multicyclic Polymers by "'a2+b4"' Polycondensations, Polym. Chem. 47 (2008) 1971–1987. https://doi.org/10.1002/POLA.
- [130] D.S. Pashankar, W.P. Bishop, V. Loening-Baucke, Long-term Efficacy of Polyethylene Glycol 3350 for the Treatment of Chronic Constipation in Children with and without Encopresis, Clin. Pediatr. (Phila). 42 (2003) 815–819. https://doi.org/10.1177/000992280304200907.
- [131] J. Kahovec, R.B. Fox, K. Hatada, J. Kahovec, COMMISSION ON MACROMOLECULAR NOMENCLATURE * NOMENCLATURE OF REGULAR SINGLE-STRAND Nomenclature of regular single-strand, 74 (2002) 1921–1956.
- [132] P.C. Nalam, J.N. Clasohm, A. Mashaghi, N.D. Spencer, Macrotribological studies of poly(L-lysine)-graft-Poly(ethylene glycol) in aqueous glycerol mixtures, Tribol. Lett. 37 (2010) 541–552. https://doi.org/10.1007/s11249-009-9549-9.
- [133] G. Karlström, O. Engkvist, Theory of Poly (ethylene glycol) in Solution, (1997) 16–30.
- [134] A. Jain, H.S. Ashbaugh, Helix stabilization of poly(ethylene glycol)-peptide conjugates, Biomacromolecules. 12 (2011) 2729–2734. https://doi.org/10.1021/bm2005017.

- [135] C.Y. Gong, S. Shi, X.H. Wang, Y.J. Wang, S.Z. Fu, P.W. Dong, L.J. Chen, X. Zhao, Y.Q. Wei, Z.Y. Qian, Novel composite drug delivery system for honokiol delivery: Self-assembled poly(ethylene glycol)-poly(ε-caprolactone)-poly(ethylene glycol) micelles in thermosensitive poly(ethylene glycol)-poly(ε-caprolactone)-poly(ethylene glycol) hydrogel, J. Phys. Chem. B. 113 (2009) 10183–10188. https://doi.org/10.1021/jp902697d.
- [136] S. Ahmadi, D. Winter, Identification of Poly(ethylene glycol) and Poly(ethylene glycol)-Based Detergents Using Peptide Search Engines, Anal. Chem. 90 (2018) 6594–6600. https://doi.org/10.1021/acs.analchem.8b00365.
- [137] J.G. Huddleston, T.K. Looney, G.A. Broker, S.T. Griffin, S.K. Spear, R.D. Rogers, Comparative Behavior of Poly(ethylene glycol) Hydrogels and Poly(ethylene glycol) Aqueous Biphasic Systems, Ind. Eng. Chem. Res. 42 (2003) 6088–6095. https://doi.org/10.1021/ie030351x.
- [138] A.P. Chemist, Poly(ethylene glycol): a poor chemist's crown, (1983) 77–78.
- [139] S.G. Roy, U. Haldar, P. De, Remarkable swelling capability of amino acid based cross-linked polymer networks in organic and aqueous medium, ACS Appl. Mater. Interfaces. 6 (2014) 4233–4241. https://doi.org/10.1021/am405932f.
- [140] I. Mukherjee, A. Ghosh, P. Bhadury, P. De, Side-Chain Amino Acid-Based Cationic Antibacterial Polymers: Investigating the Morphological Switching of a Polymer-Treated Bacterial Cell, ACS Omega. 2 (2017) 1633–1644. https://doi.org/10.1021/acsomega.7b00181.
- [141] Q. Liu, W. Li, H. Wang, B.M.Z. Newby, F. Cheng, L. Liu, Amino Acid-Based Zwitterionic Polymer Surfaces Highly Resist Long-Term Bacterial Adhesion, Langmuir. 32 (2016) 7866–7874. https://doi.org/10.1021/acs.langmuir.6b01329.
- [142] J.M. Metselaar, P. Bruin, L.W.T. De Boer, T. De Vringer, C. Snel, C. Oussoren, M.H.M. Wauben, D.J.A. Crommelin, G. Storm, W.E. Hennink, A Novel Family of L-Amino Acid-Based Biodegradable Polymer-Lipid Conjugates for the Development of Long-Circulating Liposomes with Effective Drug-Targeting Capacity, Bioconjug. Chem. 14 (2003) 1156–1164. https://doi.org/10.1021/bc0340363.
- [143] S. Anantharaj, M. Jayakannan, Amyloid-Like Hierarchical Helical Fibrils and Conformational Reversibility in Functional Polyesters Based on l-Amino Acids, Biomacromolecules. 16 (2015) 1009–1020. https://doi.org/10.1021/bm501903t.
- [144] W. Li, Q. Liu, L. Liu, Antifouling gold surfaces grafted with aspartic acid and glutamic acid based zwitterionic polymer brushes, Langmuir. 30 (2014) 12619–12626. https://doi.org/10.1021/la502789v.
- [145] R. Liu, F. Sanda, T. Masuda, Synthesis and properties of glutamic acid-derived optically active phenyleneethynylene-based helical polymers, Macromolecules. 41

- (2008) 5089–5097. https://doi.org/10.1021/ma800674f.
- [146] F. Sanda, K. Terada, T. Masuda, Synthesis, chiroptical properties, and pH responsibility of aspartic acid- And glutamic acid-based helical polyacetylenes, Macromolecules. 38 (2005) 8149–8154. https://doi.org/10.1021/ma051529p.
- [147] M. Talelli, M.J. Vicent, Reduction sensitive poly(l-glutamic acid) (PGA)-protein conjugates designed for polymer masked-unmasked protein therapy, Biomacromolecules. 15 (2014) 4168–4177. https://doi.org/10.1021/bm5011883.
- [148] Y. Ogasawara, M. Shigematsu, S. Sato, H. Kato, T. Dairi, Involvement of Peptide Epimerization in Poly-γ-glutamic Acid Biosynthesis, Org. Lett. 21 (2019) 3972–3975. https://doi.org/10.1021/acs.orglett.9b01121.
- [149] S. Saxena, A. Pradeep, M. Jayakannan, Enzyme-Responsive Theranostic FRET Probe Based on l -Aspartic Amphiphilic Polyester Nanoassemblies for Intracellular Bioimaging in Cancer Cells , ACS Appl. Bio Mater. (2019). https://doi.org/10.1021/acsabm.9b00450.
- [150] D. Juriga, K. Nagy, A. Jedlovszky-Hajdú, K. Perczel-Kovách, Y.M. Chen, G. Varga, M. Zrínyi, Biodegradation and Osteosarcoma Cell Cultivation on Poly(aspartic acid) Based Hydrogels, ACS Appl. Mater. Interfaces. 8 (2016) 23463–23476. https://doi.org/10.1021/acsami.6b06489.
- [151] T. Nakato, M. Yoshitake, K. Matsubara, M. Tomida, T. Kakuchi, Relationships between structure and properties of poly(aspartic acid)s, Macromolecules. 31 (1998) 2107–2113. https://doi.org/10.1021/ma971629y.
- [152] P. Mishra, R.K. Dey, Co-delivery of docetaxel and doxorubicin using biodegradable PEG-PLA micelles for treatment of breast cancer with synergistic anti-tumour effects, J. Macromol. Sci. Part A Pure Appl. Chem. 55 (2018) 310–316. https://doi.org/10.1080/10601325.2018.1426390.
- [153] P. Mishra, R.K. Dey, Development of docetaxel-loaded PEG–PLA nanoparticles using surfactant-free method for controlled release studies, Int. J. Polym. Mater. Polym. Biomater. 67 (2018) 535–542. https://doi.org/10.1080/00914037.2017.1354193.
- [154] K. Prusty, S.K. Swain, Release of ciprofloxacin drugs by nano gold embedded cellulose grafted polyacrylamide hybrid nanocomposite hydrogels, Int. J. Biol. Macromol. 126 (2019) 765–775. https://doi.org/10.1016/j.ijbiomac.2018.12.258.
- [155] K. Prusty, A. Biswal, S. Bhusan, S.K. Swain, Synthesis of soy protein / polyacrylamide nanocomposite hydrogels for delivery of ciprofloxacin drug, Mater. Chem. Phys. (2019). https://doi.org/10.1016/j.matchemphys.2019.05.038.
- [156] P.Y. and P.H. P. Sagunthala1, V. Veeravazhuthi2, GROWTH, CHARACTERISATION, ANTIMICROBIAL AND ANTICANCER ACTIVITIES OF L ALANINE ADDED NICKEL SULPHATE CRYSTALS, World J. Pharm. Res.

- 5 (2016) 414–425. https://doi.org/10.20959/wjpr20168-6738.
- [157] X. Zhu, K. Pathakoti, Green synthesis of titanium dioxide and zinc oxide nanoparticles and their usage for antimicrobial applications and environmental remediation, 2019. https://doi.org/10.1016/B978-0-08-102579-6.00010-1.
- [158] Z. Yu, W. Qin, J. Lin, S. Fang, J. Qiu, Antibacterial mechanisms of polymyxin and bacterial resistance, Biomed Res. Int. 2015 (2015). https://doi.org/10.1155/2015/679109.
- [159] W.W. UMBREIT, Mechanisms of antibacterial action, Pharmacol. Rev. 5 (1953) 275–284. https://doi.org/10.1146/annurev.mi.08.100154.001123.
- [160] N.G. Vasconcelos, J. Croda, S. Simionatto, Antibacterial mechanisms of cinnamon and its constituents: A review, Microb. Pathog. 120 (2018) 198–203. https://doi.org/10.1016/j.micpath.2018.04.036.
- [161] C.C. Homes, T. Vogt, Colossal permittivity materials: Doping for superior dielectrics, Nat. Mater. 12 (2013) 782–783. https://doi.org/10.1038/nmat3744.
- [162] X. Hao, A review on the dielectric materials for high energy-storage application, J. Adv. Dielectr. 03 (2013) 1330001. https://doi.org/10.1142/S2010135X13300016.
- [163] F.T. A. Deschanvres, B. Ravenau, Remplacement de metal bivalent par le cuivre dans les titanates de type perowskite, Bull. Chim. Soc.Fr. (1967) 4077–4078. https://doi.org/10.1016/j.ceramint.2019.07.166.
- [164] M. a. A. Subramanian, D. Li, N. Duan, B. a. A. Reisner, a. W.W. Sleight, High Dielectric Constant in ACu3Ti4O12 and ACu3Ti3FeO12 Phases, J. Solid State Chem. 151 (2000) 323–325. https://doi.org/10.1006/jssc.2000.8703.
- [165] C.C. Homes, T. Vogt, S.M. Shapiro, S. Wakimoto, A.P. Ramirez, Optical response of high-dielectric-constant perovskite-related oxide, Science (80-.). 293 (2001) 673–676. https://doi.org/10.1126/science.1061655.
- [166] P. Lunkenheimer, S. Krohns, S. Riegg, S.G. Ebbinghaus, A. Reller, A. Loidl, Colossal dielectric constants in transition-metal oxides, Eur. Phys. J. Spec. Top. 180 (2009) 61–89. https://doi.org/10.1140/epjst/e2010-01212-5.
- [167] P. Thomas, K. Dwarakanath, K.B.R. Varma, T.R.N. Kutty2*, Synthesis of the Giant Dielectric Constant Material CaCu 3 Ti 4 O 12 by Wet-Chemistry Methods †, Chem. Mater. 95 (2009) 267–272. https://doi.org/10.1021/cm0716553.
- [168] W. Si, E.M. Cruz, P.D. Johnson, P.W. Barnes, P. Woodward, A.P. Ramirez, Epitaxial thin films of the giant-dielectric-constant material CaCu 3Ti4O12 grown by pulsed-laser deposition, Appl. Phys. Lett. 81 (2002) 2056–2058. https://doi.org/10.1063/1.1506951.

- [169] L. Singh, U.S. Rai, K.D. Mandal, N.B. Singh, Progress in the growth of CaCu3Ti4O12and related functional dielectric perovskites, Prog. Cryst. Growth Charact. Mater. 60 (2014) 15–62. https://doi.org/10.1016/j.pcrysgrow.2014.04.001.
- [170] I.F. Chang, S.S. Mitra, J.N. Plendl, L.C. Mansur, Long-Wavelength Longitudinal Phonons of Multi-Mode Crystals, Phys. Status Solidi. 28 (1968) 663–673. https://doi.org/10.1002/pssb.19680280224.
- [171] R.G.Sa. R. H. LYDDANF, On the Polar Vibrations of Alkali Halides., Phys. Rev. 59 (1941) 673–676.
- [172] M.H. Wang, B. Zhang, F. Zhou, Preparation and characterization of silica-coated CaCu3Ti 4O12, J. Electron. Mater. 43 (2014) 2607–2613. https://doi.org/10.1007/s11664-014-3156-8.
- [173] L. He, J.B. Neaton, M.H. Cohen, D. Vanderbilt, C.C. Homes, First-principles study of the structure and lattice dielectric response of CaCu3Ti4O12, Phys. Rev. B. 65 (2002) 214112. https://doi.org/10.1103/PhysRevB.65.214112.
- [174] L. He, J.B. Neaton, D. Vanderbilt, M.H. Cohen, Lattice dielectric response of CdCu3Ti4O12 and CaCu3Ti4O12 from first principles, Phys. Rev. B Condens. Matter Mater. Phys. 67 (2003) 121031–121034. https://doi.org/10.1103/PhysRevB.67.012103.
- [175] C.C. Homes, T. Vogt, S.M. Shapiro, S. Wakimoto, M.A. Subramanian, A.P. Ramirez, Charge transfer in the high dielectric constant materials CaCu3Ti4O12 and CdCu3Ti4O12, Phys. Rev. B. 67 (2003) 092106. https://doi.org/10.1103/PhysRevB.67.092106.
- [176] D.C. Sinclair, T.B. Adams, F.D. Morrison, A.R. West, CaCu3Ti4O12: One-step internal barrier layer capacitor, Appl. Phys. Lett. 80 (2002) 2153–2155. https://doi.org/10.1063/1.1463211.
- [177] T. Adams, D. Sinclair, A. West, Giant barrier layer capacitance effects in CaCu 3 Ti 4 O 12 ceramics, Adv. Mater. 14 (2002) 1321–1323. https://doi.org/10.1002/1521-4095(20020916)14:18<1321::AID-ADMA1321>3.0.CO;2-P.
- [178] W. Hu, Y. Liu, R.L. Withers, T.J. Frankcombe, L. Norén, A. Snashall, M. Kitchin, P. Smith, B. Gong, H. Chen, J. Schiemer, F. Brink, J. Wong-Leung, Electron-pinned defect-dipoles for high-performance colossal permittivity materials, Nat. Mater. 12 (2013) 821–826. https://doi.org/10.1038/nmat3691.
- [179] M. Ahmadipour, M.F. Ain, Z.A. Ahmad, A Short Review on Copper Calcium Titanate (CCTO) Electroceramic: Synthesis, Dielectric Properties, Film Deposition, and Sensing Application, Nano-Micro Lett. 8 (2016) 291–311. https://doi.org/10.1007/s40820-016-0089-1.
- [180] H.J. Chen, Y.W. Chen, Hydrothermal synthesis of barium titanate, Ind. Eng. Chem.

- Res. 42 (2003) 473-483. https://doi.org/10.1021/ie010796q.
- [181] S.P. More, R.J. Topare, The review of various synthesis methods of barium titanate with the enhanced dielectric properties, AIP Conf. Proc. 1728 (2016) 1–7. https://doi.org/10.1063/1.4946611.
- [182] M.C. de Andrade, G.N. Carneiro, E.L. Moreira, J.C. Araújo, V.C.A. Moraes, Synthesis and characterization of barium titanate by solid-state reaction, Mater. Sci. Forum. 802 (2014) 285–290. https://doi.org/10.4028/www.scientific.net/MSF.802.285.
- [183] B. Jiang, J. Iocozzia, L. Zhao, H. Zhang, Y.W. Harn, Y. Chen, Z. Lin, Barium titanate at the nanoscale: Controlled synthesis and dielectric and ferroelectric properties, Chem. Soc. Rev. 48 (2019) 1194–1228. https://doi.org/10.1039/c8cs00583d.
- [184] Z. Nurbaya, M. Rusop, Dielectric property of lead titanate thin films prepared on glass substrate at low temperature, Proc. RSM 2013 2013 IEEE Reg. Symp. Micro Nano Electron. (2013) 197–199. https://doi.org/10.1109/RSM.2013.6706507.
- [185] M. Kumari, A. Singh, J. Mandal, Structural and Dielectric Properties of PZT Ceramics Prepared by Solid-state Reaction Route, Internatinal J. Sci. Eng. Res. 5 (2014) 404– 406.
- [186] V.A. Chaudhari, G.K. Bichile, Synthesis, Structural, and Electrical Properties of Pure PbTiO 3 Ferroelectric Ceramics, Smart Mater. Res. 2013 (2013) 1–9. https://doi.org/10.1155/2013/147524.
- [187] W. Stober, A. Fink, Controlled Growth of Monodispersed Silica Spheres in the Micron Size Range, J. Colloid Interface Sci. 26 (1968) 62–69.
- [188] W. Volksen, R.D. Miller, G. Dubois, Low Dielectric Constant Materials, Chem. Rev. 110 (2010) 56–110.
- [189] L. Esposito, G. Ottaviani, E. Carollo, M. Bacchetta, Thermal stability of low dielectric constant porous silica films, Appl. Phys. Lett. 87 (2005) 1–3. https://doi.org/10.1063/1.2159093.
- [190] P. Article, The rise of graphene, Nat. Mater. 6 (2007) 183–191. https://doi.org/10.1038/nmat1849.
- [191] Y. Kopelevich, P. Esquinazi, Graphene Physics in Graphite, Adv. Mater. 19 (2007) 4559–4563. https://doi.org/10.1002/adma.200702051.
- [192] F. Bonaccorso, Z. Sun, T. Hasan, A.C. Ferrari, Graphene photonics and optoelectronics, Nat. Photonics. 4 (2010) 611–622. https://doi.org/10.1038/nphoton.2010.186.
- [193] S. Stankovich, D.A. Dikin, G.H.B. Dommett, K.M. Kohlhaas, E.J. Zimney, E.A. Stach, R.D. Piner, S.B.T. Nguyen, R.S. Ruoff, Graphene-based composite materials,

- Nature. 442 (2006) 282–286. https://doi.org/10.1038/nature04969.
- [194] C. Lee, X. Wei, J.W. Kysar, J. Hone, Measurement of the elastic properties and intrinsic strength of monolayer graphene, Science (80-.). 321 (2008) 385–388. https://doi.org/10.1126/science.1157996.
- [195] R. Zeng, Z. Luo, L. Zhang, D. Tang, Platinum Nanozyme-Catalyzed Gas Generation for Pressure-Based Bioassay Using Polyaniline Nanowires-Functionalized Graphene Oxide Framework, Anal. Chem. 90 (2018) 12299–12306. https://doi.org/10.1021/acs.analchem.8b03889.
- [196] J. Shu, Z. Qiu, D. Tang, Self-Referenced Smartphone Imaging for Visual Screening of H2S Using CuxO-Polypyrrole Conductive Aerogel Doped with Graphene Oxide Framework, Anal. Chem. 90 (2018) 9691–9694. https://doi.org/10.1021/acs.analchem.8b03011.
- [197] G. Cai, Z. Yu, R. Ren, D. Tang, Exciton-Plasmon Interaction between AuNPs/Graphene Nanohybrids and CdS Quantum Dots/TiO2 for Photoelectrochemical Aptasensing of Prostate-Specific Antigen, ACS Sensors. 3 (2018) 632–639. https://doi.org/10.1021/acssensors.7b00899.
- [198] J.S. Bunch, S.S. Verbridge, J.S. Alden, A.M. Van Der Zande, J.M. Parpia, H.G. Craighead, P.L. McEuen, Impermeable atomic membranes from graphene sheets, Nano Lett. 8 (2008) 2458–2462. https://doi.org/10.1021/nl801457b.
- [199] D.R. Dreyer, S. Park, C.W. Bielawski, R.S. Ruoff, The chemistry of graphene oxide, Chem. Soc. Rev. 39 (2010) 228–240. https://doi.org/10.1039/b917103g.
- [200] C. Berger, Z. Song, X. Li, X. Wu, N. Brown, C. Naud, D. Mayou, T. Li, J. Hass, A.N. Marchenkov, E.H. Conrad, P.N. First, W.A. De Heer, Electronic confinement and coherence in patterned epitaxial graphene, Science (80-.). 312 (2006) 1191–1196. https://doi.org/10.1126/science.1125925.
- [201] H. Chen, M.B. Müller, K.J. Gilmore, G.G. Wallace, D. Li, Mechanically strong, electrically conductive, and biocompatible graphene paper, Adv. Mater. 20 (2008) 3557–3561. https://doi.org/10.1002/adma.200800757.
- [202] T.K. Gupta, B.P. Singh, V.N. Singh, S. Teotia, A.P. Singh, I. Elizabeth, S.R. Dhakate, S.K. Dhawan, R.B. Mathur, MnO2 decorated graphene nanoribbons with superior permittivity and excellent microwave shielding properties, J. Mater. Chem. A. 2 (2014) 4256. https://doi.org/10.1039/c3ta14854h.
- [203] R.K. Singh, R. Kumar, D.P. Singh, Graphene oxide: Strategies for synthesis, reduction and frontier applications, RSC Adv. 6 (2016) 64993–65011. https://doi.org/10.1039/c6ra07626b.
- [204] P.B. Arthi G, L. BD, A Simple Approach to Stepwise Synthesis of Graphene Oxide Nanomaterial, J. Nanomed. Nanotechnol. 06 (2015) 1–4. https://doi.org/10.4172/2157-

- 7439.1000253.
- [205] H. Yu, B. Zhang, C. Bulin, R. Li, R. Xing, High-efficient Synthesis of Graphene Oxide Based on Improved Hummers Method, Sci. Rep. 6 (2016) 1–7. https://doi.org/10.1038/srep36143.
- [206] V. Sharma, Y. Jain, M. Kumari, R. Gupta, S.K. Sharma, K. Sachdev, Synthesis and Characterization of Graphene Oxide (GO) and Reduced Graphene Oxide (rGO) for Gas Sensing Application, Macromol. Symp. 376 (2017) 1–5. https://doi.org/10.1002/masy.201700006.
- [207] P. Ranjan, S. Agrawal, A. Sinha, T.R. Rao, J. Balakrishnan, A.D. Thakur, A Low-Cost Non-explosive Synthesis of Graphene Oxide for Scalable Applications, Sci. Rep. 8 (2018) 1–13. https://doi.org/10.1038/s41598-018-30613-4.
- [208] K.S. Kumar, S. Pittala, S. Sanyadanam, P. Paik, A new single/few-layered graphene oxide with a high dielectric constant of 10 6: contribution of defects and functional groups, RSC Adv. 5 (2015) 14768–14779. https://doi.org/10.1039/C4RA10800K.
- [209] W.L. Zhang, H.J. Choi, Silica-graphene oxide hybrid composite particles and their electroresponsive characteristics, Langmuir. 28 (2012) 7055–7062. https://doi.org/10.1021/la3009283.
- [210] S.D. Kim, W.L. Zhang, H.J. Choi, Y.P. Seo, Y. Seo, Electrorheological activity generation by graphene oxide coating on low-dielectric silica particles, RSC Adv. 4 (2014) 62644–62650. https://doi.org/10.1039/c4ra13357a.
- [211] S. Song, Y. Zhai, Y. Zhang, Bioinspired Graphene Oxide/Polymer Nanocomposite Paper with High Strength, Toughness, and Dielectric Constant, ACS Appl. Mater. Interfaces. 8 (2016) 31264–31272. https://doi.org/10.1021/acsami.6b08606.
- [212] J.H. Kang, T. Kim, J. Choi, J. Park, Y.S. Kim, M.S. Chang, H. Jung, K.T. Park, S.J. Yang, C.R. Park, Hidden Second Oxidation Step of Hummers Method, Chem. Mater. 28 (2016) 756–764. https://doi.org/10.1021/acs.chemmater.5b03700.
- [213] H. He, J. Klinowski, M. Forster, A. Lerf, A new structural model for graphite oxide, Chem. Phys. Lett. 287 (1998) 53–56. https://doi.org/10.1016/S0009-2614(98)00144-4.
- [214] T. Miyazaki, K. Igarashi, Y. Matsumoto, H. Cabral, One-Pot Synthesis of PEG–Poly(amino acid) Block Copolymers Assembling Polymeric Micelles with PEG-Detachable Functionality, ACS Biomater. Sci. Eng. (2019). https://doi.org/10.1021/acsbiomaterials.8b01549.
- [215] V. Ladmiral, A. Charlot, M. Semsarilar, S.P. Armes, Synthesis and characterization of poly(amino acid methacrylate)-stabilized diblock copolymer nano-objects, Polym. Chem. 6 (2015) 1805–1816. https://doi.org/10.1039/c4py01556h.
- [216] S. Kumar, R. Acharya, U. Chatterji, P. De, Side-chain amino-acid-based ph-responsive

- self-assembled block copolymers for drug delivery and gene transfer, Langmuir. 29 (2013) 15375–15385. https://doi.org/10.1021/la403819g.
- [217] M. Levit, N. Zashikhina, A. Vdovchenko, A. Dobrodumov, T. Scheper, T. Tennikova, E. Korzhikova-vlakh, Bio-Inspired Amphiphilic Block-Copolymers Based, (n.d.).
- [218] Y. Liang, W. Ouyang, P. Wang, W. Zhang, S. Wang, L. Tian, Y. Ju, G. Li, Block copolymer assisted topochemical polymerization: A facile and efficient route to robust polymeric nanoporous membranes decorated with versatile amino acids, Chinese Chem. Lett. (2019). https://doi.org/10.1016/j.cclet.2019.07.035.
- [219] K. Osada, R.J. Christie, K. Kataoka, Polymeric micelles from poly(ethylene glycol)-poly(amino acid) block copolymer for drug and gene delivery, J. R. Soc. Interface. 6 (2009). https://doi.org/10.1098/rsif.2008.0547.focus.
- [220] A. Ponta, Y. Bae, PEG-poly(amino acid) block copolymer micelles for tunable drug release, Pharm. Res. 27 (2010) 2330–2342. https://doi.org/10.1007/s11095-010-0120-z.
- [221] C.J. Hawkins, P.J. Lawson, Circular dichroism spectra of amino acid complexes. Carboxylatopentaamminecobalt(III) compounds, Inorg. Chem. 9 (1970) 6–11. https://doi.org/10.1021/ic50083a002.
- [222] K. Bauri, S.G. Roy, S. Pant, P. De, Controlled synthesis of amino acid-based pH-responsive chiral polymers and self-assembly of their block copolymers, Langmuir. 29 (2013) 2764–2774. https://doi.org/10.1021/la304918s.
- [223] M.P. Bevilacqua, D.J. Huang, B.D. Wall, S.J. Lane, C.K. Edwards, J.A. Hanson, D. Benitez, J.S. Solomkin, T.J. Deming, Amino Acid Block Copolymers with Broad Antimicrobial Activity and Barrier Properties, Macromol. Biosci. 17 (2017) 1–9. https://doi.org/10.1002/mabi.201600492.
- [224] J. Szczeblinska, K. Fijalkowski, J. Kohn, M. El Fray, Antibiotic loaded microspheres as antimicrobial delivery systems for medical applications, Mater. Sci. Eng. C. 77 (2017) 69–75. https://doi.org/10.1016/j.msec.2017.03.215.
- [225] I. Mukherjee, A. Ghosh, P. Bhadury, P. De, Side-Chain Amino Acid-Based Cationic Antibacterial Polymers: Investigating the Morphological Switching of a Polymer-Treated Bacterial Cell, ACS Omega. 2 (2017) 1633–1644. https://doi.org/10.1021/acsomega.7b00181.
- [226] R.P. Gandhiraman, C. Volcke, V. Gubala, C. Doyle, L. Basabe-Desmonts, C. Dotzler, M.F. Toney, M. Iacono, R.I. Nooney, S. Daniels, B. James, D.E. Williams, High efficiency amine functionalization of cycloolefin polymer surfaces for biodiagnostics, J. Mater. Chem. 20 (2010) 4116–4127. https://doi.org/10.1039/b925737c.
- [227] S. Lv, M. Li, Z. Tang, W. Song, H. Sun, H. Liu, X. Chen, Doxorubicin-loaded amphiphilic polypeptide-based nanoparticles as an efficient drug delivery system for

- cancer therapy, Acta Biomater. 9 (2013) 9330–9342. https://doi.org/10.1016/j.actbio.2013.08.015.
- [228] G. Zhu, F. Wang, K. Xu, S. Dong, Y. Liu, Properties study of poly(l-lactic acid)/poly(γ-benzyl l-glutamate)-graft-poly(ethylene glycol) blend film, Res. Chem. Intermed. 41 (2015) 1097–1106. https://doi.org/10.1007/s11164-013-1256-3.
- [229] I.C. Reynhout, J.J.L.M. Cornelissen, R.J.M. Nolte, Self-assembled architectures from biohybrid triblock copolymers, J. Am. Chem. Soc. 129 (2007) 2327–2332. https://doi.org/10.1021/ja066790f.
- [230] S.W. Kang, Y. Li, J.H. Park, D.S. Lee, PH-triggered unimer/vesicle-transformable and biodegradable polymersomes based on PEG-b-PCL-grafted poly(β-amino ester) for anti-cancer drug delivery, Polymer (Guildf). 54 (2013) 102–110. https://doi.org/10.1016/j.polymer.2012.10.055.
- [231] X.R. Shao, X.Q. Wei, X. Song, L.Y. Hao, X.X. Cai, Z.R. Zhang, Q. Peng, Y.F. Lin, Independent effect of polymeric nanoparticle zeta potential/surface charge, on their cytotoxicity and affinity to cells, Cell Prolif. 48 (2015) 465–474. https://doi.org/10.1111/cpr.12192.
- [232] Y. Yang, H. Sun, D. Yin, Z. Lu, J. Wei, R. Xiong, J. Shi, Z. Wang, Z. Liu, Q. Lei, High performance of polyimide/CaCu3Ti4O12@Ag hybrid films with enhanced dielectric permittivity and low dielectric loss, J. Mater. Chem. A. 3 (2015) 4916–4921. https://doi.org/10.1039/c4ta05673f.
- [233] P. Barber, S. Balasubramanian, Y. Anguchamy, S. Gong, A. Wibowo, H. Gao, H.J. Ploehn, H.C. Zur Loye, Polymer composite and nanocomposite dielectric materials for pulse power energy storage, 2009. https://doi.org/10.3390/ma2041697.
- [234] M.S.D. Satia, M. Jaafar, Properties of treated calcium copper titanate filled epoxy thin film composites for electronic applications, J. Appl. Polym. Sci. 133 (2016). https://doi.org/10.1002/app.43313.
- [235] X. Wang, S. Yan, L. Song, H. Shi, H. Yang, S. Luan, Y. Huang, J. Yin, A.F. Khan, J. Zhao, Temperature-Responsive Hierarchical Polymer Brushes Switching from Bactericidal to Cell Repellency, ACS Appl. Mater. Interfaces. 9 (2017) 40930–40939. https://doi.org/10.1021/acsami.7b09968.
- [236] Y. Yang, J. Cai, X. Zhuang, Z. Guo, X. Jing, X. Chen, PH-dependent self-assembly of amphiphilic poly(l-glutamic acid)-block-poly(lactic-co-glycolic acid) copolymers, Polymer (Guildf). 51 (2010) 2676–2682. https://doi.org/10.1016/j.polymer.2010.04.008.
- [237] H. Xu, P. Yang, H. Ma, W. Yin, X. Wu, H. Wang, D. Xu, X. Zhang, Amphiphilic block copolymers-based mixed micelles for noninvasive drug delivery, Drug Deliv. 23 (2016) 3063–3071. https://doi.org/10.3109/10717544.2016.1149743.

- [238] C. Amgoth, G. Dharmapuri, A.M. Kalle, P. Paik, Nanoporous capsules of block copolymers of [(MeO-PEG-NH)-b-(L-GluA)]-PCL for the controlled release of anticancer drugs for therapeutic applications, Nanotechnology. 27 (2016) 0. https://doi.org/10.1088/0957-4484/27/12/125101.
- [239] D. Priftis, L. Leon, Z. Song, S.L. Perry, K.O. Margossian, A. Tropnikova, J. Cheng, M. Tirrell, Self-Assembly of??-Helical Polypeptides Driven by Complex Coacervation, Angew. Chemie Int. Ed. 54 (2015) 11128–11132. https://doi.org/10.1002/anie.201504861.
- [240] A. Basu, K.R. Kunduru, J. Katzhendler, A.J. Domb, Poly(α-hydroxy acid)s and poly(α-hydroxy acid-co-α-amino acid)s derived from amino acid, Adv. Drug Deliv. Rev. 107 (2016) 82–96. https://doi.org/10.1016/j.addr.2016.08.003.
- [241] P. Paik, A. Gedanken, Y. Mastai, Enantioselective separation using chiral mesoporous spherical silica prepared by templating of chiral block copolymers, ACS Appl. Mater. Interfaces. 1 (2009) 1834–1842. https://doi.org/10.1021/am9003842.
- [242] Z. Zhou, B. Chu, V.M. Nace, Y.W. Yang, C. Booth, Self-assembly characteristics of BEB-type triblock copolymers, Macromolecules. 29 (1996) 3663–3664. https://doi.org/10.1021/ma960033s.
- [243] I.J. Oh, J.Y. Oh, C.S. Cho, K.C. Lee, Biodegradability of Poly (y-benzyl L-glutamate)/ poly (ethylene oxide) / poly (y-benzyl L-glutamate) Block Copolymer in Mice, Arch. Pharm.Res. 18 (1995) 8–11.
- [244] S.H. Hua, Y.Y. Li, Y. Liu, W. Xiao, C. Li, F.W. Huang, X.Z. Zhang, R.X. Zhuo, Self-assembled micelles based on PEG-polypeptide hybrid copolymers for drug delivery, Macromol. Rapid Commun. 31 (2010) 81–86. https://doi.org/10.1002/marc.200900473.
- [245] A.K. Yamala, V. Nadella, Y. Mastai, H. Prakash, P. Paik, Poly-: N -acryloyl-(l-phenylalanine methyl ester) hollow core nanocapsules facilitate sustained delivery of immunomodulatory drugs and exhibit adjuvant properties, Nanoscale. 9 (2017) 14006–14014. https://doi.org/10.1039/c7nr03724d.
- [246] A. Böker, A.H.E. Müller, G. Krausch, Nanoscopic surface patterns from functional ABC triblock copolymers, Macromolecules. 34 (2001) 7477–7488. https://doi.org/10.1021/ma002198d.
- [247] V. Balsamo, G. Gil, C.U. De Navarro, I.W. Hamley, F. Von Gyldenfeldt, V. Abetz, E. Canizales, Morphological behavior of thermally treated polystyrene-b-polybutadiene-b-poly(ε-caprolactone) ABC triblock copolymers, Macromolecules. 36 (2003) 4515–4525. https://doi.org/10.1021/ma020129o.
- [248] A. Ricci, M. Chiarini, C. Lo Sterzo, R. Pizzoferrato, S. Paoloni, Synthesis and photophysical properties of poly(arylene ethynylene) small-molecules and polymers

- derivatized with leucine substituents, J. Photochem. Photobiol. A Chem. 298 (2014) 1–8. https://doi.org/10.1016/j.jphotochem.2014.10.003.
- [249] R. Chen, J.E. Wulff, M.G. Moffitt, Microfluidic Processing Approach to Controlling Drug Delivery Properties of Curcumin-Loaded Block Copolymer Nanoparticles, Mol. Pharm. 15 (2018) 4517–4528. https://doi.org/10.1021/acs.molpharmaceut.8b00529.
- [250] C.V. Ramana, K. Malkappa, B.N. Rao, T. Jana, G. Suresh, Organic/inorganic hybrid nanocolloids of water dispersible polyurethanes with antibacterial activity, Colloid Polym. Sci. 296 (2017) 95–106. https://doi.org/10.1007/s00396-017-4229-z.
- [251] H.D.M. Follmann, I. Messias, M.N. Queiroz, R.A. Araujo, A.F. Rubira, R. Silva, Designing hybrid materials with multifunctional interfaces for wound dressing, electrocatalysis, and chemical separation, J. Colloid Interface Sci. 533 (2019) 106–125. https://doi.org/10.1016/j.jcis.2018.08.007.
- [252] E.R. Gillies, J.M.J. Fréchet, A new approach towards acid sensitive copolymer micelles for drug delivery, Chem. Commun. 3 (2003) 1640–1641. https://doi.org/10.1039/b304251k.
- [253] S. Abbasi, G. Yousefi, A.M. Tamaddon, Polyacrylamide–b-copolypeptide hybrid copolymer as pH-responsive carrier for delivery of paclitaxel: Effects of copolymer composition on nano micelles properties, loading efficiency and hemocompatibility, Colloids Surfaces A Physicochem. Eng. Asp. 537 (2018) 217–226. https://doi.org/10.1016/j.colsurfa.2017.09.007.
- [254] J. Araújo, C. Fernandes, M. Pinto, M. Elizabeth Tiritan, Chiral derivatives of xanthones with antimicrobial activity, Molecules. 24 (2019). https://doi.org/10.3390/molecules24020314.
- [255] L. Geng, Q. Liu, Q. Fang, J.R. Gong, Q. Xin, Chiral Nanoparticle as a New Efficient Antimicrobial Nanoagent, Adv. Healthc. Mater. 6 (2016) 1601011. https://doi.org/10.1002/adhm.201601011.
- [256] P. Paik, A. Gedanken, Y. Mastai, Chiral-mesoporous-polypyrrole nanoparticles: Its chiral recognition abilities and use in enantioselective separation, J. Mater. Chem. 20 (2010) 4085–4093. https://doi.org/10.1039/c000232a.
- [257] H. Qiu, Z. Yang, M.I. Shah, Z. Mao, J. Ling, [PCL-b-P(THF-co-CL)]m multiblock copolymer synthesized by Janus polymerization, Polymer (Guildf). 128 (2017) 71–77. https://doi.org/10.1016/j.polymer.2017.08.040.
- [258] Y. Li, S. Wang, D. Zhu, Y. Shen, B. Du, X. Liu, Y. Zheng, Reversibly cross-linked poly(ethylene glycol)-poly(amino acid)s copolymer micelles: A promising approach to overcome the extracellular stability versus intracellular drug release challenge, RSC Adv. 5 (2015) 20025–20034. https://doi.org/10.1039/c4ra12255k.
- [259] T. Tay, E. Köse, R. Keçili, R. Say, Design and preparation of nano-lignin peroxidase

- (NanoLiP) by protein block copolymerization approach, Polymers (Basel). 8 (2016). https://doi.org/10.3390/polym8060223.
- [260] B. Kalita, B. Gogoi, N. Sen Sarma, Cholesterol-amino acid conjugates treated filter paper-based photoluminescence indicator for nitroaromatic chemicals, Mater. Res. Bull. 115 (2019) 211–218. https://doi.org/10.1016/j.materresbull.2019.03.025.
- [261] R.N.S. Disna P. Samarakoon, Nirmal Govindaraju, CALCIUM COPPER TITANATE BASED HIGH DIELECTRIC CONSTANT MATERIALS FOR ENERGY STORAGE APPLICATIONS, SMEHATRC. (1392) 131–140.
- [262] P. Samanta, A comprehensive technique for estimation of process-induced fixed charges and effective work function of the metal gate on high-SiO2 stack, Semicond. Sci. Technol. 34 (2019) 115008. https://doi.org/10.1088/1361-6641/ab4375.
- [263] D. Grebinişan, M.N. Holban, C. Lionte, C. Peptu, V. Şunel, M. Popa, J. Desbrieres, Drug-Polymer Conjugates with Tuberculostatic Activity, Based on Poly (N-Vinyl Pyrrolidone-alt-Itaconic Anhydride) and Novel Amino acid Hydrazides, Polym. Plast. Technol. Eng. 52 (2013) 1213–1219. https://doi.org/10.1080/03602559.2013.798824.
- [264] E. Pellizzoni, M. Tommasini, E. Marangon, F. Rizzolio, G. Saito, F. Benedetti, G. Toffoli, M. Resmini, F. Berti, Fluorescent molecularly imprinted nanogels for the detection of anticancer drugs in human plasma, Biosens. Bioelectron. 86 (2016) 913–919. https://doi.org/10.1016/j.bios.2016.07.087.
- [265] Sharma YR, Elementary Spectroscopy, 2010
- [266] H. Gleiter, H. Hahn, T. Schimmel, Advances in nanomaterials, 2013. https://doi.org/10.3762/bjnano.4.91.
- [267] R.K. Jammula, S. Pittala, S. Srinath, V.V.S.S. Srikanth, Strong interfacial polarization in ZnO decorated reduced-graphene oxide synthesized by molecular level mixing, Phys. Chem. Chem. Phys. 17 (2015) 17237–17245. https://doi.org/10.1039/c5cp02196k.
- [268] A.P. Ramirez, M.A. Subramanian, M. Gardel, G. Blumberg, D. Li, T. Vogt, S.M. Shapiro, Giant dielectric constant response in a copper-titanate, Solid State Commun. 115 (2000) 217–220. https://doi.org/10.1016/S0038-1098(00)00182-4.
- [269] T. Abdel-Baset, M. Elzayat, S.Mahrous, Characterization and Optical and Dielectric Properties of Polyvinyl Chloride / Silica Nanocomposites Films, Int. J. Polym. Sci. 2016 (2016) 13. https://doi.org/10.1155/2016/1707018.
- [270] S.-Y. Chung, I.-D. Kim, S.-J.L. Kang, Strong nonlinear current-voltage behaviour in perovskite-derivative calcium copper titanate., Nat. Mater. 3 (2004) 774–778. https://doi.org/10.1038/nmat1238.

- [271] W.L. and Y.J. Chao Xie, Fei Liang *, Min Ma, Xizi Chen, School, Microstructure and Dielectric Properties of PTFE-Based Composites Filled by Micron/Submicron-Blended CCTO, Crystals. 7 (2017) 126. https://doi.org/10.3390/cryst7050126.
- [272] C. Ehrhardt, C. Fettkenhauer, J. Glenneberg, W. Münchgesang, H.S. Leipner, M. Diestelhorst, S. Lemm, H. Beige, S.G. Ebbinghaus, A solution-based approach to composite dielectric films of surface functionalized CaCu 3 Ti 4 O 12 and P(VDF-HFP), J. Mater. Chem. A. 2 (2014) 2266–2274. https://doi.org/10.1039/C3TA14379A.
- [273] J. Mohammed, T.T. Carol T., H.Y. Hafeez, B.I. Adamu, Y.S. Wudil, Z.I. Takai, S.K. Godara, A.K. Srivastava, Tuning the dielectric and optical properties of Pr–Co–substituted calcium copper titanate for electronics applications, J. Phys. Chem. Solids. 126 (2019) 85–92. https://doi.org/10.1016/j.jpcs.2018.09.034.
- [274] F. Branda, B. Silvestri, G. Luciani, A. Costantini, F. Tescione, Synthesis structure and stability of amino functionalized PEGylated silica nanoparticles, Colloids Surfaces A Physicochem. Eng. Asp. 367 (2010) 12–16. https://doi.org/10.1016/j.colsurfa.2010.05.036.
- [275] T. Kawasaki, Y. Araki, K. Hatase, K. Suzuki, A. Matsumoto, T. Yokoi, Y. Kubota, T. Tatsumi, K. Soai, Helical mesoporous silica as an inorganic heterogeneous chiral trigger for asymmetric autocatalysis with amplification of enantiomeric excess, Chem. Commun. 51 (2015) 8742–8744. https://doi.org/10.1039/c5cc01750e.
- [276] S. Jesurani, S. Kanagesan, R. Velmurugan, T. Kalaivani, Phase formation and high dielectric constant of calcium copper titanate using sol-gel route, J. Mater. Sci. Mater. Electron. 23 (2012) 668–674. https://doi.org/10.1007/s10854-011-0468-9.
- [277] F. Amaral, M. Valente, L.C. Costa, Synthesis and characterization of calcium copper titanate obtained by ethylenediaminetetraacetic acid gel combustion, Mater. Chem. Phys. 124 (2010) 580–586. https://doi.org/10.1016/j.matchemphys.2010.07.016.
- [278] N. Kolev, R.P. Bontchev, A.J. Jacobson, V.N. Popov, V.G. Hadjiev, A.P. Litvinchuk, M.N. Iliev, Raman spectroscopy of CaCu 3 Ti 4 O 12, Phys. Rev. B. 66 (2002) 132102. https://doi.org/10.1103/PhysRevB.66.132102.
- [279] R. j H. kathleen j kingma, Raman spectroscopic study of microcrystalline silica, Am. Mineral. 79 (1994) 269–273.
- [280] M. Hass, Raman spectra of vitreous silica, germania and sodium silicate glasses, J. Phys. Chem. Solids. 31 (1970) 415–422. https://doi.org/10.1016/0022-3697(70)90081-8.
- [281] P.G. Puranik, K.V. Ramiah, Raman and infra-red spectra of amines, Proc. Indian Acad. Sci. Sect. A. 54 (1961) 146–154. https://doi.org/10.1007/bf03048974.
- [282] V.G. Gavrilyachenko, Y. V. Kabirov, E.M. Panchenko, E.I. Sitalo, T. V. Gavrilyachenko, E. V. Milov, N. V. Lyanguzov, Specific features of the dielectric

- spectrum of CaCu3Ti4O12 in the low-frequency range, Phys. Solid State. 55 (2013) 1651–1654. https://doi.org/10.1134/S1063783413080131.
- [283] J. Li, A.W. Sleight, M.A. Subramanian, Evidence for internal resistive barriers in a crystal of the giant dielectric constant material: CaCu3Ti4O12, Solid State Commun. 135 (2005) 260–262. https://doi.org/10.1016/j.ssc.2005.04.028.
- [284] M.-H. Wang, X.-Y. Ma, B. Zhang, F. Zhou, Effects of Carbon Coating on Microstructure and Dielectric Properties of CaCu3Ti4O12, J. Electron. Mater. 43 (2014) 4322–4326. https://doi.org/10.1007/s11664-014-3337-5.
- [285] Z.M. Dang, T. Zhou, S.H. Yao, J.K. Yuan, J.W. Zha, H.T. Song, J.Y. Li, Q. Chen, W.T. Yang, J. Bai, Advanced calcium copper titanate/polyimide functional hybrid films with high dielectric permittivity, Adv. Mater. 21 (2009) 2077–2082. https://doi.org/10.1002/adma.200803427.
- [286] V.S. Saji, H.C. Choe, Chemical solution deposition of CaCu3Ti4O12 thin film, Bull. Mater. Sci. 33 (2010) 203–207. https://doi.org/10.1007/s12034-010-0031-y.
- [287] A.K.& D.K. Sarita Sharma1, CAVITY PERTURBATION MEASUREMENT OF COMPLEX PERMITTIVITY OF DIELCTRIC MATERIAL AT MICROWAVE FREQUENCIES, Int. J. Emerg. Technol. Comput. Appl. Sci. 4 (2013) 116–120. https://doi.org/10.1134/S1063783413080131.
- [288] A. Reyes-Montero, P. Ramos-Alvarez, A. González, R. López-Juárez, M. Villafuerte-Castrejón, Dielectric and Impedance Analysis on the Electrical Response of Lead-Free Ba1–xCaxTi0.9Zr0.1O3 Ceramics at High Temperature Range, Appl. Sci. 7 (2017) 214. https://doi.org/10.3390/app7030214.
- [289] M. Rahmani, O. Mirzaee, M. Tajally, M.R. Loghman-Estarki, Comparison of synthesis and spark plasma sintering of YAG nano particles by variation of pH and precipitator agent, Ceram. Int. 44 (2018) 23215–23225. https://doi.org/10.1016/j.ceramint.2018.07.130.
- [290] S. Hajra, K. Mohanta, M. Sahu, V. Purohit, R.N.P. Choudhary, Studies of structural, dielectric and impedance spectroscopy of fused silica ceramics fabricated through colloidal processing, Appl. Phys. A Mater. Sci. Process. 125 (2019) 1–7. https://doi.org/10.1007/s00339-019-2671-0.
- [291] C. Qian, T. Zhu, W. Zheng, R. Bei, S. Liu, D. Yu, Z. Chi, Y. Zhang, J. Xu, Improving Dielectric Properties and Thermostability of CaCu 3 Ti 4 O 12 /Polyimide Composites by Employing Surface Hydroxylated CaCu 3 Ti 4 O 12 Particles, ACS Appl. Polym. Mater. (2019). https://doi.org/10.1021/acsapm.9b00010.
- [292] L.W. LIANG Fei, ZHAO Yifei, CHEN Xizi, WAN Qianxing, Dielectric properties of polytetrafluoroethylene/CaCu3 Ti4O12 Composites, J. Wuhan Univ. Technol. Sci. Ed. 34 (2019) 189–194. https://doi.org/10.1109/ceidp.1966.7725198.

- [293] L. Zhang, X. Shan, P. Wu, Z.Y. Cheng, Dielectric characteristics of CaCu3Ti4O12/P(VDF-TrFE) nanocomposites, Appl. Phys. A Mater. Sci. Process. 107 (2012) 597–602. https://doi.org/10.1007/s00339-012-6836-3.
- [294] P. Mao, J. Wang, S. Liu, L. Zhang, Y. Zhao, K. Wu, Z. Wang, J. Li, Improved dielectric and nonlinear properties of CaCu3Ti4O12 ceramics with Cu-rich phase at grain boundary layers, Ceram. Int. (2019) https://doi.org/10.1016/j.ceramint.2019.04.247. https://doi.org/10.1016/j.ceramint.2019.04.247.
- [295] S. Bykkam, K. Rao, Synthesis and characterization of graphene oxide and its antimicrobial activity against Klebsiella and Staphylococus, Int. J. Adv. Biotechnol. Res. 4 (2013) 142–146. https://doi.org/10.1016/j.apcata.2015.10.042.
- [296] N.R. Wilson, N.R. Wilson, P.A. Pandey, P.A. Pandey, R. Beanland, R. Beanland, R.J. Young, R.J. Young, I. a Kinloch, I. a Kinloch, L. Gong, L. Gong, Z. Liu, Z. Liu, K. Suenaga, K. Suenaga, J.P. Rourke, J.P. Rourke, S.J. York, S.J. York, J. Sloan, J. Sloan, Graphene oxide: structural analysis and application as a highly transparent support for electron microscopy, ACS Nano. 3 (2009) 2547–2556. https://doi.org/10.1021/nn900694t.
- [297] X. Pu, H.-B. Zhang, X. Li, C. Gui, Z.-Z. Yu, Thermally conductive and electrically insulating epoxy nanocomposites with silica-coated graphene, RSC Adv. 4 (2014) 15297–15303. https://doi.org/10.1039/C4RA00518J.
- [298] P. Bhawal, S. Ganguly, T.K. Chaki, N.C. Das, Synthesis and characterization of graphene oxide filled ethylene methyl acrylate hybrid nanocomposites, RSC Adv. 6 (2016) 20781–20790. https://doi.org/10.1039/C5RA24914G.
- [299] J. Song, X. Wang, C.-T. Chang, J. Song, X. Wang, C.-T. Chang, Preparation and Characterization of Graphene Oxide, J. Nanomater. 2014 (2014) 1–6. https://doi.org/10.1155/2014/276143.
- [300] K.N. Kudin, B. Ozbas, H.C. Schniepp, R.K. Prud'homme, I.A. Aksay, R. Car, Raman spectra of graphite oxide and functionalized graphene sheets, Nano Lett. 8 (2008) 36–41. https://doi.org/10.1021/nl071822y.
- [301] Y. Xu, Y. Feng, X. Li, G. Hu, Y. Luo, L. Sun, T. Tang, J. Wen, H. Wang, M. Li, Direct formation of reduced graphene oxide and graphene quantum dot composites by using ascorbic acid as high-performance binder-free supercapacitor electrodes, Int. J. Electrochem. Sci. 12 (2017) 8820–8831. https://doi.org/10.20964/2017.09.08.
- [302] Y. Miroshnikov, G. Grinbom, G. Gershinsky, G.D. Nessim, D. Zitoun, Do we need covalent bonding of Si nanoparticles on graphene oxide for Li-ion batteries?, Faraday Discuss. 173 (2014) 391–402. https://doi.org/10.1039/C4FD00089G.
- [303] A.M. Dimiev, J.M. Tour, Mechanism of graphene oxide formation, ACS Nano. 8

- (2014) 3060–3068. https://doi.org/10.1021/nn500606a.
- [304] B. Schwenzer, T.C. Kaspar, Y. Shin, D.W. Gotthold, Spectroscopic Study of Graphene Oxide Membranes Exposed to Ultraviolet Light, J. Phys. Chem. C. 120 (2016) 12559–12567. https://doi.org/10.1021/acs.jpcc.6b03033.
- [305] E.E. Havinga, the Temperature Dependence of Dielectric Constants, J. Phys. Chem. Solids Pergamon Press. 18 (1961) 253–255. https://doi.org/10.1016/0022-3697(61)90169-X.
- [306] M. Deng, R. Wang, G. Rong, J. Sun, X. Zhang, X. Chen, X. Jing, Synthesis of a novel structural triblock copolymer of poly(γ -benzyl-L-glutamic acid)-b-poly(ethylene oxide)-b-poly(ε-caprolactone), Biomaterials. 25 (2004) 3553–3558. https://doi.org/10.1016/j.biomaterials.2003.10.018.
- [307] C. Deng, G. Rong, H. Tian, Z. Tang, X. Chen, X. Jing, Synthesis and characterization of poly(ethylene glycol)-b-poly (L-lactide)-b-poly(L-glutamic acid) triblock copolymer, Polymer (Guildf). 46 (2005) 653–659. https://doi.org/10.1016/j.polymer.2004.11.100.
- [308] G.Q. Zhu, F.G. Wang, Y.Y. Liu, Effects of reaction conditions on the grafting percentage of poly(ethylene glycol)- block-poly(γ -benzyl L-glutamate)-graft-poly(ethylene glycol) copolymer, J. Braz. Chem. Soc. 21 (2010) 715–720. https://doi.org/10.1590/S0103-50532010000400019.
- [309] C. Deng, H. Tian, P. Zhang, J. Sun, X. Chen, X. Jing, Synthesis and characterization of RGD peptide grafted poly(ethylene glycol)-b-poly(L-lactide)-b-poly(L-glutamic acid) triblock copolymer, Biomacromolecules. 7 (2006) 590–596. https://doi.org/10.1021/bm050678c.
- [310] T.H. Epps, F.S. Bates, Effect of molecular weight on network formation in linear ABC triblock copolymers, Macromolecules. 39 (2006) 2676–2682. https://doi.org/10.1021/ma052132o.
- [311] Q.T. Pham, W.B. Russel, J.C. Thibeault, W. Lau, Micellar solutions of associative triblock copolymers: Entropic attraction and gas-liquid transition, Macromolecules. 32 (1999) 2996–3005. https://doi.org/10.1021/ma982007v.
- [312] J.S. Park, Y. Akiyama, F.M. Winnik, K. Kataoka, Versatile synthesis of end-functionalized thermosensitive poly(2-isopropyl-2-oxazolines), Macromolecules. 37 (2004) 6786–6792. https://doi.org/10.1021/ma049677n.
- [313] X.J. Loh, Z.X. Zhang, Y.L. Wu, T.S. Lee, J. Li, Synthesis of novel biodegradable thermoresponsive triblock copolymers based on poly[(R)-3-hydroxybutyrate] and poly(N-isopropylacrylamide) and their formation of thermoresponsive micelles, Macromolecules. 42 (2009) 194–202. https://doi.org/10.1021/ma8019865.
- [314] M.R. Libera, R.F. Egerton, Advances in the transmission electron microscopy of

- polymers, Polym. Rev. 50 (2010) 321–339. https://doi.org/10.1080/15583724.2010.493256.
- [315] W. Zhao, D. Chen, Y. Hu, G.M. Grason, T.P. Russell, ABC Triblock Copolymer Vesicles with Mesh-Like Morphology, ACS Nano. 5 (2010) 486–492.
- [316] S. Xu, C. Zhang, L. Li, S. Zheng, Polystyrene-block-polyethylene-block-polystyrene triblock copolymers: Synthesis and crystallization-driven self-assembly behavior, Polymer (Guildf). 128 (2017) 1–11. https://doi.org/10.1016/j.polymer.2017.09.002.
- [317] C. Spagnol, E.H. Fragal, M.A. Witt, H.D.M. Follmann, R. Silva, A.F. Rubira, Mechanically improved polyvinyl alcohol-composite films using modified cellulose nanowhiskers as nano-reinforcement, Carbohydr. Polym. 191 (2018) 25–34. https://doi.org/10.1016/j.carbpol.2018.03.001.
- [318] J. Sundaram, B. Park, A. Hinton, K.C. Lawrence, Y. Kwon, Detection and differentiation of Salmonella serotypes using surface enhanced Raman scattering (SERS) technique, J. Food Meas. Charact. 7 (2013) 1–12. https://doi.org/10.1007/s11694-012-9133-0.
- [319] B.A. Chalmers, C. Magee, D.L. Cheung, P.B. Zetterlund, F. Aldabbagh, CO2-responsive polyacrylamide copolymer vesicles with acid-sensitive morpholine moieties and large hydrophobic RAFT end-group, Eur. Polym. J. 97 (2017) 129–137. https://doi.org/10.1016/j.eurpolymj.2017.10.004.
- [320] Y. Cai, S.P. Armes, A zwitterionic ABC triblock copolymer that forms a "trinity" of micellar aggregates in aqueous solution, Macromolecules. 37 (2004) 7116–7122. https://doi.org/10.1021/ma048789b.
- [321] M.G. Carneiro-Da-Cunha, M.A. Cerqueira, B.W.S. Souza, J.A. Teixeira, A.A. Vicente, Influence of concentration, ionic strength and pH on zeta potential and mean hydrodynamic diameter of edible polysaccharide solutions envisaged for multinanolayered films production, Carbohydr. Polym. 85 (2011) 522–528. https://doi.org/10.1016/j.carbpol.2011.03.001.
- [322] O. Bertrand, C.A. Fustin, J.F. Gohy, Multiresponsive micellar systems from photocleavable block copolymers, ACS Macro Lett. 1 (2012) 949–953. https://doi.org/10.1021/mz300299t.
- [323] L. Zhu, Y. Yang, K. Farquhar, J. Wang, C. Tian, J. Ranville, S.G. Boyes, Surface Modification of Gd Nanoparticles with pH-Responsive Block Copolymers for Use As Smart MRI Contrast Agents, ACS Appl. Mater. Interfaces. 8 (2016) 5040–5050. https://doi.org/10.1021/acsami.5b12463.
- [324] S.L. Canning, T.J. Neal, S.P. Armes, PH-Responsive Schizophrenic Diblock Copolymers Prepared by Polymerization-Induced Self-Assembly, Macromolecules. 50 (2017) 6108–6116. https://doi.org/10.1021/acs.macromol.7b01005.

- [325] C. Li, Y. Tang, S.P. Armes, C.J. Morris, S.F. Rose, A.W. Lloyd, A.L. Lewis, Synthesis and characterization of biocompatible thermo-responsive gelators based on ABA triblock copolymers, Biomacromolecules. 6 (2005) 994–999. https://doi.org/10.1021/bm049331k.
- [326] J. Weiss, A. Laschewsky, Temperature-induced self-assembly of triple-responsive triblock copolymers in aqueous solutions, Langmuir. 27 (2011) 4465–4473. https://doi.org/10.1021/la200115p.
- [327] T. Sun, J. Zhu, M. Wang, M. Lu, J. Ding, Z. Lv, P. Hua, Y. Zhang, A glucosyl triblock copolymer: Synthesis and its injectable thermo- and pH-responsive behaviours, RSC Adv. 5 (2015) 24231–24238. https://doi.org/10.1039/c5ra01144b.
- [328] M. Hrubý, S.K. Filippov, P. Štěpánek, Smart polymers in drug delivery systems on crossroads: Which way deserves following?, Eur. Polym. J. 65 (2015) 82–97. https://doi.org/10.1016/j.eurpolymj.2015.01.016.
- [329] S.L. Anderson, K.C. Stylianou, Biologically derived metal organic frameworks, Coord. Chem. Rev. 349 (2017) 102–128. https://doi.org/10.1016/j.ccr.2017.07.012.
- [330] J. Guo, Y. Huang, X. Jing, X. Chen, Synthesis and characterization of functional poly(γ-benzyl-l-glutamate) (PBLG) as a hydrophobic precursor, Polymer (Guildf). 50 (2009) 2847–2855. https://doi.org/10.1016/j.polymer.2009.04.016.
- [331] O. Altintas, M. Artar, G. Ter Huurne, I.K. Voets, A.R.A. Palmans, C. Barner-Kowollik, E.W. Meijer, Design and Synthesis of Triblock Copolymers for Creating Complex Secondary Structures by Orthogonal Self-Assembly, Macromolecules. 48 (2015) 8921–8932. https://doi.org/10.1021/acs.macromol.5b01990.
- [332] H.R. Allcock, Y.C. Song, L.B. Steely, New amphiphilic poly[bis(2,2,2-trifluoroethoxy)phosphazene]/ poly(propylene glycol) triblock copolymers: Synthesis and micellar characteristics, Macromolecules. 39 (2006) 8334–8338. https://doi.org/10.1021/ma061531w.
- [333] N. Greenfield, G.D. Fasman, Computed Circular Dichroism Spectra for the Evaluation of Protein Conformation, Biochemistry. 8 (1969) 4108–4116. https://doi.org/10.1021/bi00838a031.
- [334] K. Matsuo, R. Yonehara, K. Gekko, Improved estimation of the secondary structures of proteins by vacuum-ultraviolet circular dichroism spectroscopy, J. Biochem. 138 (2005) 79–88. https://doi.org/10.1093/jb/mvi101.
- [335] J. Babin, J. Rodriguez-Hernandez, S. Lecommandoux, H.A. Klok, M.F. Achard, Self-assembled nanostructures from peptide-synthetic hybrid block copolymers: Complex, stimuli-responsive rod-coil architectures, Faraday Discuss. 128 (2005) 179–192. https://doi.org/10.1039/b403203a.
- [336] F. Chécot, A. Brûlet, J. Oberdisse, Y. Gnanou, O. Mondain-Monval, S.

- Lecommandoux, Structure of polypeptide-based diblock copolymers in solution: Stimuli-responsive vesicles and micelles, Langmuir. 21 (2005) 4308–4315. https://doi.org/10.1021/la0468500.
- [337] T. Luo, L. He, P. Theato, K.L. Kiick, Thermoresponsive self-assembly of nanostructures from a collagen-like peptide-containing diblock copolymera, Macromol. Biosci. 15 (2015) 111–123. https://doi.org/10.1002/mabi.201400358.
- [338] D. Bharatiya, S. Kumar, S. Raghunandan, P. Paik, Dielectrics of graphene oxide decorated with nanocomposite silica-coated calcium copper titanate (CCTO) nanoparticles, J. Mater. Sci. 54 (2019) 6272–6285. https://doi.org/10.1007/s10853-019-03336-8.
- [339] D. Bharatiya, K. Santhosh Kumar, R. Seelaboyina, P. Paik, A detailed study on the dielectric properties of CCTO@SiO2 core-shell nanoparticles: Role of SiO2-NH2 shell over CCTO core surface, J. Solid State Chem. 277 (2019) 346–355. https://doi.org/10.1016/j.jssc.2019.06.023.
- [340] L.R. Velatooru, C.B. Baggu, V.R. Janapala, Spatane diterpinoid from the brown algae, Stoechospermum marginatum induces apoptosis via ROS induced mitochondrial mediated caspase dependent pathway in murine B16F10 melanoma cells, Mol. Carcinog. 55 (2016) 2222–2235. https://doi.org/10.1002/mc.22463.
- [341] R. Mancuso, R. Amuso, B. Armentano, G. Grasso, V. Rago, A.R. Cappello, F. Galiano, A. Figoli, G. De Luca, J. Hoinkis, B. Gabriele, Synthesis and Antibacterial Activity of Polymerizable Acryloyloxyalkyltriethyl Ammonium Salts, Chempluschem. 82 (2017) 1235–1244. https://doi.org/10.1002/cplu.201700194.
- [342] S.K.I.L. Mounyr Balouiri n, Moulay Sadiki, Methods for in vitro evaluating antimicrobial activity: A review, J. Pharm. Anal. 6 (2016) 71–79. https://doi.org/10.1016/j.jpha.2015.11.005.
- [343] H. Priya James, R. John, A. Alex, K.R. Anoop, Smart polymers for the controlled delivery of drugs a concise overview, Acta Pharm. Sin. B. 4 (2014) 120–127. https://doi.org/10.1016/j.apsb.2014.02.005.
- [344] R.J.M. Nolte, R.J.R.W. Peters, J.C.M. van Hest, S.F.M. van Dongen, M. Nallani, H.-P.M. de Hoog, Biohybrid Polymer Capsules, Chem. Rev. 109 (2009) 6212–6274. https://doi.org/10.1021/cr900072y.
- [345] J.P. Lerch, L.I. Atanase, G. Riess, Adsorption of non-ionic ABC triblock copolymers: Surface modification of TiO2 suspensions in aqueous and non-aqueous medium, Appl. Surf. Sci. 419 (2017) 713–719. https://doi.org/10.1016/j.apsusc.2017.05.062.
- [346] G. Riess, Micellization of block copolymers, Prog. Polym. Sci. 28 (2003) 1107–1170. https://doi.org/10.1016/S0079-6700(03)00015-7.
- [347] P. Caliceti, S. Salmaso, G. Mantovani, M.J. Vicent, T. Matini, E. Gallon, L. Sasso, C.

- Alexander, A. Armiñan de Benito, J. Sanchis, Triblock Copolymer Nanovesicles for pH-Responsive Targeted Delivery and Controlled Release of siRNA to Cancer Cells, Biomacromolecules. 16 (2015) 1924–1937. https://doi.org/10.1021/acs.biomac.5b00286.
- [348] S. Honary, F. Zahir, Effect of zeta potential on the properties of nano-drug delivery systems A review (Part 2), Trop. J. Pharm. Res. 12 (2013) 265–273. https://doi.org/10.4314/tjpr.v12i2.20.
- [349] D. Breite, M. Went, A. Prager, A. Schulze, The critical zeta potential of polymer membranes: How electrolytes impact membrane fouling, RSC Adv. 6 (2016) 98180–98189. https://doi.org/10.1039/c6ra19239d.
- [350] Y. Chen, Z. Xu, Q. Zeng, Z. Wang, H. Fan, J. Chang, Switchable Control of Antibiotic Activity: A Shape-Shifting "Tail" Strategy, Bioconjug. Chem. 29 (2017) 74–82. https://doi.org/10.1021/acs.bioconjchem.7b00599.

Synthesis, characterization and applications of morphologically varying organic-inorganic dielectrics and amino acid based biocompatible copolymeric nanomaterials

by Debasrita Bharatiya

Submission date: 28-Jan-2020 02:58PM (UTC+0530)

Submission ID: 1247609483

File name: Thesis_Plagiarism_Check_Debasrita_Bharatiya_27_Jan_2020.pdf (3.48M)

Word count: 46245 Character count: 245385 Synthesis, characterization and applications of morphologically varying organic-inorganic dielectrics and amino acid based biocompatible copolymeric nanomaterials

ORIGINA	LITY REPORT			
SIMILA	2% RITY INDEX	4% INTERNET SOURCES	12% PUBLICATIONS	2% STUDENT PAPERS
PRIMARY	/ SOURCES			
1	Raghuna detailed s CCTO@S SiO2-NH	a Bharatiya, K. Sandan Seelaboyir study on the diele SiO2 core-shell r 2 shell over CCT of Solid State Che	na, Pradip Pai ectric propertic nanoparticles: O core surfac	k. "A es of Role of
2	link.sprin	•		2%
3	www.md			<1%
4	Raghuna graphene silica-coa	a Bharatiya, Sant Indan, Pradip Pa e oxide decorated Ited calcium copp icles", Journal of	ik. "Dielectrics d with nanoco per titanate (C	s of mposite CCTO)



Kim E. Sapsford, W. Russ Algar, Lorenzo Berti, Kelly Boeneman Gemmill et al. "Functionalizing Nanoparticles with Biological Molecules: Developing Chemistries that Facilitate Nanotechnology", Chemical Reviews, 2013 <1%

Publication

Exclude quotes On Exclude bibliography On

Exclude matches

< 14 words

Synthesis, characterization and applications of morphologically varying organic-inorganic dielectrics and amino acid based biocompatible copolymeric nanomaterials

ORIGINA	ALITY REPORT			
3 SIMILA	1% ARITY INDEX	15% INTERNET SOURCES	30% PUBLICATIONS	4% STUDENT PAPERS
PRIMAR	Y SOURCES			
1	Raghuna detailed CCTO@ SiO2-NH	a Bharatiya, K. S andan Seelaboyir study on the diele SiO2 core-shell r l2 shell over CCT of Solid State Che	na, Pradip Paik ectric propertie nanoparticles: O core surfac	c. "A es of Role of
2	link.sprin	•		11%
3	Debasrita Raghuna graphene silica-coa nanopart 2019 Publication	of mposite CTO)		
4	"Enantio	aik, Aharon Geda selective Separa ous Spherical Sil	tion Using Chi	ral \\

Their Application for Cancer Treatment", Polymers, 2017 Publication

73	Laxman Singh, U.S. Rai, K.D. Mandal, N.B. Singh. "Progress in the growth of CaCu3Ti4O12 and related functional dielectric perovskites", Progress in Crystal Growth and Characterization of Materials, 2014 Publication	<1%
74	Yong Li, Xingyi Huang, Zhiwei Hu, Pingkai Jiang, Shengtao Li, Toshikatsu Tanaka. "Large Dielectric Constant and High Thermal Conductivity in Poly(vinylidene fluoride)/Barium Titanate/Silicon Carbide Three-Phase Nanocomposites", ACS Applied Materials & Interfaces, 2011 Publication	<1%
75	Submitted to Swinburne University of Technology Student Paper	<1%
76	mfr.edp-open.org Internet Source	<1%
77	worldscientific.com Internet Source	<1%

Exclude quotes On Exclude matches < 14 words

Exclude bibliography Off